Flow boiling of pure refrigerants and binary refrigerant mixtures in a horizontal tube

Vom Fachbereich Maschinenbau
der Universität Hannover
zur Erlangung des akademischen Grades

Doktor-Ingenieur

genehmigte
Dissertation

von
MSc. Ali A. Rabah
geboren am 1. Januar 1967 im Sudan

2003

1. Referent: Prof. Dr.-Ing. S. Kabelac
2. Referent: Prof. Dr.-Ing. D. Mewes
Vorsitz der Prüfungskommission: Prof. Dr.-Ing. R. Braune

Tag der Promotion: 02. Juni 2003

Vorwort

Die vorliegende Arbeit entstand während meiner Tätigkeit als wissenschaftlicher Mitarbeiter am Institut für Thermodynamik der Universität Hannover.

Herrn Professor Dr.-Ing. S. Kabelac, dem ehemaligen Institutsleiter und dem Leiter des Instituts für Thermodynamik der Universität der Bundeswehr Hamburg, danke ich für die Anregung und die großzügige Förderung der Arbeit.

Herrn Professor Dr.-Ing. D. Mewes, dem Leiter des Instituts für Verfahrenstechnik der Universität Hannover danke ich für die Übernommene des Korreferats. Für die Übernahme des Vorsitzes der Prüfungskommission danke ich Herrn Professor Dr.-Ing. R. Braune, dem Leiter des Instituts für Getriebetechnik der Universität Hannover.

Ein besonderer Dank gilt den Kollegen und Mitarbeiten des Instituts, Studienarbeitern und wissenschaftlichen Hilfskräften. Die konstruktive und angenehme Atmosphäre am Institut habe ich sehr zu schätzen gelernt.

Meine Familie, insbesondere meiner Frau Sumya und meiner Tochter Sarah danke ich herzlich dafür, dass sie mich immer unterstützt haben.

Dem Deutschen Akademischen Austauschdienst (DAAD) danke ich für die finanzielle Unterstützung.

Hannover, im Juni 2003

Ali A. Rabah

Abstract

The reduction in chlorofluorocarbons (CFCs) and hydrochlorofluorocarbons (HCFCs) production and the scheduled phase-out of these ozone-depleting refrigerants have called for the development of environmentally safe refrigerants for use in air conditioning and refrigeration equipments. The demand for replacement of CFCs and HCFCs has led to the renewed interest in the natural fluids (hydrocarbons) and the development of new non-ozone depleting refrigerants based on hydrofluorocarbons (HFCs) and mixtures of HFCs and natural fluids. Thermodynamic data are available but there is a lack of information on the flow boiling heat transfer characteristics of the newly developed refrigerants.

In the present study the flow boiling characteristics of a pure 1,1,1,2-tetraflouroethane (R134a) and binary R134a/propane (R290) mixtures have been studied. The mixture bulk compositions covered the zeotropic region and azeotropic point; $0 < \widetilde{z} \leq 65$ mole % R290. The R134a/R290 mixture has an azeotrope at **65** mole % R290.

The experimental setup employs a plain horizontal tube of 10 mm in diameter and of 500 mm in length. The test tube is heated not by the conventional mean of electrical energy dissipation but via a condensing steam of ammonia on the outside of the horizontal tube. Thus the thermal boundary condition of **constant wall temperature** rather than the conventional one of a constant heat flux may be assumed. The experiments were carried out at **low** saturation temperatures (**-40**$\leq T_s \leq$ **5** **°C**) for a wide range of mass fluxes (**50**$\leq \dot{m} \leq$ **400 kg/m^{2}s**) and qualities (**0**$\leq \dot{x} \leq$**1**).

The experimental measurements revealed that the assumption of the thermal boundary condition of constant wall temperature is valid only at a very low heat flux. At a relatively high heat flux the measured wall temperature is found, however, to possess a profound cosine profile. Subsequently, the conservation of mass, momentum and energy equations are numerically solved for the condensate film thickness under both isothermal and non-isothermal wall temperature. It is found that the film thickness, and thus the angular heat flux, are strong functions of the cosine wall temperature profiles. However, the mean heat flux over the perimeter of the tube remained unaffected by the cosine wall temperature distribution; the solution **blended** with the original **Nusselt's theory** of film condensation.

The parametric dependency of the flow boiling heat transfer coefficients of R134a and R134a/R290 mixtures on the test variables $\dot{m}$, $\dot{x}$, T_s and concentration $\widetilde{x}$ are experimentally investigated and found to confirm the previous studies. Furthermore, a number of existing correlations for the prediction of the flow boiling heat transfer coefficients are fitted to the experimental data of the pure R134a and R134a/R290 mixtures. Besides the heat transfer coefficient, data on the pressure drop and the flow pattern for both pure R134a and R134a/R290 mixtures are presented in this work.

Keywords: Flow boiling, R134a, Mixtures

Kurzfassung

Die gesetzlichen Auflagen zur Verringerung der Produktion von ozonschädlichen Kühlmitteln wie Fluorchlorkohlenwasserstoffe (FCKW) und Fluorchlorkohlenstoffe (FCK) haben die Entwicklung umweltschonender Kühlmittel für den Gebrauch in Klimaanlagen- und Abkühlungsausrüstungen erfolderlich gemacht. Die Nachfrage nach Ersatzstoffen für FCK und FCKW hat das erneuerte Interesse an den natürlichen Fluiden (Kohlenwasserstoffe) geweckt und zu der Entwicklung von neuen nichtozonschädigenden Kühlmitteln, die auf Fluorkohlenwasserstoffe (FKW) basieren, sowie Gemischen aus FKW und natürlichen Fluiden geführt. Thermodynamische Daten sind zwar vorhanden, aber es besteht Informationsbedarf über die Wärmeübertragungseigenschaften beim Strömungssieden dieser neu entwickelten Kältemittel.

In der vorliegenden Arbeit sind die Eigenschaften des Strömungssieden von 1,1,1,2-Tetraflouroethane (R134a) und der binären Gemisch aus R134a und Propan (R290) untersucht worden. Die Zusammensetzung des Gemisches umfasste das zeotrope Gebiet und den azeotropen Punkt ($0 \leq \tilde{z} \leq 65$). R134a/R290 hat einen azeotropen Punkt bei 65 Mole % R290.

Die Versuche wurden an einem glatten waagerechres Rohr mit 10 mm Durchmesser und 500 mm Länge durchgeführt. Das horizontale Rohr wurde nicht elektrisch, sondern durch Filmkondensation von Ammoniak in einem umhüllenden äußeren Rohre beheizt. So wurde als thermische Randbedingung eine **konstante Wandtemperatur** anstatt einer konstanten Wärmestromdichte näherungsweise realiziert. Die Versuche wurden bei tiefen Temperaturen ($\mathbf{-40} \leq T_s \leq \mathbf{5}\ \ ^\circ\mathbf{C}$) in einem Parameterbereich der Massenstromdichte von ($\mathbf{50} \leq \dot{m} \leq \mathbf{400\ kg/m^2s}$)) und einem Dampfgehalt von ($\mathbf{0} \leq \dot{x} \leq \mathbf{1}$) durchgeführt.

Die Untersuchungen zeigten, dass eine konstante Wandtemperatur als thermischen Randbedingung nur bei sehr niedrigen Wärmestromdichten gegeben ist. Bei verhältnismäßig hohen Wärmestromdichten wird die gemessene Wandtemperatur jedoch durch ein ausgeprägtes Kosinusprofil dargstellt. Daher werden die Massen-, Impuls- und Energiegleichungen für die Kondensatschichtstärke numerisch sowohl für die isothermeals auch für die nichtisotherme Wandtemperatur gelöst. Es konnte gezeigt werden, daß die Schichtstärke und lokale Wärmestromdichte stark von dem kosinusförmigen Wandtemperaturprofil abhängt. Die mittlere Wärmestromdichte blieb über dem Umfang des Rohres jedoch von der kosinusförmigen Temperaturverteilung unberührt. Die Lösung vermengte sich mit der ursprünglichen Nußelt'sche Theorie der Filmkondensation.

Die Abhängigkeit der Wärmeübertragungskoeffizienten beim Strömungssiedens von R134a und R134a/R290 mit den den Parametern $\dot{m}$, $\dot{x}$, T^s und Konzentration $\tilde{x}$ werden experimentell untersucht und ausgewertet, um die vorhergehenden Untersuchungen zu bestätigen. Außerdem wurden eine Anzahl von vorhandenen Berechnungsmethoden zur Berechnung von Wärmeübertragungskoeffizienten von R134a und R134a/R290 angepasst. Neben dem Wärmeübertragungskoeffizienten werden in dieser Arbeit Daten bezüglich des Druckverlustes und den Strömungsformen für R134a und R134a/R290 dargestellt.

Schlüsselwörter: Strömungssieden, R134a, Gemisch

Table of contents

Nomenclature **xi**

1 Introduction **1**

2 Literature review **3**

2.1 Previous experimental work 4

2.2 Heat transfer coefficient 6

2.2.1 Flow boiling of pure components 6

2.2.2 Flow boiling of mixtures 10

2.3 Pressure drop 16

2.4 Flow pattern 16

2.5 Objectives of this work 18

3 Experimental apparatus **21**

3.1 Experimental setup 21

3.1.1 Test circuit 21

3.1.2 Secondary evaporator 23

3.1.3 Refrigeration cycle 23

3.2 Measurement techniques 24

3.2.1 Temperature 26

3.2.2 Pressure 28

3.2.3 Pressure difference 31

3.2.4 Flow rate 32

3.2.5 Electrical heat 32

3.2.6 Gas chromatography 34

3.2.7 Observation of flow pattern 38

3.3 Data acquisition system 38

3.4 Experimental procedure 39

3.4.1 Charging procedure 39

3.4.2 Test programm 40

4 Data reduction **42**

4.1 Heat transfer coefficient 42
4.1.1 Angular heat transfer coefficient 42
4.1.2 Mean circumferential heat transfer coefficient 43
4.2 Energy balance 43
4.3 Saturation temperature 46
4.3.1 Pure R134a and azeotropic R134a/R290 mixture 46
4.3.2 Zeotropic R134a/R290 mixture 48
4.4 Wall temperature 51
4.5 Wall superheat 54
4.6 Heat flux 55
4.6.1 Angular heat flux 56
4.6.2 Axial heat flux 63
4.6.3 Validation of the heat flux model 65
4.7 Vapor quality 69
4.8 Equilibrium composition 70
4.9 Summary 76

5 Heat transfer coefficient **77**
5.1 Results for pure R134a 80
5.1.1 Influence of vapor quality 82
5.1.2 Influence of the mass flux 85
5.1.3 Influence of the saturation temperature 86
5.1.4 Comparisons with correlations 87
5.1.5 Comparisons with previous experimental work 91
5.1.6 Repeatability of R134a data 91
5.2 Results for R134/R290 mixtures 93
5.2.1 Influence of the concentration 93
5.2.2 Influence of the mass flux 98
5.2.3 Influence of the saturation pressure 99
5.2.4 Influence of the vapor quality 100
5.2.5 Comparisons with correlations 101
5.2.6 Repeatability of R134a-R290 data 104

6 Pressure drop **105**

6.1 Pure R134a . . . 107

6.2 R134a/R290 mixtures . . . 109

7 Flow pattern **111**

7.1 Pure R134a . . . 114

7.2 R134a/R290 mixtures . . . 115

8 Recommendation **117**

9 Conclusion **118**

Bibliography **121**

A Uncertainty and statistical analysis **133**

A.1 Uncertainty . . . 133

A.2 Statistical parameters . . . 134

B Thermophysical properties **136**

B.1 1,1,1,2- Tetrafluoroethane (R134a) . . . 136

B.1.1 General specifications and critical properties of R134a . . . 136

B.1.2 Equation of state (EOS) for R134a . . . 136

B.1.3 Liquid dynamic viscosity of R134a . . . 139

B.1.4 Vapor dynamic viscosity of R134a . . . 139

B.1.5 Thermal conductivity of R134a . . . 141

B.1.6 Surface tension of R134a . . . 141

B.2 Propane (R290) . . . 142

B.2.1 General specifications and critical properties of R290 . . . 142

B.2.2 EOS for R290 . . . 142

B.2.3 Dynamic viscosity of R290 . . . 142

B.2.4 Thermal conductivity of R290 . . . 144

B.2.5 Surface tension of R290 . . . 144

B.3 Ammonia (R717) . . . 145

B.3.1 General specifications and critical properties of R717 . . . 145

B.3.2 EOS for R717 . . . 145

B.3.3 Thermal conductivity of R717 . . . 146
B.3.4 Dynamic viscosity of R717 . . . 146
B.4 R134a/R290 mixtures . . . 148
B.4.1 EOS for R134a/R290 mixtures . . . 148
B.4.2 Liquid dynamic viscosity of R134a/R290 mixtures . . . 150
B.4.3 Vapor dynamic viscosity of R134a/R290 mixtures . . . 150
B.4.4 Liquid thermal conductivity of R134a/R290 mixtures . . . 151
B.4.5 Vapor thermal conductivity of R134a/R290 mixtures . . . 151
B.4.6 Surface tension of R134a/R290 mixtures . . . 152

C Heat transfer coefficient **153**
C.1 Two phase flow: Pure fluid . . . 153
C.1.1 Steiner [128] correlation . . . 153
C.1.2 Kattan et al. [73] correlation . . . 155
C.1.3 Kandlikar [66] correlation . . . 157
C.1.4 Chen [17] correlation . . . 158
C.1.5 Gungor and Winterton [48] correlation . . . 158
C.1.6 Shah [118] correlation . . . 159
C.1.7 Schrock and Grossman [117] correlation . . . 159
C.1.8 Dembi et al. [27] correlation . . . 160
C.1.9 Klimenko [79] correlation . . . 160
C.1.10 Jung et al. [60] correlation . . . 160
C.2 Two phase flow: Mixture . . . 161
C.2.1 Steiner [128] correlation . . . 161
C.2.2 Kandlikar [67] correlation . . . 161
C.2.3 Bennett and Chen [7] correlation . . . 162
C.2.4 Palen [104] correlation . . . 162
C.2.5 Jung et al. [60] correlation . . . 163
C.3 Single phase . . . 163
C.3.1 Free convection . . . 163
C.3.2 Radiation . . . 164

D Steiner [128] flow pattern map **165**

E Pressure drop **168**

E.1 Friedel [38] model 168

E.2 Lockhart and Martinelli [85] model 168

E.3 Chisholm [20] model 169

F Experimental Data **170**

Nomenclature

Latin letters

Symbol	SI Unit	Quantity
a	m^2/s	thermal diffusivity
A	m^2,-	cross sectional area, amplitude of the cosine wall temperature distribution equation 4.38
b	-	laplace constant
C	-	constant
c_p	J/(kg K)	isobar specific heat
c_v	J/(kg K)	isochoric specific heat
d	m	diameter
D_{12}	m^2/s	binary diffusion coefficient
F	-,-	parameter equation 4.50, suppression factor
$\dot{F}$	mol/s	bulk molar flow rate
g	m/s^2	acceleration due to gravity
$\dot{G}$	mol/s	vapor molar flow rate
h	J/(kg K)	enthalpy
$\widetilde{h}_L$	m	height of the stratified liquid film
I	A	electric current
k	W/(m^2 K)	overall heat transfer coefficient
K	W/(m^2 K)	fugacity coefficient ratio
L	m	length
$\dot{L}$	mol/s	liquid molar mass
$\dot{m}$	kg/(m^2 s)	mass flux
$\dot{M}$	kg/s	mass flow rate
$\widetilde{M}$	kg/kmol	molecular weight
p	Pa	pressure
p_c	Pa	critical pressure
p_r	-	reduced pressure
P	-,W	pressure function equation 4.63, electric power
$\dot{q}$	W/m^2	heat flux
$\dot{Q}$	W	heat flow rate
r	m	radial coordiante
s	m	tube thickness
T	K	thermodynamic temperature
T_c	K	critical temperature
T_W	K	wall temperature
T_f	K	fluid bulk temperature
T_s	K	saturation temperature
T_∞	K	ambient temperature
u	m/s	condensate velocity

U	V	electric voltage
U_∞	m/s	steam velocity
X	-, -	Martinelli parameter, parameter
$\dot{x}$	-	quality
$\widetilde{x}$	-	liquid mole fraction
y	-	coordinate
$\widetilde{y}$	-	vapor mole fraction
z	-	coordinate
$\widetilde{z}$	-	mixture bulk mole fraction
$\widetilde{Z}$	-	mixture bulk weight fraction

Greek letters

Symbol	SI Unit	Quantity
α	W/(m^2 K)	local heat transfer coefficient
α_c	W/(m^2 K)	convective boiling heat transfer coefficient
α_n	W/(m^2 K)	nucleate boiling heat transfer coefficient
β	1/K, m/s	thermal expansion coefficient, mass transfer coefficient
Δh_V	J/kg	enthalpy evaporation
ΔT_sup	K	$T_\mathrm{W} - T_\mathrm{s}$
$\delta = \rho/\rho_\mathrm{c}$	-	reduced density
δ	m	condensate film thickness
δ^*	-	dimensionless condensate film thickness
ε	-	void fraction
η	kg/(m s)	dynamic viscosity
λ	W/(m K)	thermal conductivity
$\dot{\lambda}$	kmol/kmol	molar quality
ν	m^2/s	kinematic viscosity
ρ	kg/m^3	density
σ	N/m, -	surface tension, standard deviation
	W/(m^2 K^4)	Stefan-Boltzman constant
Φ	-	Helmholtz free energy
ξ	-	friction factor
$\tau = T_\mathrm{c}/T$	-	reciprocal of reduced temperature
ϕ	-	fugacity coefficient
φ	rad,^{o}	angle, circumferential angle
ω	-	eccentric factor

Subscripts

Symbol	Quantity
bub	bubble point
c	critical state, condensation, convection
calc	calculated

eff	effective
el	electrical
G	gas
Gr	*Grenze* (boundary)
i	inside, index
id	ideal
j	index
L	liquid
max	maximum
meas	measured
min	minimum
n	nucleate
o	outside
r	reduced
s	saturated
sub	subcooling
sup	superheat
t	turbulent
tot	total
v	viscous
0	reference state
∞	infinite distance

Superscript

Symbol	Meaning
$^\circ$	degree

Abbreviations

CFCs	Chlorofluorocarbons
COP	Coefficient of performance
DKD	*Der Deutsche Kalibrierdienst*
EOS	Equation of state
FCK	Fluorchlorkohlenstoffe
FCKW	*Fluorchlorkohlenwasserstoffe*
FKW	*Fluorkohlenwasserstoffe*
GC	Gas Chromography
GPIB	General Purpose Interface Bus
HCFCs	Hydrochlorofluorocarbons
HFCs	Hydrofluorocarbons
IEEE	Institute of Electrical and Electronic Engineers
ISA	Industry-Standard Architecture
PCI	Peripheral Component Interconnect

PTB *Physikalisch-Technischen-Bundesanstalt*

Dimensionless groups

$Bo = \dot{q}/\dot{m}\Delta h_v$	boiling number
$Co = (\rho_G/\rho_L)[(1-\dot{x})/\dot{x}]^{0.8}$	convection number
$Fr_d = \dot{m}/(\rho_L\ g\ d)$	Froude number
$Gr_d = g\beta\Delta T d^3/\nu^2$	Grashof number
$Ja = \rho_L c_{\mathrm{pL}}\Delta T/(\rho_G \Delta h_{\mathrm{V}})$	Jacob number
$Nu = \alpha d/\lambda$	Nusselt number
$Pr = \nu/a$	Prandtl number
$Ra = Gr_d Pr$	Rayleigh number
$Re = \dot{m}d/\nu$	Reynolds number

1 Introduction

Flow boiling is defined as being the addition of heat to a flowing fluid in such a way that generation of vapor occurs; liquid and vapor flowing simultaneously (*i.e.* two phase). Two-phase processes are important in unit operations almost in every chemical and energy plant. In energy processes, for example in power, refrigeration and in air conditioning, pure substances and/or azeotropic mixtures are usually used as working fluids. In a thermal separation process, for example distillation and rectification, the variable composition of zeotropic mixtures are separated via simultaneous vaporization and condensation. For the past few decades, the ozone depleting chlorofluorocarbons (CFCs) and hydrochlorofluorocarbons (HCFCs) refrigerants have been used extensively in heat pumps, air conditioners and refrigerators. Dichlorodifluoromehtane (R12) and chlorodifluoromethane (R22) were the most widely known CFC and CHFC refrigerants respectively.

The reduction in CFC and HCFC production and the scheduled phase-out of these ozone depleting refrigerants require the development and characterization of new environmentally safe refrigerants for use in air conditioning and refrigeration equipments. The most successful, to date, has been the development of 1,1,1,2-tetraflouroethane (R134a) as a substitute for R12. R134a has similar saturation pressure and coefficient of performance (COP) as R12 (Granryd [45]). The search for a R22 alterative has produced; as yet; no single component having a reasonably close saturation pressure curve to R22 (Kim et al. [76]). However, several zeotropic and azeotropic mixtures resulting in vapor pressure and COP similar to R22 have been identified. Among these the R134a/propane (R290) mixture is a possible substitute to R22 (Jung et al. [62] and Morrison and McLinden [93]). The R134a/R290 mixture has an azeotrope at approximately 65 mol % R290 in the temperature range of -40 to 40 °C (Didion and Bivens [29]), R290 being the more volatile component. In addition to its favorable thermodynamic and refrigeration properties, the R134a/R290 mixture has the merit of incorporating a natural fluid: R290. Incorporation of a natural fluid is likely to offer the additional advantage of making the mixture soluble for mineral oil (Domanski and Didion [31]).

Besides environmental considerations and thermodynamics properties, the flow boiling heat transfer characteristics play an important rule in the selection of the substitute refrigerant. The heat transfer characteristics include heat transfer coefficient (α), pressure drop (Δp) and flow pattern; to mention a few. That is to say if the heat transfer characteristics of an alternative refrigerant deviates too much from that of the reference fluid, the existing equipment must be redesigned completely which would be quite costly. For example, for a sizing purpose, the heating surface A of a heat exchanger is

$$A = \frac{\dot{Q}}{\alpha \Delta T} \ , \tag{1.1}$$

where $\dot{Q}$ is the heat load and $\Delta T = T_w - T_s$, where T_w is the wall temperature and T_s is the saturation temperature. To maintain the same size A of the existing heat exchanger for a given energy demand (*e.g.* cooling load) $\dot{Q}$, under same working conditions, the heat transfer coefficient α of the old and new refrigerant should not deviate too much.

The thermodynamic experimental data as well as calculation methods are available, but there is a lack of information on heat transfer of the newly developed refrigerants and their mixtures. Over years, owing to the extensive utilization of flow boiling in industry, a number of models have been developed for the prediction of α, Δp and the flow pattern, for instance those presented in VDI-Wärmeatlas [143]. Most of the existing prediction methods, for example those for the prediction of α, are however developed based on a data bank of old refrigerants. In the recent past some experimental works on flow boiling of newly developed refrigerants have been published. It has been reported that some of the existing correlations fairly fit the flow boiling data of the new refrigerants (Wetterman [148]). However, the experimental work on the new refrigerants was carried out at relatively high saturation temperature and under a thermal boundary condition of constant heat flux. In most of the real applications the thermal boundary conditions are close to uniform wall temperature.

In the present work experimental studies on the flow boiling of pure R134a and the binary mixture of R134a/R290 have been carried out. The measurement covers the region of low saturation temperature for a wide range of mass flux ($\dot{m}$), quality ($\dot{x}$) and mixture composition ($\widetilde{x}$). Furthermore the study was carried out under the assumption of thermal boundary condition of constant wall temperature.

In order to present the purpose and results of this thesis, it is divided into a number of chapters. In chapter 2 of this work a comprehensive literature review of the existing work on the flow boiling of pure substance and mixture is given. A brief account of the existing correlations for the prediction of α, Δp and flow pattern is also given. In chapter 3 a detailed description of the experimental setup is presented. Here the measurement and calibration procedures as well as the level of uncertainty for the various devices are presented. Methods of reducing the measured parameters to yield the desired parameter of α and $\dot{x}$, among other parameters, are presented in chapter 4. In the subsequent chapters the result of measurements on α, Δp and flow pattern of flow boiling of pure R134a and binary mixtures of R134a/R290 on a plain horizontal tube are presented, discussed and compared with the existing work successively. In addition, a detailed comparison between the experimental results and the existing predictive methods for the local heat transfer coefficient, pressure drop and flow pattern is presented. Predictive methods for physical properties of R134a, R290, ammonia and R134a/R290 mixture and the existing correlations for the prediction of α, Δp and flow pattern are given in the appendices of this works.

Besides the experimental study, a numerical method is presented which was employed to investigate the assumption of thermal boundary conditions of constant wall temperature. The method employs the numerical solution of the conservation of mass, momentum and energy equations for the film-wise condensation problem. The result of the numerical analysis is presented and compared with experimental results and Nusselt's theory of film condensation.

2 Literature review

Research work from many fields of engineering has contributed to the knowledge of flow boiling inside tubes. Notably, work has been published in the technical journals covering mechanical, chemical, refrigeration, petroleum, boiler plant and nuclear engineering amongst other. Although, the studies in this field goes back to the nineteenth century, it is only in the last three or so decades that important contributions have been made towards understanding the processes involved in flow boiling along a tube. The lack of progress in the earlier studies may be attributed, in part, to two main reasons. One reason is the presence of a large number of experimental variables. The second reason is the consequence of the fact that early workers in the field of evaporation reported only *effects* on the performance of the evaporator resulting from independent variables altered by the operator.

In the early experiments long evaporator tubes heated with water (liquid) or condensing steam were used. In this case the heat flux along the length of the tube is a dependent variable. Its magnitude, at any point, is set by the *overall* heat transfer coefficient k, and overall temperature difference ΔT_{lm} (logarithmic mean temperature difference) at that point. In addition, the quality or weight faction vaporized at any point is a function of the total heat added to the fluid up to that point. It has been established that the heat transfer coefficient in flow boiling is strongly dependent upon the local conditions of heat flux and quality (Collier and Thome [23]). Clearly the case of a long evaporator tube or, in other words, the overall heat transfer coefficient is a complex one to analyse.

Two experimental approaches have been used which considerably simplify the situation. Firstly, is the use of electrically heated tubular test sections. This configuration allows a uniform heat flux distribution and linear variation of quality along the tube length. Under such circumstances the thermal boundary conditions of **constant heat flux** is conventionally assumed. Secondly, considering only a very short section of the evaporator was a big advantage. In this case, it may be assumed that the conditions along the test tube are approximately constant. Two modes of heating are possible for this short tube configuration: single phase flow of water or condensing steam. For a short water-heated evaporator the thermal boundary condition of **nearly constant wall temperature** is generally assumed, while for a short steam-heated evaporator the thermal boundary conditions of **constant wall temperature** is conventionally assumed.

The following sections do not attempt to review all the available literature on the field of saturated flow boiling. The intention is rather to:

1. present and classify the existing experimental data on the flow boiling of pure R134a and R290 and their mixtures in a horizontal plain tube,

2. provide a brief account of the present state of knowledge on the flow boiling heat transfer coefficient, pressure drop and flow pattern of pure components and mixtures.

2.1 Previous experimental work

Table 2.1 shows some of the available experimental work on the flow boiling of pure R134a and R290 and their mixtures. The available literature is classified in a way shown in Fig. 2.1, which is summarized as:

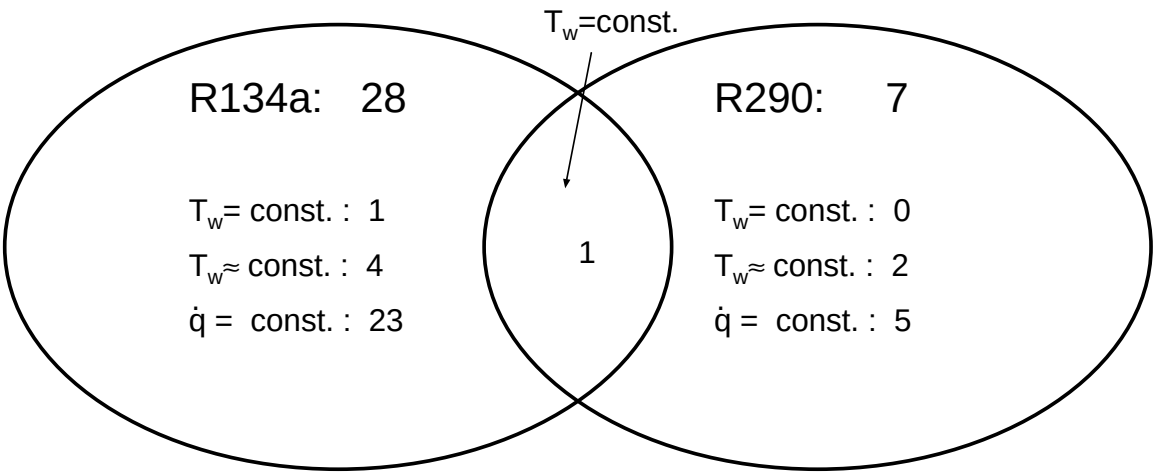

Figure 2.1. Classification of the available experimental data on the flow boiling of R134a, R290 and their mixture in the time period 1990-2003. Symbols: $\dot{q}$: heat flux, T_w: wall temperature.

- No experimental data for flow boiling of a R134a/R290 mixture is available, save the work of Kabelac and Rabah [65] which was made in the context of the present study and covered the region of low concentration ($\widetilde{z}$ =10 mole % R290).
- There exist 28 research papers on the flow boiling of pure R134a on a plain horizontal tube. These papers are further classified according to the thermal boundary condition (constant heat flux or constant wall temperature) as:
  1. The intersection of the key word R134a with the key words constant heat flux yields 23 papers. These include the work of Wettermann [148], Hambraeus [49] and Shin et al. [123], to mention a few. All the existing works under this category are for moderate to high saturation pressures (3.5 bar to 32.4 bar).
  2. The search for R134a data with *nearly* constant wall temperature (*i.e.* water as a heating medium) yields only 4 hits. These include among other the work of Eckels et al. [32] and Kattan et al. [72]. These works are at saturation pressures of greater than 2.7 bar.
  3. The combination of the key word R134a with key words constant wall temperature (film condensation) yields only one hit. This is the work of Kabelac and Rabah [65] at saturation pressures of less than 2 bar.
- The search for flow boiling data of R290 produced 7 hits. All these R290 data are for the thermal boundary condition of constant heat flux save the two papers of Melin and Vamling [90]. Their work was carried out using water as a heating medium.

Table 2.1. Summary of some of the existing recent work on flow boiling of pure R134a and R290 and their mixtures in a plain horizontal tube.

Author	Refrigerant	d mm	$\dot{m}$ kg/m^{2}s	$\dot{x}$ -	$\dot{q}$ kW/m^2	$[T_s], (p_s)$ °C, bar	Heating medium
Wettermann [148]	R134a	14.0	74.1 - 405.7	0.08 - 0.84	0.9 - 75.5	(4 - 32.4)	Electrical [a]
Kattan et al. [72]	R134a	12.0	100 - 500	0.05 - 1.0	0.4 - 36.5	(2.79 - 4.19)	Water[b]
Shin et al. [123]	R134a, R290	07.7	265 - 583	0.05 - 0.85	10-30	[12]	Electrical
Hambraeus [49]	R134a	12.0	17.6 - 195		2 - 10	[-20 - 10]	Electrical
Eckels et al. [32]	R134a	09.5	85 - 375	0.05 - 0.88		(3.5)	Water
Eckels and Pate [35]	R134a	08.0	125 - 400	0.1 - 0.9	12.1	(3.5 - 4.9)	Electrical
Melin and Vamling [90]	R134a, R290	10.0	85 - 316	0.05 - 1.0	1 - 45	[0 - 30]	Water
Zhang [153]	R134a	06.0	150 - 400	0.05 - 0.80	10 - 20	[20]	Electrical
Mathur [87]	R290	02.0	50 - 200	0.0 - 1.0	5 - 20	[5 - 31]	Electircal
Murata and Hashizume [96]	R134a	10.3	100 - 300	0.1 - 1	10 - 30	(2.2 - 2.4)	Electrical
Kabelac and Rabah [65]	R134a	10.0	100 - 300	0 - 1.0	2- 16.5	(0.84 - 2.0)	Condensation[c]
Kabelac and Rabah [65]	R134a/R290	10.0	100 - 300	0 - 1.0	2- 16.5	(0.84 - 2.0)	Condensation
Wongwieses et al. [149]	R134a	09.5	160 - 470	0.0 - 1.0	8 - 55	[4 - 25]	Water

[a] thermal boundary condition of constant heat flux
[b] thermal boundary condition of nearly constant wall temperature
[c] thermal boundray condition of constant wall temperature

2.2 Heat transfer coefficient

2.2.1 Flow boiling of pure components

Chen [17] has postulated that the heat transfer in flow boiling occurs by two mechanisms: nucleate boiling and convective boiling. In the convective boiling, the evaporation occurs at the vapor-liquid interface in the bulk flow away from the wall, so that heat is transferred by convection and conduction across an intervening layer of liquid film. In contrary to the convective boiling, in the nucleate boiling heat transfer region, the vapor bubble activities of nucleation, bubble growth and bubble departure associated with pool nucleate boiling are responsible for transferring heat in this region; analogous to the nucleate boiling in the pool boiling.

Over years systematic experimental studies have been carried out to investigate the effect of the thermal, hydrodynamic, fluid and wall parameters on the flow boiling mechanisms. In the following paragraphs a brief account to some of the existing studies on the influence of these parameters on the flow boiling mechanisms are given.

- Schmidt [116] has investigated the effect of the thermal boundary conditions of constant heat flux and constant wall temperature on the local flow boiling heat transfer coefficient. He measured the local heat transfer coefficient for R12 in two tubes made of Copper and Nickel. The measurements were carried out under thermal boundary condition of both constant heat flux and constant wall temperature. The thermal boundary conditions of constant wall temperature was created by applying a non-uniform heat flux around the tube. Due to the high wall temperature at the dry part of the tube and continuous decrease in the wetted boundary (increase in the dry part), the circumferential average heat transfer coefficient at constant heat flux was found to be lower than that for constant wall temperature. Furthermore, he indicated that the heat transfer coefficient is affected by tube wall thermal conductivity λ_w and wall thickness s. These effects were also observed by Bonn [11].

- Niederkrüger and Steiner [100] have used the Schmidt [116] experimental setup with some modification and measured the local heat transfer coefficient for R12 and sulphur hexafluoride (R846). They have found that the nucleate boiling local heat transfer coefficient is dependent on the heat flux $\dot{q}$, saturation pressure p_s as well as the surface roughness and the type of fluid. Furthermore, the investigation of Jung et al. [60] and Hihara et al. [53] on a horizontal copper tube ($\lambda_w s \geq 0.7$) indicated that, in contrast to a vertical tube, the hydrodynamic parameters ($\dot{m}$, $\dot{x}$) have a strong influence on the nucleate boiling heat transfer coefficient.

- Bonn [11] and Bonn et al. [12] have investigated the circumferential distribution of wall temperature at the surface of a horizontal tube. They have measured the wall temperature at 5 positions per axial location in an electrically heated horizontal copper tube of various wall thickness s. The test fluid were R12, nitrogen (N_2) and argon (Ar). They have observed that, due to non-symmetrical distribution of the vapor-liquid phase in a horizontal tube, the upper side of the tube is less wetted by

the liquid than the lower side. This effect is specially noticeable when the tube wall is thin. Subsequently the measured wall temperature is found to be non-uniform in the circumferential direction. This effect is also observed by Fuchs [39] for flow boiling of R12 in a stainless steel tube at constant heat flux and Müller-Steinhagen [94] und Müller-Steinhagen and Schlünder [95] for flow boiling of Ar, N_2 in a Nickel tube at constant heat flux. Müller-Steinhagen [94] has validated his experimental result with a calculation model. He solved the conduction equation $\nabla^2 T(r, \varphi) = 0$ for the wall temperature using numerical methods.

Kabelac and de Buhr [63] have measured the wall temperature at 4 positions per axial location. Their experiment was carried out under the assumption of thermal boundary conditions of constant wall temperature realised via film condensation. The measured wall temperature was found to be none uniform in the circumference of the tube due to the variable thickness of the condensate film (see Chapter 4). Similar results were also observed by Kabelac and Rabah [65] who used the same experimental setup as that used by Kabelac and de Buhr [63].

- Niederkrüger [98] and Niederkrüger et al. [99] have investigated the effect of flow pattern on the local heat transfer coefficient using R12 and R846 at constant heat flux. Their test section is a modified form of that used by Schmidt [116]. Their results showed that under stratified flow conditions the local heat transfer coefficient at the top of the tube is lower than that at the bottom. The top part of the tube is dry while the bottom part is completely wet. They have indicated that the heat transfer coefficient in the wetted part of the tube is much higher (by a factor of 2 to 3) compared with those at the top part of the tube (dry region). Wettermann [148] has measured the flow boiling heat transfer coefficient for R134a and R846 in a similar experimental setup as that used by Niederkrüger [98]. He has confirmed the early observation of Niederkrüger [98] and Niederkrüger et al. [99] on stratified flow pattern. Furthermore, Wettermann [148] has investigated the flow boiling heat transfer coefficient under a fully developed annular flow pattern. He has indicated that at a low wall superheat the heat transfer coefficient at the top side of the tube is higher than that at bottom side. He attributed this to the fact that the film thickness at the top is thinner than that at the bottom of the tube due to gravity.

  In contrary to the stratified and annular flow pattern, there is a relative lack of experimental work on the intermittent flow patterns like plug/slug, churn flow pattern and annular flow pattern with partial dry out. Wadekar [146] attributed the lack of the information in this area to complexity of the phenomena. Nevertheless, there exist some investigation on this area. These include the work of Niederkrüger [98] with R12, Baumann [5] with N_2 and Köhler et al. [81] with water in intermittent flow patterns. Their experimental results suggested a uniform angular wall temperature and thus uniform heat transfer coefficient around the tube.

- The influence of vapor quality on heat transfer coefficient has been investigated by a number of researchers. The investigations were carried under both low and high

pressure conditions. Those for high pressure conditions include the work of Schroch and Grossman [117] for water, Jallouk, [57] for dichlorotetrafluoroethane (R114), Khanpara [75] for trichlorotrifluoroethane (R113) and Jensen and Bensler [58] for R113 as well. Those under low pressure conditions include the work of Kabelac and de Buhr [63] for ammonia, Kabelac and Rabah [65] for R134a, Kenning and Cooper [74] and Kandlikar [66] for water and Kattan et al. [71] for R134a. The high pressure (low liquid-vapor density ratio) data produced a decreasing heat transfer coefficient with quality while those at low pressure (high liquid-vapor density ratio) data produced an increasing trend. Kandlikar et al. [69] have attributed this effect to the relative contribution of the two boiling mechanisms (*i.e.* nucleate and convective). The nucleate boiling contributions is expected to decrease with increasing quality, while the convective contribution is expected to increase (VDI-Wärmeatlas [143]). The overall trend is thus dependent on the relative contributions from these two mechanisms.

Clearly most of the investigations on flow boiling were carried out with old refrigerants. Due to the scheduled phase-out of the CFCs and HCFCs, in the recent past a number of new, ozone friendly refrigeration fluids have been investigated. A number of good surveys reviewing this experimental work are found in Collier and Thome [23] and Kandlikar et al. [69].

For the prediction of the flow boiling heat transfer coefficient there exists in the literature a number of correlations. A brief review of some of the existing correlations is given in the following paragraphs. A number of good surveys reviewing these correlations in depth are found in VDI-Wärmeatlas [143], Kandlikar et al. [69] and Collier and Thome [23].

Chen [17] has developed a correlation based on the additive of the nucleate and convective boiling. The convective contribution is enhanced due to the two-phase effects, while nucleate boiling is suppressed due to the flow effects. Chen [17] used 600 experimental data points for water, trichlorofluoromethane (R11), R12, R22, R113, R114, ethylene glycol, n-butanol, ethanol in vertical flow in arriving at his correlation. The Chen [17] correlation works well with low pressure water data but large deviations are observed with old refrigerants. Jung and Radermacher [61] have modified Chen [17] correlation using a suppression factor to the nucleate part and enhancement factor to the convective part. The modified form of Chen [17] correlation is tested with experimental data of R12, R22, 1,1-difluoroethane (R152a) and R114.

Shah [118] proposed a graphical chart as an alternative to the Chen [17] correlation. The Shah [118] method can be used for flow boiling in both horizontal and vertical tubes. The ordinate of his chart is the ratio between the two phase heat transfer coefficient α and liquid single phase heat transfer coefficient α_L and its abscissa is the Martinelli parameter X, which is defined as

$$X^2 = \left(\frac{dp}{dz}\right)_L \Big/ \left(\frac{dp}{dz}\right)_G, \tag{2.1}$$

where $(dp/dz)_L$ and $(dp/dz)_G$ are the liquid and vapor frictional pressure gradients re-

spectively. Shah [120] has also developed equations that presents his chart method. The Shah [120] correlation is developed using a data bank of water, R11, R12, R22 and R113.

Gungor and Winterton [48] have developed a correlation that combines the Chen [17] and Shah [120] models. As in the Chen [17] model the correlation is based on the additive contributions of the nucleate and convective boiling. The two phase convection is calculated from the single phase correlation of Dittus-Boelter [30]. The nucleate part is calculated from Cooper [25] correlation of pool boiling with a suppression factor. The suppression factor is based on Froude number ($Fr{=}\dot{m}^2/\rho_L g d$); a criteria previous used by Shah [120] for stratified flow conditions. Liu and Winterton [84] have further modified the Gungor and Winterton [48] model's using a suppression factor based on boiling number, $Bo = \dot{q}/\dot{m}.\Delta h_V$. The correlation was developed on a data bank of water, R11, R12, R22, R113, R114 and ethylene glycol.

Kandlikar [66] has proposed a Shah-like correlation that utilizes in addition to the Froude number Fr, a boiling number Bo, a vapor-liquid density ratio and what is called a fluid-surface parameter: The fluid-surface parameter is a function of the surface finish of the tube and the fluid. Kandlikar's correlation was based on data bank of water, R11, R12, bromotrifluoromethane (R13B1), R22, R113, R114, R152a, N_2, Ne and cryogens[1] as a liquified N_2 and He. It is recommended in the wetted wall region below a quality of about 0.8.

Schrock and Grossman [117] also proposed an additive form of correlation using Bo and X as parameters. Their correlation was developed based on a data bank of water, n-butanol, R12, R22 and R113. They also proposed a chart based correlation which was latter refined by Shah [118].

A generalized correlation has been proposed by Steiner [128] for the prediction of flow boiling heat transfer coefficient. He employed an asymptotic model as

$$\alpha = \sqrt[3]{\alpha_c^3 + \alpha_n^3}\ , \tag{2.2}$$

where α_c and α_n are the convective and the nucleate heat transfer coefficient respectively. The correlation was developed using a data bank of R11, R12, R113, R114, N_2, NH_3 a number of natural fluids as R290 and R600. The Steiner [128] model is the most accurate correlation that is currently available as attested by Collier and Thome [23] and VDI-Wärmeatlas [143].

The Kattan et al. [73] correlation is also based on an asymptotic model. The convective and the nucleate boiling heat transfer coefficients are calculated from the single phase correlations of Dittus-Boelter [30] and Cooper [25] respectively. The correlation was developed based on a data bank of R134a, 1,1-dichloro-2,2,2-trifluoroethane (R123), and R502 (azeotropic mixture of R22 and chloropentafluoroethane (R115), 48.8/51.2 mass %) and R404A (near-azeotropic mixture of R125/R134a/R143a, 44/4/52 mass %).

[1] A liquid, such as liquid nitrogen, that boils at a temperature below about 110 K (-160 °C) and is used to obtain very low temperatures; a refrigerant.

Other correlations which are available include those of Dembi et al. [27], Klimenko [79] and Jung et al. [60], to mention a few.

Clearly most of the correlations were developed on a data bank of old refrigerants. Fig. 2.2 shows comparisons between some of the existing correlations and the existing experimental R134a data of Kattan et al. [72]. To be remembered is that Kattan et al. [72] data is obtained by using liquid phase water as a heating medium. Most of the correlations show a mean deviation of 20-40% from the experimental data of Kattan et al. [72]. Furthermore, the various correlations do deviate from one another with a mean deviation of order 20-40%. Collier and Thome [23] in their review to the existing correlations indicated that a mean deviation of order of 20-50% is typical to the most correlations. A critical review to the existing models which identifies the sources of deficiency is found in Kattan et al. [73].

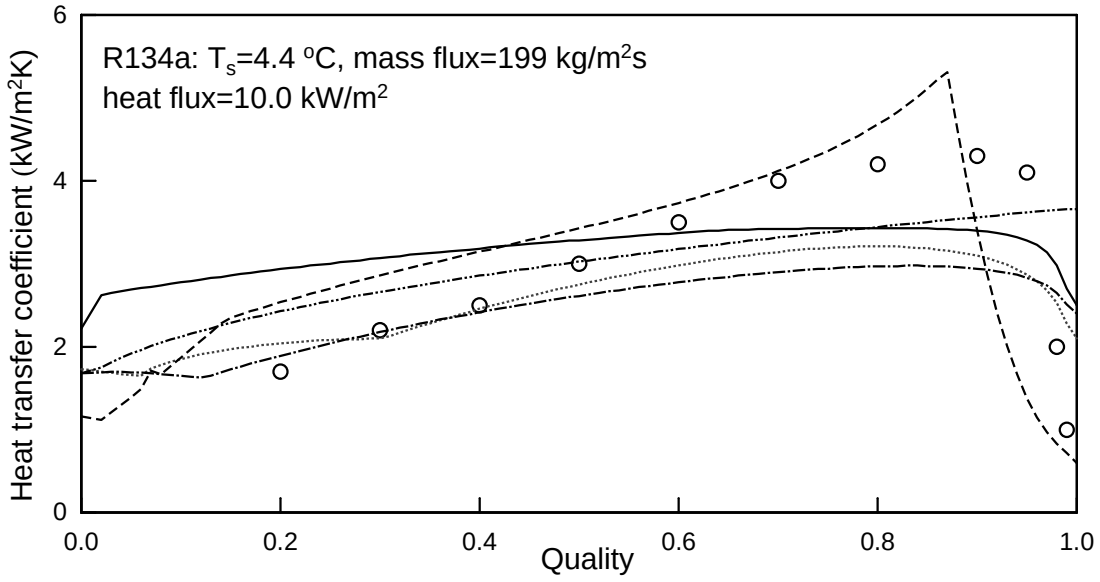

Figure 2.2. Comparison of five different correlations for flow boiling heat transfer coefficient with the experimental data of Kattan et al. [72] for R134a. Legend: (· · · · · ·) Shah [120], (— ··—) Gungor and Winterton [48], (—·—·—) Kandlikar [66], (- - -) Kattan et al. [73], (——) Steiner [128] and (○) Kattan et al. [72] experimental data.

2.2.2 Flow boiling of mixtures

In contrary to the flow boiling of pure substances there exists only limited work in the open literature in the field of flow boiling of mixtures. These works are not listed in the present work, nevertheless, reference is to be made to VDI-Wärmeatlas [143], Collier and Thome [23]) and Kandlikar et al. [69] for more literature on the flow boiling of mixtures. The existing works are on horizontal and vertical tubes made of copper, nickel and stainless steel. As working fluids binary, ternary and multicomponent mixtures were used. As in the case for a pure substance, most of the available experimental work is for old refrigerant mixtures. Furthermore the existing data on flow boiling of mixtures is obtained using either electrical or liquid single phase flow of water as a heating medium.

The previous experimental and theoretical work for flow boiling of mixtures indicates that, as for the case of pure substances, the flow boiling of the mixture is also governed by two mechanisms: nucleate and convective boiling. It is also shown that nucleate boiling heat transfer coefficients during evaporation of a mixture is substantially smaller than those obtained by linear interpolation between their respective pure components. An ideal nucleate boiling heat transfer coefficient for a mixture is defined as

$$\alpha_{id} = \left[\sum \frac{\widetilde{x}_i}{\alpha_{n,i}} \right]^{-1}, \tag{2.3}$$

where $\alpha_{n,i}$ is nucleate boiling heat transfer coefficient for the component i evaluated at the system pressure and heat flux. $\widetilde{x}_i$ is the liquid mole fraction of the component i. Various mechanisms are considered being responsible for the degradation of the mixture heat transfer coefficient. They are grouped as flows:

1. increase in the effective wall superheat relative to those obtained by linear interpolation between their respective pure components (Thome [135] and Stephan [129]). The increase in the wall superheat was explained as the combined results of several effects. These effects are best explained with the help of a phase diagram. Fig. 2.3 shows the phase diagram for the binary refrigerant mixture of R134a/R290. The $T - \widetilde{x}\widetilde{y}$ data are obtained using the fundamental equation of state of Tillner-Roth [137] for R134a/R290 mixtures.

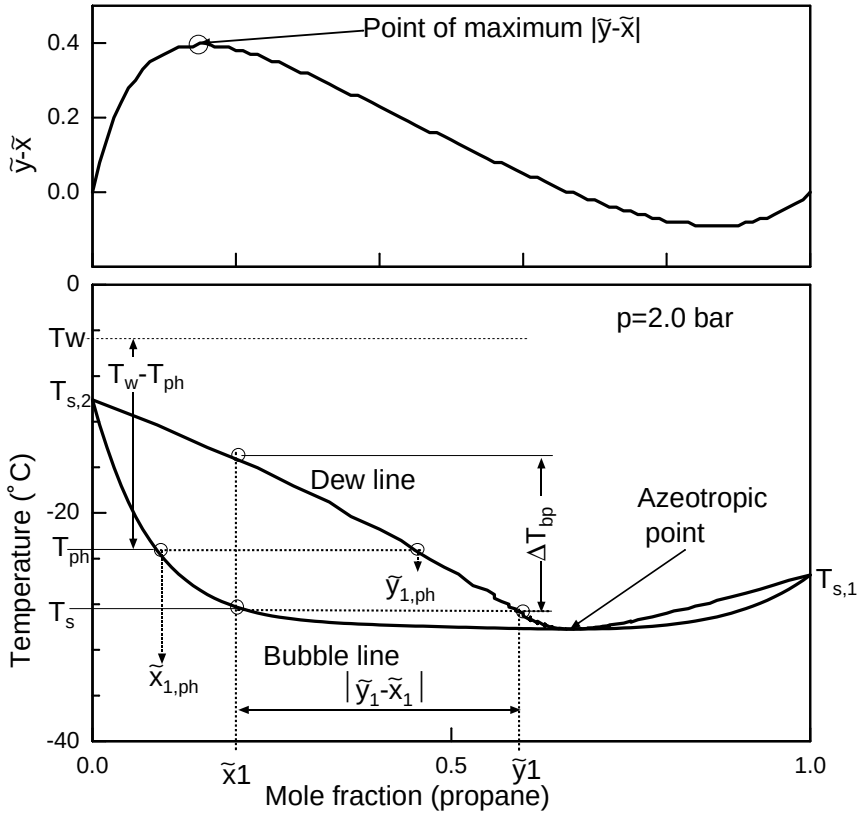

Figure 2.3. Phase diagram for a binary R134a/R290 mixture.

- Schlünder [115] and Van Wijik et al. [141] postulated that since the equilibrium vapor mole fraction of the more volatile component $\widetilde{y}_1$ is greater than that in the corresponding liquid $\widetilde{x}_1$, for a binary system, the local bubble point temperature T_s rises as the liquid composition of the more volatile component $\widetilde{x}_1$ decreases; $\widetilde{y}_1$, $\widetilde{x}_1$ and T_s are shown in Fig. 2.3. The wall temperature T_w must therefore rise in order to transfer the imposed heat flux in compensation for the rise in the local bubble point temperature at the vapor-liquid interface. The wall superheat increases by an amount equal to the rise in the local bubble point temperature such that it becomes equal to

$$\triangle T = \triangle T_{ideal} + \triangle \theta \ , \tag{2.4}$$

  where $\triangle\theta$ is the positive deviation of the wall superheat from the ideal wall superheat. The ideal wall superheat is defined using a linear mixing law as

$$\triangle T_{ideal} = \sum \widetilde{x}_i \triangle T_i \ , \tag{2.5}$$

  where $\triangle T_i = T_w - T_{s,i}$ is the pure component wall superheat. T_w is the wall temperature and $T_{s,i}$ is the saturation temperature of the component i. Since the heat transfer coefficient can be defined by the following expression

$$\alpha = \frac{\dot{q}}{\triangle T} = \frac{\dot{q}}{\triangle T_{ideal} + \triangle \theta} \ , \tag{2.6}$$

  the heat transfer coefficient decreases as the local boiling point rises.

- Thome [134] showed that the maximum rise in the local bubble point temperature is limited by the boiling range ΔT_{bp}. ΔT_{bp} is defined as the temperature difference between the dew point and the bubble point temperature at the bulk liquid composition of the more volatile component as defined in Fig. 2.3.

2. reduction in nucleation sites. Stephan and Körner [130] analyzed nucleation conditions in a mixture and showed that the reversible isothermal work required for bubble formation is greater in mixtures than in a pure liquid of the same physical properties. Thus nucleation sites activated under the same wall superheat are expected to be fewer in a mixture than in an equivalent pure fluid. This may cause a reduction of the heat transfer coefficient in mixtures.

3. mass transfer resistance. Liquid layer around growing bubbles is depleted in the more volatile component as a result of preferential evaporation of the more volatile component. Thus a concentration difference $(\widetilde{y}_1 - \widetilde{x}_1)$ exists between the interface and the bulk liquid and the more volatile component has to diffuse from the bulk liquid to the interface. The mass transfer resistance in this process is attributed to a slower bubble growth rate and the resulting reduction in heat transfer coefficients.

4. retardation in main heat transport process. Latent heat transport due to evaporation into bubbles and sensible heat transport as a result of stripped and accompanied

thermal boundary layer by bubbles are retarded in mixture boiling because of the slower bubble growth rate, lower departure frequency and fewer bubble generation sites (Thome [134]).

5. non-linear variation of physical properties with composition: Stephan and Preusser [131] have attributed part of the reduction in the mixture boiling heat transfer coefficient, in addition to the mass diffusion, to the effect of non-linear variations in the pertinent mixture physical properties.

Furthermore a remarkable degradation in the heat transfer coefficient has been noted if one of the components constituting the mixture is a surface-actant. Mixtures of organic and inorganic components contain, however, surface actant components only in certain cases, for example addition of surface wetting agents (Stephan [129]).

Fig. 2.4 from Baehr and Stephan [2] shows the variation of the heat transfer coefficient for an azeotropic mixture of methanol-benzene at various saturation pressures and constant heat flux and mass flux. The results support the above mentioned hypothesis of Schlünder [115], Van Wijik et al. [141], Thome [134] and Stephan and Preusser [131]. It is also recognized that there is a clear decrease in the heat transfer coefficient in the region where $|\widetilde{y} - \widetilde{x}|$ is large. This is the point of maximum mass diffusion. Furthermore, the results show that the heat transfer coefficient increases toward the azeotropic point. This is attributed to the diminishing of the mass diffusion effect; $|\widetilde{y} - \widetilde{x}| \rightarrow 0$. Similar results were previously observed by Chen et al. [19] for a mixture of R22 and N,N-Dimethyl Formamide (DMF), Gorenflo and Bieling [43] for an azeotropic mixture of R22/R115, Varma et al. [142] for R12/R22, Singal et al. [125] for R13/R12, Jain and Dhar [56] for R12/R13 and Jung et al. [60] for R22/R114.

The influence of the working parameters of $\dot{m}$, $\dot{q}$, p, $\dot{x}$, $\widetilde{x}$, d, $\lambda_w s$ and the flow pattern on the flow boiling heat transfer coefficient of mixtures have been investigated by a number of researchers in the recent past. The experimental results obtained by Ross et al. [114] for R152a/R13B1, Niederkrüger [98] with R12/R846 and Gropp [46] with R11/R113 show that similar to pure fluids, the mixture heat transfer coefficient is influenced by the hydrodynamic and thermal conditions. Niederkrüger [98] has indicated that the influence of the $\dot{q}$ and p on the mixture nucleate boiling heat transfer coefficient is smaller than that for a pure component. These affects are also confirmed by Wetterman [148] with a R134a/R12 mixture.

In convective boiling, VDI-Wärmeatlas [143] and Gropp [46] indicated that for a liquid mixture which possesses normal viscosity, the effect of mass diffusion resistance on the convective heat transfer can be neglected. That is to say in contrary to nucleate boiling the mixture composition has no influence on the convective boiling heat transfer coefficient. It depends rather on $\dot{m}$ and $\dot{x}$. Mixtures of normal viscosity include liquid-liquid miscible mixtures or azeotropic or near azeotropic mixtures. For high viscosity mixtures Palen [104], who investigated mixtures of ethylene glycol-water and propylene glycol-water, indicated that the resistance of mass diffusion on the convective heat transfer is

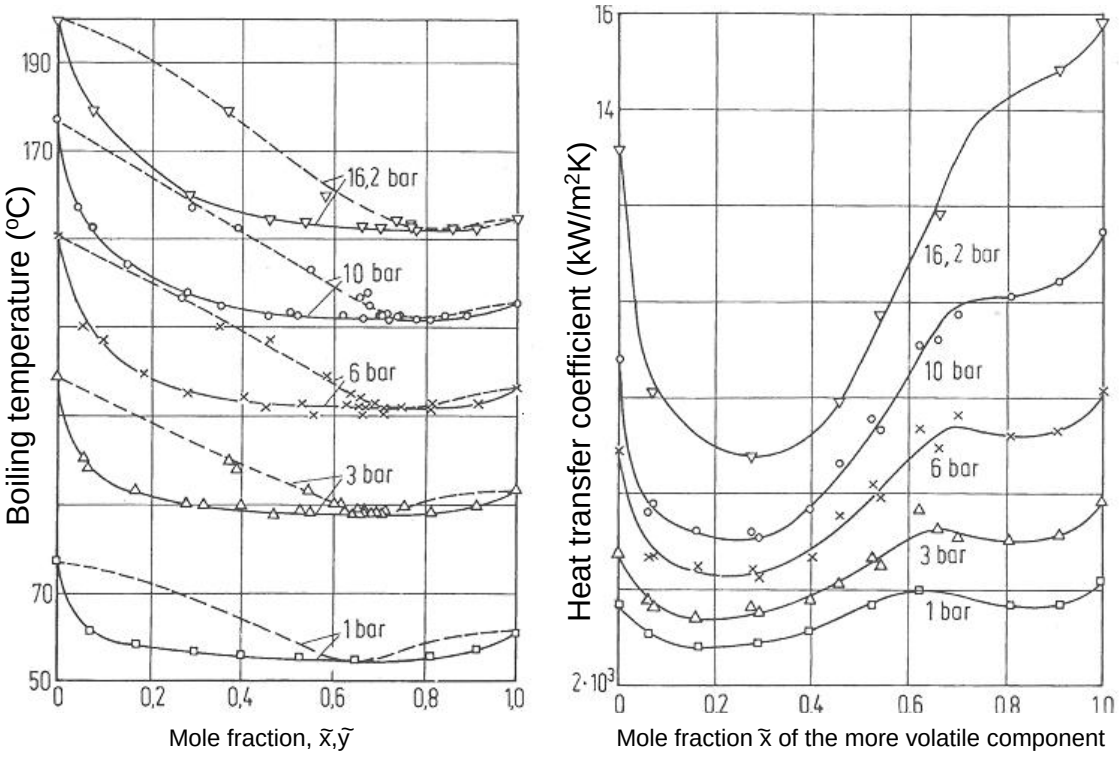

Figure 2.4. A phase diagram (left) and heat transfer coefficient for methanol-benzene mixtures in accordance with Baehr and Stephan [2].

significant. The relationship between the viscosity and the mass diffusion resistance could be explained as that the mass transfer coefficient is inversely proportional to the dynamic viscosity of the liquid (VDI-Wärmeatlas [143]). Therefore the diffusion coefficient for a liquid mixture of a high viscosity is smaller than that for a liquid mixture of a normal viscosity.

In contrary to a pure component there are relatively few studies available in the open literature on the modeling of the flow boiling heat transfer coefficient for binary mixtures. In the following paragraphs a brief account to some of the existing correlations is given. More details about the existing correlations may be found in VDI-Wärmeatlas [143] and in the book of Collier and Thome [23].

Bennett and Chen [7] presented a correlation scheme based on the Chen [17] correlation for a pure component. The convective term was modified to incorporate the bubble interface temperature. The suppression factor suggested by Calus and Leonidopoulos [15] for pool boiling was introduced in the nucleate boiling term with some modifications. The mass transfer coefficient in the liquid phase near a bubble interface was calculated from a correlation with the same form as in the Dittus-Boelter [30] correlation for heat transfer, but employing a Sherwood number $Sh_d = \alpha_m d/D_{AB}$ and a Schmidt number $Sc = \nu/D_{AB}$. The Bennett and Chen [7] correlation was tested for R22/R114 and R11/R114 data. Other correlations based on the Chen [17] idea include those of Palen [104], Hihara et al. [53], Murata and Hashizume [97] and Murata and Hashizume [96].

Jung et al. [60] developed a correlation based on a data bank of R12/R152a, R500 (azeotropic mixture of R12/R152a, 73.8/26.2 mass %) and R22/R114. They used an ideal heat transfer coefficient for mixtures in flow boiling, similar to that employed for pool boiling by earlier investigators. Their approach implicitly incorporates the convective component of flow boiling in the averaging scheme. The Jung et al. [60] correlation utilizes the phase equilibrium data and critical pressure and temperature along with some empirical constants, which were determined experimentally from their own experimental data bank. The Jung et al. [60] correlation has been tested by Jung and Radermacher [61] using difluoromethane (R32)/R142b and R32/R152a mixtures and by Wettermann [148] for R12/R134a.

Steiner [128] has extended his pure component asymptotic model for mixtures (equation 2.2). In his treatment the nucleate part of the heat transfer coefficient is

$$\alpha_n = \alpha_{n,id} F_n^{-1}. \tag{2.7}$$

The ideal nucleate heat transfer coefficient, $\alpha_{n,id}$, is given by equation 2.3. The suppression factor F_n is the one given by Schluender [115] as

$$F_n = \left\{ 1 + \frac{\alpha_{id,n}}{\dot{q}} (T_{bk} - T_{bj})(\widetilde{y}_j - \widetilde{x}_j) \left[1 - \exp \frac{B_o \dot{q}}{\rho_L \Delta h_V \beta_L} \right] \right\}, \tag{2.8}$$

where the indices, j and k stand for the more volatile and the less volatile components respectively. $B_o/\beta_L = 5 \times 10^3$, ρ_L and Δh_V is a mass transfer coefficient, the ideal liquid density and latent heat of evaporation of the mixture respectively. $\widetilde{x}_j$ and $\widetilde{y}_j$ are the liquid and vapor mole fraction of the more volatile component respectively.

The same treatment, as for the nucleate boiling, also applies to the convective boiling heat transfer coefficient for the case of a liquid-liquid immiscible mixture. For liquid-liquid miscible mixture the convective heat transfer coefficient is not suppressed but it is calculated from the pure component relation with pseudo-properties of the mixture. The Steiner [128] model was tested by Niederkrüger and Steiner [100] for R12/R846 mixtures and by Wettermann [148] for R134a/R12 mixtures. It was found to predict both the trend and the value of the heat transfer coefficient fairly well. However, they have indicated that a better agreement can be achieved if the mass transfer coefficient in the Schlünder [115] model is given by

$$\frac{B_o}{\beta_l} = \frac{\alpha_{n,id}}{c_{pL} \rho_L}. \tag{2.9}$$

Here c_{pL} and ρ_L is the ideal isobaric specific heat and the density of the liquid phase respectively.

Kandlikar [68] has extended his pure component (Kandlikar [66]) flow boiling correlation to binary mixtures. Only the nucleate part of the two phase heat transfer coefficient is suppressed using the diffusion-induced-suppression factor for pool boiling (Kandlikar [67])

$$F_n = 0.678 \left[1 + (c_{pL}/\Delta h_V)(\kappa/D_{12}) \left| (\widetilde{y}_1 - \widetilde{x}_1) \frac{dT}{d\widetilde{x}_1} \right| \right]^{-1}. \tag{2.10}$$

where κ is the thermal diffusivity and D_{12} is the diffusion coefficient.

2.3 Pressure drop

For the design of evaporators, beside the heat transfer coefficient, the pressure drop is of paramount importance. There exist a number of models for the prediction of the pressure drop. These include among other homogenous and separated flow models. The latter is also widely known as *heterogenous* model. VDI-Wärmealtas [143], Spindler [127] and Müller-Steinhagen [94] provided detailed reviews of the existing models for two phase pressure drop. Müller-Steinhagen [94] has compared some of the existing pure component correlations for the pressure drop with Ar data. Storek and Brauer [132], Niederkrüger [98] and Wettermann [148] have compared some of the existing models with experimental data of hexafluoroethane (R116)/R846 and R134a/R846/R116 mixtures respectively. They have indicated that the existing models work good for pure substances, however, a relatively high level of uncertainty is observed for mixtures.

2.4 Flow pattern

When a liquid is vaporized in a heated channel the liquid and vapor take up a variety of configurations known as flow patterns. Fig. 2.5 from Baehr and Stephan [2] depicts the flow patterns for flow boiling on a horizontal adiabatic flow. There exist in the literature a

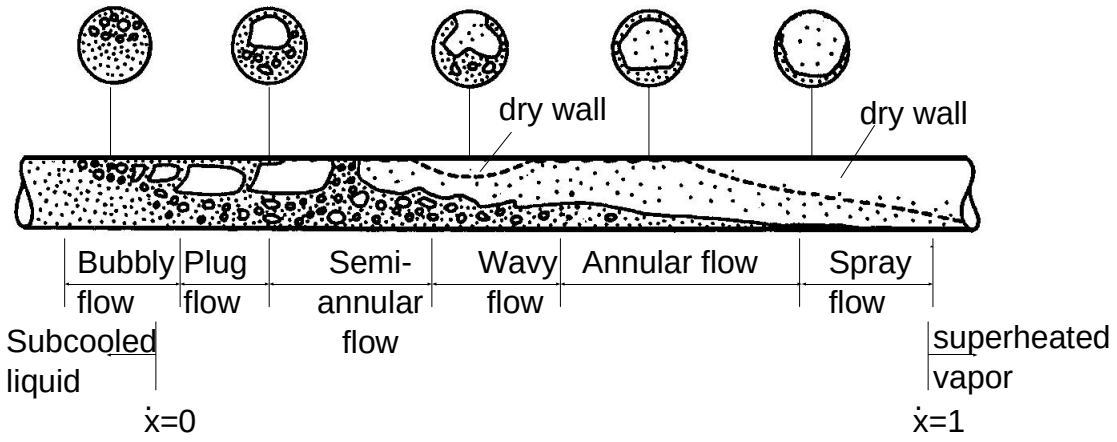

Figure 2.5. Flow patterns in a horizontal tube according to Baehr and Stephan [2].

multitude of terms describing the various possible phase distribution however, the primary flow pattern include bubbly, stratified, wavy, plug, slug, annular and mist or spray flow pattern.

The particular flow pattern depends on the conditions of pressure, mass flux, heat flux and channel geometry. Furthermore the flow pattern depends on the hydrodynamic and the thermal entrance length as well as on the thermal boundary conditions. Weismann et al. [147] have investigated the influence of the start length on the flow pattern using various fluids (water-air, glycerin-water-air, potassium carbonate solution in air and R113) in glass tubes with different pipe diameters. He indicates a thermal (start) length of l/d = 60 (related to the pipe diameter) was necessary for the development of the flow pattern.

The heating effect (i.e adiabatic or diabetic) on the flow pattern has been investigated by Zahn [152] for flow boiling of R22. He indicates that the particular flow patten (annular, plug, mist) depends on the thermal boundary condition: adiabatic or none adiabatic. This was also confirmed by Schmidt [116] by means of a gamma density measuring instrument using R12.

Over years numerous flow pattern maps have been developed for horizontal, adiabatic two phase flow in tubes. Baker [3] has developed a flow pattern map of two phase flow of an oil-air system and extended it to a water-air system. For the transition boundaries between the flow pattern Baker [3] used the vapor momentum flux as an ordinate and the liquid momentum as the abscissa to his map. Hashizume [50] has tested Baker's [3] flow pattern map using R12 and R22 for a wide range of pressure (5.7-19.6 bar). He indicated a poor match to his data. Subsequently he further modified the Baker [3] flow pattern map.

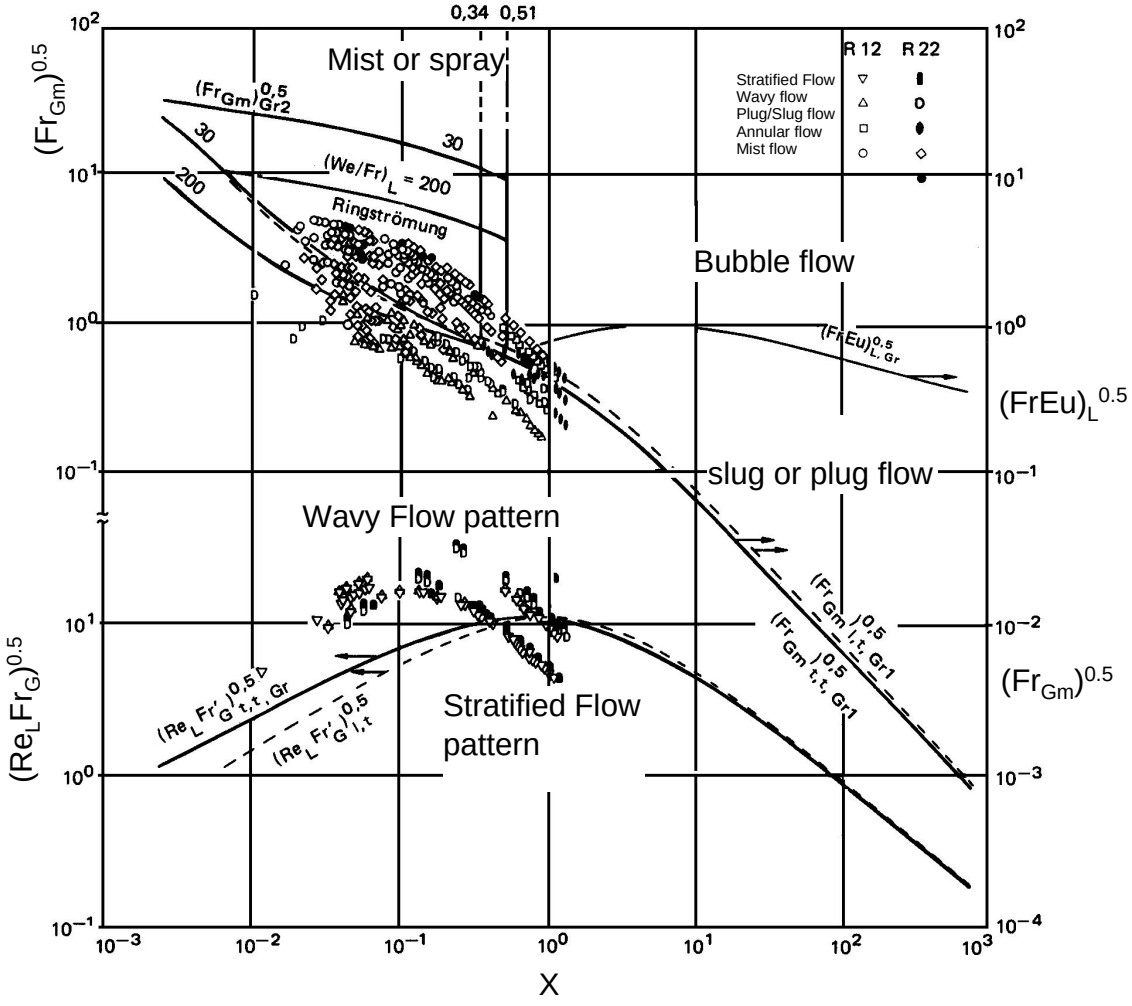

Figure 2.6. The flow pattern map of Steiner [128] from VDI-Wärmeatlas [143].

Taitel and Dukler [133] and Taitel and Dukler [133] have developed a unified flow pattern model based on dimensionless parameters. The unified flow pattern map is latter modified

by Steiner [128]. The Steiner [128] flow pattern map is based on the two fluid model. Its abscissa is Martineilli parameter X given by equation 2.1. Its outstanding feature is that different ordinates are used. A detailed description of the Steiner [128] flow pattern map is found in the VDI-Wärmeatlas [143]. The Steiner's flow pattern map is developed based on a data bank of R12 and R22, among other substances. An illustration to the Steiner's flow pattern map is shown in Fig. 2.6.

Niederkrüger [98] and Wettermann [148] have tested Steiner's flow pattern map using experimental data for pure substances R12, R134a and R846 and their mixtures at various working conditions. Their results indicate that the Steiner's flow pattern map predicted the experimental results with high level of accuracy.

Another flow pattern map is that of Kattan et al. [71]. They have converted the coordinate of the Steiner [128] flow pattern map. The Martinelli parameter (*i.e.* abscissa) X is being replaced by the quality $\dot{x}$ and the other dimensionless parameters (*i.e.* ordinates) are being replaced by the mass flux $\dot{m}$.

2.5 Objectives of this work

In the present study the flow boiling characteristics of pure R134a and R134a/R290 mixtures in a horizontal plain tube are studied. The study is intended to address the following objectives:

- **Heat transfer coefficient for pure R134a:** Being one of the constituents of the R134a/R290 mixture, in the first part of this study the local heat transfer coefficient of pure R134a is measured. Measurements are made to cover low saturation temperature ranges of less than 0 °C for a wide range of mass flux, vapor quality and wall temperature. The measurements were carried out under the assumption of the thermal boundary condition of a constant wall temperature. The constant wall temperature thermal boundary condition is tried via film condensation of ammonia on the external side of the horizontal test tube. These working conditions are selected because film condensation on the outside provides a higher heat flux as compared to one phase water flow. In addition, it provides experimental data that may contribute to bridge the gap in the literature of the flow boiling of pure R134a. This gap is created by the lack of:

  i experimental data at the thermal boundary condition of constant wall temperature,

  ii flow boiling data at low saturation temperatures $T_s < 0$ °C.

  Furthermore, the results of this part are meant to

  i lay down the basics of flow boiling phenomena,

  ii test the validity of the existing pure fluid correlations for the prediction of the heat transfer coefficients for R134a and

  iii test the validity of the experimental setup for the use for mixtures.

- **Heat transfer coefficient for R134a/R290 mixtures:** In the second part of this study measurements on the local heat transfer coefficient for R134a/R290 mixtures are made in the same range of parameters and thermal boundary conditions as for pure R134a. The measurements cover both the zeotropic and azeotropic regions of the mixture composition. Here the result is thought to provide experimental data that can be used for the design of the evaporation equipment in the range of the investigated parameters. Additionally, the experimental data are used to test the validity of the existing correlations for the prediction of the flow boiling heat transfer coefficient for R134a/R290 mixtures.

  Due to the fact that there does not exist any experimental data on the flow boiling of R134a/R290 mixtures in the literature, the result is sought further to verify the assumptions that the:

  i flow boiling heat transfer coefficient for R134a/R290 mixture is smaller than what would have been obtained by linear interpolation between the respective pure components,

  ii large decrease occurs at the point where $|\widetilde{y} - \widetilde{x}|$ is large,

  iii heat transfer coefficient increases towards the azeotropic point.

- **Pressure drop:** Beside the flow boiling local heat transfer coefficient, the pressure drop is an important parameter in the design of flow boiling equipment. In the present work the pressure drop in the flow boiling of both pure R134a and R134a/R290 mixtures is measured parallel to the heat heat transfer coefficient. Firstly, the pressure drop measurement is meant to facilitate the calculation of the refrigerant saturation temperature at the exist of the evaporator. Secondly, the results is sought to validate the existing pressure drop correlations for pure R134a and R134a/R290 mixtures under low saturation temperature conditions.

- **Flow pattern:** For the calculation of the local heat transfer coefficient some of the existing correlations, for example the Steiner [128] correlation, require a prior knowledge of the flow pattern. Against this background, simultaneously with the measurement of the local heat transfer coefficient and pressure drop the the flow pattern is observed in the sight glass. Subsequently, it is recorded with hand notes and documented with a camera. Firstly, the results of flow pattern is sought to facilitates the correct application of the existing correlations for the prediction of the local heat transfer coefficient. Secondly, the results is intended to be used to test the validity of the existing flow pattern maps.

A great part of this work is devoted to the validation of the assumption of the thermal boundary condition of constant wall temperature. To investigate this assumption measurements of the angular wall temperature distribution at the film condensation side on the external side of the horizontal tube have been made. The effect of the wall temperature distribution on the heat flux is assessed, as in Nusselts theory of film condensation,

via solution of conservation of mass, momentum and energy equations for the condensate film.

3 Experimental apparatus

3.1 Experimental setup

The test facilities used in the present work have been designed and built by Kabelac and de Buhr [63]. It is presented schematically in Fig. 3.1. The experimental setup consists of three circuits, namely a test circuit utilizing the tested refrigerant, a secondary evaporator providing the heat load necessary for evaporating the refrigerant in the test section and a refrigeration cycle. In the following subsections a detailed description of these three loops is given.

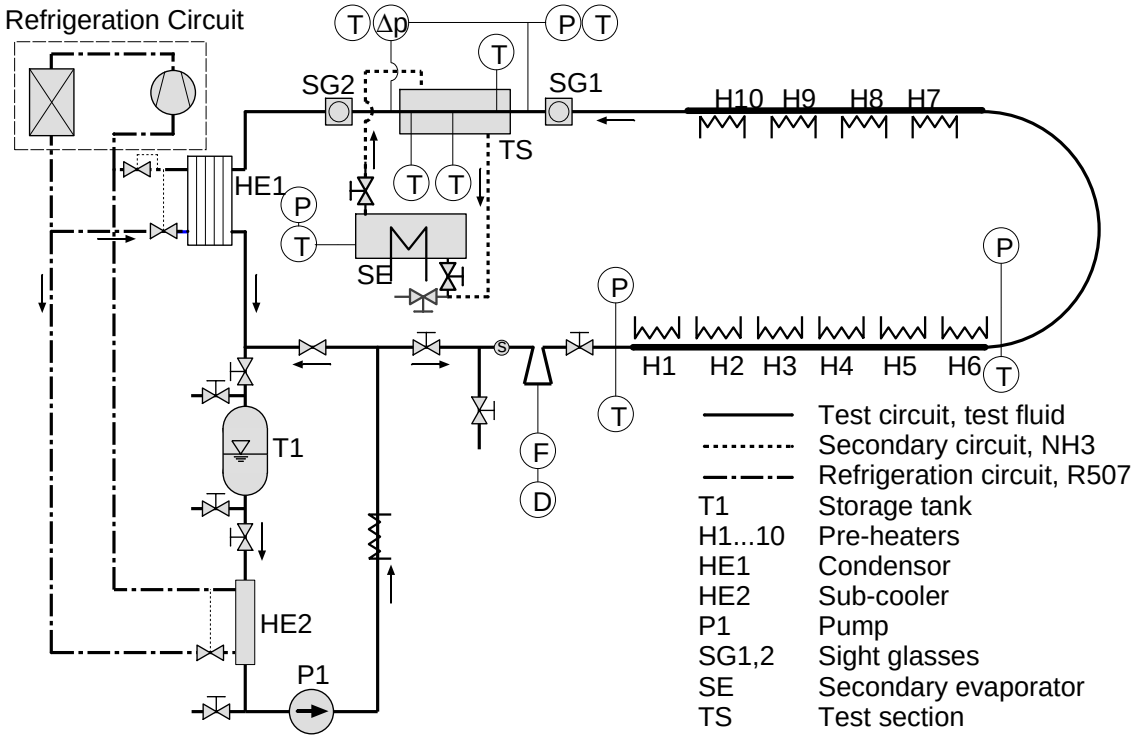

Figure 3.1. Layout of the test facility.

3.1.1 Test circuit

The locus of the test loop is indicated by the thick solid line in Fig. 3.1. The test loop consists of a test section (**TS**), condensor (**HE1**), storage tank (**T1**), second condensor (**HE2**), positive-displacement pump (**P1**), two sets of preheaters (**H1...6** and **H7...10**), and two sight glasses (**SG1** and **SG2**). The refrigerant (liquid) in the storage tank **T1**, (a horizontal cylinder with semi-spherical ends) is pumped into the test circuit using a positive displacement pump **P1**. At the negative suction side of the pump a plate-type subcooler **HE2** is installed. This is made to ensure that the refrigerant entering the pump contains no vapor. The pump produces a constant volume flow of refrigerant. To control the flow rate into the test loop as well as to provide the minimum flow rate necessary for the cooling and lubrication of the pump a bypass line is installed. The bypass line diverts a certain portion of the flow and returns it back to the storage tank **T1**. Before

it enters into the first set of preheaters **H1...6** the temperature, pressure, mass flow rate and density of the incoming subcooled refrigerant is measured. Knowledge of these parameters facilitates the calculation of the enthalpy at the inlet of the test loop which is required for the determination of the vapor quality. Heat is added to the refrigerant as it passes through the two sets of preheaters **H1...6** and **H7...10**. This is made to bring the refrigerant to the desired vapor quality, temperature and pressure at the inlet of the test section. Before it enters into the test section the temperature and pressure of the test refrigerant is measured. At the outlet of the test section the temperature and pressure drop are also measured. Parallel to the temperature and pressure measurements, the prevailing flow patterns at the inlet and outlet of the test section are observed at the sight glass **SG1** and **SG2**. The two phase refrigerant leaving the test section is then condensed and passed into the storage tank. The condenser **HE1** is a plate type heat exchanger.

The different sections of the test loop are held together using appropriate joints. The leakage between the joints is eliminated using O-rings as a seal. This type of connection eases the frequent change of the tested tubes as well as the frequent soldering and dismantling. Additionally, it ensures adequate firmness. The thermal loss to the surrounding at all the test loop tubes and apparatus save the sight glasses is minimized using Armaflex[1] as an insulation. To avoid a possible disruption of the hydrodynamic development by the bending or inclination a zero angle of inclination to the horizontal is maintained by all tubes of the test circuit up to the end of the test section.

The test section: The test section consists of a horizontal concentric pipe (Fig. 3.2); similar in configuration to a double pipe heat exchanger.

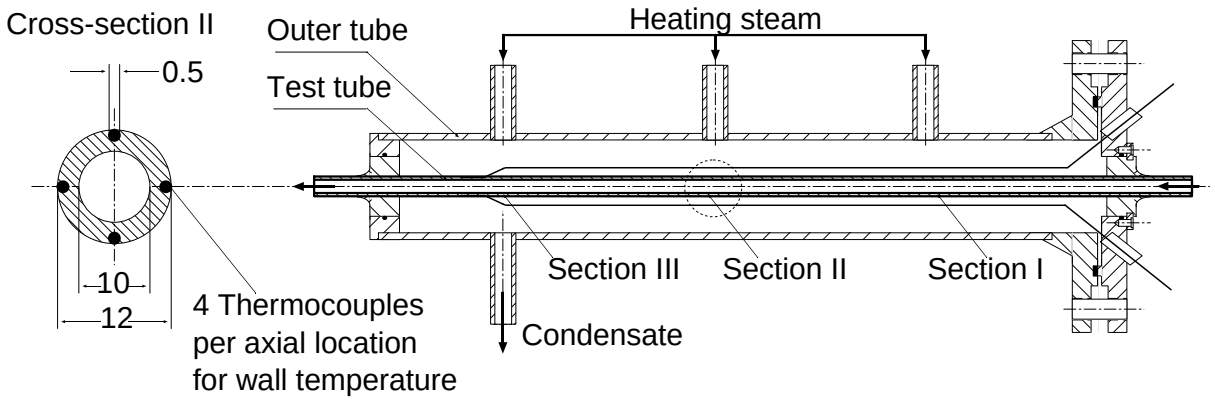

Figure 3.2. The test section and the axial and angular locations of thermocouples in the test tube.

The inner tube is made of stainless steel with an inner diameter of d_i=10 mm, a wall thickness of 1 mm and a 500 mm long. It is instrumented with a number of thermocouples along its length. The thermocouples are soldered at three axial locations along the tube. At each axial location, the thermocouples are distributed at the top, bottom, left and

[1]synthetic foam material (Elastomer)

right hand side of the tube. The outer tube is provided with three inlet ports for the incoming vapor (heat supply). One port at the bottom of the outer tube is provided to work as an outlet for the condensate leaving the test section.

Preheaters: To control the quality at inlet of the test section, the refrigerant is passed through a number of preheaters (H1,...,H10) distributed along the test loop. The distribution of the preheaters in the test loop is shown in Fig. 3.1. The tubes housing the various preheaters are an outside-grooved ones made of stainless steel. The last 4 preheaters (H7,...,10) are located 3.5 m down stream of the first set of preheaters (H1,...,6). This is made to a void the local over heating. Each preheater is eclectically heated using an electrical coil (1 kW). The electrical coil is wrapped in the outside of the grooved tube. The power is supplied to the electric coil utilizing a variable resistance regulated transformer. To avoid overheating and the subsequent damage of the electric coil a thermostat is used as a control.

3.1.2 Secondary evaporator

Fig. 3.3 shows the schematic presentation of the secondary evaporator. Having a high enthalpy of evaporation Δh_V as compared to other refrigerants, ammonia vapor is used as a heating medium in the present work. The ammonia vapor is generated in a cylindrical-shaped stainless steel container (300×ϕ 71.0 mm), with a liquid charge of more than 50 Vol %. The liquid container is equipped with two 1-kW rod-type electric immersion heaters. The power to the electric heater is supplied from a variable resistance regulated transformer. The ammonia vapor flows vertically down a calming section to the test section and condenses at the outside of the test tube. The condensate is returned to the boiler by gravity.

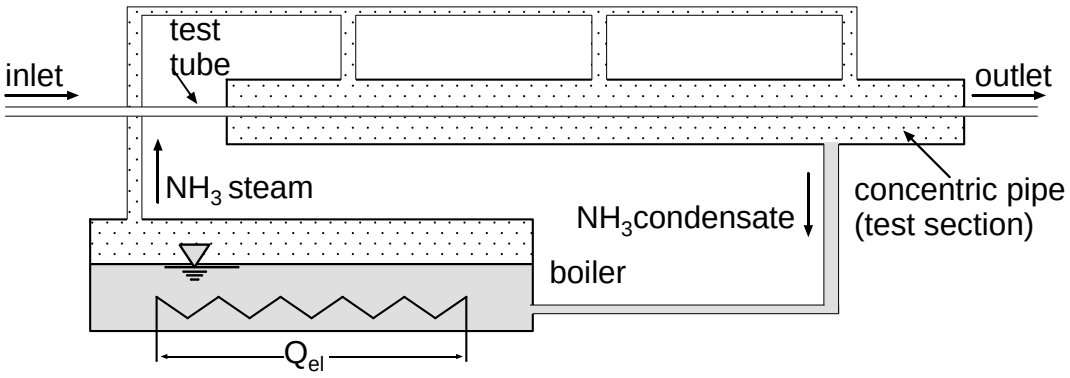

Figure 3.3. Loop of the secondary evaporator.

3.1.3 Refrigeration cycle

The refrigeration capacity needed for condensation and subsequent subcooling of the test refrigerant leaving the test section is realised by a 2-stage vapor compression cycle utilizing R507 as a working refrigerant. A schematic presentation of the 2-stage vapor compression

cycle is shown in Fig. 3.4. The refrigeration unit has a cooling rate in the range of 10 kW (-50 ^{o}C) to 25 kW (0 ^{o}C).

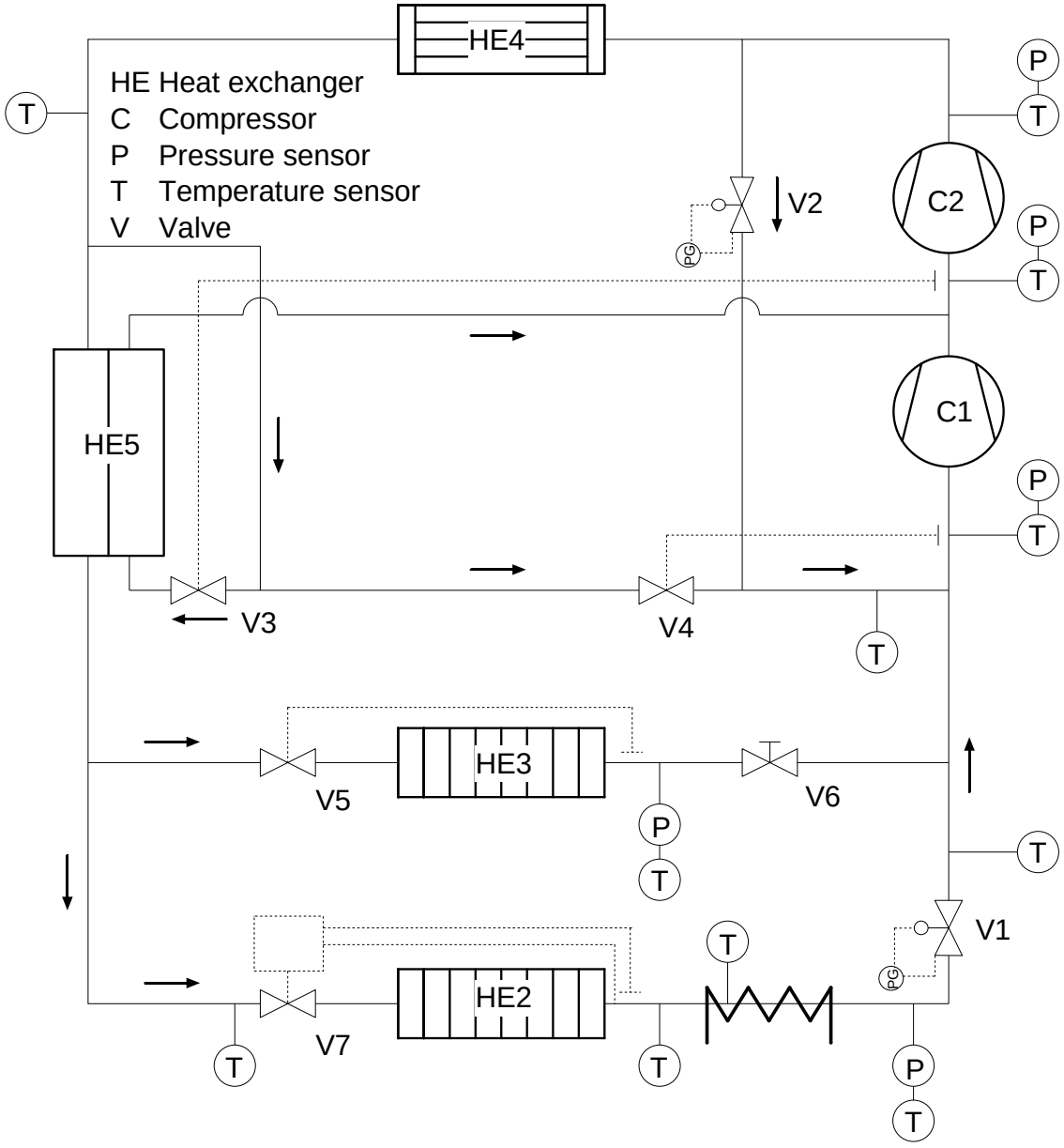

Figure 3.4. Schematic presentation of the 2-stage vapor compression cycle.

3.2 Measurement techniques

To evaluate the flow boiling heat transfer characteristics the following parameters are to be measured:

- temperature
- pressure (absolute and pressure drop)
- flow rate

- electrical power
- mixture bulk composition

Parallel to these parameters the flow pattern is observed using two sight classes mounted inline with the inlet and outlet of the test section. The distribution of the various measur-

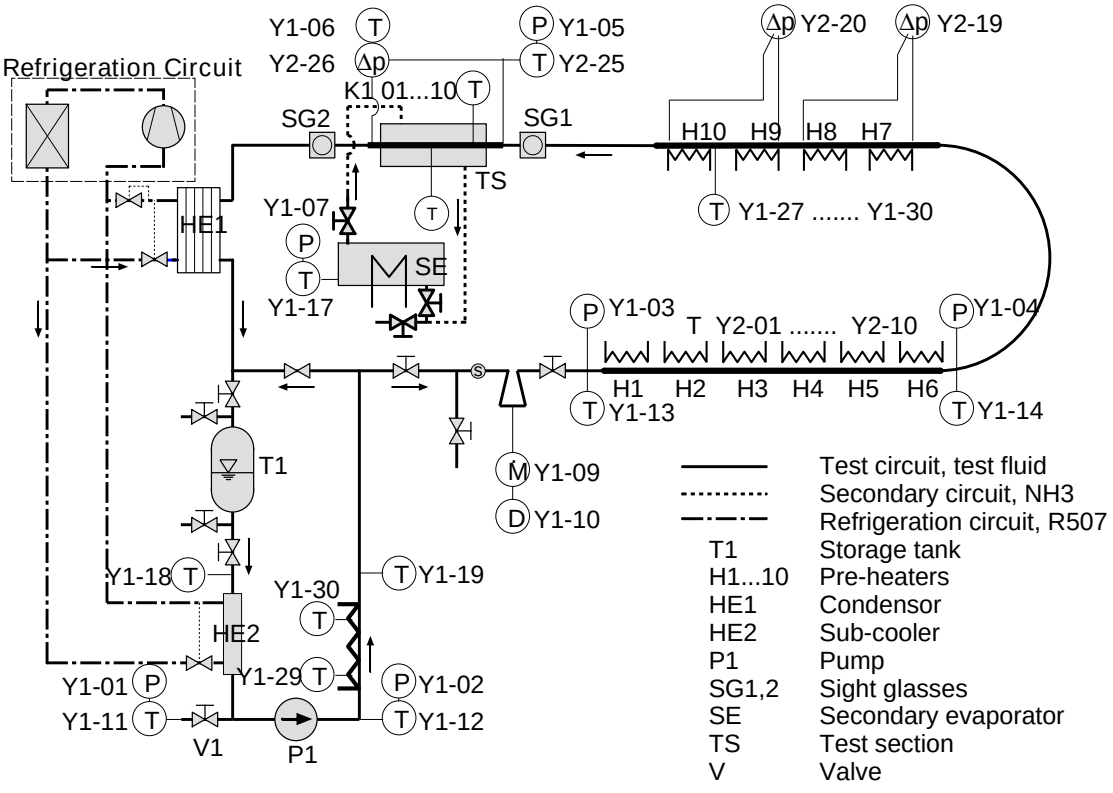

Figure 3.5. Distribution of the pressure, temperature, flow rate and electrical power measuring devices on the test circuit.

ing devices in the test loop are shown in Fig. 3.5. Those used in the secondary evaporator and refrigeration cycle are shown in Fig. 3.6 and Fig. A.1 respectively. Each measured parameter is given a special identifier having the form "**Parameter-name X-YY**". The "**Parameter**"can be either temperature T, pressure p, pressure drop Δp, mass flow rate $\dot{m}$, voltage U, current I or density, D. "**name**" stands for the name of the multimeter used for the measurement of the output signal of the sensor. It can be the hybridrecorder Yokogawa HR 3760, Keithley 2010 or Keithley 177. "**X**" has values of 1 or 2 and is the serial number of the hybridrecorder Yokogawa HR 3760 device (*i.e.* in the present work two Yokogawa HR 3760 devices, designated as Y1 and Y2, have been used). "**XX**" has values from 01 to 30 which are the number of channels of the multimeter. *For example the identifier "**T Y2-25**" means that the value of the temperature measured at this position is recorded by the second hybridrecorder Yokogawa HR 3760 at channel 25.*

The various devices used for the measurement of temperature, pressure, flow rate and electric power were originally calibrated by Kabelac and de Buhr [64]. However, due to

the possible aging of the sensors, their applicability to the present work needed to be validated. In the following subsections the measurement and the calibration procedure as well as the level of uncertainty of each device is given.

3.2.1 Temperature

For the purpose of temperature measurement different temperature sensors were used. The wall temperature is measured using a Nickel-Chrome thermocouple (NiCr NiAl, ϕ 0.5 mm). For the fluid bulk temperature a platinum resistance thermometer (Pt100, ϕ 1 mm) and in some cases a Nickel-Chrome thermocouple (NiCr NiAl, ϕ 0.5 mm) is used. For wall temperature the thermocouple is soldered in a groove (0.5 mm deep) on the external wall of the tube. For the refrigerant bulk temperature the temperature sensor is made to protrude inside the tube in which the refrigerant flows; at approximately 1/2 the diameter of the tube.

The level of uncertainty of the uncalibrated thermocouple is ±(0.05% of the reading +0.7 °C) in the temperature range of -200 to 100 °C and for Pt100 is ±(0.05% of the reading +0.3 °C) in the temperature range of -200 to 550 °C according to manufacturer [2]. An error of ±0.7 °C in the measured wall temperature yields an inaccuracy of about 30-80 % in the measured heat transfer coefficient ($\alpha = \dot{q}/\Delta T$) for a temperature difference of 5 to 2 K. In turn this necessitates the calibration of the temperature sensors to obtain a better accuracy in the measurement. For this purpose all temperature sensors were calibrated in the temperature range between -40 to 40 ^{o}C. The output voltage signal of the temperature sensors is proportional to the sensed temperature as

$$X = a + bU \ . \tag{3.1}$$

For a Pt100 thermometer $X = T$ and for a thermocouple $X = \Delta T$, where ΔT is the temperature difference in K between the temperature of the thermocouple and the reference junction temperature. The reference junction temperature is taken as 0 ^{o}C; realised using a thermostat. For both temperature sensors X is measured with a Pt25 thermometer calibrated by the "*Physikalisch-Technischen-Bundesanstalt* (PTB)". It has a level of uncertainty of ±1.5 mK. The corresponding output voltage U of the sensor in Volt V is measured using a hybridrecorder Yokogawa HR 3760. It has a data acquisition error of ±(0.05 % of reading+2 mV) for -50≤U≤ 50 V according to manufacturer[3]. For some of the thermocouples a *Kiethley* 2010 voltmeter is used. It has a data acquisition error of ±(35 ppm of reading+5 ppm of the range) in the range of -100≤U ≤100 V, as given by the manufacturer [4].

The value of the constants a and b of equation 3.1 are determined via minimizing the sum

[2]THERMOCOAX, UB der Panta Electronics, Vertriebs-GmbH, Meiendorfer Str. 205, 22145 Hamburg, Germany

[3]Bedienungsanleitung: Modell 3760 und 4082 Hybriddrucker. pp. 11-2

[4]User's Manual: Keithley Model 2010 Multimeter. PP. A-2

10 parts per million (ppm)=0.001 %

of squares of residual as

$$\sum \left(X_i - X(U_i)\right)^2 = \sum \left(X_i - (a + bU_i)\right)^2 \rightarrow Minimum. \tag{3.2}$$

For all temperature sensors the values of the coefficients for the calibration equation 3.1 are summarized in Table A.1 of the Appendix A.

Uncertainty evaluation of the temperature is performed in accordance with a 95 % confidence limit to satisfy the proposal given by the *"Deutsche Kalibrierdienst* (DKD)" [28]. For each temperature sensor the level of uncertainty $\mathbf{U}_T$ consists of the bias error **B** and the precision error **P** as

$$\mathbf{U}_T = \sqrt{\mathbf{B}_T^2 + \mathbf{P}_T^2} \tag{3.3}$$

In turn the bias error consists of the calibration error and data acquisition error. The calibration error is taken as that for the calibrated BTP reference thermometer. The acquisition error is the error of the voltmeter used to measured the output signal of the temperature sensor, for example Kiethley 2010 voltmeter. For convenience the calibration error and data acquisition error are designated by the symbols **C** and **A** respectively. The bias error is thus

$$\mathbf{B}_T = \sqrt{\mathbf{C}_T^2 + \mathbf{A}_T^2} \tag{3.4}$$

The precision error is defined in accordance with DKD [28] as

$$\mathbf{P}_T = \frac{t_{\lambda,95\%} S_T}{\sqrt{N}} \tag{3.5}$$

where t is the estimation of the precision error, in accordance with the student test, in the repeated measurements at 95% confidence. λ is the degree of freedom $\lambda = N - 1$. N is the number of the data points and S_T is the standard deviation defined as

$$S_T^2 = \frac{\sum \left[X_i - \overline{X}\right]^2}{N - 1} \ , \tag{3.6}$$

where $\overline{X}$ is the arithmetic mean given as

$$\overline{X} = \frac{1}{N} \sum_{j=1}^{N} X_i \ . \tag{3.7}$$

The above outlined uncertainty evaluation procedure is illustrated in the following example.

Illustration example: *As a basis for calculation a maximum possible temperature of 40° C is considered in this illustration example. The calibration equation of the temperature seonsor designated the identifier* ***T Y2 25*** *in Fig. 3.5 is*

$$T = -0.501147 + 1.009014U \ , \tag{3.8}$$

in the temperature range of -40 °C≤ T ≤40 °C with a standard deviation of 0.08481. The number of data points used to obtain this calibration equation are N=18 and

hence $t_{17,95\%}$=2.11 (Adunka [1]). Using equation 3.5 the estimated precision error is thus $\boldsymbol{P}_T = \pm 42.422$ mK.

The data acquisition error is taken as that supplied by the manufacturer of the corresponding voltmeter. The "hybridrecorder Yokogawa HR 3760" has a "quoted" uncertainty of ±(0.05 % of reading+2 mV) for U≤ 50 V. This is converted into a quantity in accordance with 95% confidence limit for an output voltage of 40.139 V which correspond to 40° C as (DKD [28])

$$\boldsymbol{A}_U = \frac{0.05 \times 40.139 \times 10^{-2} + 2 \times 10^{-3}}{\sqrt{3}} V = 12.742 \times 10^{-3} V \ . \tag{3.9}$$

A_U is then converted into temperature as

$$\boldsymbol{A}_T = \frac{\partial T}{\partial U} \boldsymbol{A}_U \ . \tag{3.10}$$

With the partial derivative $\partial T/\partial U$ evaluated using the calibration equation 3.8, the data acquisition error is thus $A_T = 12.857 \times 10^{-3}$ K.

The calibration error is taken to be equivalent to that for a PTB Pt25 thermometer i.e. $\boldsymbol{C}_T$=1.5 mK. Upon substitution of A_T and $\boldsymbol{C}_T$ in equation 3.4 the total bias error is

$$\boldsymbol{B}_T = \sqrt{(12.857 \times 10^{-3} K)^2 + (1.5 \times 10^{-3} K)^2} = \pm 12.944 \times 10^{-3} K \ . \tag{3.11}$$

Upon substitution of $\boldsymbol{P}_T$ and $\boldsymbol{B}_T$ in equation 3.3 the maximum level of uncertainty of the temperature sensor for a maximum temperature of 40° C is

$$\boldsymbol{U}_T = \sqrt{(42.422\ mK)^2 + (12.944\ mK)^2} = \pm 44.353\ mK \ . \tag{3.12}$$

The level of uncertainty of the various temperature sensors are summarized in Table A.1 of the Appendix A. For all temperature sensors the level of uncertainty does not exceeded ±55.0 mK.

3.2.2 Pressure

In the field of flow boiling the saturation temperature which is required for the calculation of the heat transfer coefficient is obtained from the measured vapor pressure using a suitable equation of state or vapor pressure correlation, for example the Antoine vapor pressure correlation. Therefore a precise measurement of the vapor pressure is of paramount importance.

Various high precision DMS[5]-pressure transducers (Bruster 8206 and 8206R) and piezoresistance P99 series pressure transducers were used for the measurement of the absolute pressure. The former is manufactured by Bruster[6] and the latter by Johnson Controls[7].

[5]Dehnungsmessstreifen (Strain-Gauges)

[6]Buster Präzisionsmeßtechnik GmbH & Co Kg, Talstraße 1-7, 7562 Gernsbach, Germany.

[7]Johnson Controls, JCI Regelungstechnik GmbH, Vertrieb Regelgeräte, Raiffeisenstrraße 6, 61191 Rosbach, Germany

The output voltage signal U of the pressure transducer is proportional to the sensed pressure p as

$$p = a + bU \ . \tag{3.13}$$

The constant a and b may be evaluated using the data supplied by the manufacturer and U is measured using a hybridrecorder Yokogawa HR 3760. *For the P99 pressure transducer for example the constants a and b are* -1 bar*and* 0.9 bar/V *respectively for a gauge pressure of* $p < 8$ bar *with uncertainty of 0.5 % according to manufacturer.* For all pressure transducers the level of uncertainty is 0.1-0.5 % according to manufacturer. This corresponds to an error 0.01-0.05 bar (or 10-50.0 mbar) for a maximum pressure of 10 bar. This yields a maximum error of about ± 0.2 °C in the calculated saturation temperature of R134a when the fundamental equation of state of Tillner-Roth and Baehr [138] for R134a is used. In turn this results in an error of about 8-20% in the heat transfer coefficient for a temperature difference of 5 to 2 K. To improve the level of uncertainty each pressure transducer is calibrated using a PTB calibrated pressure balance (a piston manometer type 21710 of the company Desgranges & Huot). Its calibration error[8] is

$$C_{p_{PTB}} = \sqrt{1.4 \times 10^{-7} + 1.6 \times 10^{-9} p^2} \ , \tag{3.14}$$

where p is the absolute pressure in bar in the range of $p \leq 10$ bar. *For example for a maximum absolute pressure of* 10 bar $C_{p_{PTB}}$ *is 0.55* mbar.

With p measured using the piston manometer the value of the constants a and b are obtained via minimizing of sum of residual (see equation 3.2). Table A.2 of the Appendix A presents the value of constants a and b for the various pressure transducers used in the present work.

The level of uncertainty for each pressure transducer is determined using the same procedure as that employed for temperature sensors. The level of uncertainty for the various pressure transducer are presented in Table A.2. For all pressure transducers the level of uncertainty does not exceed ± 11 mbar for $p \leq 10$ bar. It is to be remembered that for all pressure transducers used in the test circuit the maximum allowable pressure is 13.8 bar.

For some pressure measurements it was not possible to measure the pressure at the desired position. For example the saturation pressure of ammonia designated the identifier **P Y1-07** in Fig. 3.5 is measured in the calming section of the secondary evaporator rather than in its desired position. For convenience this is identified with p_1 and that the desired position is identified with p_2 as shown in Fig. 3.6. Under such conditions the desired pressure is corrected as

$$p_2 = p_1 - \Delta p, \tag{3.15}$$

where Δp is the pressure drop. The pressure drop for a single vapor phase in a vertical tube consists of the frictional and hydrostatic pressure drop as

$$\Delta p = \Delta p_f + \Delta p_h \ . \tag{3.16}$$

[8]Physikalisch-Technische Bundesanstalt. Prüfschein: Kolbenmanometer mit 2 Meßbereichen

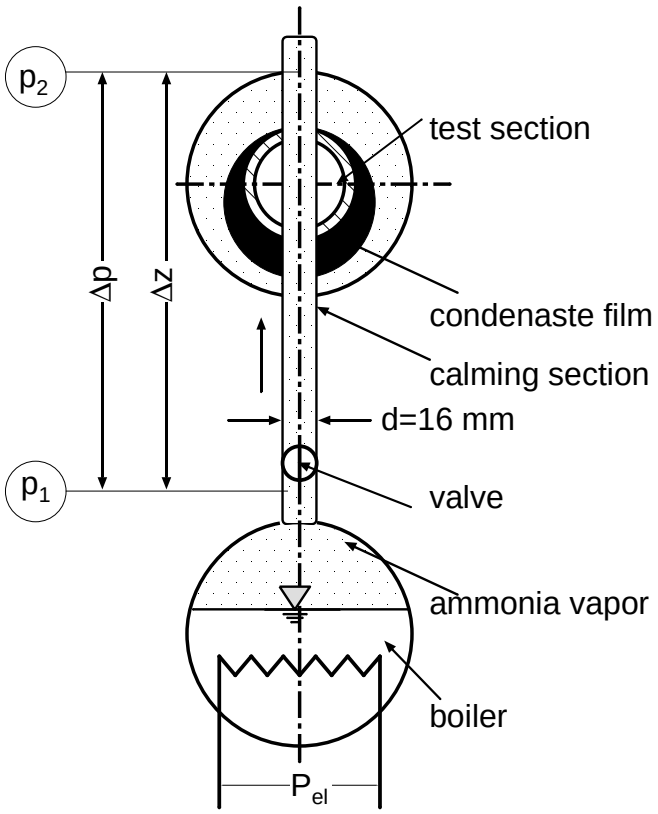

Figure 3.6. Left hand side view of the secondary evaporator shown in Fig. 3.3.

The hydrostatic pressure drop is

$$\Delta p_h = \rho_G g \Delta z \ , \tag{3.17}$$

where Δz=0.5 m is the height of the calming section as shown in Fig. 3.6. The acceleration due to gravity[9] is taken as g=(9.812629 ± 10^{-6}) m/s^2 . The saturated vapor density ρ_G is calculated using the fundamental equation of state of Tillner-Roth [137] for ammonia at the mean saturation pressure p_m =$(p_1 + p_2)/2$. Due to complex configuration of the calming section of the secondary evaporator, the frictional pressure drop is made up of the sum of the pressure drops due to the tube wall, presence of the valve and the bending as

$$\Delta p_f = \left(\xi \frac{\Delta z}{d} + \xi_V + \xi_b \right) \frac{\rho_G w^2}{2} \ , \tag{3.18}$$

where $d = 16$ mm is the calming section diameter, w is the vapor velocity. ξ, ξ_V and ξ_b are the friction factors due to the tube, valve and the bending respectively. The maximum friction factor due to the valve and the bending are taken as 9 and 15 respectively (see Chapter Lc of VDI-Wärmeatlas [143]). The friction factor for the tube is given as (VDI-Wärmeatlas [143])

$$\xi = \begin{cases} \frac{0.3164}{Re^{0.25}} & Re \ \geq 2320 \\ \\ \frac{64}{Re} & Re \ < 2320 \end{cases} \ .$$

[9]personal contact: Prof. Dr.-Ing. J. Müller, Institut für Erdmessung, Universität Hannover, Schneiderberg 50, 30167 Hannover, Germany, May 2002

Reynolds number is

$$Re = \frac{\rho_G w d}{\mu_G} \ , \tag{3.19}$$

where μ_G is the vapor viscosity of ammonia (see appendix B) calculated at $T(p_m)$ and w is the vapor velocity calculated from an energy balance as

$$w = \frac{\dot{Q}_{el}}{A \rho_G \Delta h_V} \ , \tag{3.20}$$

where $A = \pi d^2/4$ and $\dot{Q}_{el}$ is the electrical heat applied to evaporate the ammonia and Δh_V is enthalpy of evaporation. Δh_V is calculated using the fundamental equation of state of Tillner-Roth [137] for ammonia. Fig. 3.7 shows the pressure drop in the calming section of the secondary evaporator for a wide range of working conditions. The maximum pressure drop under the present working conditions does not exceeded 200 Pa (2 mbar).

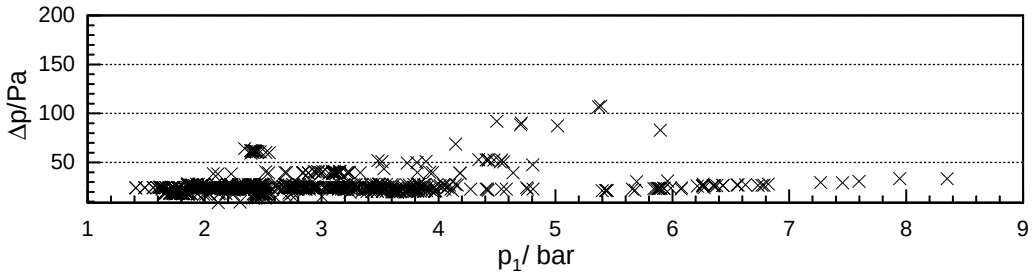

Figure 3.7. Pressure drop in the calming section of the secondary evaporator.

3.2.3 Pressure difference

For the differential pressure measurement high precision DMS-differential pressure transducers (Bruster 8310Z and 8311A5) were used. The level of uncertainty of the DMS-differential pressure transducer does not exceeded 0.25 % as given by the manufacturer. This corresponds to 1.25 mbar for a maximum pressure drop of 500 mbar. As for the case of absolute pressure the differential pressure transducer is calibrated using a calibrated PTB pressure balance (DW10-piston manometer type 21710 of the company Desgranges & Huot). The functional relationship between the differential pressure Δp and the output voltage U of the *DMS*-differential pressure transducer is

$$\Delta p = a + bU \ . \tag{3.21}$$

The constants a and b are determined via minimizing the sum of residual of the pressure drop. Table A.2 presents the value of a and b as well as the level of uncertainty for various DMS-differential pressure transducers. For the various differential pressure transducers the maximum level of uncertainty does not exceeded $U_{\Delta p}$=0.25 mbar for $\Delta p \leq$500 mbar.

3.2.4 Flow rate

The mass flow rate is directly measured utilizing a "Coriolis" density flow meter (model RFT9739 with FSK modems). The flow meter has a range of 0-17 g/s. The output voltage U in Volt is proportional to the sensed flow rate in g/s as

$$\dot{M} = a + bU \ . \tag{3.22}$$

The constant a and b are -4.1675 g/s and 10.4875 g/sV respectively. These are determined from the data supplied by the manufacturer[10]. The flow meter has a level of uncertainty of ± 0.4 % of the reading according to the manufacturer. The mass flux is then calculated as ratio between the mass flow rate and the tube cross section area.

3.2.5 Electrical heat

An electrical coil (P=1 kW) is used as a source of heat for the preheater and a rod-type electrical heater is used in the secondary evaporator. The electric coil is wrapped in the outside of the grooved tube. The electric rod is submerged in the boiler of the secondary evaporator. The voltage is supplied to the heater utilizing a variable resistance regulated transformer. The power P of the electrical heater is measured via measurement of the voltage U supplied by the transformer and the current I passing across the resistance of the electric heater as

$$P = IU \ . \tag{3.23}$$

The voltage in V is directly measured using a digital voltmeter (Keithley 177). The voltmeter has a level of uncertainty of ±(0.035 % of reading+ 0.1 V) for $U \leq$1 kV. This is equivalent to a data acquisition error of 0.1042 V for a maximum possible voltage of U= 230 V. The current is indirectly measured by analog treatment using a PTB calibrated shunt resistance R_s as shown in Fig. 3.8. Thus with Ohm's law

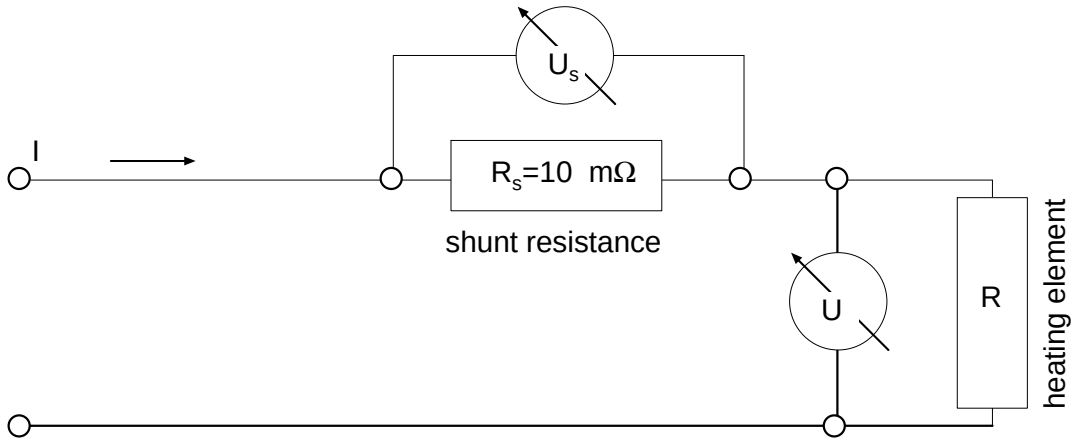

Figure 3.8. Analog measurement of the electric current using shunt resistance.

[10]Micro Motion, SMR GmbH, Technisches Büro der Fisher-Rosemount GmbH, Pankower Straße 8b, 21502 Geesthacht, Germany

$$I = \frac{U_s}{R_s} \ , \tag{3.24}$$

the electric current may be evaluated. Here $R_s = 10 \pm 0.003$ mΩ and the shunt output voltages U_s is measured using a digital voltmeter Keithley 177. The voltmeter has a level of uncertainty of $\pm$(0.2 % of reading+ 2 μ V) for $U \leq$1 V. This correspond to a data acquisition error of 1.556×10^{-4} V for a maximum possible shunt voltage of U_s=43.5 mV. Upon substitution of equation 3.24 into equation 3.23 the electric power may be written as

$$P = \frac{UU_s}{R_s} \ . \tag{3.25}$$

As for the case of temperature the combined standard uncertainty of the electrical power P designated by U_P consists of bias and precision error as given by equation 3.3 with P replaces T. The electric power being not a directly measured parameter but a derived one, both the bias error and precision error are evaluated using the law of propagation of error in accordance with the DKD [28]. That is to say for an out parameter y derived from N other parameters $x_1, x_2, \cdots, x_N$ through a functional relationship f:

$$y = f(x_1, x_2, \cdots, x_N) \ , \tag{3.26}$$

the propagated error is

$$E_y^2 = \sum_{i=1}^{N} \left(\frac{\partial y}{\partial x_i} \right)^2 E_{x_i}^2 \ , \tag{3.27}$$

where E may be bias error B, precision error P or total error U. Application of equation 3.27 to the electric power equation 3.25 yields the bias and the precision error as

$$\frac{B_P}{P} = \sqrt{\frac{B_U^2}{U^2} + \frac{B_{U_s}^2}{U_s^2} + \frac{B_{R_s}^2}{R_s^2}} \ , \tag{3.28}$$

and

$$\frac{P_P}{P} = \sqrt{\frac{P_U^2}{U^2} + \frac{P_{U_s}^2}{U_s^2} + \frac{P_{R_s}^2}{R_s^2}} \ , \tag{3.29}$$

respectively. The bias error is taken as the data acquisition error supplied by the manufacturer of the respective devices (*e.g.* voltmeter). The precision error of each parameter (U, U_s) is evaluated using equation 3.5 with U or U_s replaces T. The precision error for the shunt resistance is taken to be equivalent to the bias error supplied by the manufacturer. As an illustration table 3.1 shows the level of uncertainty of the heating element designated H10 in Fig. 3.5 for a maximum power of 1 kW.

Table 3.1. Estimation of the level of uncertainty for the heating element H10.

Reading	U=230 V	U_s=43.5 V	R_s 10 mΩ	I= 4.35 A	P=1000 W
			Uncertainty		
B_P	0.104	1.556×10^{-4}	1.732×10^{-6}	15.578×10^{-3}	3.609
P_P	0.050	1.000×10^{-4}	1.732×10^{-6}	13.220×10^{-3}	2.007
U_P	0.116	1.850×10^{-4}	2.449×10^{-6}	15.847×10^{-3}	4.130

For the various heating elements the level of uncertainty in the measurement of the power does not exceed 5.0 W for $P \leq 1$ kW.

To control the aging effect on the heating element a frequent check has been made at various time intervals. Fig. 3.9 shows specimen of the measurement at various time intervals. The results indicated that the aging effect on the heating element is negligible.

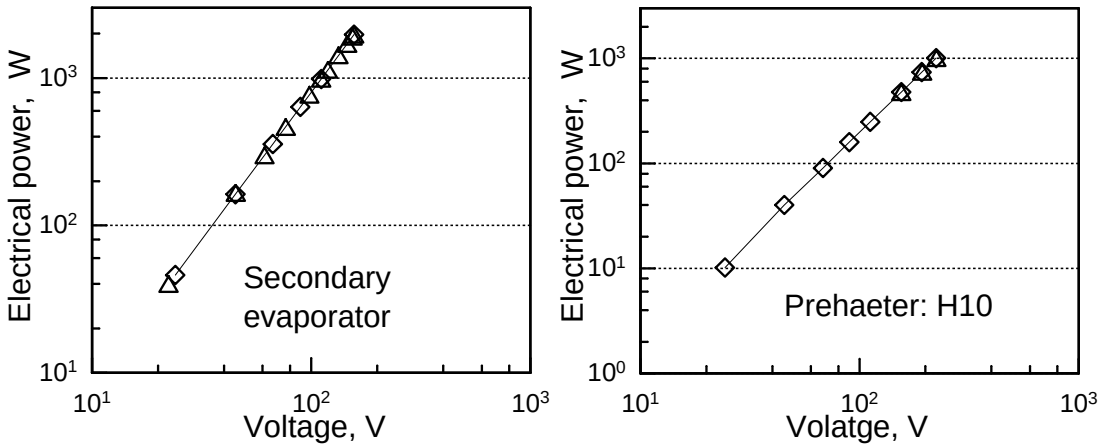

Figure 3.9. Aging effect on the heating elements. Legend: (△) Augest 2000, (♢) March 2003.

3.2.6 Gas chromatography

For the determination of the composition of the R134a/R290 mixture a *Perkin Elmer* modell 1022 gas chromatography (GC) was used. The output signal of GC is related to the mole fraction of a binary mixture $\widetilde{z}$ as (Kleemiß [77])

$$\widetilde{z}_1 = \frac{1}{1 + f\frac{A_2}{A_1}} \,, \tag{3.30}$$

where A is the output signal of the GC which is expressed as the peak area. The subscripts 1, 2 signify R290 and R134a respectively. f is a respond or a calibration factor. The respond factor f is particular to each mixture (*i.e.* depend on the mixture compositions). Therefore the GC requires to be calibrated to determine the calibration factor for the R134a/R290 mixture used in the present work. For this purpose a number of reference samples of the R134a/R290 mixture were prepared. The preparation procedure of the sample is shown schematically in Fig. 3.10. To eliminate the possibility of traces, the refrigerant vessel as well as the reference sample vessel were connected to the suction side of a vacuum pump. Thus the tube connecting the vessels is evacuated before the charging process. To ease refrigerant charge the reference sample vessel is cooled to about 0 °C using an ice bath and the refrigeration vessel is heated to about 40 °C. This is made to create a pressure difference between the sample and refrigerant vessels. Thus easing the flow from the refrigerant vessel to the sample vessel and avoiding the reverse flow. The

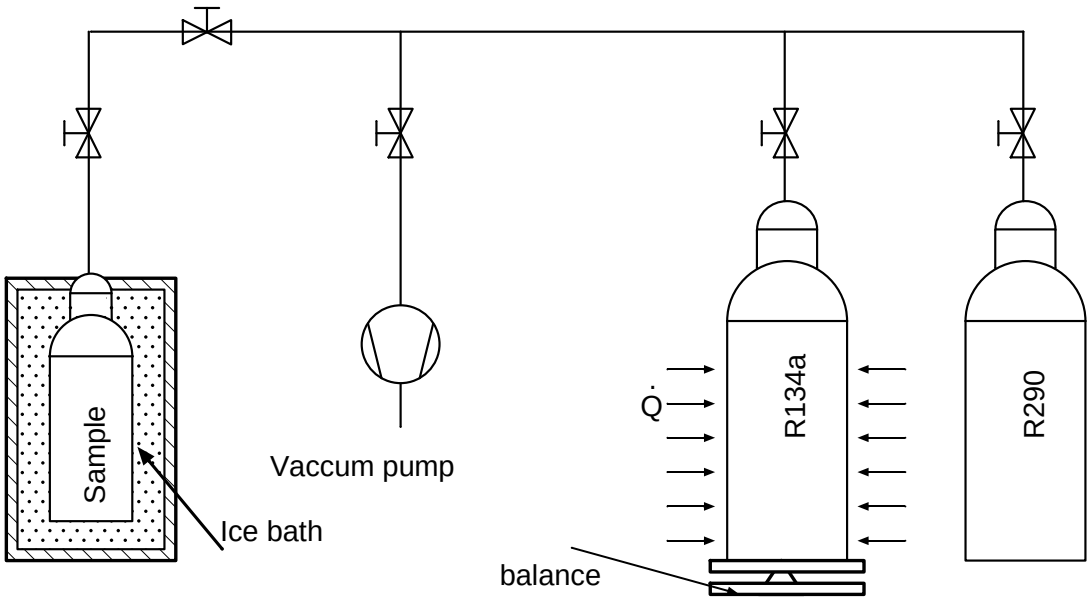

Figure 3.10. Setup for the preparation of the reference sample.

mass fraction of the mixture $\widetilde{Z}$ of the reference sample is determined as

$$\widetilde{Z}_1 = \frac{M_1}{M_1 + M_2} \ , \tag{3.31}$$

where M_1 and M_2 is the weight (in g) of propane and R134a respectively. These are determined using a *Mettler Pt15* balance. The mole fraction of propane may be calculated from the mass fraction and knowledge of the pure components molecular weights as

$$\widetilde{z}_1 = \frac{\widetilde{Z}_1}{\widetilde{Z}_1 + \frac{\widetilde{M}_1}{\widetilde{M}_2}(1 - \widetilde{Z}_1)} \ , \tag{3.32}$$

where $\widetilde{M}_1$ and $\widetilde{M}_2$ is the molecular weights of propane and R134a respectively. In accordance with Tillner-Roth [136] these are 44.0965 g/gmole and 102.032 g/gmole of propane and R134a respectively. *As an illustration to equation 3.32,* $\widetilde{z}_1$*(0.45)=0.65.*

The prepared reference sample of the gaseous R134a/R290 mixture of known composition is then charged into the GC. The output signals of the GC, which are the peak areas A_1 and A_2, are recorded and subsequently the value of the respond factor is determined using equation 3.30 for each sample of known composition $\widetilde{z}$. Fig. 3.11 shows the calibration factor f as a function of mole fraction $\widetilde{z}$. The result of the best fit suggested that the respond factor is a quadratic function of the mole fraction as

$$f = 4.7867 - 10.2662\widetilde{z}_1 + 6.405\widetilde{z}_1^2 \ . \tag{3.33}$$

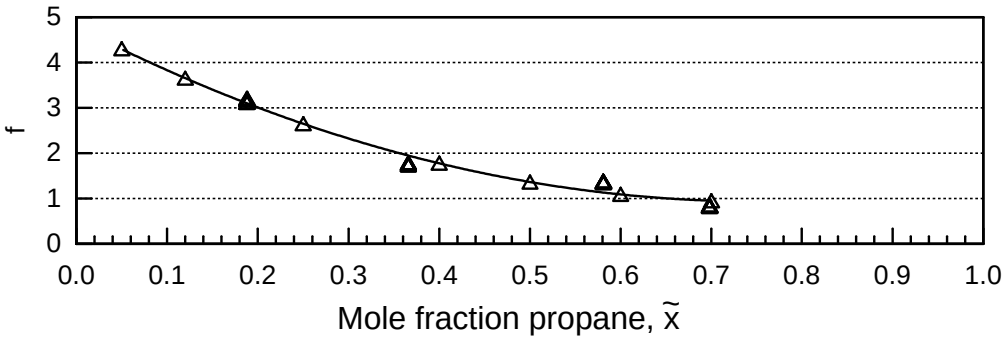

Figure 3.11. Calibration factor f for the gas chromatography as a function of propane mole fraction.

Upon substitution of f in equation 3.30 the resulted calibration equation of the GC is

$$\tilde{z}_1 = \frac{1}{1 + (4.7867 - 10.2662\tilde{z}_1 + 6.405\tilde{z}_1^2)\frac{A_2}{A_1}} \ . \tag{3.34}$$

Equation 3.34 is valid in the range of $\tilde{z} \leq 0.7$ mole fraction propane. For further application equation 3.34 may be solved iteratively to determined the unknown composition $\tilde{z}$ of a R134a/R290 sample.

The level of uncertainty in the measurement of mole fraction $\tilde{z}$ using GC is evaluated in accordance with a 95% confidence limit as given by equation 3.3 with $\tilde{z}$ replacing T as

$$U_{\tilde{z}} = \sqrt{B_{\tilde{z}}^2 + P_{\tilde{z}}^2} \tag{3.35}$$

The bias error $B_{\tilde{z}}$ and the precision error $P_{\tilde{z}}$ is derived applying the law of propagation (cf. equation 3.27) to equation 3.30 as

$$\frac{B_{\tilde{z}}}{\tilde{z}} = \sqrt{\frac{B_f^2}{f^2} + \frac{B_{A_1}^2}{A_1^2} + \frac{B_{A_2}^2}{A_2^2}} \ , \tag{3.36}$$

and

$$\frac{P_{\tilde{z}}}{\tilde{z}} = \sqrt{\frac{P_f^2}{f^2} + \frac{P_{A_1}^2}{A_1^2} + \frac{P_{A_2}^2}{A_2^2}} \ , \tag{3.37}$$

respectively. The bias error for the calibration factor f is

$$B_f = \left(\frac{\partial f}{\partial \tilde{z}}\right) B_{\tilde{z}} = (b + 2c\tilde{z}_1) B_{\tilde{z}} \ , \tag{3.38}$$

where the bias error in the mole fraction $B_{\tilde{z}_1}$ is given as

$$B_{\tilde{z}_1} = \frac{\partial \tilde{z}_1}{\partial \tilde{Z}_1} B_{\tilde{Z}_1} \ . \tag{3.39}$$

The partial derivatives of the mole fraction $\tilde{z}$ with respect to mass fraction $\tilde{Z}$ is evaluated by using equation 3.32. The bias error in the mass fraction is given as

$$B_{\tilde{Z}_1} = \sqrt{\left(\frac{\partial \widetilde{Z_1}}{\partial M_1}\right)^2 U_{M_1}^2 + \left(\frac{\partial \widetilde{Z_1}}{\partial M_2}\right)^2 U_{M_2}^2} \ , \tag{3.40}$$

with the partial derivatives of $\widetilde{Z}_1$ with respect to M_1, M_2 evaluated by using equation 3.31, equation 3.40 becomes

$$B_{\widetilde{Z}} = \frac{\widetilde{Z}_1 B_M}{M_1 + M_2}\sqrt{1 + \left(\frac{M_2}{M_1}\right)^2} \ . \tag{3.41}$$

For the case of $\widetilde{Z}$=0.45 (*i.e.* $\widetilde{z}$=0.65) the corresponding mass of propane is 200 g. The $MettlerPt15$ balance used in the present work has an error of ± 0.1 g as given by the manufacturer. A further error of 5 g is considered to compensate for the losses resulted from the gas remained in the tube connecting the sample and the refrigerant vessels (cf. Fig. 3.10). Therefore the total error in the measurement of the weight of the sample is approximated as

$$B_M = B_{M_1} = B_{M_2} = \sqrt{0.1^2 + 5^2} = 5.001 \text{ g} \ . \tag{3.42}$$

Hence

$$\begin{cases} B_{\widetilde{Z}} & = 0.007995 \text{ weight fraction} & \text{equation 3.41} \\ B_{\widetilde{z}} & = 0.005025 \text{ mole fraction} & \text{equation 3.39} \\ B_f & = 0.009745 & \text{equation 3.38} \end{cases} .$$

The bias error for the peak area is taken as the tolerance[11] of the GC given by the manufacturer, which amount to $B_{A_1}/A_1 = B_{A_2}/A_2 = 1 \times 10^{-3}$. Thus equation 3.36 yields $B_{\widetilde{z}}/\widetilde{z}$=0.01196.

For a limited number of data points the precision error in accordance with a 95 % confidence limit is given by equation 3.5. In the present work each test is repeated 10 times. Thus $t_{9,95\%}$=2.26 (Adunka [1]). The standard deviation S_{A_i} is given by equation 3.6 when A_i replacing X. For a binary mixture we have

$$P_{A_1} = P_{A_2} \ . \tag{3.43}$$

For the case at hand (*i.e.* $\widetilde{z}$=0.65) $\overline{A}_1$=65.869 % and $\overline{A}_2$=34.131 % while the standard deviation is 0.2546%. Using equation 3.5

$$P_{A_1} = P_{A_2} = \frac{t_{\lambda,95\%} S_{A_i}}{\sqrt{N}} = \frac{2.26 \times 0.2546}{\sqrt{10}} = 0.18196\% \ . \tag{3.44}$$

For the calibration factor f given by equation 3.33 the standard deviation is 0.0152. Thus

$$P_f = \frac{2.26 \times 0.0152}{\sqrt{10}} = 0.0108 \ . \tag{3.45}$$

With values of P_{A_1}, P_{A_2} and P_f equation 3.37 yields $P_{\widetilde{z}}/\widetilde{z}$=0.01455. The total propagated error in the measurement of $\widetilde{z}$=0.65 mole fraction is

$$\frac{U_{\widetilde{z}}}{\widetilde{z}} = \sqrt{\left(\frac{B_{\widetilde{z}}}{\widetilde{z}}\right)^2 + \left(\frac{P_{\widetilde{z}}}{\widetilde{z}}\right)^2} = \sqrt{0.01196^2 + 0.0145^2} = 0.018796 \ . \tag{3.46}$$

Or $U_{\widetilde{z}}/\widetilde{z}$=1.8796%. For the whole range of mole fraction $0 < \widetilde{z} \leq 0.7$ the level of uncertainty in the measurement does not exceeded 2.0%.

[11] 1022 GC Plus, Installation and setup guide, 1993, pp. 14.4

3.2.7 Observation of flow pattern

As indicated in the literature review besides the mass flow flux, heat flux, saturation temperature and vapor quality the flow pattern has a strong influence on the flow boiling heat transfer coefficient. Thus knowledge of flow pattern is of paramount importance in the correct prediction of the heat transfer coefficient. With this in mind two sight glasses are mounted inline to the inlet and outlet of the test evaporator. Thus recording the flow pattern with a video system, camera or direct visual observation with written notes are made possible. On the other hand it has to be kept in mind that the sight glass before the test section may have influence on the heat transfer coefficients.

3.3 Data acquisition system

The block diagram shown in Fig. 3.12 presents the scheme used to facilitate the measurement of the various parameters. The output signals of the temperature sensors,

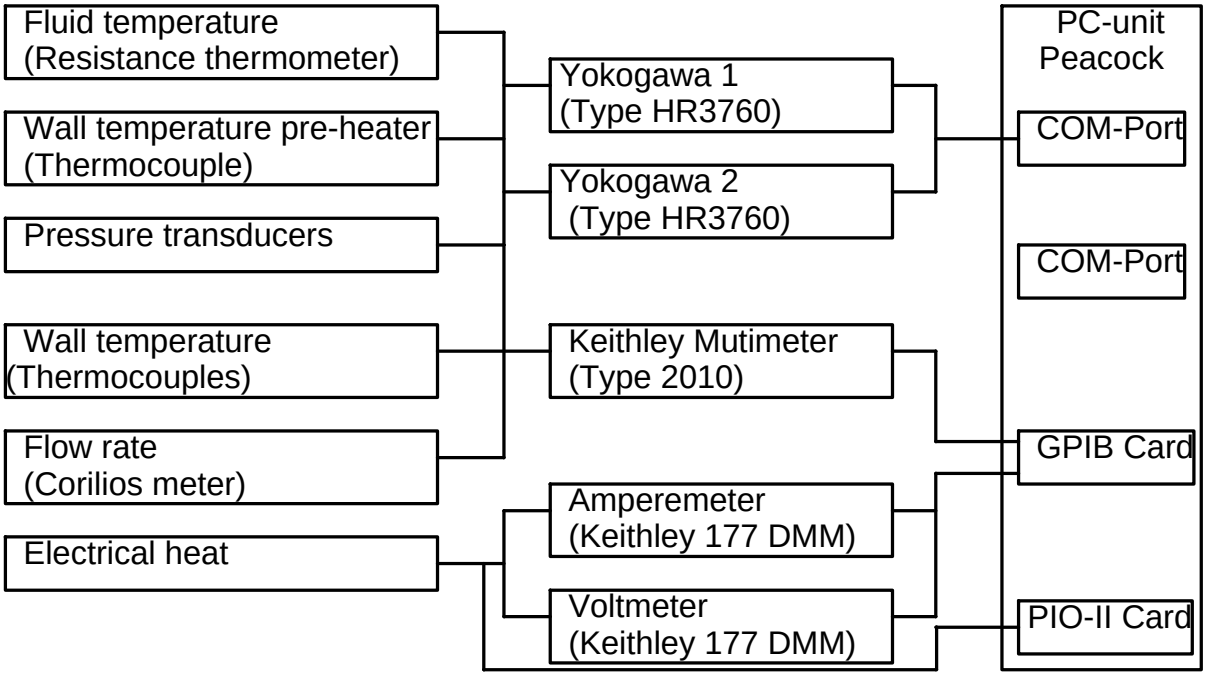

Figure 3.12. Schematic presentation of the data acquisition system setup.

pressure transducers and the mass flow meter are logged to a PC via serial interfaces (*i.e.* the PCI and ISA-slots) for storing and processing. The output signals of these devices are measured, as reported, using two hybridrecorder Yokogawa HR 3760 each employs 30 chanals. The output voltages of the heating elements and some of the temperature sensors are logged to the PC via GPIB card employing an IEEE-488.2 Bus System. To be remembered is that the output voltages of the heating elements and the temperature sensors are measured using Keithley 177 and Keithley 2010 voltmeters respectively. The successive measurement of the output signals of the heating elements are facilitated using a PIO24II rely card.

The reading and the subsequent storing of the measured data are facilitated using the software *Labview* version 4.1 with *Window* 95 as a PC working system. Measurements are taken in 5 second intervals. The measured data is stored as an "ASCII-text" for further processing and analysis. The data analysis is facilitated using a computer code employing the software package of "Fortran 90". The measurements are averaged over a period of 5 to 30 minutes of steady state condition. As an illustration Fig 3.13 shows specimen of the steady state measurement of some of the parameters.

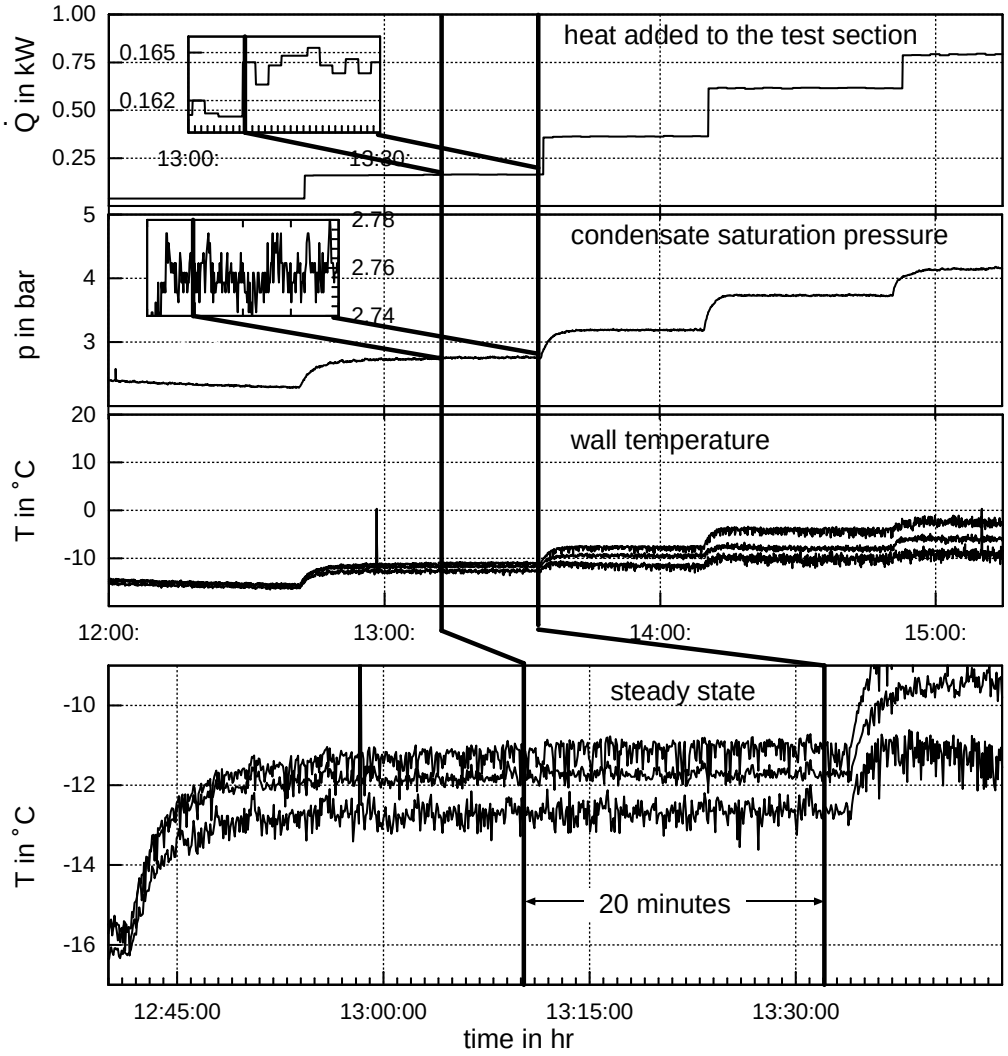

Figure 3.13. Specimen of the steady state measurement.

3.4 Experimental procedure

3.4.1 Charging procedure

Before charging the test system with the new refrigerant the old one is drained. The system is then washed with nitrogen and evacuated to an absolute pressure of about 1-5 mbar utilizing a *PFEIFFER* vacuum pump, with no leakage detected over 48 hr. To eliminate the possibility of traces, the refrigerant vessel was connected to the suction side

of a vacuum pump. Thus the tube between the vessel and the test system is evacuated before the charging process. To ease refrigerant charge into the system the test circuit is cooled to about -30 °C and the refrigerant vessel is heated to about 40 °C. This is made to create a pressure difference between the test circuit and refrigerant vessel. Thus easing the flow from the vessel to the test circuit and avoiding the reverse flow. For the case of a mixture, first the required mass of R134a is charged into the test circuit, then followed by the required mass of propane. After the charging process the charge is circulated in the test circuit in a state of single phase liquid, to ensure a proper mixing. A sample is taken from the circulating mixture (liquid) and analyzed using a *Perkin Elmer* gas chromatography. The sample is collected at the positive suction side of the pump (*i.e.* the valve labelled "V1" in Fig. 3.5). The result of the analysis (see Fig. 3.14) indicated that most of the data deviate by as much as ±5 % from the desired composition; the charged mass ratio. This indicates the adequacy of the charging procedure employed in the present work. The refrigerant R134a and propane used in the present work were supplied by the company Solvay AG, Hannover, Germany. The purity of pure R134a and propane as indicated by the manufacturer are 99.9 % (*i.e.* Grade 2.5) and 99.95 % (*i.e.* Grade 3.5) respectively.

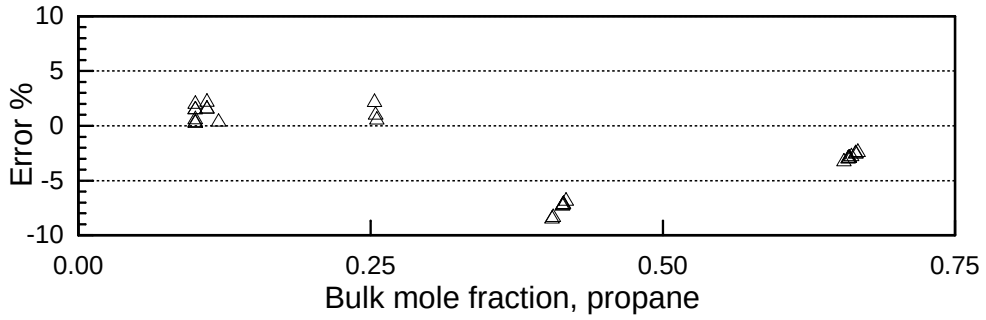

Figure 3.14. Deviation between the desired and charged composition of R134a/propane mixture.

3.4.2 Test programm

For flow boiling of pure components and mixtures the parameters of concern generally include p, $\dot{q}$, mixture composition and tube diameter d. For flow boiling in a horizontal tube, in addition to these parameters the mass flux $\dot{m}$, vapor quality $\dot{x}$, tube thickness s, and the thermal conductivity of the tube λ_w are to be considered. To facilitate the systematic investigation of these parameters on the flow boiling of pure R134a and R134a/propane mixtures the test program shown in Table 3.2 was executed.

Due to the flammability problem associated with propane neither pure propane tests nor R134a/propane mixture tests of bulk composition of more that 65 mole % (azeotropic point) were carried out. Furthermore, for the azeotropic mixture, there was carried out no experiment with a pressure of less than 1 bar. This condition requires a cooling rate of more than 10 kW (-50 °C), which is beyond the capacity of the refrigeration unit (maximum cooling rate 10 kW: -50 °C) used in the present work. Finally due to temporal

reasons the test program is shortened for mixtures (a variation of the parameters in the whole range as for pure R134a would have required about 5000 test runs; 5000-10000 hr).

Table 3.2. Test program.

Parameter	Refrigerant			Unit
	R134a	R290	R134a/R290	
p	0.84,$\cdots$, 3.4	-	0.84,$\cdots$, 3.4	bar
$\dot{q}$	2.0,$\cdots$, 40.5	-	2.0, $\cdots$, 40.5	kW/m^2
$\widetilde{z}$	-	-	10.0,$\cdots$, 65.0	mole % R290
$\dot{m}$	100,$\cdots$, 300	-	100,$\cdots$, 300	kg/m^{2}s
$\dot{x}$	0,$\cdots$, 1.0	-	0,$\cdots$, 1.0	
d	10	-	10	mm
N	330	-	800	

N=number of test runs

4 Data reduction

In the field of flow boiling the heat transfer coefficient and quality are not directly measured parameters, they are rather derived from the measured temperature, pressure, pressure drop, mass and heat flow rate. Therefore the reduction procedures of these parameters to yield, among other, the heat transfer coefficient and quality need to be outlined.

4.1 Heat transfer coefficient

4.1.1 Angular heat transfer coefficient

For a horizontal tube the angular heat transfer coefficient at the axial position z is defined as

$$\alpha(\varphi, z) = \frac{\dot{q}_i(\varphi, z)}{T_{wi}(\varphi, z) - T_s(z)} \ , \tag{4.1}$$

where $T_{wi}(\varphi, z)$ and $\dot{q}_i(\varphi, z)$ are the inside wall temperature and heat flux at the angular position φ and the axial position z respectively. $T_s(z)$ is the saturation temperature for the pure refrigerant or the bubble point temperature for a mixture at the axial position z. The evaluation procedure of the saturation temperature or bubble temperature is shown in section 4.3. The inside wall temperature is calculated from the measured outside wall temperature $T_{wo}(\varphi, z)$ utilizing a one dimensional steady state conduction equation as

$$T_{wi}(\varphi, z) = T_{wo}(\varphi, z) - \dot{Q}(\varphi, z)\frac{\ln(d_o/d_i)}{2\pi L\lambda} \ , \tag{4.2}$$

where L is the heated length of the tube, d_i and d_o are the inside and outside diameter of the tube respectively. λ is the thermal conductivity of the tube, which is assumed to be independent of temperature. For stainless tube it is taken as λ= 15 W/m K (VDI-Wärmeatlas [143]). $\dot{Q}(\varphi, z)$ is the heat added to the test section taken into account the heat lost or gained as

$$\dot{Q}(\varphi, z) = \dot{Q}_c(\varphi, z) + \dot{Q}_{loss} \ . \tag{4.3}$$

The heat added to test section via condensation $\dot{Q}_c(\varphi, z)$ is calculated from Nusselt's theory of film condensation (section 4.6). The heat loss to the surrounding based on the outer tube $\dot{Q}_{loss}$ is

$$\dot{Q}_{loss} = kA\Delta T_{lm} \ , \tag{4.4}$$

where $A = \pi dL$, is the heating surface. L and d are the length and the diameter of the tube respectively. k is the overall heat transfer coefficient and ΔT_{lm} is logarithmic mean temperature different. The calculation model used to estimate the heat loss is shown in section 4.2. The local heat flux, given by equation 4.1, is therefore

$$\dot{q}_i(\varphi, z) = \frac{\dot{Q}_i(\varphi, z)}{A_i} \ , \tag{4.5}$$

where A_i is the heating surface based on the inside diameter d_i of the tube.

4.1.2 Mean circumferential heat transfer coefficient

Integration of equation 4.1 over the entire perimeter of the tube yields the local mean heat transfer coefficient as

$$\alpha(z) = \frac{1}{2\pi}\int_0^{2\pi} \alpha(\varphi, z)d\varphi = \frac{1}{2\pi}\int_0^{2\pi} \frac{\dot{q}_i(\varphi, z)d\varphi}{T_{wi}(\varphi, z) - T_s(z)} \ . \tag{4.6}$$

For the case of thermal boundary conditions of constant wall temperature equation 4.6 reduces to

$$\alpha(z) = \frac{\dot{q}_i(z)}{T_{wi}(z) - T_s(z)} \ , \tag{4.7}$$

where

$$\dot{q}(z) = \frac{1}{2\pi}\int_0^{2\pi} \dot{q}(\varphi, z)d\varphi \ . \tag{4.8}$$

For the case of a complex scenario the integration of equation 4.6 requires knowledge of the wall temperature distribution.

4.2 Energy balance

Although the test circuit is insulated to minimize the effect of the surrounding, the heat loss to the surrounding may not be completely eliminated. Therefore it needs to be quantified. To estimate the heat loss to the surrounding a number of test runs were carried out using liquid single phase under subcooling conditions. For convenience the test circuit is divided into four zones: two preheating zones, test section and adiabatic zone as shown in Fig. 4.1.

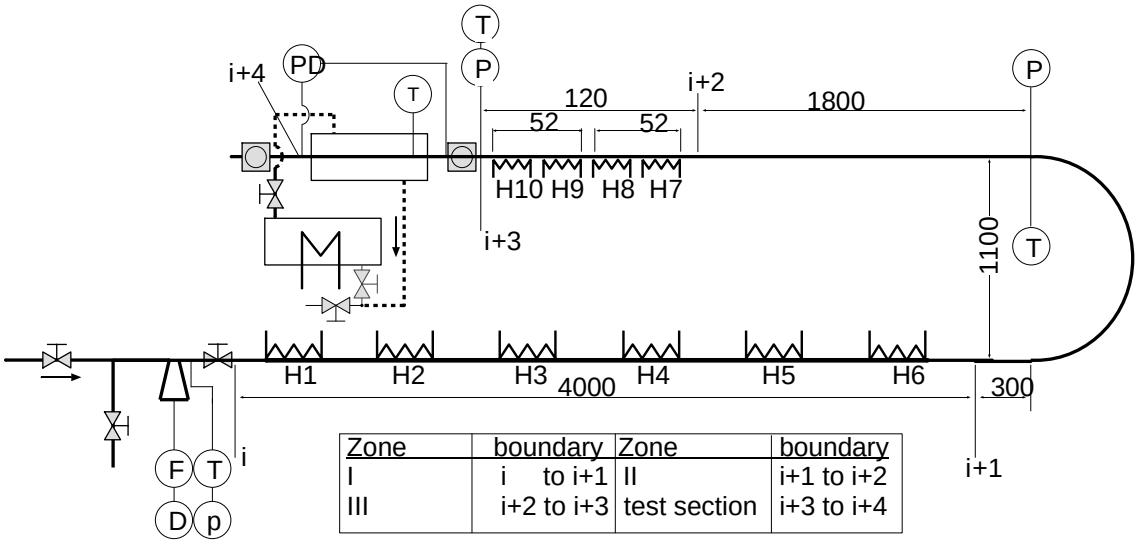

Figure 4.1. Schematic presentation of the heating zones, dimensions are in mm.

The steady state heat balance for each preheating zone j is given as

$$P_{el,j} = \dot{Q}_{f,j} + \dot{Q}_{loss,j} \ , \tag{4.9}$$

where $P_{el,j}$ is the electric power (heat) input to the heating zone j, $\dot{Q}_{f,j}$ is the heat transferred to the fluid in the zone j, $\dot{Q}_{loss,j}$ is the heat lost to surrounding of the heating zone j. The heat transferred to the fluid in the zone j is calculated from the first law of thermodynamics applied to a steady state flow process with negligible potential and kinetic energy as

$$\dot{Q}_{f,j} = \dot{M}\left[h_j(T_{i+1}, p_{i+1}) - h_j(T_i, p_i)\right] \ , \tag{4.10}$$

where $\dot{M}$ is liquid mass flow rate, h is the fluid enthalpy calculated from the fundamental equation of state of Tillner Roth and Baehr [138] for R134a for a given fluid bulk temperature T and pressure p. The subscripts i and $i+1$ specify the inlet and outlet of the heating zone j respectively. The heat loss to the surrounding is written as

$$Q_{loss,j} = k_j A_j \Delta T_{ln,j} \ , \tag{4.11}$$

where k is the overall heat transfer coefficient and $A_j = \pi d_j L_j$ is the outer surface with d_j and L_j are the outer diameter and the length of the tube of the heating zone j. $\Delta T_{ln,j}$ is the logarithmic mean temperature difference defined as

$$\Delta T_{lm,j} = \frac{\Delta T_{j,i} - \Delta T_{j,i+1}}{\ln\left[\frac{\Delta T_{j,i}}{\Delta T_{j,i+1}}\right]} \ , \tag{4.12}$$

where $\Delta T_{j,i} = T_\infty - T_{j,i}$ and $\Delta T_{j,i+1} = T_\infty - T_{j,i+1}$ are the overall temperature difference at the inlet and outlet of the heating zone j respectively. T_∞ is the ambient temperature. Equation 4.9 is solved for $k.A$ under both adiabatic ($\dot{Q}_j$=0) and none adiabatic conditions. Table 4.1 summarizes the values of $k.A$ for the various heating zones. With the values of $k.A$ the heat loss to surrounding does not exceeded 5% at all preheating zones under the extreme working conditions of a maximum mean refrigerant temperature of -40 °C. *For example for a maximum mean fluid temperature of* -40 °C *and ambient temperature of* 20 °C *the heat loss to the surrounding at the test section is* 5.166 W (*or* $\dot{q} = 0.329\ W/m^2$). Low heat loss to the surrounding is an indicative to the adequacy of the insulation used in the present work.

The experimentally measured overall heat transfer coefficient is also theoretically determined. Fig. 4.2 shows the model used to calculate the theoretical thermal resistances.

The thermal circuit is constructed by recognizing that there are resistances to heat flow associated with forced convection due to the flowing fluid at the inner side of the tube R_f and radial conduction in the tube wall R_w. Additionally, there are resistance due to radial conduction across the insulation R_s. At the outside of the insulation resistance to heat loss due to free convection R_a and radiation R_r are considered. The fouling resistances at the fluid side $R_{f,i}$ is also considered in the modelling. With these resistances the overall heat transfer coefficient for each of the preheating zone is

$$\frac{1}{kA} = \sum R_i = \frac{1}{2\pi r_i L \alpha_f} + \frac{R_{f,i}}{2\pi r_i L} + \frac{\ln(r_o/r_i)}{2\pi L \lambda_w} + \frac{\ln(r_s/r_o)}{2\pi L \lambda_s} + \frac{1}{2\pi r_s L(\alpha_\infty + \alpha_r)} \ . \tag{4.13}$$

Table 4.1. Specifications of Fig. 4.1 and the overall heat transfer coefficient at each heating zone. Abbreviations: TS: test section, HI: heating zone I, HII: heating zone II and HIII: heating zone III.

Parameter	Unit	HI	HII	HIII	TS
d_i	mm	15	15	10	10
d_o	mm	30	30	12	12
$d_{c,i}$	mm	-	-	-	57
$d_{c,o}$	mm	-	-	-	62.8
d_s	mm	100	100	100	135
L	mm	4.000	3300	1200	500
λ_w	W/m K	15	15	15	15
λ_s	W/m K	$0.036 + 10^{-4} \times T$			
kA	W/K	0.2552	0.1876	0.0978	0.0861
λ_s is the thermal conductivity of the insulation material					

For the test section where the thermal resistance due to condensation is to be accounted for, the overall heat transfer coefficient is

$$\frac{1}{kA} = \sum R_i = \frac{1}{2\pi r_i L \alpha_f} + \frac{R_{f,i}}{2\pi r_i L} + \frac{\ln(r_o/r_i)}{2\pi L \lambda_w} + \frac{R_{f,o}}{2\pi r_i L} + \frac{1}{2\pi r_o L \alpha_c} \ , \tag{4.14}$$

where the radii r_i, r_o , $r_{c,i}$, $r_{c,o}$ and r_s as well as the heated length L are defined in Fig. 4.2. Their values are given in Table 4.1. λ_w, λ_c and λ_s are the thermal conductivity of the tube carrying the fluid, the tube enclosing the condensing fluid and the insulation respectively. The thermal conductivity of the test tube is obtained from the VDI-Wärmeatlas [143] while that for the insulation material is obtained from the manufacturer[1]. These are given in Table 4.1. α_f, α_c, α_∞ and α_r are the heat transfer coefficients due to the flow of single phase fluid (forced convection), laminar film condensation, the ambient air at the outside wall of the insulation (free convection) and due to radiation between the insulation and the surrounding respectively. The liquid heat transfer coefficient α_f is calculated using Gnielinski [42] model (see Appendix C). The free convection heat transfer coefficient α_∞ is calculated using Churchil and Chu [21] correlation (see Appendix C). The radiation heat transfer coefficient α_r is calculated using Stefan-Boltzmann law (Appendix C). α_c is estimated using Nusselt's theory of film condensation (cf. equation 4.58). In the present analysis the inside and the out side fouling coefficients are neglected for the test tube is considered clean (*i.e.* initially put in to the service). The absolute deviation between the experimental and the theoretical values of the thermal conductance ($k.A$) for all the heating zones is found to be less than 10 %.

[1]FISCHER KÄLTEKLIMA, Christof Fischer GmbH, Augsburger Str. 289-29, 70327 Stuttgart, Germany.

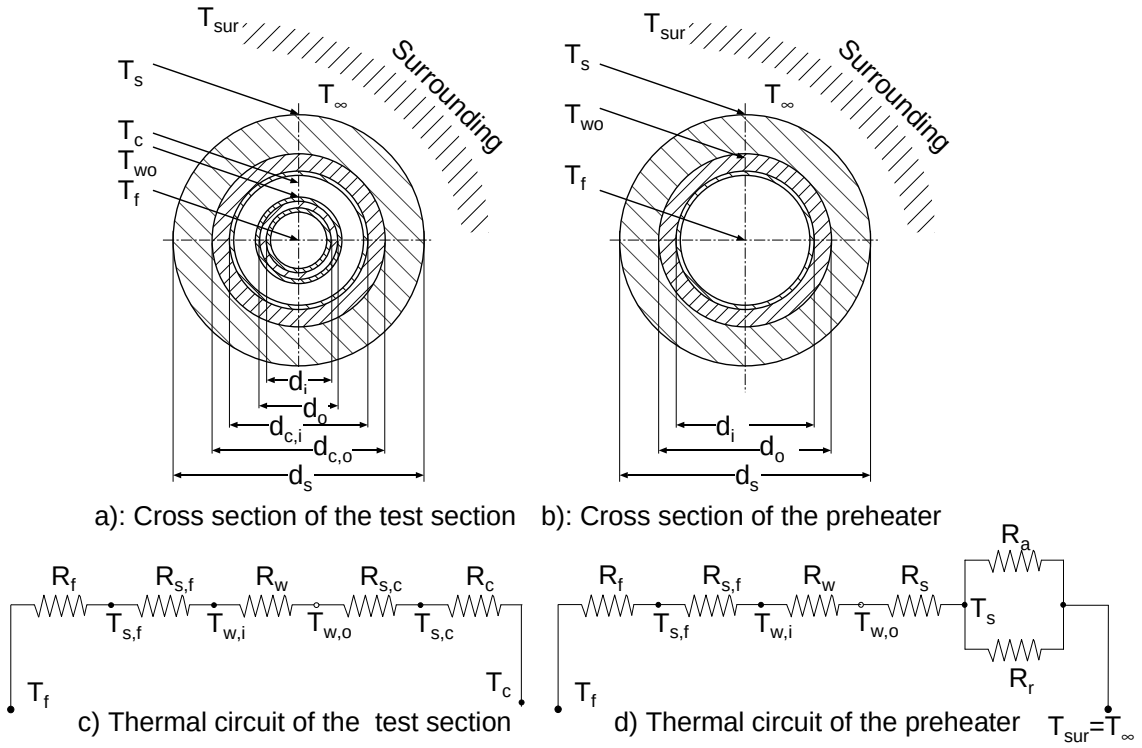

Figure 4.2. Energy balance model.

4.3 Saturation temperature

4.3.1 Pure R134a and azeotropic R134a/R290 mixture

The prediction of saturation temperature for pure R134a and azeotropic R134a/R290 mixtures are facilitated utilizing the measured saturation pressure and suitable equation of state. For a pure R134a and the R134a/R290 mixture the fundamental equation of state of Tillner-Roth and Baehr [138] and Tillner-Roth [137] respectively are used (see Appendix B). For a short test tube the local saturation pressure $p_s(z)$ at any position z along the test section is calculated from the measured inlet absolute pressure $p_{s,i}$ and the pressure drop across the test section Δp assuming a linear variation as

$$p_s(z) = p_{s,i} + \frac{\Delta z_i + z}{\Delta z_i + L + \Delta z_o} \Delta p \ , \tag{4.15}$$

where Δz_i and Δz_o are the adiabatic length of the tube at the inlet and outlet of the test section respectively (see Fig. 4.3).

The pressure transducer used for the measurement of the saturation pressure (*i.e.* "**P Y1-05**" see Fig. 3.5) has a level of uncertainty of U_p=±1.33 mbar (see Appendix A) in the range of $p \leq 10$ bar. The corresponding level of uncertainty of the saturation temperature is calculated numerically as

$$U_T = \frac{dT}{dp} U_p \ . \tag{4.16}$$

The partial derivatives of T with respect to p for pure R134a and the azeotropic R134a/R290 mixture is calculated utilizing the fundamental equation of state of Tillner-Roth and

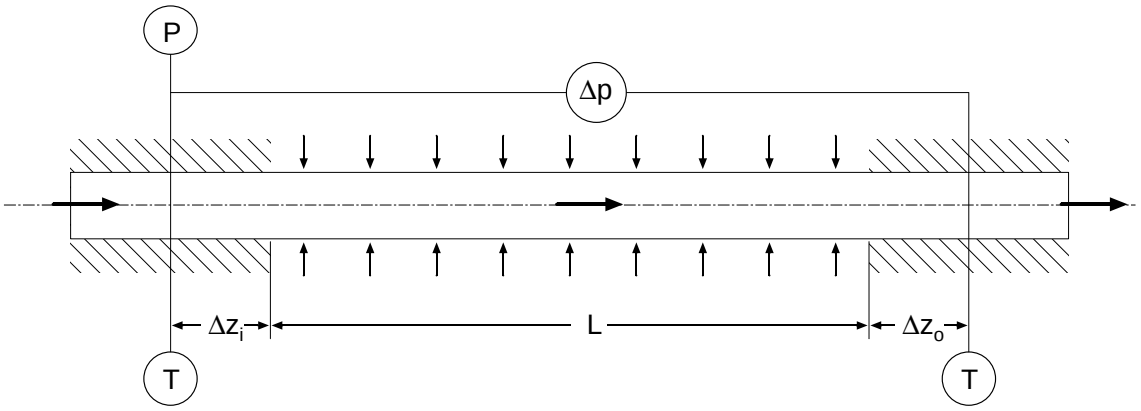

Figure 4.3. Location of bulk fluid pressure and temperature measurement in the test section.

Baehr [138] and Tillner-Roth [137] respectively (see Appendix B). Fig. 4.4a and Fig. 4.4b present the level of uncertainty for a wide range of temperatures. For both pure R134a and the azeotropic R134a/R290 mixture the level of uncertainty does exceed ±0.05 K, most of the data is within ±0.025 K.

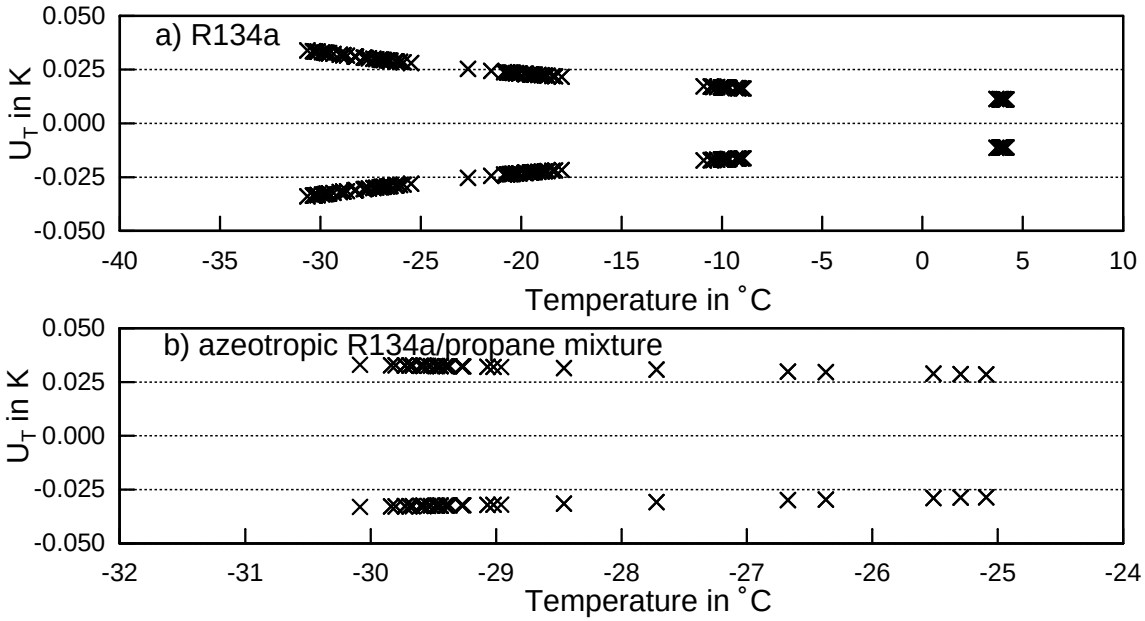

Figure 4.4. The level of uncertainty in the the calculated saturation temperature for: a) pure R134a and b) azeotropic R134a/R290 mixture.

The temperature sensor designated with the identifier **T Y2 25** in Fig. 3.5 which is used for the measurement of the bulk fluid temperature possesses a maximum level of uncertainty of ±0.044 K (see Appendix A). Clearly, with the advent of highly accurate fundamental equation of state of Tillner-Roth and Baehr [138] for R134a and Tillner-Roth [137] for the R134a/R290 mixture the saturation temperature can be precisely predicted provided that high level of accuracy in the measurement of the saturation pressure is maintained.

4.3.2 Zeotropic R134a/R290 mixture

In the flow boiling of a zeotropic mixture the saturation temperature used in equation 4.6 is defined by the VDI-Wärmeatlas [143] as the bubble point temperature. In the field of flow boiling the bubble point temperature of a zeotropic mixture is usually determined with a help of thermodynamic relationships.

The most widely used method for calculating the bubble point temperature is the method of *heat release (enthalpy) curve*. The literature refers to the change in enthalpy of a mixture during evaporation by various names: *heat release curve, evaporation curve and enthalpy curve*. The term *evaporation curve* is easily confused with *boiling curve* used in pool boiling research; thus this name should be avoided. For this reason the terminology *heat release curve* will be used here. In the following paragraph the procedure for using the heat release curve to calculated the boiling temperature is given.

During the evaporation of zeotropic mixture, the vapor composition of the more volatile component (the fluid with the lower boiling point) is in most cases greater than its composition in the liquid phase. Consequently, the local bubble-point temperature increases as the composition of the less volatile component (the fluid with a higher boiling point) in the liquid phase rises during evaporation along a heated tube at least up to the azeotropic point. The local change in enthalpy dh of a binary mixture during evaporation is composed of three contributions (Collier and Thome [23]):

1. latent heat to the fraction of liquid vaporized ($d\dot{x}$),
2. the sensible heat to the fraction of fluid in the liquid phase $(1-\dot{x})$ heated to a higher bubble point temperature,
3. sensible heat to the fraction of fluid in the vapor phase ($\dot{x}$) heated to a higher bubble point temperature.

In mathermatical terms this is

$$dh = d\dot{x}\Delta h_V + (1-\dot{x})c_{pL}dT + \dot{x}c_{pG}dT \ , \tag{4.17}$$

where Δh_V is the enthalpy of evaporation, $\dot{x}$ is quality. c_{pL} and c_{pG} is the isobaric specific heat of the liquid and vapor phase respectively. dT is the rise in the bubble point temperature. Equation 4.17 reduces to only the latent heat for a pure fluid or an azeotropic mixture as expected.

For the sake of simplicity, where only a very small change in the enthalpy is considered (or a very small heated section of the tube), the isobaric specific heat and vapor quality may be assumed constant (Zürcher et al. [154], Katten et al. [72] and Shao and Granryd [121]). Thus integration of of the heat release curve (equation 4.17) yields

$$h = h_0 + \dot{x}\Delta h_V + (1-\dot{x})c_{pL}(T-T_0) + \dot{x}c_{pG}(T-T_0) \ , \tag{4.18}$$

where h_0 and T_0 are reference enthalpy and bubble point temperature respectively, may be taken at a vapor quality of 0 % ($\dot{x}_0 = 0$). The bulk enthalpy h may be obtained from the first law of thermodynamics applied to steady state flow process with negligible potential and kinetic energy ($\dot{M}wdw$) as

$$h = h(T_f, p_f, \widetilde{z}) + \sum_{i=1}^{10} \dot{Q}_i / \dot{M} \ , \tag{4.19}$$

where $\dot{Q}_i$ is the electrical heat supplied to the preheater i, taken into account the heat loss or gain. $\dot{M}$ is the mass flow rate. T_f, p_f and $\widetilde{z}$ is the fluid bulk temperature, pressure and concentration at the inlet of the preheater respectively. It is to be remembered that the fluid conditions $T_f,\ p_f,\ \widetilde{z}$ at the inlet of the first preheater in the test circuit is at a subcooling state.

Combination of equation 4.19 and equation 4.18 yields the objective function

$$F = h(T_f, p_f, \widetilde{z}) + \sum_{i=1}^{10} \dot{Q}_i / \dot{M} - [h_0 + \dot{x}\Delta h_V + (1-\dot{x})c_{pL}(T - T_0) + \dot{x}c_{pG}(T - T_0)] = 0 \ . \tag{4.20}$$

It is to be noticed that the isobaric specific heat and the enthalpy of evaporation are functions, in addition to the temperature and pressure, of the liquid and vapor mole fraction $(\widetilde{x}, \widetilde{y})$. Thus equation 4.20 contains four unknowns: $T, \dot{x}, \widetilde{x}, \widetilde{y}$. Therefore three more independent equations are required to close equation 4.20. These three equations are obtained using:

- Material balance: Applying a component material balance to a close system yields

$$\widetilde{z}_i = \dot{\lambda}\widetilde{y}_i + (1 - \dot{\lambda})\widetilde{x}_i \ , \tag{4.21}$$

  where

$$\begin{cases} \sum \widetilde{x} = & 1 \\ \sum \widetilde{y} = & 1 \end{cases} ,$$

  and $\dot{\lambda}$ is molar quality which is related to the vapor quality as

$$\dot{x} = \frac{\dot{\lambda}}{\dot{\lambda} + \frac{\widetilde{M}_{\widetilde{x}}}{\widetilde{M}_{\widetilde{y}}}(1 - \dot{\lambda})} \ , \tag{4.22}$$

  where $\widetilde{M}_{\widetilde{x}}$ and $\widetilde{M}_{\widetilde{y}}$ is the molecular weight of the mixture in the liquid and vapor phase respectively. More details about the set of equations 4.21-4.22 will be given in the latter part of this chapter (section 4.8) in connection with the p, T-flash problem.

- Thermodynamic equilibrium: If a thermodynamic equilibrium is assumed a relationship between $\widetilde{y}$ and $\widetilde{x}$ may be obtained as

$$\frac{\widetilde{y}_i}{\widetilde{x}_i} = \frac{\phi_{i,L}(T, p, \widetilde{x})}{\phi_{i,G}(T, p, \widetilde{y})} \ , \tag{4.23}$$

  where $\phi_{i,G}(T, p, \widetilde{y})$ and $\phi_{i,L}(T, p, \widetilde{y})$ is the fugacity coefficient of the component i in the vapor and liquid phase respectively.

- Equation of state: An equation of state is required to close the problem at hand. In the present work the fundamental equation of state of Tillner-Roth [137] for the R134/R290 mixture (see Appendix B) is adopted.

Scheme of calculation: The following procedure is used in the calculation of the bubble point temperature.

1. read input variables: saturation pressure p_s, mass flow rate $\dot{M}$, bulk composition $\widetilde{z}$, electrical heat supplied to each heating zone $\dot{Q}_{el,i}$, the subcooling pressure p_f and subcooling temperature T_f at the inlet of the preheater.

2. calculate the enthalpy of the subcooling fluid at the inlet of the preheater and the reference enthalpy and temperature as

$$\begin{aligned} h_{sub} = &\quad h(T_f, p_f, \widetilde{z}) \ , \\ T_0 = &\quad h(p_s, \widetilde{x} = \widetilde{z}) \ , \\ h_0 = &\quad h(T_0, p_s, \widetilde{x} = \widetilde{z}) \ . \end{aligned}$$

   These are calculated using a software which is already available under the name "*Progs*" at the Institute for Thermodynamic, University of Hannover, Germany. The program "*Progs*" contains a number of subroutines which can be called separately by the user.

3. initial guess for bubble point temperature $T = T_{quess}$.

4. calculate the quality $\dot{x}$, the liquid mole fraction $\widetilde{x}$ and the vapor mole fraction $\widetilde{y}$. These are calculated iteratively using the set of equations 4.21-4.23 coupled with the fundamental equation of the state of Tillner-Roth [137] for the R134/R290 mixture; a calculation algorithm is shown in Fig. 4.23.

5. calculate the isobaric specific heat $c_{pl}(T, p_s, \widetilde{x})$, $c_{pg}(T, p_s, \widetilde{y})$ and the enthalpy of evaporation $\Delta h_V(T, p_s, \widetilde{x}, \widetilde{y})$. These are also calculated using the program "*Progs*" indicated above.

6. calculate the new value of the bubble point $T = T_{new}$ using equation 4.20

7. if $|T_{quess} - T_{new}| \geq 10^{-2}$ then the steps 3 - 6 are repeated until a convergence is obtained.

Based on the present formulation the level of uncertainty of the bubble point temperature is evaluated in accordance with a 95 % confidence limit as

$$U_T^2 = \left(\frac{dT}{d\dot{M}}\right)^2 U_{\dot{M}}^2 + \sum \left(\frac{dT}{d\dot{Q}_i}\right)^2 U_{\dot{Q}_i}^2 + \left(\frac{dT}{dT_0}\right)^2 U_{T_0}^2 + \left(\frac{dT}{dh}\right)^2 U_h^2 +$$

$$\left(\frac{dT}{d\Delta h}\right)^2 U_{\Delta h}^2 + \left(\frac{dT}{dh_0}\right)^2 U_{h_0}^2 + \left(\frac{dT}{d\dot{x}}\right)^2 U_{\dot{x}}^2 + \left(\frac{dT}{dc_{pl}}\right)^2 U_{c_{pl}}^2 + \left(\frac{dT}{dc_{pg}}\right)^2 U_{c_{pg}}^2 \qquad (4.24)$$

The partial derivative of T with respect to each of the various parameters is obtained from equation 4.20. The uncertainty of the mass flow rate $U_{\dot{M}}$ and the heat supplied to the preheaters $U_{\dot{Q}}$ is given in chapter 3 while that for the thermodynamic properties (*e.g.* $U_{\Delta h}$, $U_{c_{pl}}$) is obtained using the fundamental equation of state Tillner-Roth [137] for the R134a/R290 mixture. Fig. 4.5 presents the level of uncertainty for a wide range of temperatures for zeotropic R134a/R290 mixtures. The level of uncertainty in the predicted tem-

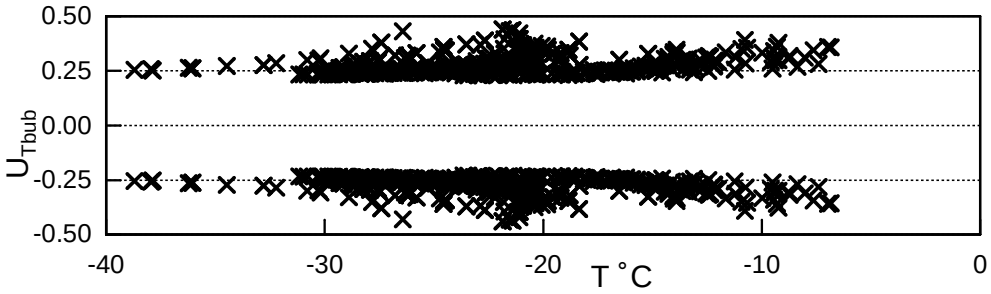

Figure 4.5. The level of uncertainty in the calculated saturation temperature for zeotropic R134a/R290 mixtures.

perature varies between 0.2 and 0.5 K. A similar level of uncertainty is obtained when the scheme of calculation is tested using the available thermodynamic tables for R32-R134a mixtures taken from Tillner-Roth et al. [139]. Clearly the simplification of equation 4.17 resulted in a relatively high error in the prediction of the bubble point temperature of zeotropic R134a/R290 mixtures. An error of 0.5 K in the saturation temperature yields an error of 10 to 20 % in the measured heat transfer coefficient ($\alpha = \dot{q}/\Delta T$) for a wall superheat of 10 to 5 K. The PTB calibrated temperature sensor designated the identifier **T Y2 25** in Fig. 3.5 which is used for the measurement of the refrigerant temperature has a maximum level of uncertainty of ±0.044 K (see Appendix A); almost $\frac{1}{5}$ to $\frac{1}{10}$ times the predicted one (cf. Fig.4.5). Against this background the measured temperature using the PTB calibrated thermometer is considered in this work rather than the predicted one.

4.4 Wall temperature

It is conventionally assumed that a constant wall temperature may be realized via film condensation on external horizontal tube. Therefore the validity of this assumption for the present work has to be validated. For this purpose the wall temperature is measured at the top, sides and bottom of at the outside of the horizontal tube. Fig. 4.6 depicts the measured wall temperature for the condensation of ammonia on external horizontal tube under various flow conditions. Clearly only at very low heat flux the measured wall temperature is nearly constant. At relatively high heat flux the measured wall temperature profile suggests a harmonic-like temperature profile as

$$T_w(\varphi) = C_1 + C_2 \cos(C_3 \varphi^n) \ . \tag{4.25}$$

where C_1, C_2, C_3 are constants and n is an exponent. The exponent n accounts for the unsymmetrical distribution of the wall temperature. The unsymmetrical distribution of the wall temperature is caused by the partial wetting of the inner surface of the tube.

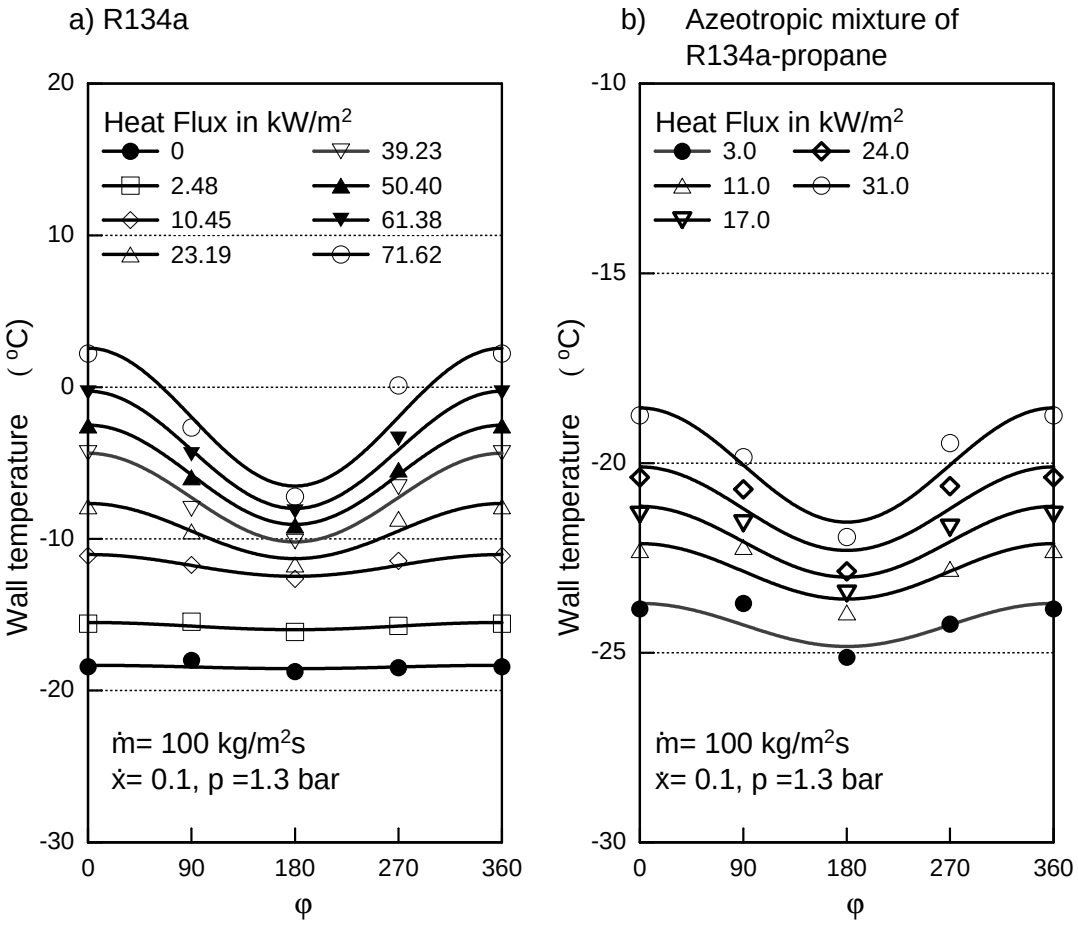

Figure 4.6. Wall temperature profiles around the condensor tube at constant quality and saturation temperature at the inlet of the test section a) the coolant is two phase R134a b) the coolant is a two phase azeotropic mixture. The solid line is a cosine fit.

Along the axis of symmetry at the bottom of the tube ($\varphi = \pi$) the film thickness becomes increasing large due to gravity. Hence the tangential heat transfer due to thermal conduction tends to diminish at this position ($\varphi = \pi$). In turn this scenario yields the following boundary condition

$$\left(\frac{dT_w(\varphi)}{d\varphi}\right)_{\varphi=\pi} = 0 \ . \tag{4.26}$$

Likewise at the top of the tube ($\varphi = 0$) where the film thickness diminishes, the tangential heat transfer due to thermal conduction tends to diminish as well, thus

$$\left(\frac{dT_w(\varphi)}{d\varphi}\right)_{\varphi=0} = 0 \ . \tag{4.27}$$

With these boundary conditions and the measured wall temperature at the top $T_w(0)$, side $T_w(\pi/2)$ and bottom $T_w(\pi)$ of the tube the constant $C_1,\ C_2,\ C_3$ and the exponent n may be evaluated as

$$C_1 = \frac{T_w(0) + T_w(\pi)}{2} \ , \tag{4.28}$$

$$C_2 = \frac{T_w(0) - T_w(\pi)}{2} \ , \tag{4.29}$$

$$C_3 = \pi^{1-n} \ , \tag{4.30}$$

$$C_4 = \frac{2T_w(\pi/2) - T_w(0) - T_w(\pi)}{T_w(0) - T_w(\pi)} \ , \tag{4.31}$$

$$n = \frac{\ln[\pi / \arccos C_4]}{\ln 2} \ . \tag{4.32}$$

For the sake of simplicity the exponent n is assumed to approach a unit ($n \to 1$). Thus equation 4.30 yields $C_3 \to 1$ and equation 4.25 reduces to a simple cosine temperature profile as

$$T_w(\varphi) = C_1 + C_2 \cos\varphi \ , \tag{4.33}$$

where C_1 is the mean wall temperature

$$C_1 = \overline{T}_w = \frac{1}{2\pi} \int_0^{2\pi} T_w(\varphi) \, \mathrm{d}\varphi \ , \tag{4.34}$$

which upon integration reduces to the arithmetic mean as

$$\overline{T}_w = \frac{1}{N} \sum_{i=1}^{N} T_w(\varphi) \ , \tag{4.35}$$

where N is the number of the measurement nodes around the tube. The constant C_2 is the amplitude of the cosine wall temperature distribution.

Similar wall temperature profiles were previously observed by Kabelac and de Buhr [63] for condensation of ammonia, Lee et al. [83] for condensation of R113 and ethanediol and Memory and Rose [91] for ethylene glycol on external film condensation on the outside of a horizontal tube.

For saturated vapor, the local temperature drop across the condensate film is

$$T_c - T_w(\varphi) = \Delta\overline{T}(1 - A\cos\varphi) \ , \tag{4.36}$$

where

$$\Delta\overline{T} = T_c - \overline{T}_w \ , \tag{4.37}$$

and

$$A = \frac{C_2}{\Delta\overline{T}} \ . \tag{4.38}$$

T_c is the interface temperature, which is supposed to be the saturation temperature. For ammonia it is calculated using the fundamental equation of state of Tillner-Roth [137]. Memory and Rose [91] have justified the existence of two possible extreme limits of the cosine amplitude C_2 as

- for a uniform condensation film thickness or in other words uniform angular wall temperature distribution, the amplitude of the cosine wall temperature profile tends to zero $C_2 \rightarrow 0$. This is clearly demonstrated in Fig. 4.6 at low heat flux ($\dot{q} \leq 30$ kW/m^2). This indicates that at low heat flux conditions the assumption of constant wall temperature may be justified.

- for a complete dryout at the top outside wall of tube where $T_w(0) \rightarrow T_c$ the amplitude of the cosine wall temperature profile is $C_2 \rightarrow T_c - \overline{T}_w$. At the lower half of the tube $\varphi = \pi$, where the film thickness becomes infinite because of gravity and hence $T_w(\pi) \rightarrow T_c$, the amplitude of the cosine wall temperature profile is $C_2 \rightarrow (T_c - \overline{T}_w)$.

Upon utilizing the above mentioned two extreme limits of C_2, equation 4.38 yields the limit of the amplitude of the temperature drop across the condensate film as $0 \leq A \leq 1$. Fig. 4.7 presents the measured amplitude of the temperature drop across the condensate film; A. The results clearly demonstrate the above mentioned two extreme limits of $0 \leq A \leq 1$.

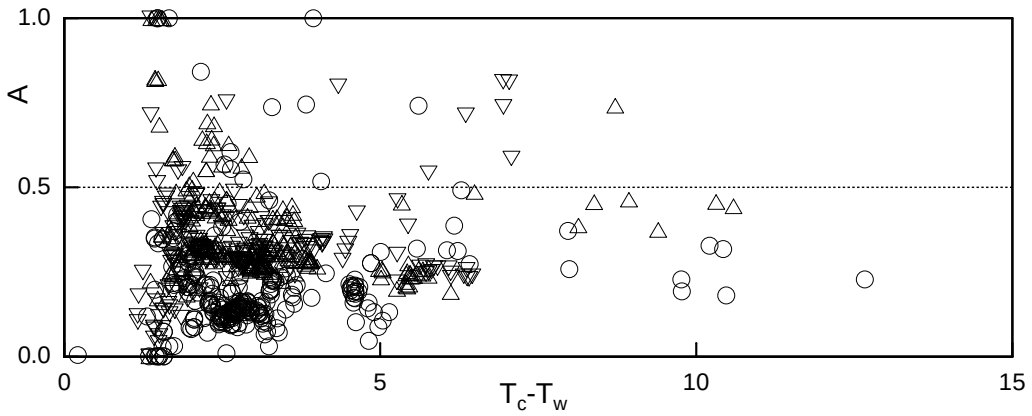

Figure 4.7. Dependency of cosine amplitude A on the local temperature drop across the condensate film. Legend: (○) S1, (△) S2 and (▽) S3.

4.5 Wall superheat

Fig. 4.8 shows a typical behavior of the inside wall temperature $\overline{T}_{wi}$, the saturation temperature T_s and condensation temperature T_c during flow boiling of R134a in a horizontal tube. At early stage of evaporation ($\dot{x} < 0.1$) the fluid temperature is slightly increased. This is the region of the onset of the nucleate boiling. In this region the bubbles formed at the wall collapse in the bulk of the liquid phase. Thus the heat is transferred by the bubble from the wall to the bulk of the liquid phase and as a consequence the bulk fluid temperature increases. Beyond this region the bulk temperature slightly decrease almost remained constant. This is attributed to the pressure drop in the tube during the evaporation process. The decrease in the wall temperature with quality is apparent, indicating improved heat transfer conditions.

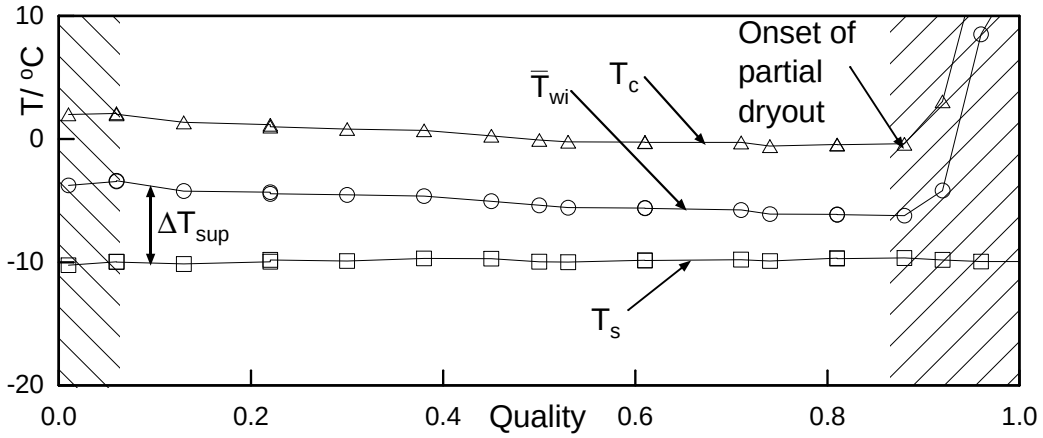

Figure 4.8. Wall, refrigerant and condensate film temperature in a saturated flow boiling of R134a ($\dot{m}$=200 kg/m^{2}s, $\dot{q}$= 16.5 kW/m^2).

As $\dot{x} \rightarrow 1$ the condensate temperature, so does the wall temperature, is sharply increased. The increase in the wall temperature is due to diminishing of the liquid film at the inside (boiling side) of the tube wall which leads to the onset of the dryout. The increase in the condensate temperature is attributed to the decrease in the overall heat transfer coefficient k as

$$T_c = T_s + \frac{\dot{q}}{k} \; . \tag{4.39}$$

The decrease in the overall heat transfer coefficient is caused by the decrease in the flow boiling heat transfer coefficient inside the tube due to dry out. That is to say as $\dot{x} \rightarrow 1$ the flow boiling heat transfer coefficient approaches that for the vapor phase which is far lower than that for the liquid or two phase. Steiner [128] indicated that the heat transfer coefficient of the liquid is 2 to 3 times the heat transfer coefficient of the vapor.

As a consequence of the saturation temperature of the boiling refrigerant and the wall temperature profiles, the wall superheat

$$\Delta T_{sup} = \overline{T}_{wi} - T_s, \tag{4.40}$$

is relatively large at the initial stage of boiling. This conditions is necessary to activate the nucleation site for the onset of the bubbles. As the nucleate boiling effect diminishes during the transition from nucleate to convective boiling region stable saturation and wall temperature profile develop and so does the wall superheat.

The overall trend of the wall superheat with progressive evaporation observed in the present work is consistent with observations reported in VDI-Wärmeatlas [143] and Urso et al. [140] for a horizontal tube.

4.6 Heat flux

In the present study the heat required for evaporating the test refrigerant was supplied via condensation of ammonia at the outside wall of the test tube. This implies a thermal boundary condition of a non-constant heat flux. Therefore the distribution of the

heat flux in the angular and axial direction need to be established. Nusselt [102], almost nine decades ago, has solved the problem of film condensation under isothermal wall temperature. In the present study the wall temperature was found, however, to be non-isothermal. Thus the effect of this non-isothermal wall temperature distribution on Nusselt [102] theory of film condensation needed to be studied.

4.6.1 Angular heat flux

Fig. 4.9 depicts the physical model and the coordinate system of the laminar condensate film on external horizontal tube. As in the Nusselt [102] theory, a momentum balance for

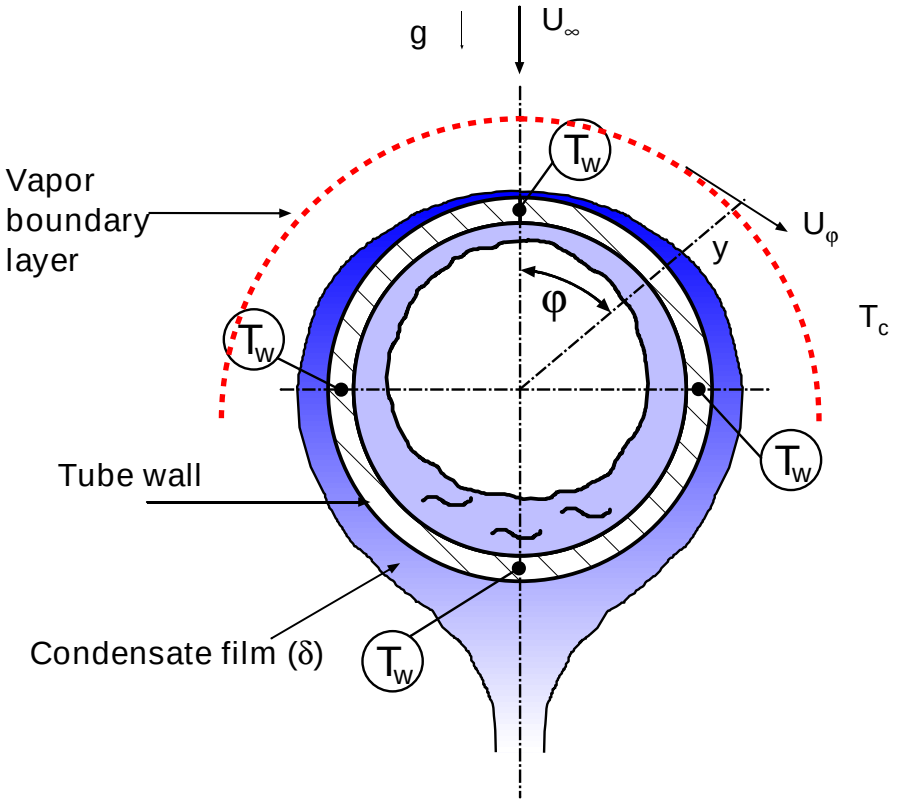

Figure 4.9. Physical Model and coordinate system.

an element in the condensate film yields

$$\frac{d}{dy}\left(\frac{du}{dy}\right) + \rho g \sin\varphi - \frac{1}{r}\frac{dp}{d\varphi} = 0, \tag{4.41}$$

where u is the tangential condensate velocity and y is the distance measured radially from the outer wall of the tube. r is the radius of the tube, g is acceleration due to gravity and ρ is liquid density of the condensate film. Integration of equation 4.41 twice with zero velocity at the tube wall

$$y = 0, \qquad u = 0,$$

and the shear stress (τ_δ) at the interface of the vapor-condensate film

$$y = \delta \qquad \tau = \tau_\delta = \frac{1}{\eta}\frac{du}{dy}\bigg|_{y=\delta} ,$$

gives the velocity distribution in the condensate film as

$$u = \frac{1}{\eta}\left[\tau_\delta y - \left(\rho g \sin\varphi - \frac{1}{r}\frac{dp}{d\varphi}\right)\left(\frac{y^2}{2} - \delta y\right)\right] . \tag{4.42}$$

The mass flow rate per unit width is given by

$$\dot{m} = \rho \int_0^\delta u dy . \tag{4.43}$$

Substitution of velocity distribution given by equation 4.42 into equation 4.43 yields

$$\dot{m} = \frac{\rho}{\eta}\left[\frac{\tau_\delta \delta^2}{2} + \frac{\left(\rho g \sin\varphi - \frac{1}{r}\frac{dp}{d\varphi}\right)\delta^3}{3}\right] . \tag{4.44}$$

If the condensate film is at the saturation temperature T_c and the wall temperature is $T_w(\varphi)$, the heat transfer by conduction to an element of length $rd\varphi$ per unit width is

$$d\dot{Q} = \frac{\lambda(T_c - T_w(\varphi))}{\delta}.rd\varphi . \tag{4.45}$$

The mass rate per unit width of condensate in this area ($rd\varphi$) is therefore

$$d\dot{m} = \frac{\lambda(T_c - T_w(\varphi))}{\delta \Delta h_V} rd\varphi , \tag{4.46}$$

where Δh_V is the enthalpy of condensation. Upon utilization of the cosine wall temperature profile, equation 4.36, into equation 4.46 the mass equation 4.44 yields the differential equation for the condensate film thickness as

$$\frac{d}{d\varphi}\left\{\frac{\rho}{\eta}\left[\frac{\tau_\delta \delta^2}{2} + \frac{\left(\rho g \sin\varphi - \frac{1}{r}\frac{dp}{d\varphi}\right)\delta^3}{3}\right]\right\} = \frac{\lambda \Delta\overline{T}(1 - A\cos\varphi)}{\delta \Delta h_V} r . \tag{4.47}$$

In order to close equations 4.47 the interfacial shear stress τ_δ and the pressure gradient $dp/d\varphi$ remained to be specified. For the determination of the shear stress and pressure gradient two types of boundary conditions have been considered: the stagnant vapor which exerts no drag ($\tau_\delta = 0$) and flowing vapor which exerts a drag ($\tau_\delta \neq 0$) at the vapor-condensate interface; y=δ.

Case I $\tau_\delta = 0$: In the case of zero vapor velocity (*i.e.* $\tau_\delta = 0$) all Nusselt's [102] assumptions of film condensation theory were maintained with exception of isothermal wall temperature. Nusselt's assumptions are listed as:

1. the vapor is considered quiescent,

2. the shear stress from the vapor at the wall of the condensate film ($y = \delta$) is negligible ($\tau_\delta = 0$),

3. the effect of the inertia and convection in the condensate film are negligible,

4. the condensate film and vapor are considered in equilibrium so that the condensate temperature is taken as the saturated vapor temperature,

5. condensate properties were assumed independent of the temperature,

6. the film thickness is assumed small in comparison with the tube radius and

7. only the hydrostatic pressure gradient

$$\frac{1}{r}\frac{dp}{d\varphi} = \rho_G g \sin\varphi, \tag{4.48}$$

is considered (*i.e.* the pressure gradient due acceleration and friction are neglected).

With these assumptions equation 4.47 becomes

$$F\left(\delta^{*3}\sin\varphi\frac{d\delta^*}{d\varphi} + \frac{\delta^{*4}}{3}\cos\varphi\right) = 2(1 - A\cos\varphi), \tag{4.49}$$

where

$$\delta^* = \delta\left[\frac{2U_\infty\rho}{d\eta}\right]^{1/2} = \sqrt{2}Re^{1/2}.\frac{\delta}{d}\ ; \quad Re = \tfrac{U_\infty\rho d}{\eta}\ ; \quad F = \frac{g\Delta h_V\eta d}{U_\infty^2\lambda\Delta\overline{T}} = \frac{Gr_d}{JRe^2}, \tag{4.50}$$

and

$$J = \frac{\lambda\Delta T}{\eta\Delta h_V},\ Gr_d = \frac{\rho\Delta\rho g d^3}{\eta^2}. \tag{4.51}$$

Here Re is defined as the two phase Reynolds number and U_∞ is the vapor velocity out side the boundary layer ($y = \infty$).

Equation 4.49 is solved for the film thickness under isothermal (A=0) and non-isothermal wall temperature ($A > 0$) conditions. The solution employs a fourth order-Rung-Kutta numerical scheme with an initial boundary condition of

$$\left.\frac{d\delta^*}{d\varphi}\right|_{\varphi=0} = 0\ . \tag{4.52}$$

The application of the this initial boundary condition to equation 4.49 yields an finite initial dimensionless film thickness as

$$\delta^*(0) = \left[\frac{6(1-A)}{F}\right]^{1/4}\ . \tag{4.53}$$

Examples of the film thickness is shown in Fig. 4.10a for isothermal wall temperature (A=0) and non-isothermal wall temperature for different values of A. At the upper part

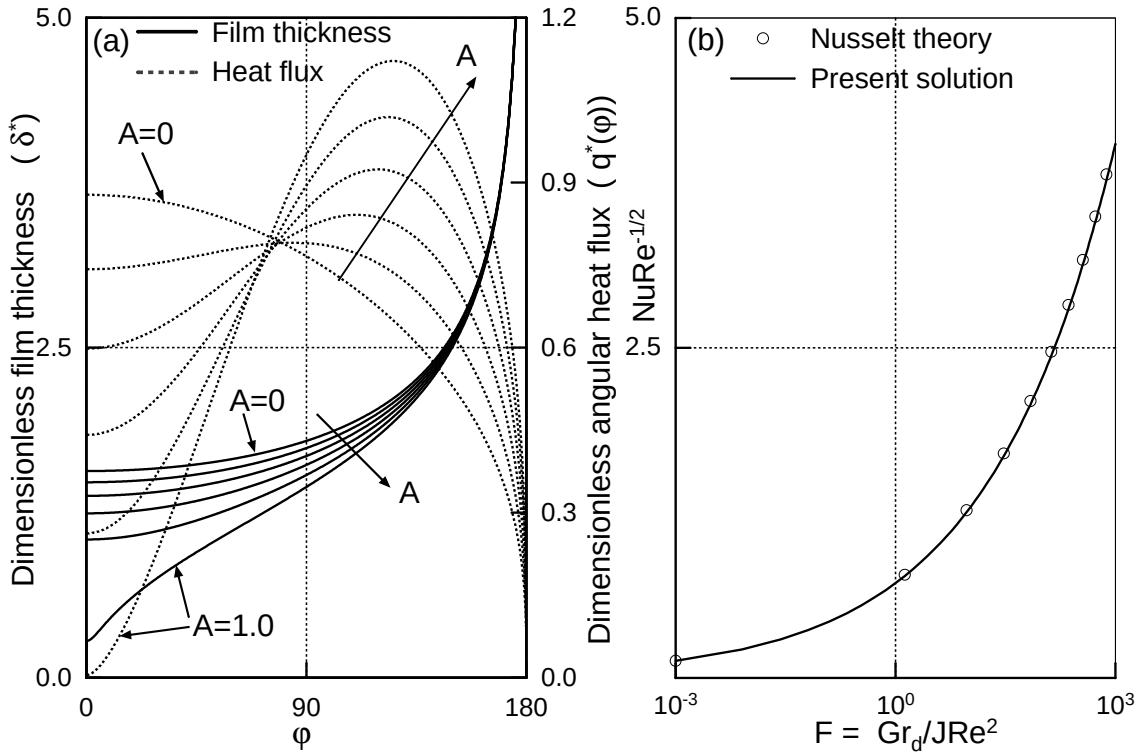

Figure 4.10. a) Specimen of the film thickness and angular heat flux for the case of $\tau_\delta = 0$, b) Comparisons between Nusselt's theory of film condensation and the result of the present solution under non-isothermal wall temperature condition. The calculation is based on $A = 0.4$.

of the tube ($\varphi \leq \pi/2$) the film thickness depends strongly on the wall temperature profile represented by A. At the rear part of the tube ($\varphi > \pi/2$) the film thickness is a weak function of the wall temperature profile. As $\varphi \to \pi$ the film thickness approaches infinity.

As in Nusselt's theory the angular heat flux up to the angle φ is given by

$$\dot{q}(\varphi) = \frac{\lambda \Delta \overline{T}(1 - A\cos\varphi)}{\delta}, \tag{4.54}$$

and the dimensionless heat flux is

$$\dot{q}^* = \frac{\dot{q}(\varphi)}{\dot{q}}, \tag{4.55}$$

where the mean circumferential heat flux is

$$\dot{q} = \frac{1}{2\pi}\int_0^{2\pi} \dot{q}(\varphi)d\varphi = \frac{1}{\pi}\int_0^{\pi} \frac{\lambda \Delta \overline{T}(1 - A\cos\varphi)}{\delta} d\varphi \ . \tag{4.56}$$

The dependence of the dimensionless angular heat flux $q^*(\varphi)$ on φ is shown in Fig. 4.10a for isothermal ($A = 0$) and non-isothermal ($A > 0$) wall temperature. It may be seen that, for isothermal wall temperature ($A = 0$), the heat flux decreases continuously around the tube. For non-isothermal wall temperature, as the amplitude A of the temperature difference across the condensate film increases, the heat flux at first rises, where the effect of the increasing value of ΔT outweighs that of increasing film thickness. The heat flux

subsequently reaches a maximum at the location on the lower half of the tube ($\varphi > \pi/2$) before decreasing to zero as the film thickness becomes infinite. It is seen that the points of intersections of the curves for different values of A are close to each other but not coincident.

The area under the curve of the heat flux shown in Fig. 4.10a, which is the mean circumferential heat flux, is found however, independent of the wall temperature distribution (*i.e.* A). To illustrate this point the corresponding mean circumferential Nusselt number

$$Nu = \frac{\dot{q}d}{\lambda \Delta T} = \sqrt{2} Re^{1/2} \frac{1}{\pi} \int_0^{\pi} \frac{(1 - A\cos\varphi)}{\delta^*} d\varphi \ , \tag{4.57}$$

is compared with the original Nusselt [102] theory of film condensation on horizontal tubes at constant wall temperature given as

$$Nu = 0.728 \left(\frac{\rho \Delta \rho g \Delta h_V d^3}{\eta \lambda \Delta T} \right)^{1/4} = 0.728 Re^{1/2} F^{1/4} \ . \tag{4.58}$$

As can be seen in Fig. 4.10b the results of the present analysis blended with the original Nusselt's solution equation 4.58; with absolutely no discrepancy. Hence, despite the wide variation of δ and $\dot{q}(\varphi)$ with angle φ the wall temperature profile has no effect on the mean Nusselt number. Thus for this case the original Nusselt model (equation 4.58) is adequate in the prediction of the mean circumferential heat flux with mean $\overline{\Delta T}$ replacing the uniform ΔT.

Case II $\tau_\delta \neq 0$: The effect of the interfacial shear stress on the film condensation of flowing vapor has been investigated by a number of researchers for example Rose [111], Fujii et al. [41] and Shekriladze and Gomelauri [122], Maekawa and Rose [113] and Rose [112], to mention a few. However, the existing works were carried out for isothermal condition (ΔT= constant). Thus the effect of non-isothermal wall temperature on film condensation needs to be investigated.

Since the primary objective here is to investigate the effect of the none uniform wall temperature on the film condensation theory, the simpler Shekriladze and Gomelauri [122] model for interfacial shear stress is adopted

$$\tau_\delta = \dot{m}' U_\varphi \ , \tag{4.59}$$

where $\dot{m}' = d\dot{m}/rd\varphi$ is the condensate mass flux and U_φ is the tangential velocity of the vapor (see Fig. 4.9). The above approximation has limitations and other models may be available, for example reference may be made to Rose [112]. However, equation 4.59 is useful in its simplicity. As in the earlier studies, potential flow outside the vapor boundary is considered so that

$$U_\varphi = 2U_\infty \sin\varphi, \tag{4.60}$$

and

$$\frac{dp}{d\varphi} = -2\rho_G U_\infty^2 \sin 2\varphi \ . \tag{4.61}$$

When equation 4.59 to equation 4.61 are used to eleminate τ_δ and $dp/d\varphi$ from equation 4.47 the resulting differential equation for the condensate film thickness is

$$\delta^* \frac{d}{d\varphi}\left[F_\delta(1 - A\cos\varphi)\sin\varphi\delta^* + \frac{\delta^{*3}}{3}\left(\frac{F}{2}\sin\varphi + 2P\sin 2\varphi\right)\right] = (1 - A\cos\varphi) \ , \qquad (4.62)$$

where

$$P = \frac{\rho_G \Delta h_v \eta}{\rho\lambda\Delta\overline{T}} = \frac{1}{J}\frac{\rho_G}{\rho} \ , \quad F_\delta = \begin{cases} 1 & : \quad \tau = \tau_\delta \\ & : \\ 0 & : \quad \tau = 0 \end{cases} \ , \qquad (4.63)$$

and F, δ^* and J are defined in equation 4.50.

The first term inside the derivative in equation 4.62 results from the shear stress while the term involving P is due to the inclusion of the pressure gradient. When both of these terms are omitted equation 4.62 reduces to equation 4.49 of the case $\tau_\delta = 0$.

Before proceeding to obtain solutions to equation 4.62 and hence to calculate the heat flux for the tube, two points may be noted. That is to say: is equation 4.62 can be solved for the case $\delta \to \infty$? and what are the conditions which lead to this problem of infinite film thickness?. First the possibility that condensate velocity gradient at the wall may go to zero is considered. This would lead to re-circulation or 'separation' of the flow in the condensate film. The separation of the flow is identified with large film thickness; $\delta \to \infty$. $(du/dy)_{y=0}$ may be obtained from equation 4.42 with the shear stress and pressure gradient is defined by equation 4.59 and equation 4.61 respectively. It may be shown that the condition

$$\left(\frac{du}{dy}\right)_{y=0} \leq 0 \ , \qquad (4.64)$$

becomes

$$1 - A\cos\varphi + \frac{\delta^{*2}}{2}\left(\frac{F}{2} + 4P\cos\varphi\right) \leq 0 \ . \qquad (4.65)$$

Evidently equation 4.65 can only be satisfied for $\pi/2 < \varphi < \pi$ and only when $P > F/8$.

Secondly the possibility that the gradient of the film thickness $d\delta^*/d\varphi$ becomes infinite. When this condition is applied to equation 4.62 the result is

$$1 - A\cos\varphi + \delta^{*2}\left(\frac{F}{2} + 4P\cos\varphi\right) = 0 \ . \qquad (4.66)$$

As in equation 4.65, equation 4.66 can only be satisfied for $\pi/2 < \varphi < \pi$ and again only when $P > F/8$. This implies that the critical angle φ_c, the value of φ satisfying equation 4.66, is

$$\varphi_c = \arccos\left(\frac{-F}{8P}\right) \ . \qquad (4.67)$$

Clearly the condition given by equation 4.66 will be met at smaller value of φ than that given by equation 4.65. Since for $P > F/8$ the solution of equation 4.62 will not be possible beyond φ_c, the conditions and associated problems given by equation 4.64 and equation 4.65 do not arise.

As for the case $\tau_\delta = 0$ a numerical solution of equation 4.62 has been obtained under isothermal ($A = 0$) and non-isothermal wall temperature ($A > 0$) conditions. The solution employs a fourth order Rung-Kutta numerical scheme with the initial boundary condition of

$$\left.\frac{d\delta^*}{d\varphi}\right|_{\varphi=0} = 0 \ . \tag{4.68}$$

The application of the this initial boundary condition to equation 4.62 yields an finite initial dimensionless film thickness as

$$\delta^*(0) = \left\{ \frac{3(1-A)}{8P+F} \left[-F_\delta + \sqrt{F_\delta^2 + \frac{2(8P+F)}{3(1-A)}} \right] \right\}^{1/2} \ . \tag{4.69}$$

For the case $F_\delta = 0$ and $P = 0$ equation 4.69 reduces to that for the case $\tau_\delta = 0$ given by equation 4.53. Examples of film thickness profiles and the dimensionless angular heat flux

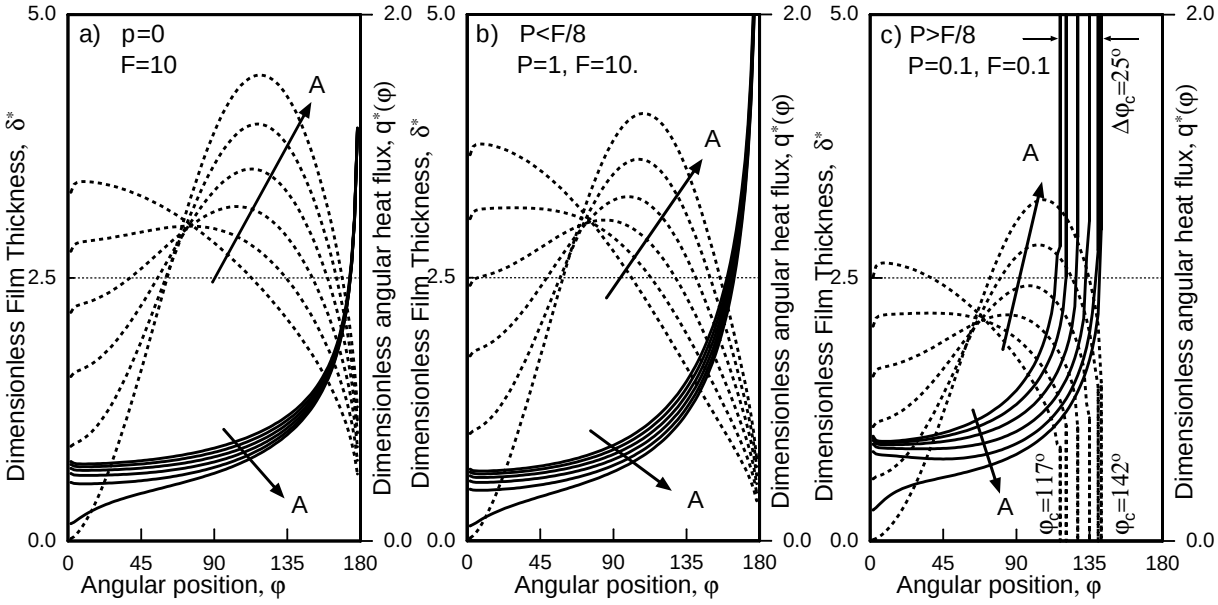

Figure 4.11. Specimen of film thickness and angular heat flux under the influence of the shear stress.

$\dot{q}^*(\varphi)$ given by equation 4.55, are shown in Fig. 4.11b-c for three cases: $P = 0$, $P < F/8$ and $P \geq F/8$ respectively. The results show similar profiles as for the case of zero vapor velocity ($\tau_\delta = 0$). Additionally, for the case of $P \geq F/8$, the present solution gives φ_c= 142 ° for the extreme case ($A = 1$) of non-isothermal wall temperature and only φ_c= 117 ° for the case of isothermal wall temperature ($A > 0$); a difference of 25 °. The significance of the increase of the critical angle will be explained in the latter part of this section.

As indicated earlier, a solution of equation 4.62 will only possible for the whole tube when $P < F/8$. For this case the dependency of the mean heat flux and it is corresponding Nusselt number on the wall temperature may be determined numerically for various values of F and P using equation 4.57. This is shown in Fig. 4.12a,b under both isothermal ($A = 0$) and non-isothermal wall temperature. It is clear that, as for the case of zero

shear stress ($\tau_\delta = 0$), the wall temperature distribution has no influence on the mean Nusselt number. The discrepancy in Nusselt number between the case of isothermal and non-isothermal wall temperature does not exceeded 1 %. The comparison with the original Nusselt's theory of film condensation indicates a large deviation in the region where the effect of vapor velocity overwhelms the gravity effect; $F < 1$. The ratio between the gravity and the vapor velocity is represented by the factor $F = Gr_d/JRe$, where the Grashhoff number Gr_d is the measure of the gravity effect while Reynolds number Re is a measure to the velocity effect. In the region where the the gravity effect overwhelms the vapor velocity $F \gg 1$ the present solution blended with the original Nusselt's model.

For the case $P \geq F/8$ it is not possible to obtain a solution for equation 4.62 for the whole tube. Under such circumstances and upon using equations 4.57 the mean Nusselt number for the whole tube may be written as

$$Nu = \sqrt{2}Re^{1/2}\frac{1}{\varphi_c}\int_0^{\varphi_c}\frac{(1 - A\cos\varphi)}{\delta^*}d\varphi + \sqrt{2}Re^{1/2}\frac{1}{\pi - \varphi_c}\int_{\varphi_c}^{\pi}\frac{(1 - A\cos\varphi)}{\delta^*}d\varphi \ . \quad (4.70)$$

Clearly, only the first term of equation 4.70 may be evaluated. The second term, where $\delta^* \to \infty$, is conventionally neglected. The previous works of Fujj [41] and Rose [111] for isothermal wall temperature ($A = 0$) indicated that the omission of the second term of equation 4.70 does not cause significant error in the prediction of the mean Nusselt number for the whole tube. This means that for an isothermal wall temperature, where $\varphi_c = 117\ ^\circ$, the heat flux is neglected almost on **35** % of the tube. While for the extreme case ($A = 1$) of non-isothermal wall temperature, where the $\varphi_c = 142^\circ$, the heat flux is neglected only in about **20** % of the tube. Clearly the inclusion of the non-isothermal wall temperature in the analysis makes the heat flux to be predicted for a large part of the tube, it is an enhancement of **15** %.

The numerical results obtained using equation 4.70 are shown in Fig. 4.12c. As for the cases of $P < F/8$ at values $F < 1$ clearly there is a weak dependency of the mean Nusselt number on the wall temperature. At values $F > 1$ the wall temperture has significant effect on the mean Nusselt number. The discrepancy between Nusselt number for the cases of isothermal and non-isothermal wall temperature exceeded 5 %. This may be attributed to the enhancement in the predicted critical angle φ_c. In the light of the above it is clear that as for the case of $\tau_\delta = 0$ the non-isothermal wall temperature distribution (*i.e.* $A > 0$) has no effect on the mean heat flux at low pressure gradient effect ($P < F/8$). At high pressure gradient effect ($P \geq F/8$) the effect of the non-isothermal wall temperature distribution must be taken into account.

4.6.2 Axial heat flux

In the preceding sections it was established that the heat flux depends on the angular position (cf. Fig. 4.10). Likewise, and despite the fact that the test tube evaporator is short in length (0.5 m), the variation of the heat flux in the axial direction may not be completely ruled out. This may be attributed to the following reasons:

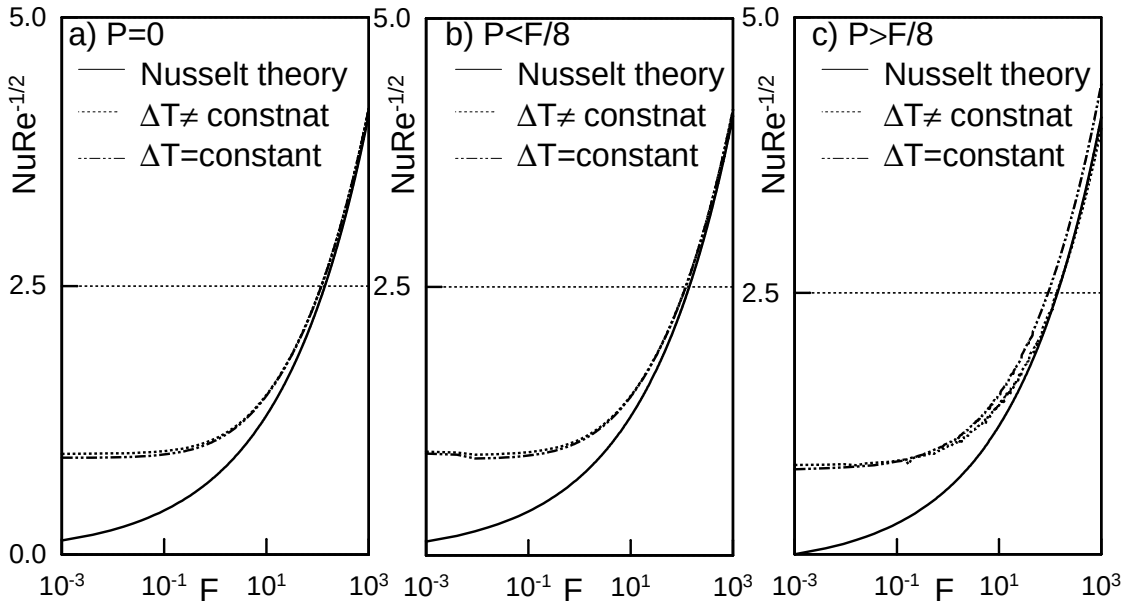

Figure 4.12. The effect wall temperature on the Nusselt's theory of film condensation under flowing vapor (*i.e.* $\tau_\delta \neq 0$) conditions.

1. the saturation temperature of the refrigerant flowing inside the tube drops in the direction of flow because of the pressure drop. As a consequence the overall driving temperature difference $T_c - T_s(z)$ increases in the direction of flow. In turn this leads to the increase in the heat flux in the direction flow, $\dot{q}(z) = k[T_c - T_s(z)]$, where k is the overall heat transfer coefficient.

2. the flow boiling inside heat transfer coefficient depends on the quality $\dot{x}$, which increases in the direction of flow due to progressive evaporation. The increase of the inside heat transfer coefficient causes the *overall* heat transfer coefficient k and subsequently the heat flux to increase in the direction of flow. The overall heat transfer coefficient based on the condensation side is defined as

$$\frac{1}{k} = \frac{1}{\alpha_c} + \frac{d_o}{2\lambda_w} \ln\left(\frac{d_o}{d_i}\right) + \frac{d_o}{d_i}\frac{1}{\alpha_i} \ , \tag{4.71}$$

   where α_c and α_i are the condensation and boiling side heat transfer coefficients.

As an illustration Fig. 4.13 shows the variation of the local heat flux with axial position. The local heat flux is calculated using the condensation model for the case $\tau_\delta = 0$ given by equation 4.56 at the three measurement sections along the test tube. The results clearly confirm the above postulations and suggest that

$$\dot{q}(z) = a + b.z \ , \tag{4.72}$$

where a and b are constants.

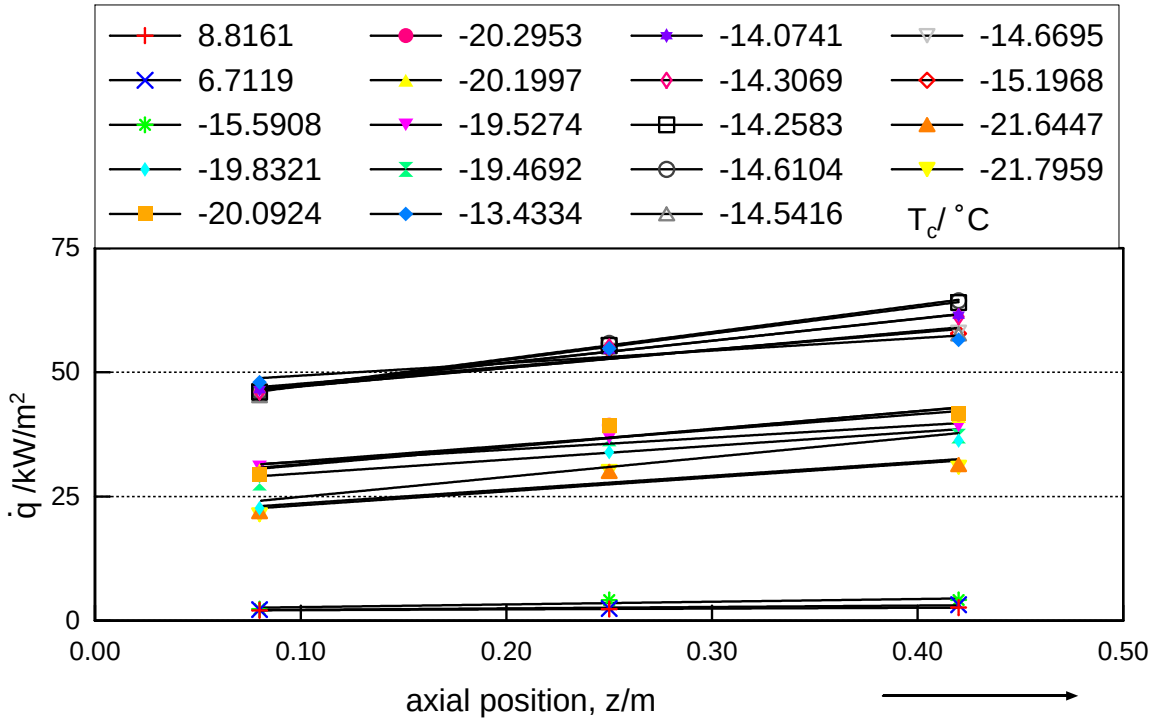

Figure 4.13. Variation of the local heat flux $\dot{q}(z)$ with axial position under various flow conditions.

4.6.3 Validation of the heat flux model

In the preceding analysis the condensation problem is solved for non-uniform wall temperature incorporating the Nusselt's assumptions which are listed earlier in subsection 4.6.1. Thus, before making comparisons with measurements, it is required to justify the applicability of Nusselt's assumptions to the present study. For this purpose the limits of the present working conditions are identified as shown in Fig. 4.14. These are summarized as:

$$10^4 \leq F(=\tfrac{Grd}{JRe^2}) \leq 10^9(\rightarrow\infty), \quad P/F \leq 10^{-5}(\rightarrow 0)$$

$$Re(=\tfrac{U_\infty \rho d}{\eta}) < 1000 \qquad J < 0.02, \qquad Pr < 1.0$$

To be remembered is that the vapor velocity U_∞ used to calculate the Reynolds number Re is defined by the VDI-Wärmeatlas [143] as the main steam vapor velocity which is calculated using the energy balance as

$$U_\infty = \frac{\dot{Q}}{\pi d_o L \rho \Delta h_V} \,, \tag{4.73}$$

where $\dot{Q}$ is the heat supplied to evaporate the ammonia, d_o and L is the outside diameter and the length of the test tube respectively.

The low value of Reynolds number ($Re < 1000$) justifies Nusselt's assumption of laminar condensate film to the present study. Additionally, being $F \rightarrow \infty$, this means that the gravity effect represented by Gr overwhelms the velocity effect represented by JRe^2.

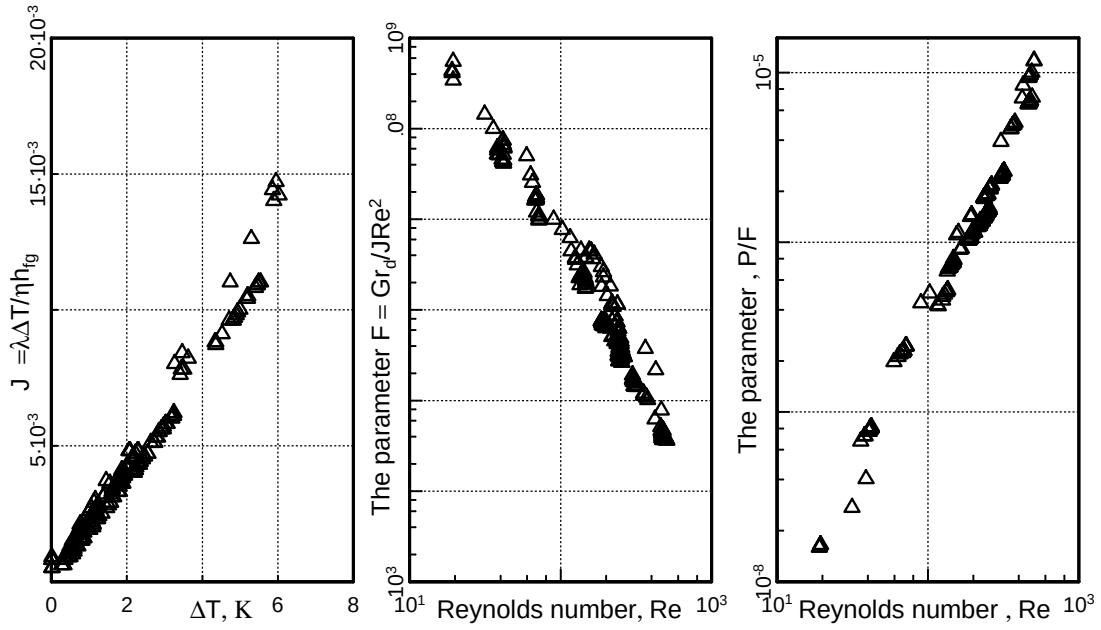

Figure 4.14. Range of parameters used in the present experimental study.

Consequently this justifies the applicability of Nusselt's assumption of quiescent vapor rather than flowing vapor to the present analysis. However, the present working conditions do hold true for Nusselt's idealization of:

- subcooling of liquid is negligible in the energy balance (i.e convection effect),
- condensate properties are considered to be independent of temperature,
- the shear stress at the condensate-vapor interface is negligible.

Thus the influence of these idealizations on Nusselt's theory of film condensation need to be quantified. These are itemized below:

- **Subcooling:** The idealization of convection in the energy equation automatically precludes condensate subcooling. There exist a number of ways of removing the idealization of subcooling, see for examples Chen [18] and Rose [112], to mention a few. However, the most widely accepted method is to include the effect of the condensate subcooling in the energy equation 4.45 as

$$\frac{d\dot{Q}}{rd\varphi} = \frac{\lambda(T_c - T_w(\varphi))}{\delta} = \Delta h_V \frac{d\dot{m}}{rd\varphi} + \frac{d}{rd\varphi}\int_0^\delta \rho c_{pl} u \Delta T dy \ . \tag{4.74}$$

  The second term in the right hand side of equation 4.74 represents the subcooling effect. The analysis of Rohsenow et al. [110] and Carey [16], among other, to equation 4.74 indicated that the effect of subcooling and energy convection can be incorporate by replacing Δh_V in Nusselt [102] model; equation 4.58 with

$$\Delta h_V^* = \Delta h_V + 0.68 c_p \Delta T \ . \tag{4.75}$$

Fig. 4.15 shows the effect of incorporation of equation 4.75 in Nusselt's theory of film condensation for the range of parameters of the present study; $J(=\frac{\lambda\Delta T}{\eta\Delta h_V}) < 0.02$ (Fig. 4.14). The results show a deviation of less than 2 % from Nusselt original model. In this respect equation 4.75 is adopted for the correction of Nusselt theory for the subcooling effect.

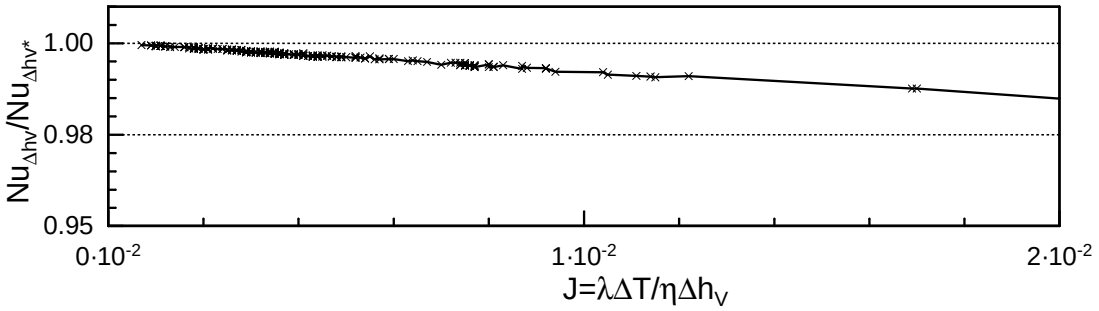

Figure 4.15. The effect of subcooling on Nusselt theory of film condensation.

- **Condensate properties:** Nusselt's assumption of the independency of the condensate properties on temperature is justified for the case of small temperature drop across the condensate film $(T_c - T_w)$. In any other case the change in the dynamic viscosity, thermal conductivity and, on a lower scale, the density of the condensate film with temperature has to be considered. There exist a number of ways to incorporate this effect. One way is to solve the momentum and energy equation for temperature dependent transport properties $(\eta = \eta(T),\ \lambda = \lambda(T),\ \rho = \rho(T))$ see for examples Voskresenskji [144] and Baehr and Stephan [2], to mention a few. However, the most widely accepted method to remove the idealization of condensate properties is to use Nusselt's's equation 4.58 with the value of the viscosity, thermal conductivity and density of the condensate film are taken at some effective condensate film temperature

$$T^* = T_c - \beta(T_c - T_w)\ . \tag{4.76}$$

  The recommended values of β differ somewhat among authors for different condensing fluids. However, the highest reported value is β =0.75 (Rohsenow et al. [110]). The vapor density ρ_G and enthalpy of evaporation Δh_V are evaluated at the saturation temperature T_c. Fig. 4.16 shows the effect of the reference temperature on Nusselt's theory of film condensation for the range of parameters investigated in the present studies. The result indicated that the idealization of the condensate properties yield a error of less than 2 % and increases with β.

- **Shear stress**: Nusselt's assumption of negligible shear stress is justified under the condition of stagnant vapor which exerts no drag; $\tau = 0$. However, for flowing vapor which exerts a drag $(\tau = \tau_\delta)$ the effect of the vapor shear stress on film condensation must be considered. To identify which case is applicable to the present study the factor $F = \frac{Gr_d}{JRe}$, which is a measure of the relative importance of gravity (stagnant

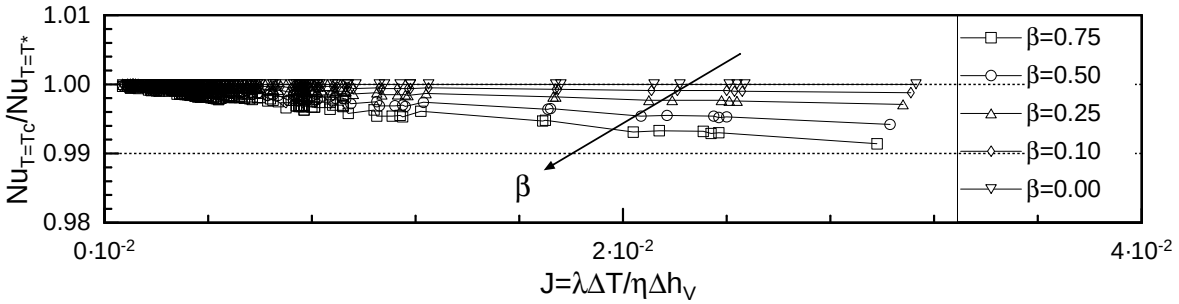

Figure 4.16. The effect of the dependency of the condensate properties on temperature on the Nusselt theory of film condensation.

vapor) and vapor velocity, is accepted as a parameter. That is to say if the gravity effect represented by the Grashoff number Gr_d overwhelms the vapor velocity effect represented by Reynolds number Re the shear stress is neglected and *vis versa*. It is to be remembered that the vapor velocity needed for the calculation of Reynolds number is given by equation 4.73.

Refereing to Fig. 4.17 it is clear that for $F > 10^4$ the shear stress has negligible effect on the Nusselt's theory of film condemnation. In the present study $10^4 < F(= \frac{Gr_d}{JRe}) \leq 10^9(\rightarrow \infty)$ as shown in Fig. 4.14. Clearly the condition of flowing vapor does not a rise in the present study (*i.e.* $\tau = 0$).

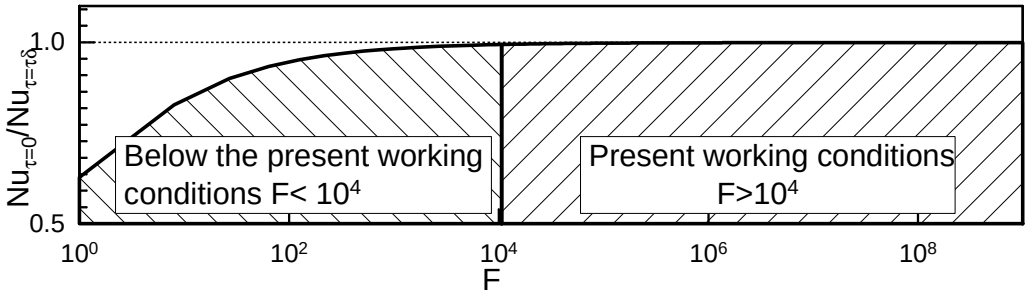

Figure 4.17. The effect of the shear stress on Nusselt theory of film condensation. $Nu_{\tau=0}$ and $Nu_{\tau=\tau_\delta}$ are given by Nusselt equation 4.58 and the present solution equation 4.70 respectively.

In the present study local measurement of heat flux on the test section was not possible. Nevertheless the total heat supplied to evaporate the heating medium, ammonia, is measured. Thus comparisons must be based on the total heat flow rate. For convenience the condensor is divided into two sections. With knowledge of linear variation of the heat flux in axial direction (cf. equation 4.72), the heat flux at each section is approximated by a linear relationship as

$$\dot{q}_I(z) = a_I + b_I.z, \quad \dot{q}_{II}(z) = a_{II} + b_{II}.z \ , \tag{4.77}$$

where

$$a_I = \dot{q}_I(z_1) - z_1 \frac{\dot{q}_I(z_2) - \dot{q}_I(z_1)}{z_2 - z_1}, \quad a_{II} = \dot{q}_{II}(z_2) - z_2 \frac{\dot{q}_{II}(z_3) - \dot{q}_{II}(z_2)}{z_3 - z_2} \ , \tag{4.78}$$

and

$$b_I = \frac{\dot{q}_I(z_2) - \dot{q}_I(z_1)}{z_2 - z_1}, \quad b_{II} = \frac{\dot{q}_{II}(z_3) - \dot{q}_{II}(z_2)}{z_3 - z_2} \ . \tag{4.79}$$

The heat load for the whole tube is

$$\dot{Q}_{tot} = \pi d_o \int_0^L \dot{q}(z)dz \ = \pi d_o \left[\int_0^{z_2} \dot{q}_I(z)dz + \int_{z_2}^L \dot{q}_{II}(z)dz \right] \ . \tag{4.80}$$

When the heat flux distribution given by equation 4.77 is used to evaluate the integral in equation 4.80 the total heat load can be written as

$$\dot{Q}_{tot} = \pi d_o \left[a_I z_2 + \frac{1}{2} b_I z_2^2 + a_{II} L + \frac{1}{2} b_{II} L^2 - a_{II} z_2 - \frac{1}{2} b_{II} z_2^2 \right] \ . \tag{4.81}$$

$\dot{q}_1$, $\dot{q}_2$ and $\dot{q}_3$ are the heat flux at axial position z_1, z_2 and z_3 of the test tube respectively. These are calculated using Nusselt's theory of film condensation given by equation 4.58. However, the wall temperature ΔT is replaced by $\Delta \overline{T}$ and the latent heat of evaporation Δh_V is replaced by Δh_V^* given by equation 4.75. Additionally, the condensate viscosity, thermal conductivity and density are evaluated at the effective temperature given by equation 4.76 with $\beta = 0.75$ while vapor density and latent heat of evaporation are evaluated at the condensate saturation temperature T_c.

Fig. 4.18 shows a comparison of the experimental results with the present analysis; equation 4.81. The present analysis deviates from the measurement by as much as 10 %, most of the data within 7 %. This is within the generally known level of uncertainty of Nus-

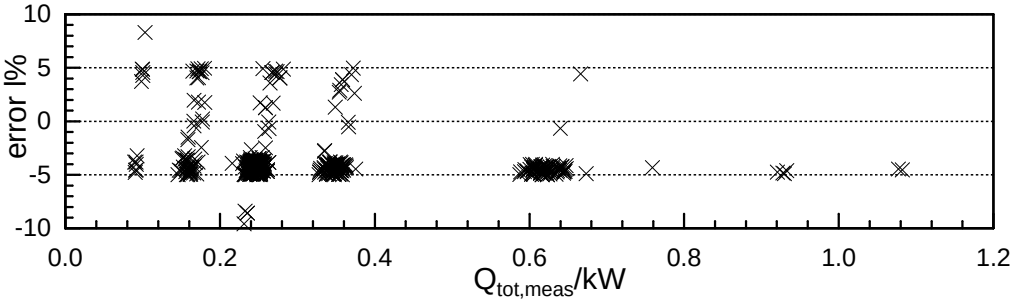

Figure 4.18. Comparison of the present solution with experimental data. Error % = $100(Q_{tot,cal} - Q_{tot,meas})/Q_{tot,cal}$.

selt's theory of film condensation (Baehr and Stephan [2] and Thome [23]). In the light of the above the original Nusselt's theory of film condensation given by equation 4.58 is accepted for the calculation of the local heat flux.

4.7 Vapor quality

One of the primary variables in the field of flow boiling is the vapor quality $\dot{x}$ or weight fraction vaporized. For zeotropic R134a/R290 mixtures the quality is calculated in section 4.8. For pure R134a and the azeotropic R134a/R290 mixture the quality at the

inlet of the test section is calculated assuming thermodynamic equilibrium from the bulk enthalpy as

$$\dot{x}_i = \frac{h(p_i, T_i) - h_L(p_i, T_i)}{h_G(p_i, T_i) - h_L(p_i, T_i)} \ , \tag{4.82}$$

where the subscript i signifies the inlet of the test section. h_L and h_G are the liquid and vapor enthalpy respectively. They are calculated utilizing the fundamental equation of state of Tillner-Roth and Baehr [138] for pure R134a and Tillner-Roth [137] for the R134a/R290 mixture (Appendix B). The bulk enthalpy at the inlet of the test section, $h(p_i, T_i)$, is calculated from the first law of thermodynamic with negligible potential and kinetic energy as

$$h(T_i, p_i) = h_1(p_1, T_1) + \sum_{i=1}^{10} \dot{Q}_i / \dot{M} \ , \tag{4.83}$$

where $\dot{Q}_i$ is the electrical heat supplied to the preheater taken into account the heat loss or gain. $\dot{M}$ is the mass flow rate. T_1, p_1 is the fluid bulk temperature and pressure respectively at the inlet of the first preheater in the test circuit. It is to be remembered that the fluid conditions at the inlet of the first preheater is in the state of subcooling.

The change in the quality across the test section is

$$\Delta\dot{x} = \frac{\dot{Q}}{\dot{M}\Delta h_V} \ , \tag{4.84}$$

where $\dot{Q}$ is the heat added to the test section taken into account the heat loss or gain. The quality at each axial position, z, in the test tube is calculated assuming a linear variation as

$$\dot{x}(z) = \dot{x}_i + \frac{z}{L}\Delta\dot{x} \ . \tag{4.85}$$

Fig. 4.19 shows the level of uncertainty $U_{\dot{x}}$ calculated in accordance with a 95 % confidence limit[2]. For both pure R134a and azeotropic R134a/R290 mixtures the level of uncertainty in the quality does exceed 0.03.

4.8 Equilibrium composition

Generally there exist two models for the calculation of the equilibrium compositions of a mixture. The first model is that of closed evaporation, widely known as "*Flash evaporation*". In this model, it is assumed that the full amount of vapor formed is in equilibrium with entire remaining liquid. The second model is that of open evaporation; widely known as "*Differential evaporation*". In this model it is assumed that at any moment the vapor formed is in equilibrium with the liquid just at this location. Schlünder [115], VDI-Wärmeatlas [143], Niederkrüger et al. [99] and Wettermann [148] have recommended

[2]

$$U_{\dot{x}} = \sqrt{(U_{h_{sub}}/\Delta h_V)^2 + (U_{\dot{Q}}/\dot{M}\Delta h_V)^2 + (\dot{Q}U_{\dot{M}}/\dot{M}^2\Delta h_V)^2 + (U_{h_L}/\Delta h_V)^2 + (\dot{x}U_{\Delta h_V}/\Delta h_V)^2}$$

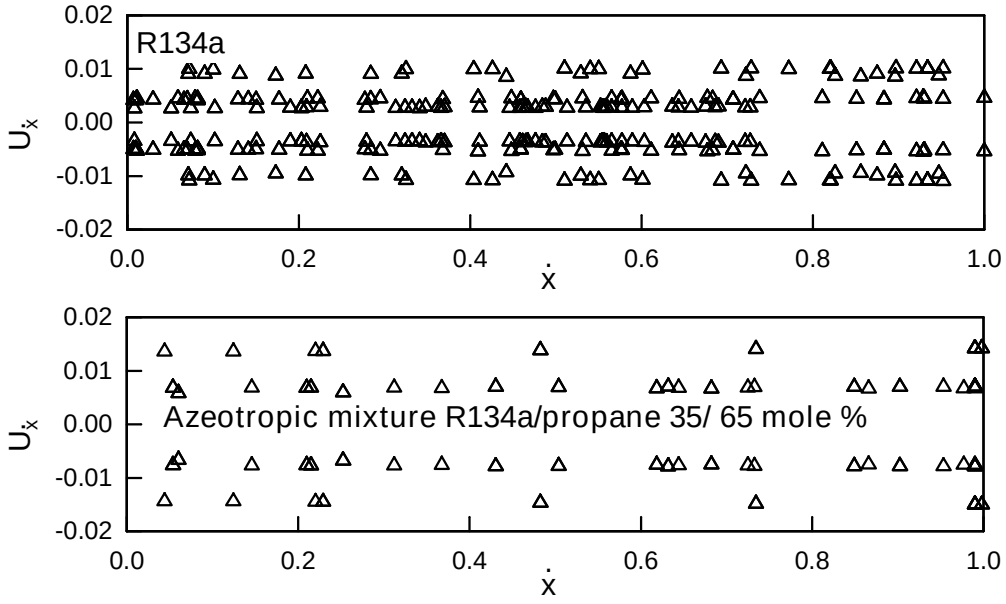

Figure 4.19. Level of uncertainty of the vapor quality $\dot{x}$.

the closed evaporation model. In the present work the closed evaporation model, which is defined as a flash problem, is adopted to calculate the equilibrium mole fraction of a mixture. The problem is to calculate for a system of known overall composition $\{\widetilde{z}_i\}$ at a given T and p the quality, the liquid mole fraction $\{\widetilde{x}_i\}$ and the vapor mole fraction $\{\widetilde{y}_i\}$. The problem is known to be determinate on the basis of Duhem's theorem, because two independent variables (T and p) are specified for a system made up of fixed quantities of its constituent species. This problem is illustrated below.

The overall material balance in a closed system may be written as

$$\dot{F} = \dot{G} + \dot{L}, \tag{4.86}$$

where $\dot{F}$, $\dot{L}$ and $\dot{G}$ are the bulk, liquid and vapor molar masses respectively. These are defined as

$$\dot{F} = \frac{\dot{M}_F}{\widetilde{M}(\widetilde{z})} , \qquad \dot{L} = \frac{\dot{M}_L}{\widetilde{M}(\widetilde{x})} , \qquad \dot{G} = \frac{\dot{M}_G}{\widetilde{M}(\widetilde{y})}, \tag{4.87}$$

where $\dot{M}_F$, $\dot{M}_L$ and $\dot{M}_G$ are the bulk, liquid and vapor mass respectively. $\widetilde{M}(\widetilde{z})$, $\widetilde{M}(\widetilde{x})$ and $\widetilde{M}(\widetilde{y})$ are the bulk, liquid and vapor molecular weight of the mixture respectively. These are calculated from the pure component molecular weight assuming a linear mixing rule as

$$\widetilde{M}(\widetilde{z}) = \sum \widetilde{z}_i \widetilde{M}_i, \qquad \widetilde{M}(\widetilde{x}) = \sum \widetilde{x}_i \widetilde{M}_i, \qquad \widetilde{M}(\widetilde{y}) = \sum \widetilde{y}_i \widetilde{M}_i \ . \tag{4.88}$$

where $\widetilde{z}_i$, $\widetilde{x}_i$, $\widetilde{y}_i$ are mole fraction of the component i in the bulk, liquid and vapor phase respectively. Solution of the component material balance

$$\dot{F}\widetilde{z}_i = \dot{G}\widetilde{y}_i + \dot{L}\widetilde{x}_i \ , \widetilde{z}_i = \dot{\lambda}\widetilde{y}_i + (1-\dot{\lambda})\widetilde{x}_i \ , \tag{4.89}$$

yields

$$\widetilde{x}_i = \frac{\widetilde{z}_i}{1 + \dot{\lambda}(K_i - 1)}, \tag{4.90}$$

and

$$\widetilde{y}_i = \widetilde{x}_i K_i = \frac{\widetilde{z}_i K_i}{1 + \dot{\lambda}(K_i - 1)} \ , \tag{4.91}$$

where $\dot{\lambda}$ is the molar vapor quality (kmol/kmol) defined as

$$\dot{\lambda} = \frac{\dot{G}}{\dot{G} + \dot{L}} \ , \tag{4.92}$$

The factor K_i of the component i is defined as

$$K_i = \frac{\widetilde{y}_i}{\widetilde{x}_i} = \frac{\phi_{i,L}(T, p, \widetilde{x})}{\phi_{i,G}(T, p, \widetilde{y})}, \tag{4.93}$$

where ϕ_i is the fugacity coefficient of the component i. It is calculated using the fundamental equation of state of Tillner-Roth [137] for R134a/R290 mixtures (Appendix B).

Since the bubble point and dew point conditions require

$$\sum \widetilde{y}_i = 1, \quad \sum \widetilde{x}_i = 1 \ , \tag{4.94}$$

respectively, the following objective functions may be defined

$$F_{\widetilde{y}} = \sum \frac{\widetilde{z}_i K_i}{1 + \dot{\lambda}(K_i - 1)} - 1 = 0, \tag{4.95}$$

$$F_{\widetilde{x}} = \sum \frac{\widetilde{z}_i}{1 + \dot{\lambda}(K_i - 1)} - 1 = 0 \ . \tag{4.96}$$

Solution of a p,T-flash problem is accomplished when a value of $\dot{\lambda}$ is found that makes either the function $F_{\widetilde{x}}$ or $F_{\widetilde{y}}$ equal to zero. However, a more convenient function for use in a general solution procedure is the difference $F_{\widetilde{y}} - F_{\widetilde{x}} = F$ (Reid et al. [108]):

$$F = \sum_1^n \frac{\widetilde{z}_i (K_i - 1)}{1 + \dot{\lambda}(K_i - 1)} = 0 \ . \tag{4.97}$$

The advantage of this function is apparent from its derivative

$$\frac{dF}{d\dot{\lambda}} = -\sum_1^n \frac{\widetilde{z}_i (K_i - 1)^2}{\left[1 + \dot{\lambda}(K_i - 1)\right]^2} = 0 \ . \tag{4.98}$$

Since $dF/d\dot{\lambda}$ is always negative, the F vs. $\dot{\lambda}$ relation is monotonic, and this makes Newton's method a rapidly converging iteration procedure well suited for the solution for $\dot{\lambda}$. Newton's method requires

$$\dot{\lambda}_{j+1} = \dot{\lambda}_j - \frac{F_j}{(dF/d\dot{\lambda})_j} \ , \tag{4.99}$$

where j is the iteration index. The convergence criteria of $|\sum_i(\widetilde{y}_i - \widetilde{x}_i| < 10^{-8}$ is adopted in the present analysis. A general solution algorithm for the flash problem is shown in a form of a block diagram of Fig. 4.23a. As a control to the scheme of calculation a bubble calculation is also needed; an algorithm for this is given in Fig. 4.23b.

The present formulation is validated using the experimental VLE-data of Kleiber [78] as shown in Fig. 4.20. The solid lines represent the bubble point calculation using the fundamental equation of state of Tillner-Roth [137] for R134a/R290 mixtures. The result gives an average deviation of 0.017 vapor mole fraction $\widetilde{y}$ (propane).

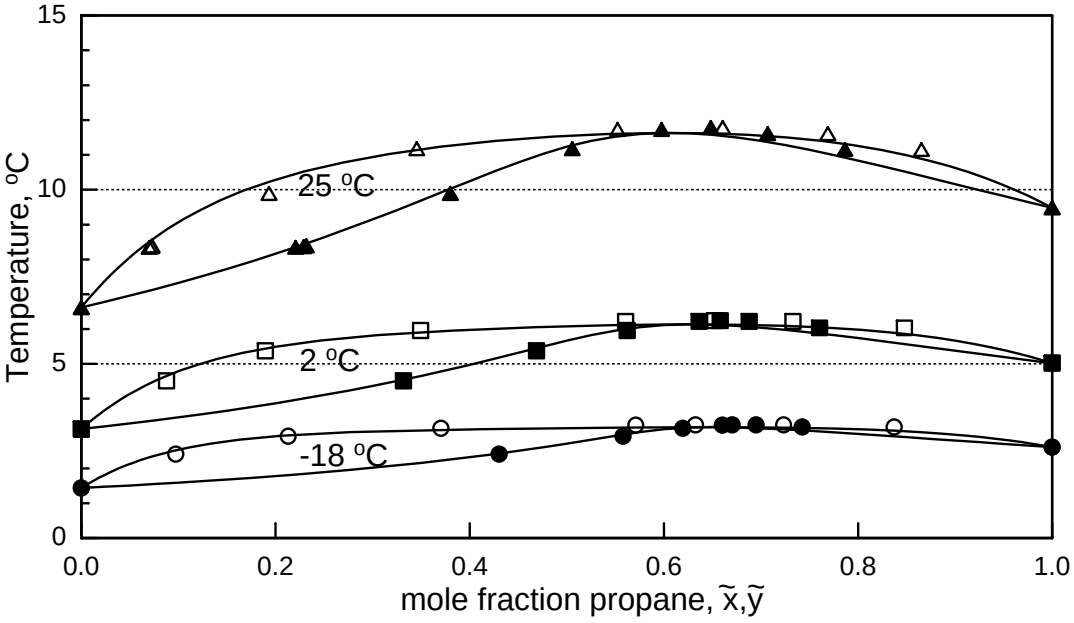

Figure 4.20. Phase diagram for the system of R134a/R290 mixture.

Besides the liquid and vapor mole fractions, the p,T-flash problem also yields the molar quality, $\dot{\lambda}$ (kmol/kmol). Knowledge of $\dot{\lambda}$ facilitates the calculation of the mass quality (kg/kg) as

$$\dot{x} = \frac{\dot{M}_G}{\dot{M}_G + \dot{M}_L} \,, \tag{4.100}$$

with

$$\dot{M}_G = \dot{G}\widetilde{M}_{\widetilde{y}}, \quad \dot{M}_L = \dot{L}\widetilde{M}_{\widetilde{x}} \,, \tag{4.101}$$

and $\dot{\lambda}$ given by equation 4.92 the relation between the molar and mass quality is

$$\dot{x} = \frac{\dot{\lambda}}{\dot{\lambda} + \frac{\widetilde{M}(\widetilde{x})}{\widetilde{M}(\widetilde{y})}\left[1 - \dot{\lambda}\right]} \,. \tag{4.102}$$

Fig 4.21 shows the relationship between the quality and the mole fraction calculated using the present formulation.

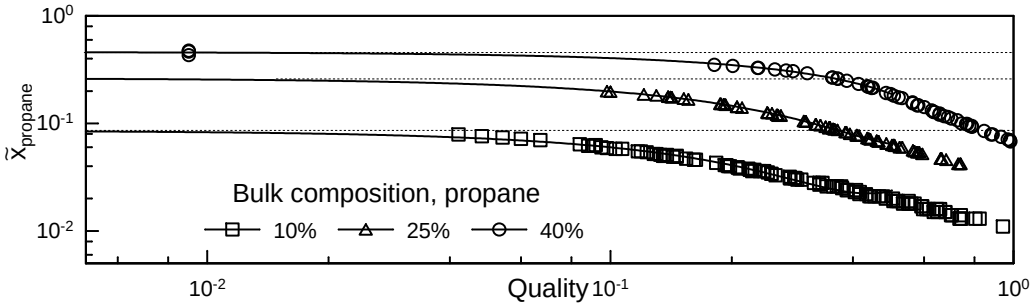

Figure 4.21. The flash curve show the relation between the quality and composition during evaporation.

Fig. 4.22 shows the level of uncertainty $U_{\dot{x}}$ in the predicted quality using the present formulation. The calculation is made in accordance with a 95 % confidence limit[3] at various bulk compositions, $\tilde{z}$. The maximum error does not exceed ± 0.05 with most of the data being within ± 0.025.

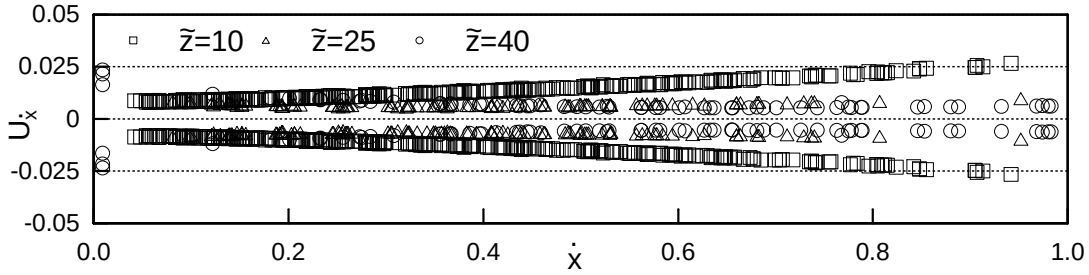

Figure 4.22. Level of uncertainty of the vapor quality of zeotropic R134a/propane mixtures.

[3]

$$U_{\dot{x}} = \sqrt{(U_{\dot{\lambda}}\widetilde{M}(\widetilde{x})/\widetilde{M}(\widetilde{y}))^2 + (U_{\widetilde{M}(\widetilde{x})}\dot{\lambda}(1-\dot{\lambda})/\widetilde{M}(\widetilde{y}))^2 + (U_{\widetilde{M}(\widetilde{y})}\dot{\lambda}(1-\dot{\lambda})\widetilde{M}(\widetilde{x})/\widetilde{M}(\widetilde{y})^2)^2}/a$$

$$U_{\dot{\lambda}} = \sqrt{(U_{\widetilde{z}}/(\widetilde{y}-\widetilde{x}))^2 + (U_{\widetilde{x}}(\widetilde{z}-\widetilde{y})/(\widetilde{y}-\widetilde{x})^2)^2 + (U_{\widetilde{y}}(\widetilde{z}-\widetilde{x})/(\widetilde{y}-\widetilde{x})^2)^2}$$

$$U_{\widetilde{M}(\widetilde{x})} = \sqrt{U^2_{\widetilde{M}(\widetilde{x})}(\widetilde{M}_1^2 + \widetilde{M}_2^2)}$$

$$U_{\widetilde{M}(\widetilde{y})} = \sqrt{U^2_{\widetilde{M}(\widetilde{y})}(\widetilde{M}_1^2 + \widetilde{M}_2^2)}$$

$$a = \dot{\lambda} + \frac{\widetilde{M}(x)}{\widetilde{M}(y)}(1-\dot{\lambda})$$

Figure 4.23. (a) Algorithm (Flash) for the calculation of $\{\widetilde{y}\}$, $\{\widetilde{x}\}$ and $\dot{x}$ for a given $\{\widetilde{z}\}$, T and p (b) Algorithm (BUBL P) for the calculation of $\{\widetilde{y}\}$ and p for a given $\{\widetilde{y}\}$ and T.

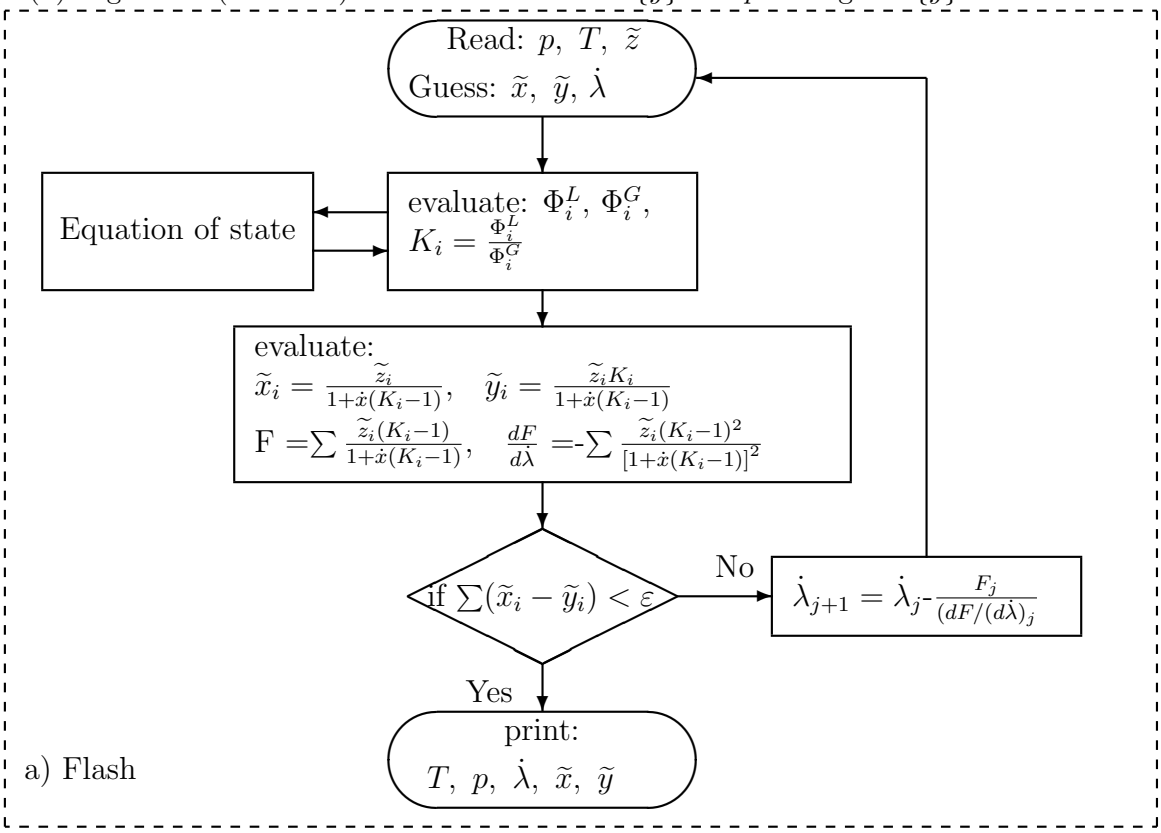

4.9 Summary

As indicated in the literature review the heat transfer coefficient, pressure drop and flow pattern are dependent on the various thermal and hydrodynamic flow parameters. Some of these parameters are directly measured. These include the wall temperature, saturation pressure, pressure drop and mass flux. The level of uncertainty of each of the measured parameters is given earlier in chapter 3. The parameters which are not measured in the present work include the saturation temperature, bubble point temperature, heat flux, quality and mole fraction.

In the preceding analysis methods and calculation procedures are developed for the evaluation of the various parameters which are not directly measured. The developed calculation methods and procedures are validated using a rigor uncertainty analysis and in some cases the result obtained by using a certain calculation model is compared with the available experimental data. For example the predicted mole fraction using the $p-T$ flash problem is compared with the experimental VLE-data of Kleiber [78].

In the field of flow boiling, to facilitate the calculation or to simplify the problem under study, some assumptions are generally made. For example a thermal boundary condition of constant wall temperature is generally assumed when the refrigerant is heated by a condensing steam. In the present work the measured wall temperature is found to posses a cosine profile rather than an isothermal profile as initially assumed. In the preceding analysis the validity of this assumption on the present study is assessed. It is found that the Nusselt theory of film condensation is not influenced by the wall temperature profile; no deviation between the calculated heat flux under the isothermal and non-isothermal wall temperature profile.

5 Heat transfer coefficient

As indicated earlier, the local heat transfer coefficient is not a directly measured parameter but a derived one. Thus it is required to determine its calculation procedure and the level of uncertainty. The algorithm shown in the block diagram of Fig. 5.2 presents the calculation procedure for the local heat transfer coefficient from the measured parameters. To facilitate the calculation procedure the algorithm is implemented as a Fortran 90 computer program running on a PC unit. The uncertainty evaluation of the local heat transfer coefficient is performed in accordance with a 95 % confidence interval to satisfy the recommendation of the DKD [28]. The local heat transfer coefficient as defined by equation 4.7 is calculated as

$$\alpha = \frac{\dot{q}}{T_{wi} - T_s} \ . \tag{5.1}$$

The 95 % confidence uncertainty of local heat transfer coefficients U_α is calculated applying the law of propagation (equation 3.27) to equation 5.1 as

$$\frac{U_\alpha}{\alpha} = \sqrt{\left(\frac{\partial \alpha}{\partial \dot{q}}\right)^2 U_{\dot{q}}^2 + \left(\frac{\partial \alpha}{\partial T_{wi}}\right)^2 U_{T_{wi}}^2 + \left(\frac{\partial \alpha}{\partial T_s}\right)^2 U_{T_s}^2} \ . \tag{5.2}$$

With the partial derivatives obtained from equation 5.1, equation 5.2 yields

$$\frac{U_\alpha}{\alpha} = \sqrt{\left(\frac{U_{\dot{q}}}{\dot{q}}\right)^2 + \left(\frac{U_{T_{wi}}}{T_{wi} - T_s}\right)^2 + \left(\frac{U_{T_s}}{T_{wi} - T_s}\right)^2} \ , \tag{5.3}$$

where

i $U_{\dot{q}}$ is the uncertainty of the heat flux. This is taken as that for the Nusselt's theory of film condensation $U_{\dot{q}}/\dot{q}$ as shown in Fig. 4.18 of section 4.6.3.

ii $U_{T_{wi}}$ is uncertainty of inside wall temperature. This is determined using the law of propagation equation 3.27 as

$$U_{T_{wi}} = \sqrt{\left(\frac{\partial T_{wi}}{\partial T_{wo}}\right)^2 U_{T_{wo}}^2 + \left(\frac{\partial T_{wi}}{\partial \dot{q}}\right)^2 U_{\dot{q}}^2} \ . \tag{5.4}$$

With partial derivatives obtained using equation 4.2, equation 5.4 reduces to

$$U_{T_{wi}} = \sqrt{U_{T_{wo}}^2 + \left(\frac{d_i \ln(d_o/d_i)}{2\lambda}\right)^2 U_{\dot{q}}^2} \ , \tag{5.5}$$

where $U_{T_{wo}}$ is the level of uncertainty of the mean outside wall temperature. The mean outside wall temperature is (see equation 4.35)

$$T_{wo} = \frac{T_{wo}(0) + T_{wo}(\pi/2) + T_{wo}(\pi)}{3} \ , \tag{5.6}$$

where $T_{wo}(0)$, $T_{wo}(\pi/2)$ and $T_{wo}(\pi)$ are the wall temperature at top, side and the bottom of the tube. The 95 % confidence uncertainty of mean wall temperature

$U_{T_{wo}}$ is calculated applying the law of propagation (equation 3.27) to equation 5.6 as

$$U_{T_{wo}} = \sqrt{\frac{U^2_{T_{wo}(0)} + U^2_{T_{wo}(\pi/2)} + U^2_{T_{wo}(\pi)}}{9}} \,, \tag{5.7}$$

where $U_{T_{wo}(0)}$, $U_{T_{wo}(\pi/2)}$ and $U_{T_{wo}(\pi)}$ are the level of uncertainty of the thermocouple used for the measurement of the outside wall temperature at top, side and bottom of the tube respectively. These are given in Appendix A.

iii U_{T_s} is the uncertainty of the saturation temperature for pure R134a or R134a/R290 mixtures. U_{T_s} was evaluated in subsection 4.3.1 and subsection 4.3.2 for pure R134a and R134a/R290 mixtures respectively.

iv U_α is the uncertainty of the local heat transfer coefficient for pure R134a or R134a/R290 mixtures as shown in Fig. 5.1a and Fig. 5.1b respectively. In the present study the level of uncertainty of local heat transfer coefficient for both pure R134a and R134a/R290 mixtures for a wide range of parameters does not exceed 10 %.

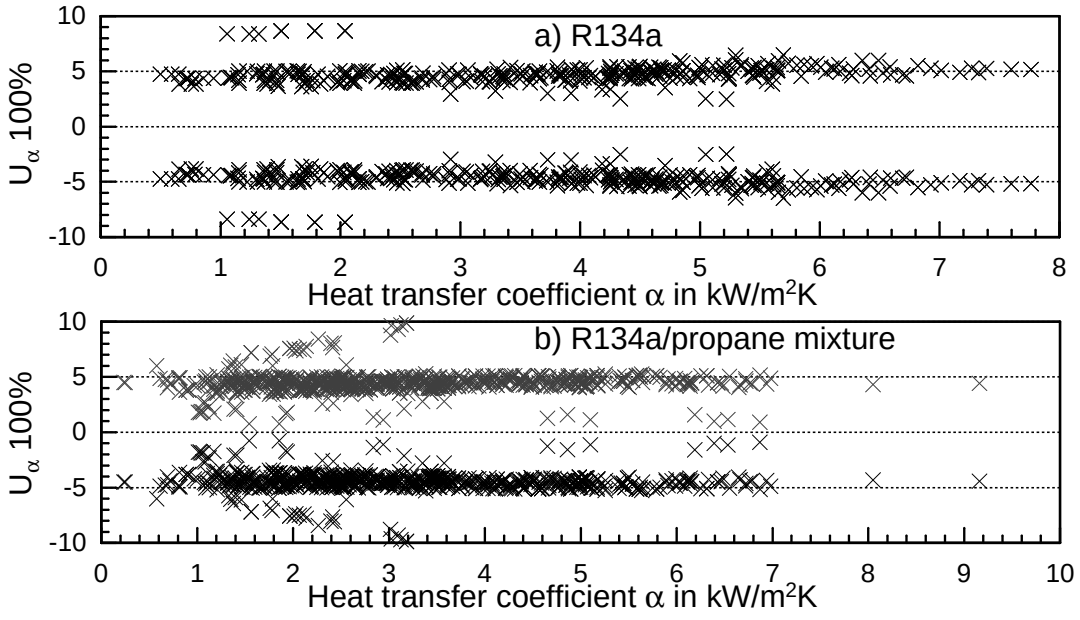

Figure 5.1. level of uncertainty of the local heat transfer coefficient a) pure R134a b) R134a/propane mixtures.

Figure 5.2. Algorithm for the calculation of the local heat transfer coefficient.

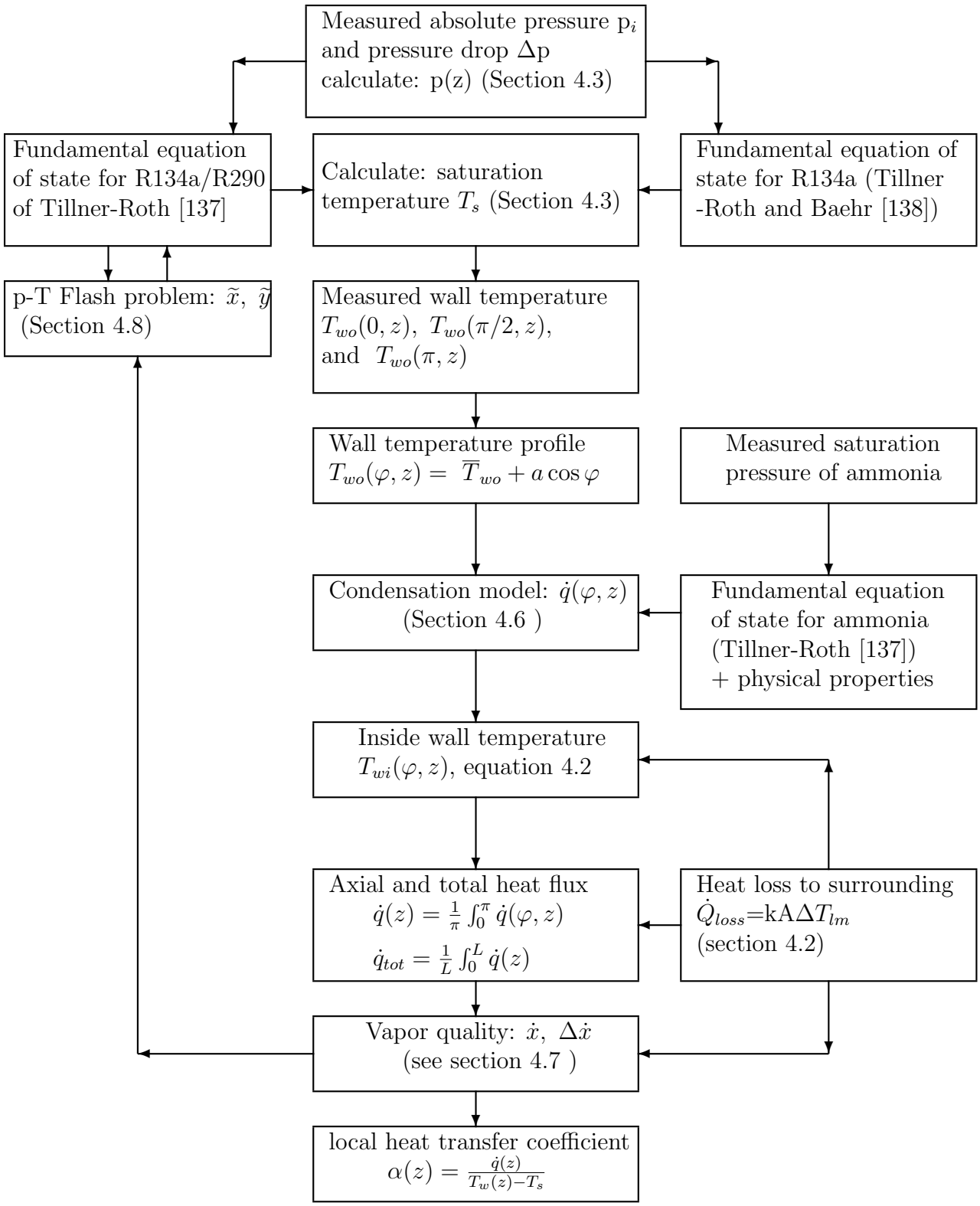

5.1 Results for pure R134a

In the present study the local heat transfer coefficient is measured at three axial positions along the test tube. However, the test section is preceded with an adiabatic zone as shown in Fig. 5.3. In turn this configuration may have some influence on the simultaneously

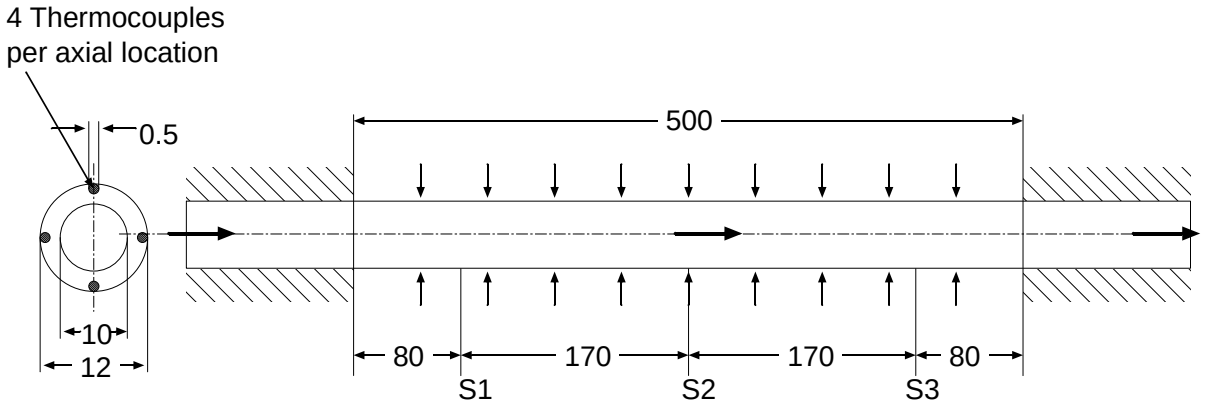

Figure 5.3. Schematic presentation of the test section. The dimensions are in mm.

developing velocity profile and temperature field in the direction of flow. Subsequently this may result in an adverse effect on the measured local heat transfer coefficient, particulary at section I. Thus the magnitude of this effect needs to be quantified. As an illustration Fig. 5.4 shows the measured local heat transfer coefficient at the three sections $S1$, $S2$ and $S3$ under same working conditions. It can be seen from this figure that the slopes of the local heat transfer coefficient as function of quality at the three different sections are almost identical in the region of $\dot{x} < 0.7$.

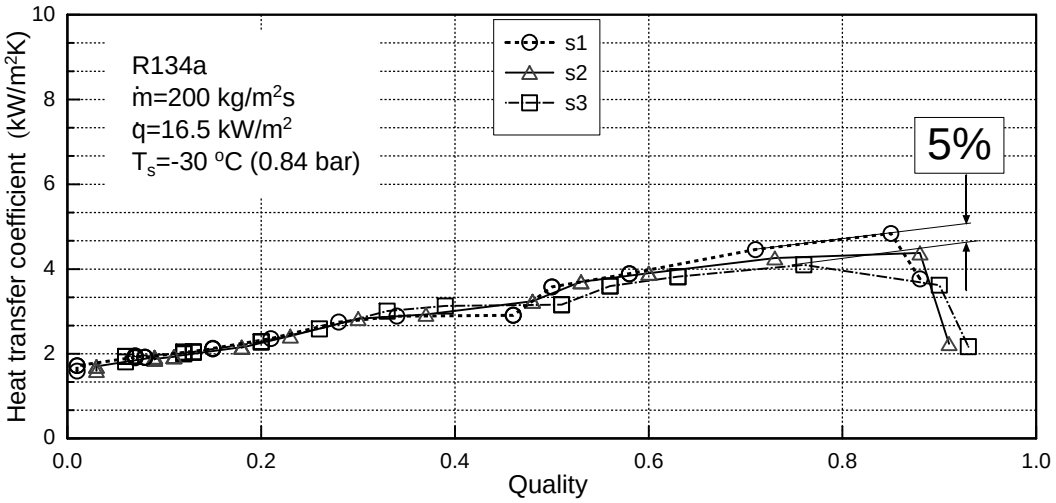

Figure 5.4. Influence of the *entrance heated length* on the local heat transfer coefficient of pure R134a.

This demonstrates that the accepted minimum thermal entrance length (heated length) of z/d =8 is satisfactory for the simultaneously developing flow. It is to be remembered that

the criteria normally accepted for simultaneously developing velocity and temperature profile in single phase turbulent flow is $z/d \geq 8$ (Rohsenow et al. [110]).

In the region where $\dot{x} \geq 0.7$ the deviation between $\alpha(S3)$ and $\alpha(S1)$ is amounted to a maximum deviation of 5 % at $\dot{x} = 0.8$. Though this deviation is considered as insignificant (*i.e.* accepted), it may be attributed to the increase in the vapor velocity. High vapor velocity (*i.e.* high Reynolds number) may require a greater thermal entrance length for simultaneously developing flow. VDI-Wärmeatls [143] has indicated that, for two phase flow boiling, the entrance affect may be greater than that for single phase flow; it may extend up to $z/d > 20$.

Similar results to the effect of the thermal entrance length on the heat transfer coefficient is also observed under other working conditions for example see Fig. 5.5.

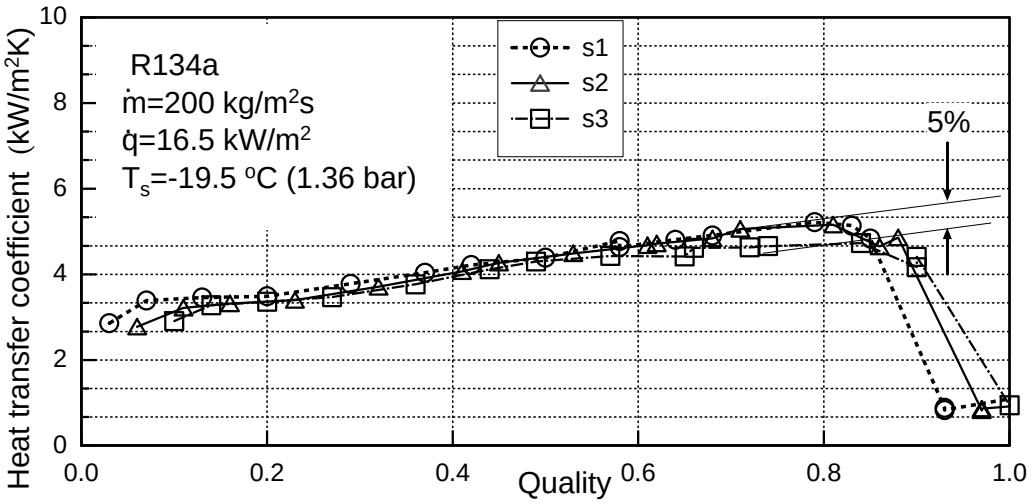

Figure 5.5. Influence of the *entrance heated length* on the local heat transfer coefficient of pure R134a.

In addition to the entrance effect, for flow boiling of pure component in a horizontal tube the local heat transfer coefficient is known to be influenced by the thermal, hydrodynamic and the tube parameters. The tube parameters include the diameter d, wall thickness s, thermal conductivity λ_w and surface roughness R_a.

$$\alpha = \alpha(\dot{m}, \dot{x}, T_s(p), T_w, d, s, \lambda_w, R_a) \ . \tag{5.8}$$

In the present study the tube parameters (d, s, λ_w, R_a) are maintained constant throughout this work. The other thermal and hydrodynamics parameters are, however, varied systematically. In the following subsections the effect of these parameters on the local heat transfer coefficient for pure R134a is considered one after another. Furthermore, a detailed comparison between the experimental data and a number of correlations is presented.

5.1.1 Influence of vapor quality

The parametric dependency of the local heat transfer coefficient on quality is an important consideration in studying the relative contributions of the two boiling mechanisms (*i.e.* nucleate and convective) and flow pattern in flow boiling. Against this background measurements have been made to cover a wide range of quality; $0 \leq \dot{x} \leq 1$. Fig. 5.6

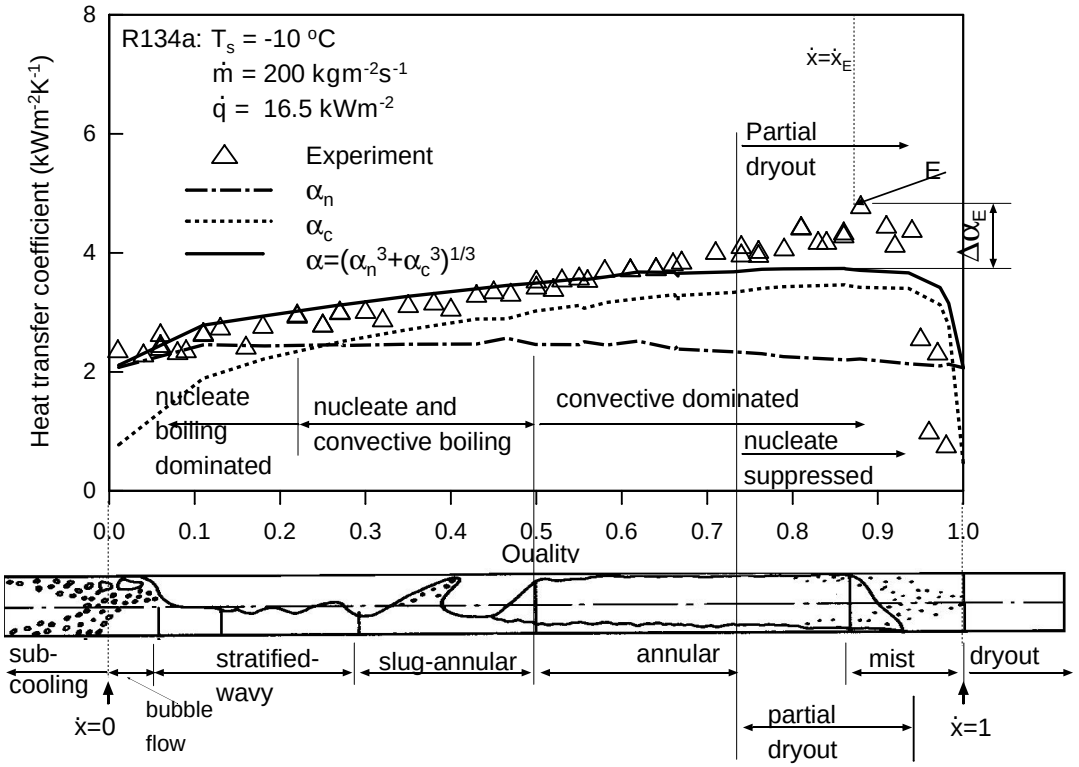

Figure 5.6. Influence of the vapor quality on the local heat transfer coefficient of pure R134a. The schematic presentation of the flow patterns shown at the bottom of the figure is adopted from VDI-Wärmeatlas [143].

shows the measured local heat transfer coefficient as function of quality at a mass flux of 200 kg/m^2 s, circumferential averaged heat flux of 16.5 kW/m^2 and saturation temperature of -10 °C (2.0 bar). The results show that the measured local heat transfer coefficient increases with quality till it reaches a peak point E followed by a sharp falloff. The variation of the slope of the local heat transfer coefficient with respect to quality may be attributed to the change in the flow pattern and the different boiling mechanisms (nucleate and convective) encountered in evaporation. For the sake of illustration a schematic presentation of the flow patterns generally observed in the field of flow boiling is shown in the lower part of Fig. 5.6. It is also shown the "theoretical" convective and nucleate boiling heat transfer coefficients and their combined contribution calculated from the asymptotic model of Steiner [128] as

$$\alpha = \sqrt[3]{\alpha_c^3 + \alpha_n^3} \ . \tag{5.9}$$

The convective α_c and the nucleate boiling α_n heat transfer coefficient are calculated using Steiner [128] correlation. The Steiner [128] correlation is given in Appendix C.

In the early stage of evaporation ($\dot{x}$ <0.1) the observed flow patterns was identified as bubbly flow. In bubbly flow pattern, nucleate boiling is generally known to be the dominant mechanism of flow boiling. Thus the result of the measurement in this region may be identified as nucleate boiling dominated data. In fact the result matches very well with the calculated nucleate boiling curve (centered line) and deviate widely from the convective curve (dotted line) presented in Fig. 5.6.

As more vapor is generated in the flow and the quality increases ($0.1 \leq \dot{x} \leq 0.65$), the flow was observed to undergo a transition to annular followed by a fully developed annular flow pattern. The flow patterns were identified as stratified-way, slug-annular to annular flow pattern. Under these conditions the convective evaporation at the vapor-liquid interface become increasing important. Simultaneously the nucleate boiling in the liquid film is decreasing yet remaining active. Thus in this region the measured local heat transfer coefficient may be identified as neither for convective dominated nor for nucleate dominated boiling, it is rather a contribution of both mechanisms. The calculated combined contribution of nucleate and convective boiling (solid line) matches very well with measurements in this region.

Acceleration of the vapor at the core during the latter annular flow stages of the evaporation process was observed and found to be producing entrainment of liquid drops (mist flow). This effect, together with direct vaporization of the annular film, tends to reduce the film thickness further as the quality increases. Nucleate boiling may be completely suppressed when the film thickness is so thin that it can no longer support a bubble to grow. Eventually the liquid film was found to disappear completely from the upper portions of the tube wall; because of the tendency of the gravity. This is usually referred to as near or partial dryout of the tube wall. Thus point E is the point of onset of dryout.

In the region of near dryout, just before the onset of dryout the point E causes a deterioration, the heat transfer coefficient shows an enhancement by a factor of 10-25 %. This factor is defined as the ratio between the measured local heat transfer and the ideal one at a quality $\dot{x}_E$. The ideal heat transfer coefficient is defined as that one would have obtained if the slope of the measured local heat transfer coefficient remained constant up to the point E. (In fact the calculated local heat transfer coefficient using Steiner [128] correlation (solid line) has the same slope as the measured one in the region $0 < \dot{x} < 0.7$. Beoletti et al. [8], Costigan et al. [26] and Urso et al. [140] have previously observed more than 40 % enhancement in the local heat transfer coefficient in the near dryout region. Their vertical tube measurements were, however, carried under a thermal boundary condition of constant heat flux realised using electrical heating. Beattie and Lawther [6] have attributed this peculiar phenomena to the structural changes of the nucleate boiling sublayer to a froth layer, while Hewitt et al. [52] have attributed to the axial conduction from the dry to wet region. The net effect of this process is a decrease in the wall superheat in the wet region near the dryout front and thus to a higher heat transfer coefficient.

Beyond the onset of dryout (point E), when the tube wall is partially dry, heat transfer from dry portions of the wall surface is negligible compared to that at locations wetted

by liquid where film evaporation is occurring. Because these dry locations are inactive, the convective local heat transfer coefficient, averaged around the perimeter of the tube, is lower than that if the entire perimeter were covered by the liquid. Furthermore, as the wetted fraction of the wall decreases with quality, more of the wall becomes inactive and the local heat transfer coefficient, averaged over the perimeter, also progressively decreases. At a complete wall dryout the local heat transfer coefficient approaches a value near to that expected for heat transfer by forced convection to a saturated vapor. For the case at hand the measured local heat transfer coefficient at $\dot{x}_2 = 0.98 \rightarrow 1.0$ is 478 W/m^{2}K and that calculated using Gnielinski [42] model is α_G= 416 W/m^{2}K. The subscript "2" signifies that the measurement corresponds to section 2.

The overall trend of the measured local heat transfer coefficient in the quality range of $0 \leq \dot{x} \leq 1$ is in line with the earlier investigations reported in VDI-Wärmeatlas [143], Kenning and Cooper [74], Kandlikar [66], Kattan et al. [72] and Kabelac and de Buhr [63], to mention a few. A similar dependency of the local heat transfer coefficient on the quality is observed for other working conditions, see for example Fig. 5.7. More data points are presented in Appendix F

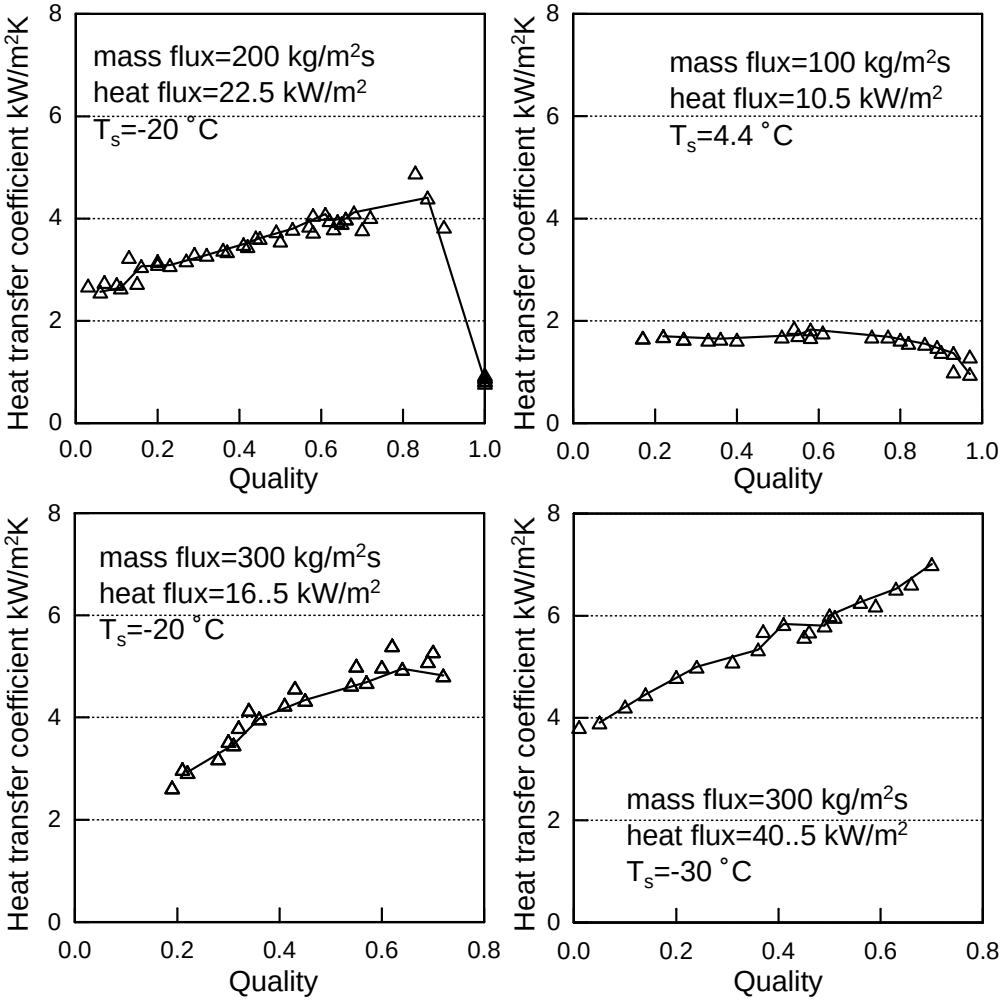

Figure 5.7. Influence of the vapor quality on the local heat transfer coefficient of pure R134a.

5.1.2 Influence of the mass flux

Besides the quality the mass flux plays an important role on the influence of the convective boiling mechanisms in the local flow boiling heat transfer coefficient. Against this background a number of test runs were carried out covering a wide range of mass fluxes (100-300 kg/m^2 s). Fig. 5.8a shows the variation of the measured local heat transfer coefficient with mass flux at a saturation temperature of -30 °C. The result indicates a strong

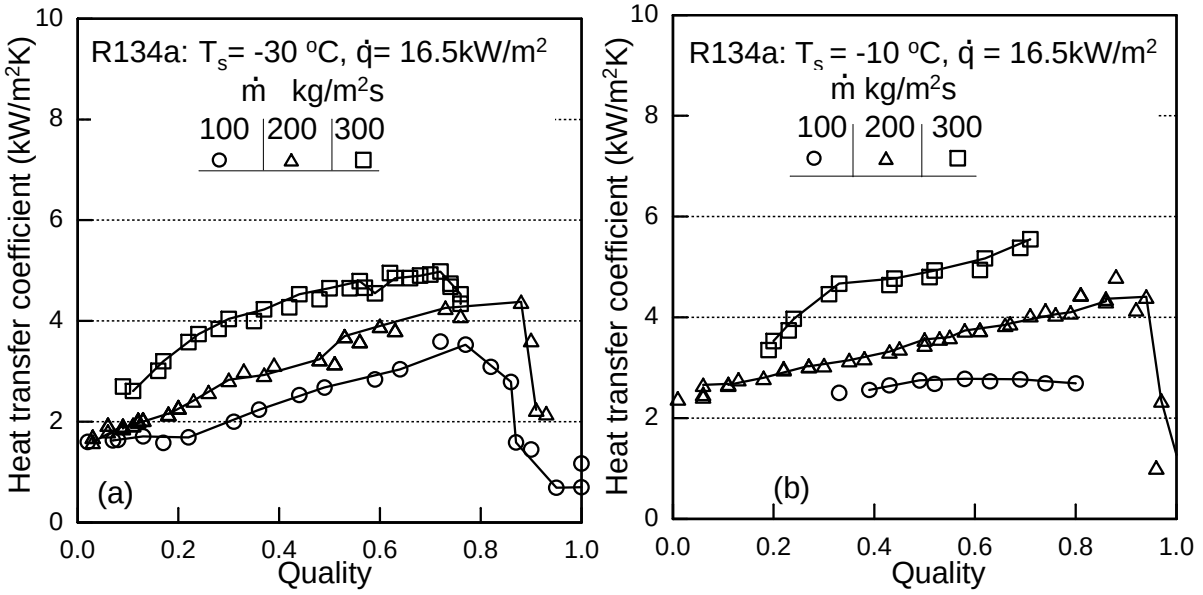

Figure 5.8. Influence of the mass flux on the flow boiling heat transfer coefficient for pure R134a.

influence of the mass flux on the local heat transfer coefficient, particularly at vapor quality in the range of $0.1 < \dot{x} \leq 0.8$. This is a typical convective flow boiling behavior. In fact the observed flow patterns in this region varied between a transition annular to fully developed annular flow pattern. In convective boiling, when the velocity of the fluid increases, the heat supplied to the tube can be taken away faster, which eventually increases heat transfer. In other words, high velocity yield high Reynolds numbers ($Re = \dot{m}d/\mu$), thus higher heat transfer coefficients analogous to single phase force convection.

In contrast, in the low quality region ($\dot{x} < 0.1$), the result shows a week influence of mass flux on the local heat transfer coefficient, particularly at low mass fluxes of 100 and 200 kg/m^{2}s. In this region the observed flow patterns at these mass fluxes are bubbly to stratified flow patterns. Thus the heat transfer coefficient may be identified as that for nucleate dominated boiling. VDI-Wärmeatlas [143] and Niederkrüger [98] indicated that the nucleate boiling is influenced by the heat flux $\dot{q}$ rather than the hydrodynamic parameters ($\dot{m}$, $\dot{x}$). At a mass flux of 300 kg/m^{2}s the observed flow pattern was annular flow rather than stratified or bubbly flow patterns. For this test run ($\dot{m} = 300$ kg/m^2 s, $\dot{x} < 0.1$) the measured local heat transfer coefficient seems to be dominated by convective boiling flow. This may justify the strong influence of mass flux on the local heat transfer coefficient in this low quality region. The experiment was repeated for a saturation

temperature of -10 °C (2 bar) and is graphically presented in Fig. 5.8b. As for the case of saturation temperature of -30 °C, a similar influence of the mass flux on the local heat transfer coefficient can be clearly recognized at a saturation temperature of -10 °C.

A similar influence of mass flux on the local heat transfer coefficient was previously observed by Kabelac and de Buhr [64] for ammonia, Wetterman [148] for R134a and R12 and Niederkrüger [98] for R12 and R846 in a horizontal tube.

5.1.3 Influence of the saturation temperature

To investigate the influence of saturation temperature on the flow boiling mechanisms (convective and nucleate) a number of test runs were performed. For the sake of studying the influence of saturation temperature on the pure convective boiling test runs with a high mass flux were performed. This is made to create an annular flow pattern, thus diminishing the influence of the nucleate boiling. Fig. 5.9a shows data of heat transfer coefficient for R134a at a high mass flux of 300 kg/m^2 s at two saturation temperatures of -10 °C and -30 °C. The result shows an increase in the local convective heat transfer coefficient with an increase in the saturation temperature. This is attributed to the liquid-vapor density ratio. The liquid-vapor density ratio decreases with increasing saturation temperature/pressure.

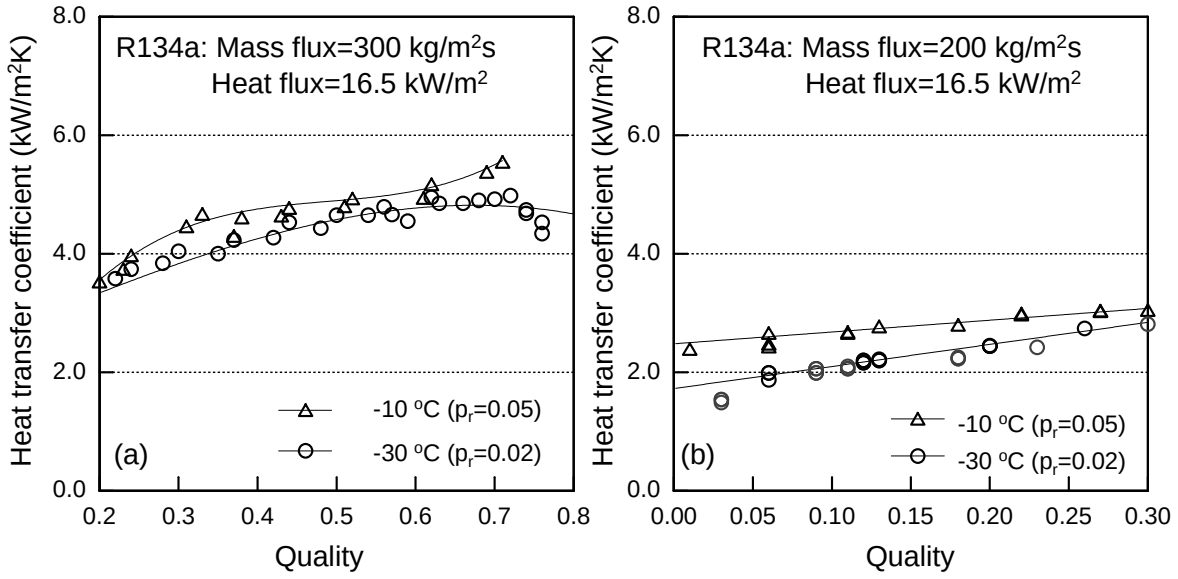

Figure 5.9. Influence of the saturation temperature/pressure on the flow boiling heat transfer coefficient for pure R134a.

For example for the case at hand

$$\begin{pmatrix} T\ °C & -10 & -30 \\ \rho_L/\rho_G & 132 & 313 \end{pmatrix}$$

where ρ_L and ρ_G are the liquid and vapor density respectively. They are calculated from the fundamental equation of state of Tillner-Roth and Baehr [139] for R134a. The

decrease in the liquid-vapor density ratio leads to a decrease in the slip ratio (vapor-liquid velocity ratio) and shear stress at the vapor-liquid interface, thus high convective boiling heat transfer coefficient; analogous to single liquid phase.

A nucleate boiling dominated data has been tried by using a relatively low mass flux and vapor quality. Under these conditions the observed flow pattern was a bubbly to stratified flow pattern. The results of these test runs are shown in Fig. 5.9b for two saturation temperatures of -10 °C and -30 °C at a mass flux of 200 kg/m^2 s. As for the case of convective flow boiling the nucleate boiling is also influenced by the saturation temperature, it increases with saturation pressure. This is attributed to the reduced pressure p_r. The reduced pressure is defined as ratio between the saturated and critical pressure of the R134a. The critical pressure of R134a as given by Tillner-Roth [136] is 40.563 bar. A more elaboration and a comprehensive review about the influence of the reduced pressure on the nucleate boiling is found in VDI-Wärmeatlas[143]. Similar dependency of the local nucleate boiling heat transfer coefficient on the saturation pressure/temperature was previously observed by Wettermann [148], Niederkrüger [98] and Steiner [128].

5.1.4 Comparisons with correlations

As indicated in the literature review R134a is one of the newly developed refrigerants as a substitute for R12. Therefore, the validity of existing correlations for the prediction of the local flow boiling heat transfer coefficient for R134a need to be tested. In the present work ten (10) of the most widely accepted correlations were fitted to the the experimental data. Namely these are the Steiner [128], Kattan et al. [73], Shah [118], Kandlikar [66], Gungor and Winterton [48], Schrock and Grossman [117], Klimenko [79], Jung et al. [60], Bennett and Chen [7] and Dembi et al. [27] correlations. These correlations are given in Appendix C. It is to be remembered that these correlations are valid only in the region prior to the point of the dryout; prior to the critical quality $\dot{x}_c$. Thus all data points at dryout and beyond ($\dot{x} \geq \dot{x}_c$) are excluded in the comparisons. The critical quality $\dot{x}_c$ is calculated using the method of Kon'kov [82] which is recommended by VDI-Wärmealtas [143]. The thermodynamic and transport properties required for the calculation of the local heat transfer coefficient from the correlation are given in appendix B.

Fig. 5.10a to Fig. 5.11d show comparisons of the ten (10) correlations with the R134a data. Table 5.1 summarizes the mean error and the standard deviation associated with each correlation. Additionally, the number of data points that falls within an error band of ±30 % is also indicated for each correlation. The total number of the data point is 3×330 (*i.e.* 330 test runs at each of the test runs the heat transfer coefficient is measured at three (3) axial positions along the test tube). The methods for estimating the mean error and the standard deviation are given in Appendix A.

Table 5.1. Comparison of ten (10) correlations with flow boiling experimental data of pure R134a.

Correlation	Mean error %	Standard deviation %	Percentage of data points within an error band of 30%
Steiner [128]	15.48	28.05	89.20
Kattan et al. [73]	21.58	32.56	70.53
Shah [118]	50.95	111.74	68.05
Kandlikar [66]	17.99	25.50	80.50
Gungor and Winterton [48]	20.96	28.85	69.71
Schrock and Grossmann [117]	28.54	35.48	50.62
Kliminko [79]	41.55	61.13	55.19
Jung et al. [60]	70.94	145.00	47.00
Bennett and Chen [7]	42.61	63.00	34.85
Dembi et al. [27]	41.32	57.40	36.93

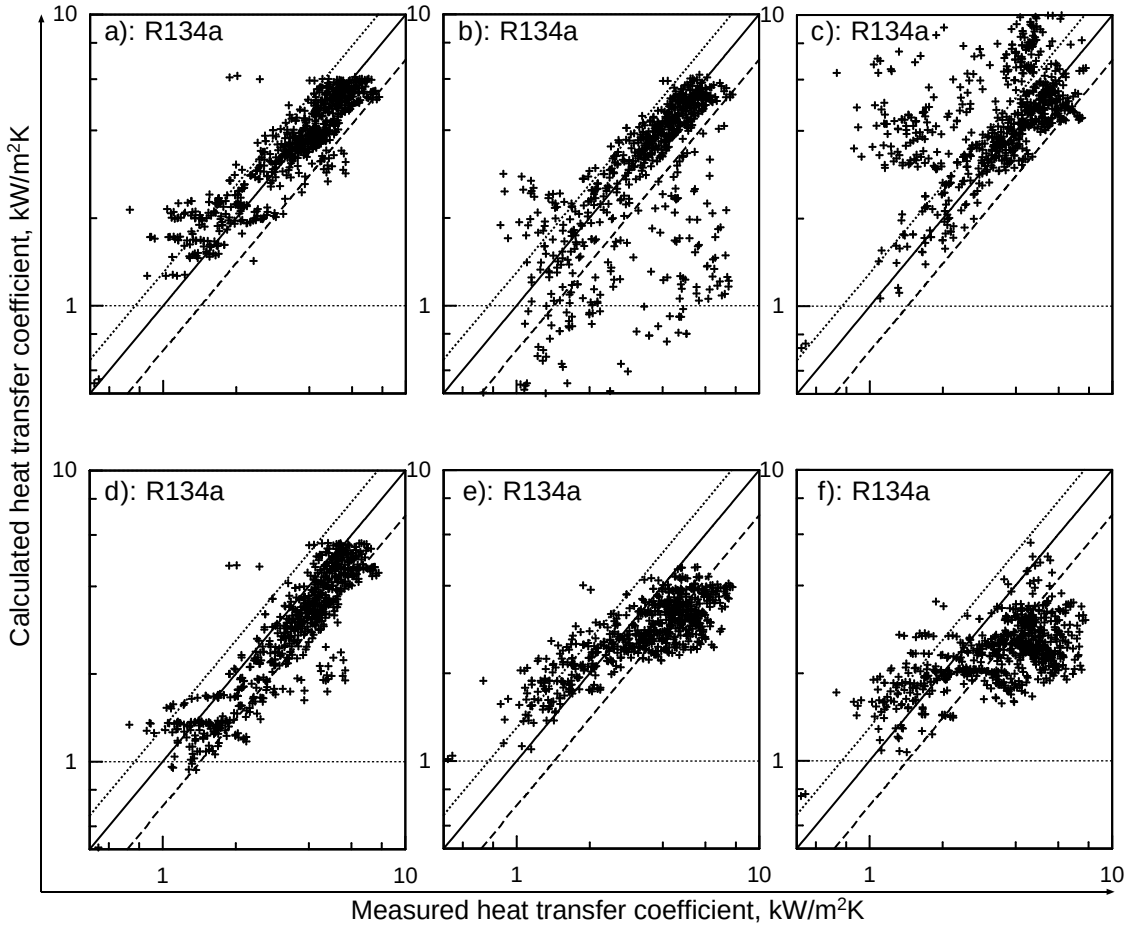

Figure 5.10. Comparison of the experimental heat transfer coefficient for R134a data with: a) Steiner [128], b) Kattan et al. [73], c) Shah [118], d) Kandlikar [66], e) Gungor and Winterton [48] and f) Schrock and Grossman [117] correlation. Legend: (——) correlation, (△) experiment, (· · ·) +30%, (- - -) -30%.

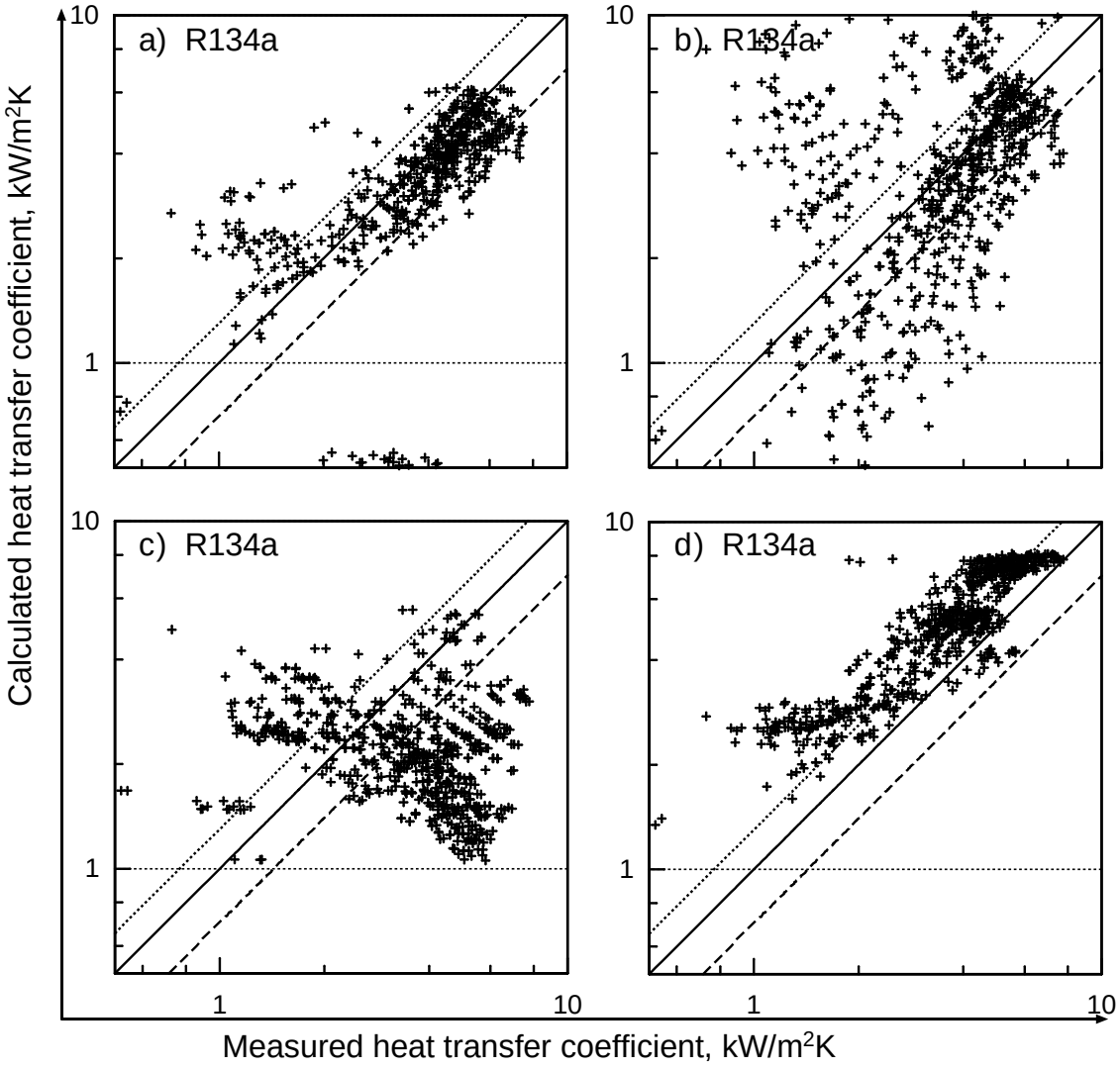

Figure 5.11. Comparison of the experimental heat transfer coefficient for R134a data with: a) Klimenko [79], b) Jung et al. [60], c) Bennett and Chen [7] and d) Dembi et al. [27] correlation. Legend: (——) correlation, (△) experiment, (· · ·) +30%, (- - -) -30%.

Among the existing correlations the Steiner [128] correlation gives the best fit to the data with a mean deviation of 15.48 %, standard deviation of 28.05 % and 89.92 % of the data falls within an error band of ± 30 %. A similar level of uncertainty of the Steiner [128] correlation was previously reported by Wettermann [148] for R134a at saturation pressure of more than 5 bar under thermal boundary condition of constant heat flux. Other models which have mean error of less than 30 % include the Kattan et al. [73], Kandlikar [66] and Gungor and Winterton [48] and Schrock and Grossmann [117] correlations. Jung et al. [60], Shah [118], Kliminko [79], Bennett and Chen [7] and Dembi et al. [27] correlations give the poorest fit to the data with mean deviation of 40-70 %. A similar level of inaccuracy associated with the latter five correlations were reported in Kattan et al. [73] and Collier and Thome [23]. The latter authors have attributed the high level of inaccuracy associated with these correlations to the fact that these are vertical tube correlations. In vertical upflow, dryout tends to occur at qualities far below

than that for horizontal flow. In addition these correlations were developed based on a data bank obtained with electrical heating of the test sections. Electrical heating has an adverse influence on the heat transfer coefficients measured with partially wetted tube walls. Furthermore, these correlations do not take the flow pattern into account.

More detailed comparisons were also made by dividing the data into small ranges according to different dimensionless groups and parameters (*i.e.* Re, Pr, $\dot{x}$). Over the different range of $\dot{x}$ and at a constant Reynolds number Re and Prandtl number Pr the Steiner [128] correlation gives a good result. Specimen of this type of comparison is shown in Fig. 5.12a and Fig. 5.12b. The slope of the correlation is similar to the experimental data from about 5 to 70 percent vapor quality. It can be seen that there is a wide deviation towards the point of maximum peak (dryout). This is expected since the Steiner [128] correlation is recommended strictly in the region prior to the point of dryout. The critical qualities, for example of the two cases at hand, predicted using Kon'kov [82] model are 0.85 and 0.9 for a saturation temperature of -20 ^{o} C and -10 ^{o} C respectively. This yields a deviation of less than 15% from the measurements.

For relatively low Reynold number region ($2300 \geq Re_L \geq 5.0 \times 10^4$) all correlations in which the convective boiling was modeled using Dittus-Boelter [30] correlation give poor results than those based on Gnielinski [42] correlation. Those correlations which are based on Dittus-Boelter [30] include Kattan et al. [73], Shah [118], Kandlikar [66], Gungor and Winterton [48], Jung et al. [60], Bennett and Chen [7]correlation. Boelter-Dittus [30] is recommended in the range of $Re_L \leq 5 \times 10^4$. For small Prandtl number ($Pr_L < 5.0$) all correlations works evenly. In the present wok the Prandtl number is within the range of $1 < Pr_L < 5.0$.

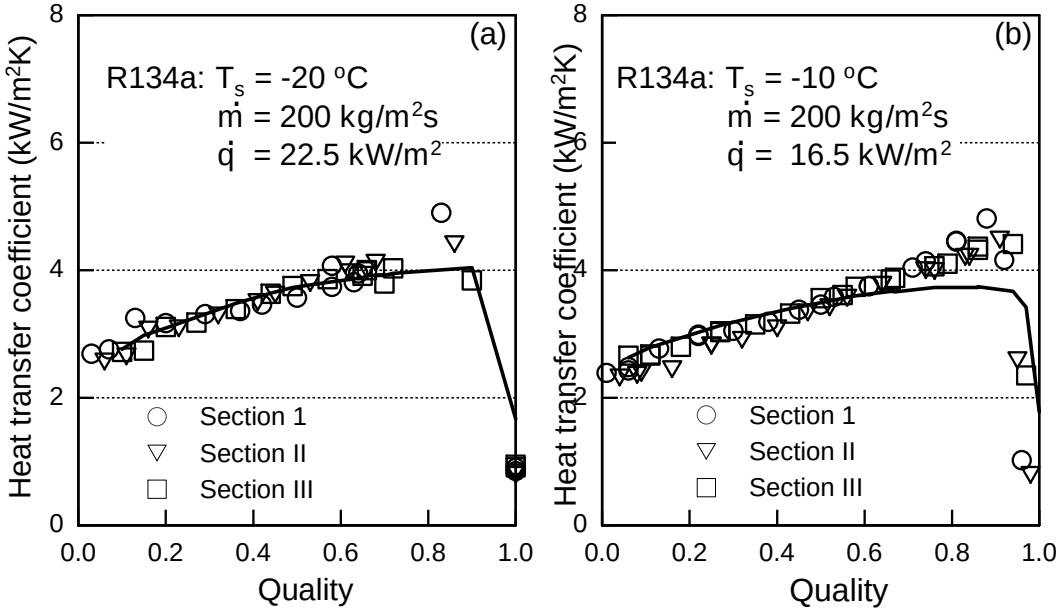

Figure 5.12. The heat transfer coefficient vs quality. The solid line represents the Steiner [128] correlation in the range $0 \leq \dot{x} \leq 1$.

5.1.5 Comparisons with previous experimental work

As is indicated earlier in chapter 2 there exists a number of experimental data for the flow boiling of the pure R134a on a plain horizontal tube. However, most of the available experimental data were carried out under the thermal boundary condition of constant heat flux realised by using electrical heating. There exists no experimental data with the thermal boundary condition of constant wall temperature; heating with a condensing steam. Nevertheless there exists very few experimental data with *nearly* constant wall temperature; heating with the liquid water. In turn most of these data of nearly constant wall temperature are at relatively high saturation pressure/temperature.

For the sake of comparison with the available experimental data of nearly constant wall temperature, a number of test runs are carried out at the same saturation temperature and mass flux and nearly the same heat flux to that of the previous work. Fig. 5.13 shows the result of the comparison between the present work and the previous work of Kattan et al. [72]. The results show a relatively wide scatter from the Kattan et al. [72] experimental data. This is expected because the Kattan et al. [72] experimental data is obtained using a single liquid phase of water as a heating medium. Heating with water yields a lower heat flux than the heating with a condensing steam.

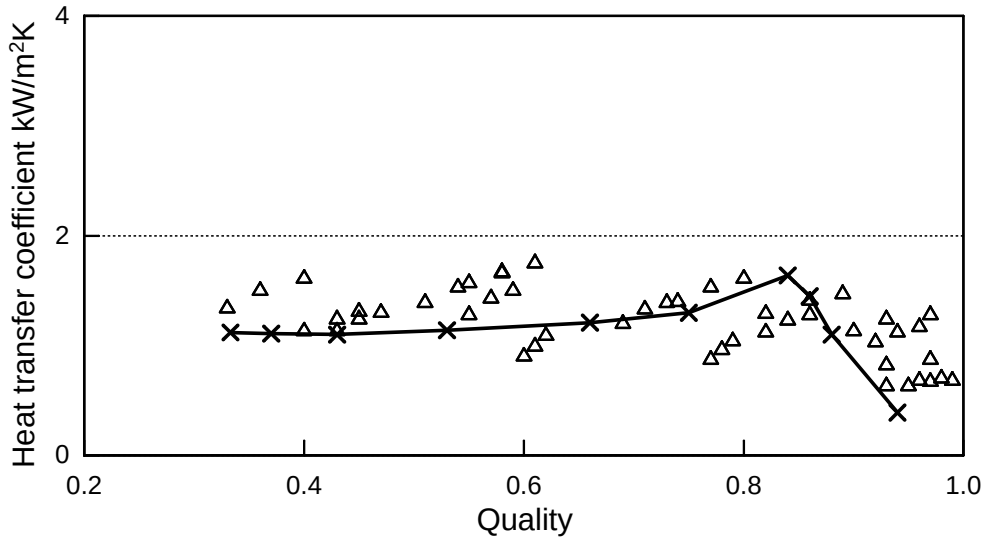

Figure 5.13. Comparison between the present work and the previous work of Kattan et al. [72] at $\dot{m}$=100 kg/m^{2}s and T_s=4.4 °C. Legend: (△) the present work $\dot{q}$=2-8 kW/m^2, (×) the Kattan et al. [72] experimental data at $\dot{q}$=1.2-7.2 kW/m^2.

5.1.6 Repeatability of R134a data

In the open literature the author is unaware of flow boiling heat transfer data for R134a within the range of the current work and under a thermal boundary condition of constant wall temperature. In this work a number of measurements were repeated under the same measurement procedure and conditions over a period time. Fig. 5.14 shows the repeatability of the heat transfer coefficient for R134a at a mass flux of 200 kg/m^2s, heat

flux 16.5 kw/m^2 and two saturation temperature of -30 °C and -10 °C for a wide range of vapor qualities. The data were repeatable within a mean deviation of less than ±8 %.

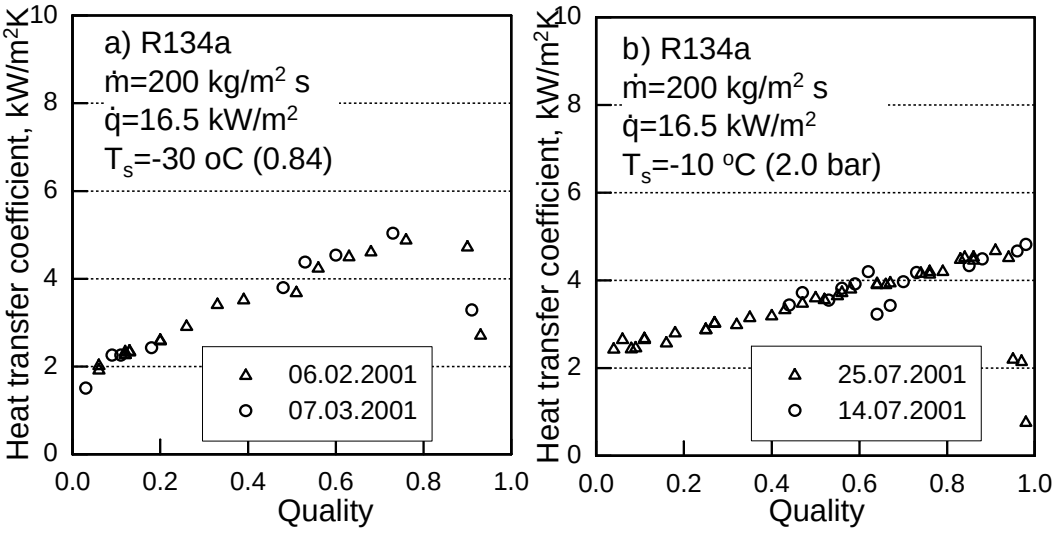

Figure 5.14. Reproducibility of the local heat transfer coefficient for R134a.

5.2 Results for R134/R290 mixtures

The existing correlations and experimental data on the evaporation of mixtures generally indicate that the heat transfer coefficient, in addition to the thermal and hydrodynamic parameters, is strongly influenced by the mixture concentration and mass transfer across the two phases. Against this background the local heat transfer coefficient is measured for a wide range of bulk composition $0 < \widetilde{z} < 65$ mole % propane. The measurements were carried out under the same thermal and hydrodynamic working conditions as for pure R134a. In the following subsections the influence of the various working parameters on the local heat transfer coefficient of R134a-R290 mixtures is presented. Additionally, as for the case of pure R134a, a detailed comparison between the results and the available correlations is made.

5.2.1 Influence of the concentration

It is indicated earlier that, as for the case of pure component, the flow boiling of mixtures is also caused by nucleate boiling, convective boiling or a combination of both mechanisms. In turn both mechanisms and their combined contribution are strongly influenced by the mixture concentration $\widetilde{x}$ and the resistance to mass transfer. In this subsection the influence of the R134a-R290 concentration and the resistance to mass transfer on these mechanisms and their combined contribution is investigated. It is to be remembered, that throughout this work the mass transfer resistance is represented by the concentration difference $\widetilde{y} - \widetilde{x}$.

In the nucleate boiling region Schlünder [115] has postulated that the reduction in the mixture heat transfer coefficient relative to the heat transfer coefficient of the pure components of the mixture is caused by the reduction of the driving temperature difference $T_w - T_{ph}$. Here T_w and T_{ph} are the wall temperature and the vapor-liquid interface temperature respectively. The vapor-liquid interface temperature T_{ph} is defined in the phase diagram of a binary R134a-R290 mixture shown in Fig. 5.15 as an illustration. Because of the preferential evaporation of the more volatile component R290, the concentration of the more volatile component at the liquid-vapor interface $\widetilde{x}_{1,ph}$ is smaller than that in the liquid phase, $\widetilde{x}_1$. Therefore, under thermodynamic equilibrium; the **actual** bubble point temperature $T_{ph}(\widetilde{x}_{1,ph})$ at the vapor-liquid interface is higher than the bubble point temperature $T_s(\widetilde{x}_1)$ in the liquid phase (cf. Fig. 5.15). Against this background Schlünder [115] has defined an effective nucleate boiling heat transfer coefficient in the vapor-liquid interface as

$$\alpha_{n,eff} = \frac{\dot{q}}{T_w - T_{ph}} \ . \tag{5.10}$$

And the nucleate boiling heat transfer coefficient in the liquid film is defined as

$$\alpha_n = \frac{\dot{q}}{T_w - T_s} \ . \tag{5.11}$$

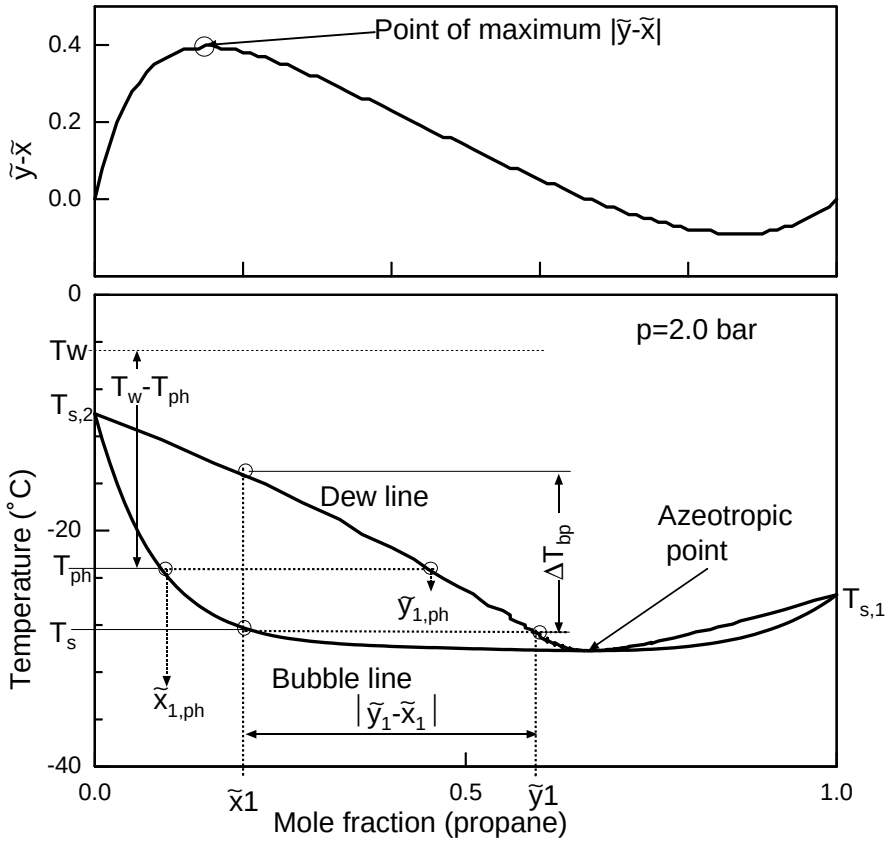

Figure 5.15. Phase diagram for a binary R134a-R290 mixture.

Combination of equation 5.10 and equation 5.11 yields

$$\frac{\alpha_n}{\alpha_{n,eff}} = \frac{1}{1 + \frac{\alpha_{n,eff}}{\dot{q}}(T_{ph} - T_s)} \ . \tag{5.12}$$

Schlünder [115] replaced the effective nucleate boiling heat transfer coefficient in equation 5.12 with an ideal nucleate boiling heat transfer coefficient $\alpha_{n,id}$. Hence equation 5.12 becomes

$$\frac{\alpha_n}{\alpha_{n,id}} = \frac{1}{1 + \frac{\alpha_{n,id}}{\dot{q}}(T_{ph} - T_s)} \ . \tag{5.13}$$

The ideal nucleate boiling heat transfer coefficient can be derived for a binary mixture as

$$\alpha_{n,id} = \frac{\dot{q}}{\Delta T_{id}} \ , \tag{5.14}$$

where the ideal wall superheat is

$$\Delta T_{id} = \sum \widetilde{x}_i \Delta T_i = \widetilde{x}_1 (T_w - T_{s,1}) + \widetilde{x}_2 (T_w - T_{s,2}) \ . \tag{5.15}$$

$T_{s,1}$ and $T_{s,2}$ are the saturation temperatures of the mixture components at the system pressure. Upon substitution of equation 5.15 into equation 5.14 and with some mathematical manipulation the ideal nucleate boiling heat transfer coefficient is

$$\alpha_{n,id} = \frac{\widetilde{x}_1}{\alpha_{n,1}} + \frac{\widetilde{x}_2}{\alpha_{n,2}} \ , \tag{5.16}$$

where $\alpha_{n,1}$ and $\alpha_{n,2}$ are the nucleate boiling heat transfer coefficients of the pure component of the binary mixture components. Equation 5.13, besides the nucleate heat transfer coefficient α_n contains the unknown temperature T_{ph}. To close equation 5.13 the interface temperature T_{ph} needs to be determined. Schlünder [115] derived the mole fractions of the liquid-vapor interface $\widetilde{y}_{1,ph}$ and $\widetilde{x}_{1,ph}$ based on the film theory as follows

$$\frac{\widetilde{y}_{1,ph} - \widetilde{x}_1}{\widetilde{y}_{1,ph} - \widetilde{x}_{1,ph}} = exp\left(-\frac{B_o.\dot{q}}{\rho_l \beta_L \Delta h_V}\right) \ , \tag{5.17}$$

where $\widetilde{y}_{1,ph}$, $\widetilde{x}_1$, $\widetilde{y}_{1,ph}$ and $\widetilde{x}_{1,ph}$ are defined in the phase diagram shown in Fig. 5.15. ρ_L and Δh_V are the ideal mixture's liquid density and the latent heat of evaporation respectively. β_L is a mass transfer coefficient and B_o is a constant. For practical application Schlünder [115] has approximated the bubble line curve as

$$T_{ph} - T_s \approx \frac{\partial T_s}{\partial \widetilde{x}_1}.(\widetilde{x}_{1,ph} - \widetilde{x}_1) \ , \tag{5.18}$$

$$\frac{\partial T_s}{\partial \widetilde{x}_1} \approx -(T_{s,2} - T_{s,1}) \ , \tag{5.19}$$

and

$$\widetilde{y}_{1,ph} - \widetilde{x}_{1,ph} \approx \widetilde{y}_1 - \widetilde{x}_1 \ . \tag{5.20}$$

Combination of equations 5.17-5.20 into equation 5.13 yields the well known Sclünder [115] model for nucleate boiling

$$\frac{\alpha_n}{\alpha_{n,id}} = \frac{1}{1 + \frac{\alpha_{n,id}}{\dot{q}}.(\widetilde{y}_1 - \widetilde{x}_1).\left(1 - \exp\left(-\frac{B_o.\dot{q}}{\rho_L \beta_L \Delta h_V}\right)\right)} \ . \tag{5.21}$$

The locus of Schlünder [115] equation 5.21 is shown for two different cases in Fig. 5.16a and Fig. 5.16b. Here the ideal nucleate boiling heat transfer coefficient is predicted using the Steiner [128] correlation, and the mass transfer coefficient is defined as (Wettermann [148])

$$\frac{B_o}{\beta_L} = \frac{\alpha_{n,id}}{c_{pL}\rho_L} \ . \tag{5.22}$$

The concentrations of the liquid and vapor phases $\widetilde{x}$ and $\widetilde{y}$ are predicted using the flash program presented in section 4.8. The physical properties of the R134a-R290 are given in Appendix B. For both cases presented in Fig. 5.16a and Fig. 5.16b the locus of the nucleate boiling curve shows strong influence of the mixture concentration on the nucleate boiling heat transfer coefficient. That is to say, in the region prior to the azeotropic point, the nucleate boiling decreases with increasing concentration till it reaches a minimum point, then it increases towards the azeotropic point. The similar cycle is repeated in the region beyond the azeotropic point. The point of the minimum corresponds to the point where the concentration difference $|\widetilde{y} - \widetilde{x}|$ is maximum. The corresponding $(\widetilde{y} - \widetilde{x}) - \widetilde{x}$ diagrams are shown in the upper parts of Fig. 5.16a and Fig. 5.16b.

In the convective boiling region, VDI-Wärmeatlas [143] and Gropp [46] indicated that for a liquid mixture which possesses normal viscosity, the effect of mass diffusion resistance

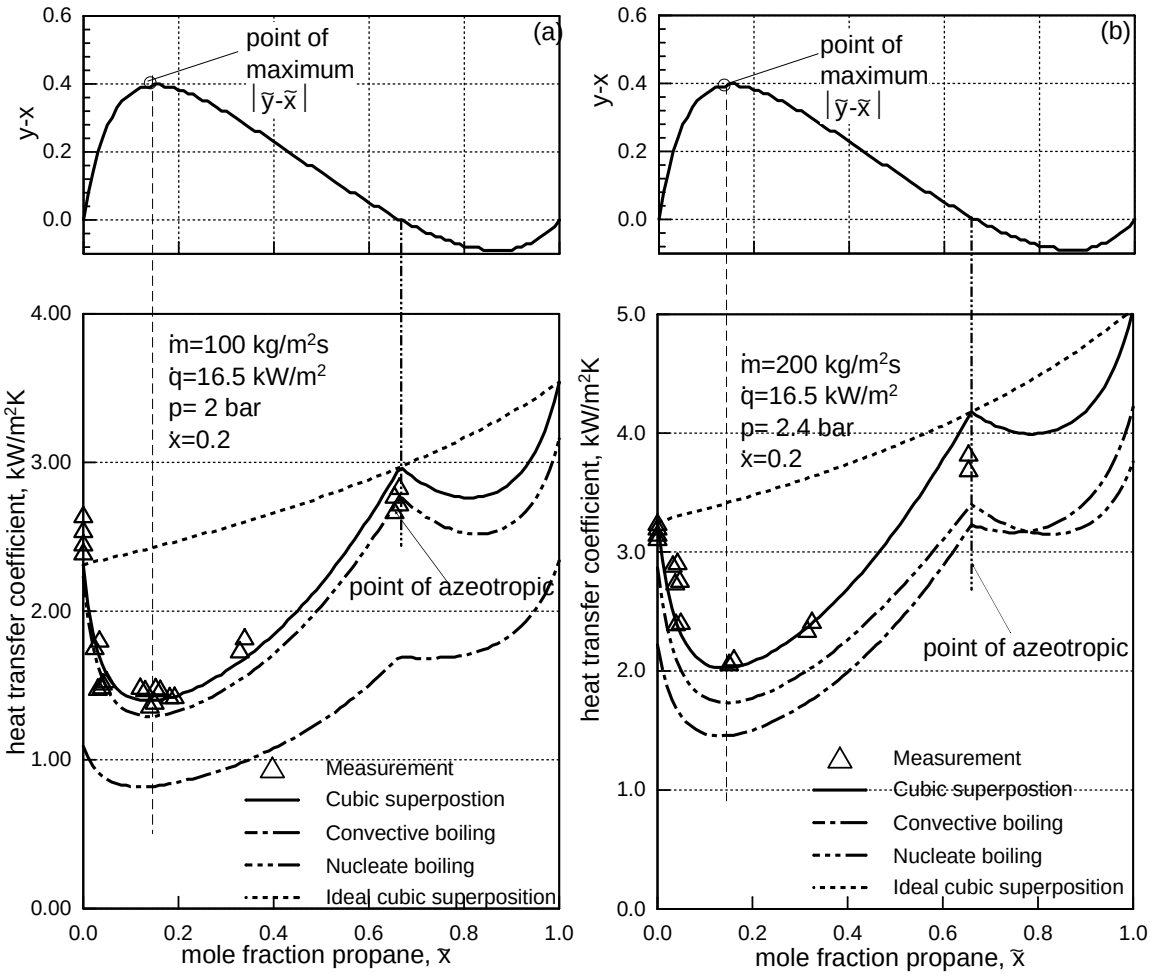

Figure 5.16. Influence of mole fraction on the local heat transfer coefficient for R134a/R290 mixtures.

on the convective heat transfer can be neglected. Mixtures of normal viscosity include liquid-liquid miscible mixtures or azeotropic or near azeotropic mixtures. For high viscosity mixtures Palen [104], who investigated flow boiling of ethylene glycol-water and propylene glycol-water mixtures; indicated that the resistance of mass diffusion on the convective heat transfer is significant. The high viscosity fluid include mixtures which possess liquid-liquid immiscibility. According to Tillner-Roth [137] and Holcomb et al. [54] the R134a-R290 mixture possesses a liquid-liquid immiscibility at low temperatures of $T < 270$ K. VDI-Wärmeatlas [143] has recommended that for a liquid-liquid miscible mixture, the convective boiling heat transfer coefficient is treated as though it were a pure component with pseudo-properties of the mixture. For a liquid-liquid immiscibility mixture the convective heat transfer coefficient is also strongly influenced by the diffusion coefficient. Under such circumstances the convective heat transfer coefficient is modelled analogous to nucleate boiling as

$$\frac{\alpha_c}{\alpha_{c,id}} = \frac{1}{1 + \frac{\alpha_{c,id}}{\dot{q}}.(\widetilde{y}_1 - \widetilde{x}_1).\left(1 - \exp\left(-\frac{B_o.\dot{q}}{\rho_L \beta_L \Delta h_V}\right)\right)} \ , \tag{5.23}$$

where $\alpha_{c,id}$ is an ideal convective boiling heat transfer coefficient. It is obtained by equa-

tion 5.16 with pure component convective boiling heat transfer coefficients $\alpha_{c,1}$ and $\alpha_{c,2}$ replacing $\alpha_{n,1}$ and $\alpha_{n,2}$ respectively. The locus of equation 5.23 with $\alpha_{c,1}$ and $\alpha_{c,2}$ obtained using Steiner [128] correlation for convective boiling heat transfer coefficient, is shown also for two different cases in Fig. 5.16a and Fig. 5.16b. As can be seen from these two figures; similar to nucleate boiling, the concentration $\widetilde{x}$ and concentration difference $\widetilde{y} - \widetilde{x}$ have also strong influence on the convective boiling.

In the region where both the convective and nucleate boiling heat transfer mechanisms are present, the local heat transfer coefficient is generally made up as a contribution of both mechanisms. There exist a number of ways to describe the interactions of the two boiling mechanisms however, it appears that the asymptotic model of Steiner [128] is the most practical one. Steiner [128] asymptotic model is given as:

$$\alpha = \left(\alpha_n^3 + \alpha_c^3\right)^{1/3} \quad . \tag{5.24}$$

The locus of the cubic asymptotic model given by equation 5.24 is shown for two cases in Fig. 5.16a and Fig. 5.16b. The convective (α_c) and the nucleate (α_n) boiling heat transfer coefficient are predicted using equation 5.23 and equation 5.21 respectively. As for the cases of nucleate and convective boiling mechanisms it can be seen in both figures the concentration $\widetilde{x}$ and concentration difference $\widetilde{y} - \widetilde{x}$ have strong influence on the mixture local heat transfer coefficient in the region where both mechanisms are present.

It is indicated earlier that, as for the case of pure component, the heat transfer in flow boiling of mixtures occurs by nucleate and convective boiling or their combined interaction. Therefore it is in the interest of the present study to verify the validity of this assumption by the data of R134a-R290 mixtures. For this purpose the measured local heat transfer coefficients are superimposed as triangle symbols on the calculated nucleate and convective boiling and their combined contribution as shown for two different cases in Fig. 5.16a and Fig. 5.16b. The measured local heat transfer coefficient for R134a-R290 mixture (triangle symbols) matches very well with the locus of the local heat transfer coefficient predicted using the asymptotic model of Steiner [128] (solid line). However, the measured local heat transfer coefficient (triangle symbols) lays slightly away from the locus of the nucleate boiling curve (double centered line) and wide away from the locus of the convective boiling curve (centered line), for the data presented in Fig. 5.16a. This suggests that, for this particular set of data, the local heat transfer coefficient may not be convective dominated boiling. It may may either be for nucleate dominated boiling or a combination (interaction) of both boiling mechanisms. It is to be remembered that this particular set of data is obtained at relatively low mass flux (100 kg/m^{2}s) and quality (*i.e.* low Reynolds number). Additionally most of the observed flow patterns, at this particular set of data, are identified with stratified to wavy flow patterns. Under these flow boiling conditions the domination of the nucleate boiling may be justified. A detailed discussion about this point is presented earlier in subsection 5.1.1. For the set of data presented in Fig. 5.16b the measured local heat transfer coefficient (triangle symbols) lis wide away from the locus of both the nucleate boiling curve (double centered line) and the convective boiling curve (centered line). It however, matches very well the asymptotic curve (solid

line). Again it is to be remembered that this set of data is rather at an intermediate mass flux (200 kg/m^{2}s) and most of the observed flow patterns are identified as transition to annular flow pattern. Under these flow patterns both flow boiling mechanisms are known to be present. For more elaboration about this point reference is made to subsection 5.1.1.

Besides the confirmation of the strong influence of the concentration and concentration difference on the local heat transfer coefficient of R134a-R290 mixtures due to the nucleate boiling, convective boiling and their combined contribution, the following observations may be drawn as well to Fig. 5.16a and Fig. 5.16b.

i the mixture local heat transfer coefficient is smaller than the ideal heat transfer coefficient. The ideal heat transfer coefficient is presented with a dotted line in Fig. 5.16a and Fig. 5.16b. It is calculated using equation 5.24 with $\alpha_{n,id}$ and $\alpha_{c,id}$ being the ideal nucleate and convection boiling heat transfer coefficient. These are estimated from the mixture component using Steiner [128] correlation at the system pressure, mass flux, heat flux and quality.

ii both nucleate and convective boiling mechanisms and their combined effect are influenced by the the concentration difference $\widetilde{y} - \widetilde{x}$. It can be seen that a maximum decrease in the local heat transfer coefficient occurs at the point where the concentration difference $|\widetilde{y} - \widetilde{x}|$ is maximum. The maximum point of $(\widetilde{y} - \widetilde{x})$ is shown in the upper part of Fig. 5.16a. The values of $\widetilde{x}$, $\widetilde{y}$ for a given temperature and pressure are calculated using the flash problem (section 4.8). The maximum difference $(\widetilde{y} - \widetilde{x})$ occurs at a mole fraction of 12 percent R290. At this mole fraction the mixture heat transfer coefficient decreases by factor of **2** relative to that for pure R134a and by factor of **2.5** relative to pure R290. It is to be remembered that the local flow boiling heat transfer coefficient for pure R290 used to obtain the latter ratio is predicted by using Steiner [128] correlation.

iii the local heat transfer coefficient increases towards the point of azeotrope. This due to the diminish of the diffusion effect, which is caused by the decrease of the concentration difference between the liquid and vapor phases $(\widetilde{y} - \widetilde{x})$ towards the point of azeotropic; at the point of azeotropic $|\widetilde{y} - \widetilde{x}| \rightarrow 0$. The local heat transfer coefficient at the azeotropic point, for example for the case presented in Fig. 5.16a, is enhanced by factor of **1.2** relative to that for pure R134a. However, it is degraded by factor **1.2** relative to the theoretical value of pure R290.

5.2.2 Influence of the mass flux

Fig. 5.17 shows the influence of mass flux on the local heat transfer coefficient at a mass flux of 100, 200 and 300 kg/m^{2}s at the same working pressure, heat flux and vapor quality. The solid line in Fig. 5.17 represents the predicted local heat transfer coefficient as calculated with equation 5.24. As for the case of a pure component, it is clear that there is a significant effect of the mass flux on the local heat transfer coefficient; the local heat transfer coefficient increases with mass flux. Furthermore, the influence of mass

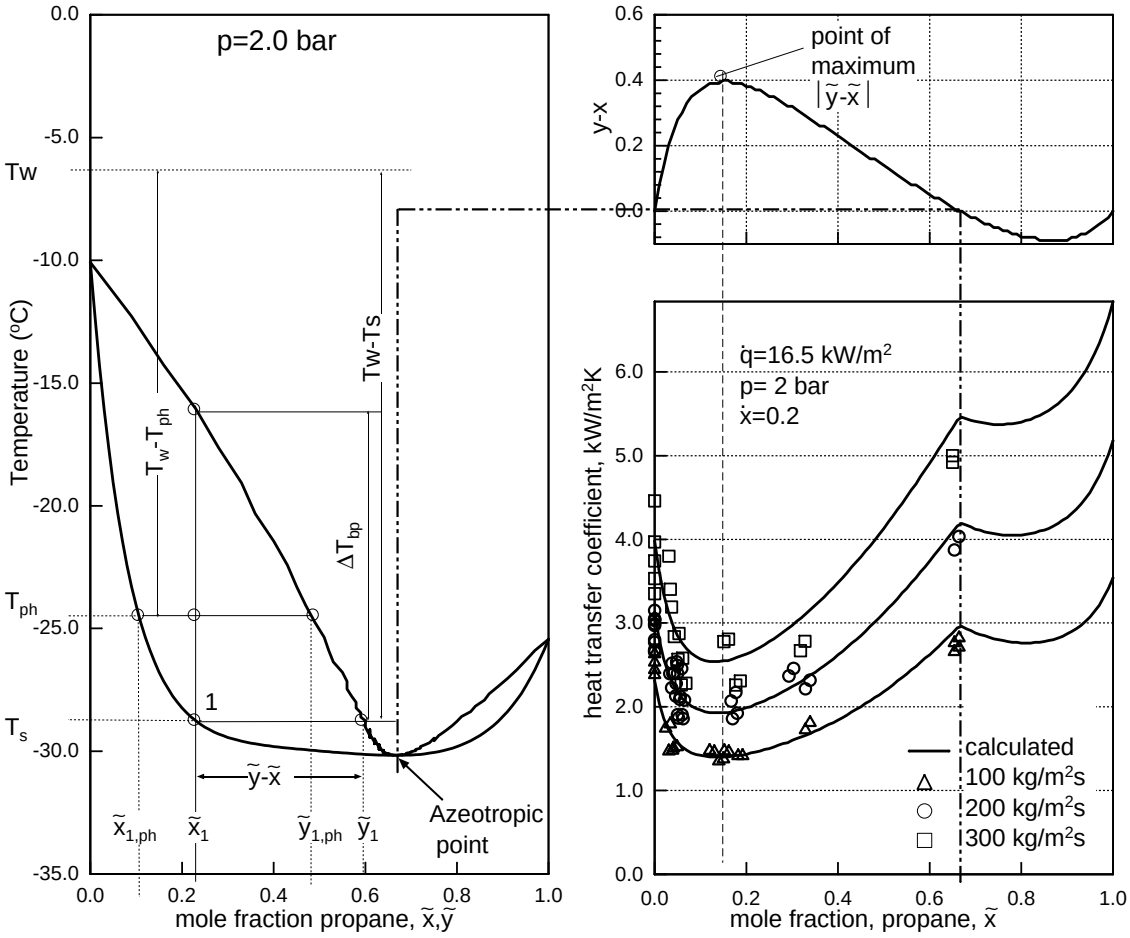

Figure 5.17. Influence of mass flux on the local heat transfer coefficient heat transfer coefficient for R134a/R290 mixtures.

flux on the local heat transfer coefficient increases with the mole fraction of the more volatile component R290. For example, at a mole fraction of 0.18 R290, the difference between the local heat transfer coefficients at 200 and 100 kg/m^{2}s does not exceed 0.5 kW/m^{2}K and that at the point of azeotropic exceeds 1.0 kW/m^{2}K. Such dependency of mass flux on the concentration depletion was previously observed by Niederkrüger et al. [99] and Wettermann [148]. They have attributed this effect to the change in mass transfer coefficient with mass flux.

5.2.3 Influence of the saturation pressure

Fig. 5.18 shows the local heat transfer coefficient for two pressures of 2 and 2.4 bar at the same heat flux, mass flux and vapor quality. The solid line in Fig. 5.18 represents the predicted local heat transfer coefficient calculated with equation 5.24. The concentration difference $(\widetilde{y}-\widetilde{x})$ is also dependent on the saturation pressure as can be seen in the $(\widetilde{y}-\widetilde{x})$-$\widetilde{x}$ diagram shown in the upper part of Fig. 5.18. The local heat transfer coefficient increases with pressure. With increasing pressure the maximum concentration difference $(\widetilde{y}-\widetilde{x})$ rises and is being shifted slightly to smaller mole fractions of the more volatile component

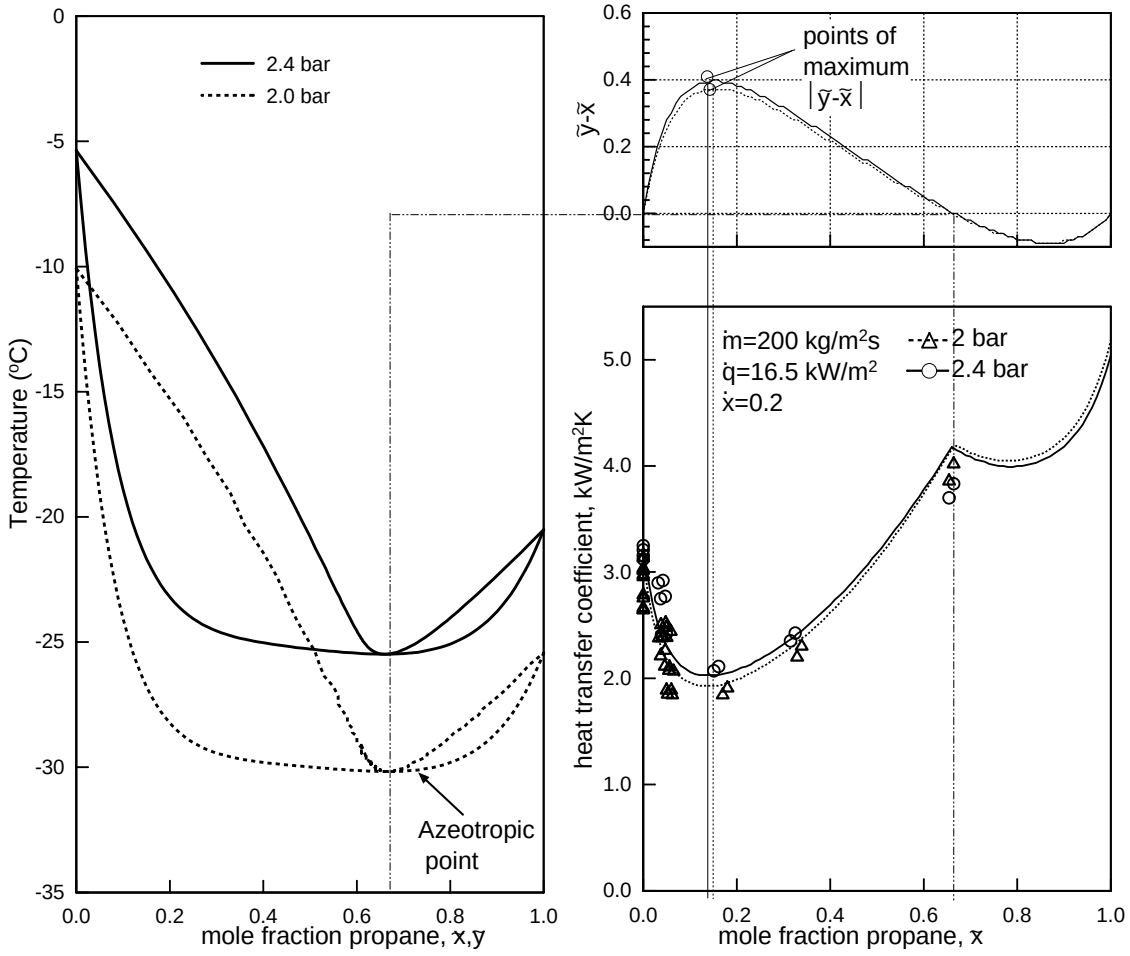

Figure 5.18. Influence of pressure on the local heat transfer coefficient for R134a/R290 mixtures.

R290. As a consequence the point of the minimum of the local heat transfer coefficient is being shifted to a smaller mole fraction of R290 as shown in Fig. 5.18. Furthermore, the relative reduction in heat transfer coefficients is higher with increasing pressure and is in contrast to the vapor-liquid composition difference. That is to say, the influence of pressure on the local heat transfer coefficient is greater in the zeotropic region than that at the azeotropic point, near azeotropic or pure R134a region.

5.2.4 Influence of the vapor quality

One useful way to present the influence of vapor quality in the mixture is to plot the local heat transfer coefficient as an ordinate and the quality as an abscissa similar to that for a pure component. Fig. 5.19a and Fig. 5.19b show the local heat transfer coefficient for R134a-R290 mixtures with bulk composition of 0 to 65 mole percent R290 at various working conditions. Fig. 5.19a corresponds to runs at a mass flux of 200 kg/m^{2}s and a heat flux of 16.5 kW/m^2. Fig. 5.19b corresponds to runs at different mass fluxes however, at the same pressure, heat flux and bulk composition of the mixture. As for the case of pure component, the heat transfer coefficient increases steadily with quality until it

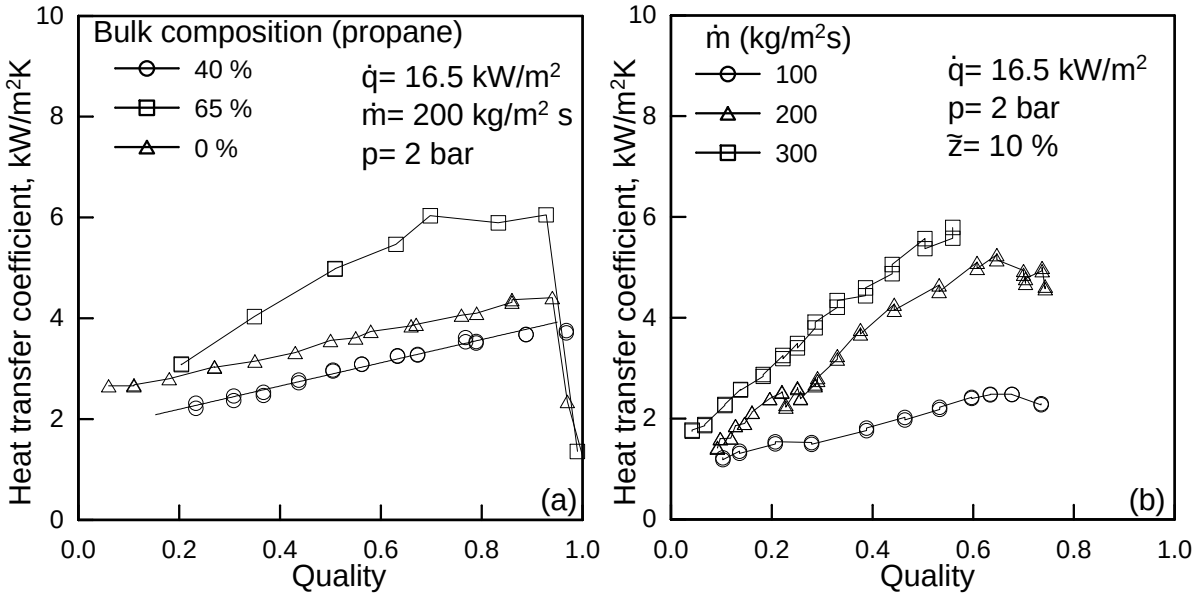

Figure 5.19. Heat transfer coefficient vs. quality at various working conditions for flow boiling of R134a/R290 mixtures.

reaches a peak point, onset of partial dryout, followed by a sharp falloff. As for the case of pure component, the change in the slope of the heat transfer coefficient with respect to quality is attributed to the change in the flow pattern and the relative contribution of both flow boiling mechanisms: nucleate and convective. A detailed elaborations about this point was presented earlier in subsection 5.1.1. More experimental data on the flow boiling of R134a/R290 mixtures is presented in Appendix F.

5.2.5 Comparisons with correlations

In contrary to pure fluid there exists a limited number of correlations for the prediction of the local heat transfer coefficient for mixtures. In all correlations the diffusion effect in nucleate boiling is taking into account. This is generally employed by using a suppression factor. There exists in the literature a number of models which describe the suppression factor. However, the most widely ones used are those of Schluender [115] and Thome [134], for they are physical based. The Schlünder [115] suppression factor, which is derived earlier, is reproduced as

$$F = \left\{ 1 + \frac{\alpha_{n,id}}{\dot{q}} (T_{b,k} - T_{b,j})(\tilde{y}_j - \tilde{x}_j) \left[1 - \exp \frac{B_o \dot{q}}{\rho_L \Delta h_V \beta_L} \right] \right\} \ , \tag{5.25}$$

and that for Thome [134] is

$$F = \left\{ 1 + \frac{\alpha_{n,id}}{\dot{q}} \Delta T_{bp} \left[1 - \exp \frac{B_o \dot{q}}{\rho_L \Delta h_V \beta_L} \right] \right\} \ . \tag{5.26}$$

With respect to the convective boiling heat transfer coefficients, most of the existing correlation do not account for the diffusion resistance to convective heat transfer even for mixtures which possesses liquid-liquid immiscibility.

In the present study five (5) correlations have been fitted to the R134a-R290 data. Namely these are the Steiner [128], Jung et al. [60], Kandlikar [67], Bennet and Chen [7] and Palen [104] correlation. The calculation procedure for each of these correlations is given in Appendix C. The thermodynamics and transport properties required for the calculation of the local heat transfer coefficient for R134a-R290 mixtures are given in appendix B. It is to be remembered, as for pure components, that these correlations are valid only in the region prior to the point of the dryout; $\dot{x} < \dot{x}_c$. Thus all data points that are at dryout and beyond, $\dot{x} \geq \dot{x}_c$, are excluded in the comparisons. Fig. 5.20a to Fig. 5.20d show a

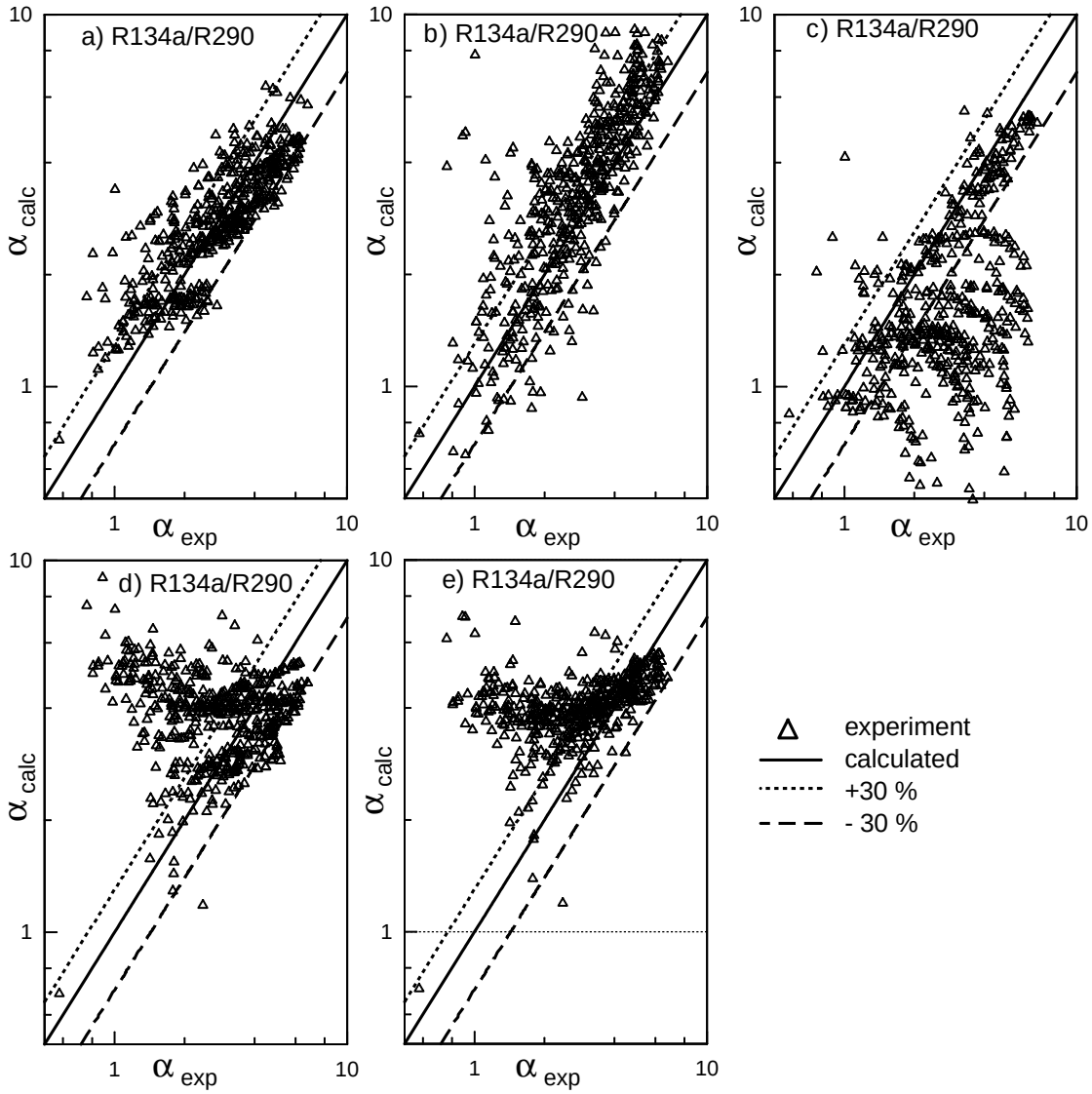

Figure 5.20. Comparison of five correlations with experimental data of R134a/R290 mixtures under a wide range of parameters. Correlation: a) Steiner [128] b)Jung et al. [60], c) Kandlikar [67], d) Bennett and Chen [7] and e) Palen [104].

comparison between the measured and the calculated local heat transfer coefficient for R134a-R290 mixtures using the five correlations. Table 5.2 summarizes the mean error and standard deviation associated with each correlation. Additionally the number of the data points that fall within the threshold of an error band of ±30 % are given for each

correlation. The total number of data points is 3×800.

Table 5.2. Comparison of five (**5**) different correlations with experimental data of flow boiling of R134a-R290 mixtures.

Correlation	Mean error %	Standard deviation %	Percentage of data points within an error band of 30%
Steiner [128]	24.39	27.61	76.43
Jung et al. [60]	37.63	54.35	55.53
Kandlikar [67]	39.63	30.55	42.62
Bennett and Chen [7]	86.03	124.97	46.93
Palen [104]	73.58	102.96	48.98

As for the case of pure R134a the Steiner [128] correlation gives the best fit to the R134a-R290 data with a mean error of 24.39 %, standard deviation of 27.6 % and 76.43 % of the data lying with an error band of ± 30 %. This may be attributed to the fact that the correlation takes into account the diffusion effect in both the nucleate and convective boiling mechanisms particulary for liquid-liquid immiscible mixture as R134a-R290. Interestingly the Jung et al. [60] correlation gives a better fit to the mixture data than that for pure R134a. It has a mean deviation of 37.63 %, standard deviation of 54.35 % and 55.53 % of the data are within an error band of ± 30 %. While for pure R134a it had 70.94 % mean deviation (cf. table 5.1). This may be attributed to the fact that the correlation, as for the case of Steiner [128] correlation, takes the diffusion effect into account. That is to say both boiling mechanisms (*i.e.* nucleate and convection) were suppressed. The Kandlikar [67] correlation gives a mean deviation of ± 39.63 % and standard deviation of 30.55 % with only 42.62 % of the data lying within an error band of ± 30 %. The Bennett and Chen [7] correlation gives the poorest fit to the data with a mean deviation of 86.03 %, standard deviation of 124.97 % and 46.93 % of the data falls within an error band of ± 30 %. The Palen [104] correlation gives almost the same mean error as the Bennett and Chen [7] correlation. It is to be remembered that the Palen [104] correlation is a modified form of the Bennett and Chen [7] correlation.

More detailed comparisons were also made by dividing the data into to zeotropic and azeotropic regions. Fig. 5.21 shows the mean error as a function of the bulk mole fraction of R290 ($\tilde{z}$) for each correlation. Clearly all correlations give a better accuracy (*i.e.* $< 30\%$) for azeotropic ($\tilde{z}= 0.65$) data than zeotropic one ($0 < \tilde{z} < 0.65$). This may be attributed to the complete suppression of the diffusion effect at the azeotropic point. That is to say the nucleation suppression factor $F= 1.0$ (for example that defined by Schlünder [115] equation 5.25 or Thome [134] equation 5.26 is valid for all correlations). Or in other words the correlation reduces to that for a pure component with pseudo properties of the mixture. The relatively high mean error associated with all correlations in the zeotropic region may be attributed to a number of reasons:

1. the high level of uncertainty associated with the prediction of the mixture physical properties,

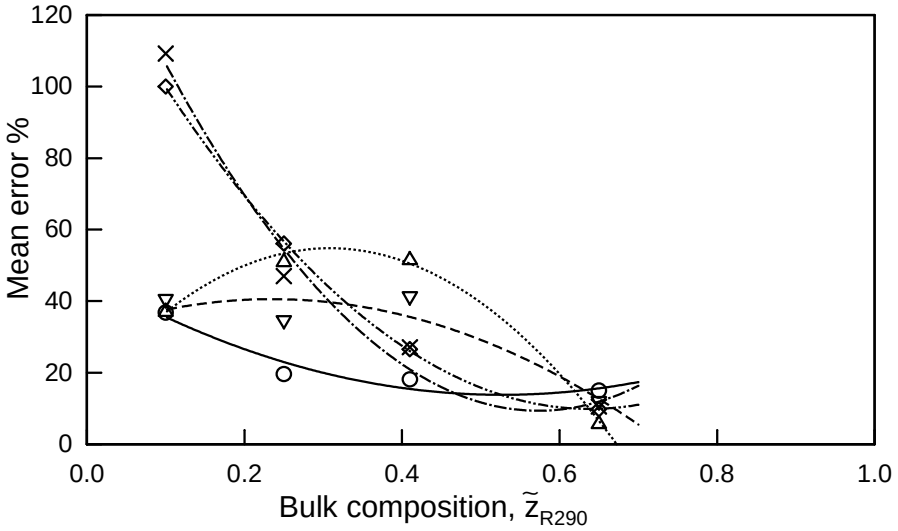

Figure 5.21. Mean error of various correlations as a function of bulk composition. Legend: (o) Steiner [128], (×) Bennet and Chen [7], (△) Kandlikar [67], (▽) Jung et al. [60] and (♢) Palen [104].

2. most of the correlation, save the Steiner [128] correlation, do not take into account the diffusion effect in the convective part of the local heat transfer coefficient even for the liquid-liquid immiscible mixture where the influence of mass diffusion on the convective heat transfer is severe,
3. most of the correlations for example the Bennett and Chen [7] and Palen [104] correlations, are basically developed for vertical tube boiling heat transfer.

5.2.6 Repeatability of R134a-R290 data

As for the case of the pure component a number of test runs were repeated to validate the experimental results for R134a-R290 mixtures. Fig. 5.22 shows the local heat transfer

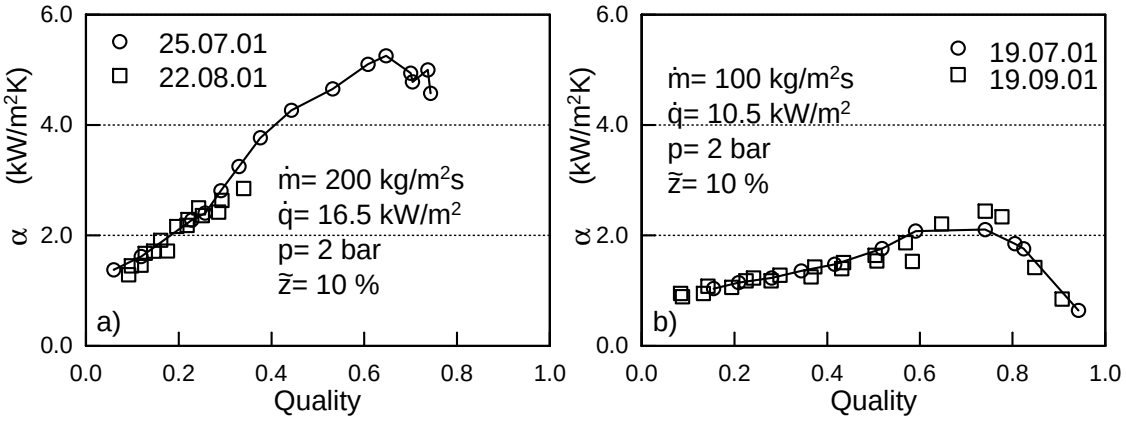

Figure 5.22. Repeatability of the R134a-R290 data.

coefficient for R134a-R290 mixture at a bulk composition of 10% mole fraction of R290 for two cases. The results indicate that the measurements are repeatable within an error band of <10 %.

6 Pressure drop

In flow boiling, the temperature drops in the direction of flow as a result of the pressure drop. This results in a change in the driving force (temperature difference) for the heat transfer along the flow path. Thus beside the heat transfer coefficient, knowledge of the pressure drop is of paramount importance in the design of the evaporator. In the present work the pressure drop is measured simultaneously with the heat transfer coefficient along the test section.

The momentum balance implies that the two phase pressure gradient is composed of three components as

$$\frac{dp}{dz} = \left(\frac{dp}{dz}\right)_f + \left(\frac{dp}{dz}\right)_a + \left(\frac{dp}{dz}\right)_h \ , \tag{6.1}$$

where dp/dz, $(dp/dz)_f$, $(dp/dz)_a$ and $(dp/dz)_h$ is the total, friction, acceleration and hydrostatic pressure gradient respectively. For a horizontal tube the hydrostatic pressure gradient diminishes. The acceleration pressure drop is caused by the change in momentum in both the liquid and vapor phases. The change in the momentum stems from the change in the velocity of the two phases, which is brought about by the added (or withdrawn) heat to/from the test section. For the case of adiabatic flow the acceleration pressure drop diminishes for $\Delta p_a/p_s \to 0$ (Baehr and Stephan [2]), where p_s is the saturation pressure.

There exist in the literature a number of approaches for modelling the change in the static pressure drop due to acceleration. The most widely accepted models include homogenous or separated flow models. The separated flow model is also widely known as the *heterogenous* model. In the homogenous model the static pressure drop due to acceleration is

$$-\left(\frac{dp}{dz}\right)_a = \dot{m}^2 \frac{d}{dz}\left[\dot{x}\left(\frac{1}{\rho_L} - \frac{1}{\rho_G}\right) + \frac{1}{\rho_L}\right] \ . \tag{6.2}$$

The energy balance in a small unit length dz along the test tube yields

$$\frac{d\dot{x}}{dz} = \frac{4\dot{q}}{\dot{m}\Delta h_v.d} \ . \tag{6.3}$$

Substitution of equation 6.3 into equation 6.2 yields the pressure drop due to acceleration as

$$\Delta p_a = \frac{4\dot{q}\dot{m}}{d.\Delta h_v \rho_G}\left(1 - \frac{\rho_G}{\rho_L}\right)\Delta L \ . \tag{6.4}$$

In the separated flow model the static pressure drop due to acceleration can be derived from the momentum balance as

$$-\left(\frac{dp}{dz}\right)_a = \dot{m}^2 \frac{d}{dz}\left[\frac{\dot{x}^2}{\varepsilon\rho_G} + \frac{(1-\dot{x})^2}{(1-\varepsilon)\rho_L}\right] \ . \tag{6.5}$$

Integration of equation 6.5 between the inlet i and outlet o of the test section yields

$$-\Delta p_a = -(p_o - p_i)_a = \dot{m}^2\left[\frac{\dot{x}_2^2}{\varepsilon_o\rho_{G,o}} + \frac{(1-\dot{x}_o)^2}{(1-\varepsilon_o)\rho_{L,o}} - \frac{\dot{x}_i^2}{\varepsilon_i\rho_{G,i}} - \frac{(1-\dot{x}_i)^2}{(1-\varepsilon_i)\rho_{L,i}}\right] \ . \tag{6.6}$$

The void fraction ε may be obtained using the Rauhani [107] model which is given as:

$$\varepsilon = \frac{\dot{x}}{\rho_G}\left\{(1+0.12(1-\dot{x}))\left(\frac{\dot{x}}{\rho_G}+\frac{1-\dot{x}}{\rho_L}\right)+\frac{1.18(1-\dot{x})[g\sigma(\rho_L-\rho_G)]^{1/4}}{\dot{m}\rho_L^{1/2}}\right\}^{-1} , \quad (6.7)$$

where ρ_L and ρ_G is the liquid and vapor density respectively, which are calculated from the fundamental equation of state of Tillner-Roth and Baehr [138] for R134a. g is acceleration due to gravity, σ is the surface tension, $\dot{m}$ is the mass flux and $\dot{x}$ is the quality. The surface tension is calculated using the method of Lucus [86] given in VDI-Wärmeatlas [143].

The pressure drop due to friction exists because of the shear stress between the fluid and the tube wall. Estimation of the friction pressure drop is somewhat more complex and various approaches have been taken, for example in homogenous or separated flow models. In the homogenous model the frictional pressure gradient is given as

$$-\left(\frac{dp}{dz}\right)_f = \frac{4\tau_o}{d} = \frac{2\xi\dot{m}^2}{d\rho_H} , \quad (6.8)$$

where ξ is the two phase friction factor calculated by a Blasius-type model as

$$\xi = \begin{cases} \frac{0.3164}{Re^{0.25}} & Re \geq 2320 \\ \\ \frac{64}{Re} & Re < 2320 . \end{cases}$$

and the homogenous densityρ_H is given as

$$\frac{1}{\rho_H} = \frac{1-\dot{x}}{\rho_L}+\frac{\dot{x}}{\rho_G} . \quad (6.9)$$

The two phase Reynolds number Re is

$$Re = \frac{\dot{m}d}{\eta_{TP}} , \quad (6.10)$$

where η_{TP} is a two-phase viscosity. A variety of methods have been proposed to calculate the two phase viscosity, a commonly used one being that proposed by McAdams et al. [88]

$$\frac{1}{\eta_{TP}} = \frac{1-\dot{x}}{\eta_L}+\frac{\dot{x}}{\eta_G} , \quad (6.11)$$

where η_L and η_G are the liquid and vapor viscosity.

In the separated flow model the two phase frictional pressure drop is related to that for single phase as

$$\left(\frac{dp}{dz}\right)_f = \left(\frac{dP}{dz}\right)_{f,L/G}\Psi_{G/L} , \quad (6.12)$$

where Ψ is the two phase multiplier. There exist a number of correlations for the prediction of Ψ. These include Friedel [38], Chishlom [20] and Lockhart and the Martinelli [85] model. These models are presented in Appendix E.

6.1 Pure R134a

The result presented in the this section is based on the frictional pressure drop

$$\Delta p_f = \Delta p_{Exp} - \Delta p_a \ , \tag{6.13}$$

where Δp_{Exp} is the measured total pressure drop and Δp_a is the calculated pressure drop due to acceleration.

Typical profiles of frictional pressure drop as a function of quality are shown in Fig. 6.1a for pure R134a for a wide range of mass fluxes. The results indicate that the pressure drop increases with quality until it reaches a peak point followed by a sharp falloff. Furthermore, the pressure drop increases with mass flux. This is attributed to the increase in the two phase velocity. It is known that as the velocity increases the shear stress between the fluid and the tube wall increases.

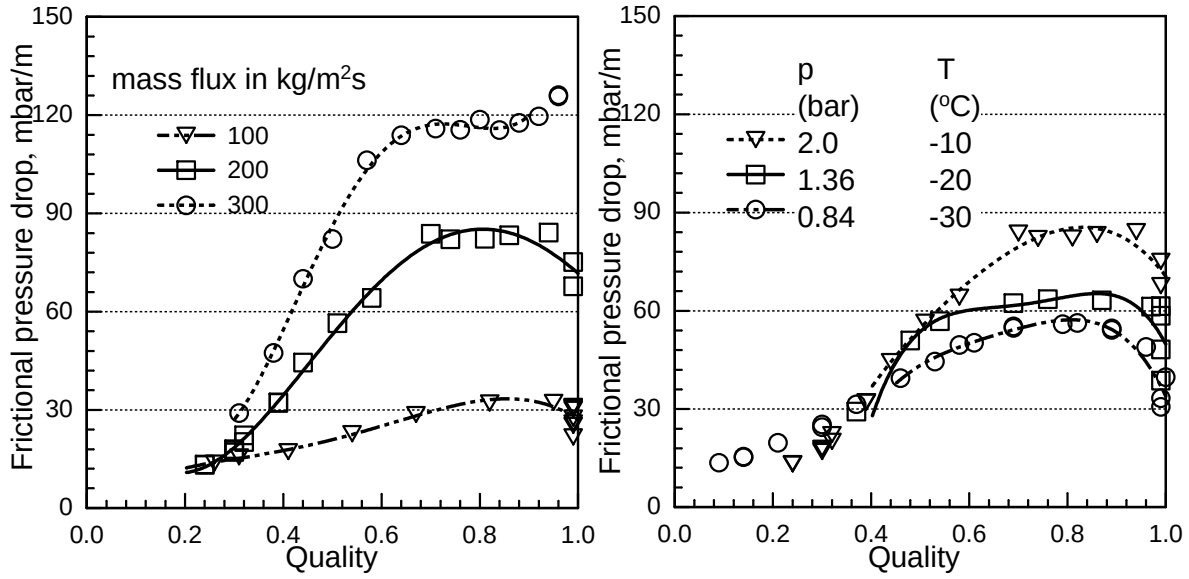

Figure 6.1. a) Influence of the mass flux on the frictional pressure drop at T_s= -10 °C and $\dot{q}$=16.5 kW/m^2 b) Influence of the saturation temperature on the frictional pressure drop at $\dot{m}$= 200 kg/m^{2}s and $\dot{q}$=16.5 kW/m^2.

Fig. 6.1b shows the pressure drop variation at different saturation temperatures. The increase in pressure drop with the saturation temperature may be attributed to liquid-vapor density ratio. It is to be remembered that the liquid-vapor density ratio decreases with the saturation temperature. The lower the density ratio the higher the void fraction and thus higher friction factor between the fluid and the tube wall. A similar dependency of the pressure drop on quality, mass flux and saturation temperature are previously reported in Baehr and Stephan [2] and Kabelac and de Buhr [63].

In the present work four correlations are fitted to the pure R134a pressure drop data. Namely these are the homogenous model and the separated flow models by Friedel [38], Lockhart and Martinelli [85] and Chisholm [20] correlations. The calculation procedures of all the correlations are given in Appendix C. As for the case of the local heat transfer

coefficient, the existing correlations are valid for the range prior to the critical heat flux. Thus all the data that are at the critical heat flux and beyond are excluded from the comparison. Fig. 6.2a-Fig. 6.2d show a comparison between the measured frictional pressure drop of pure R134a with the four correlations. Table 6.1 summarizes the mean error and the standard deviation associated with each correlation. Furthermore, the number of data points that fall within an error band of ± 30 % is also given.

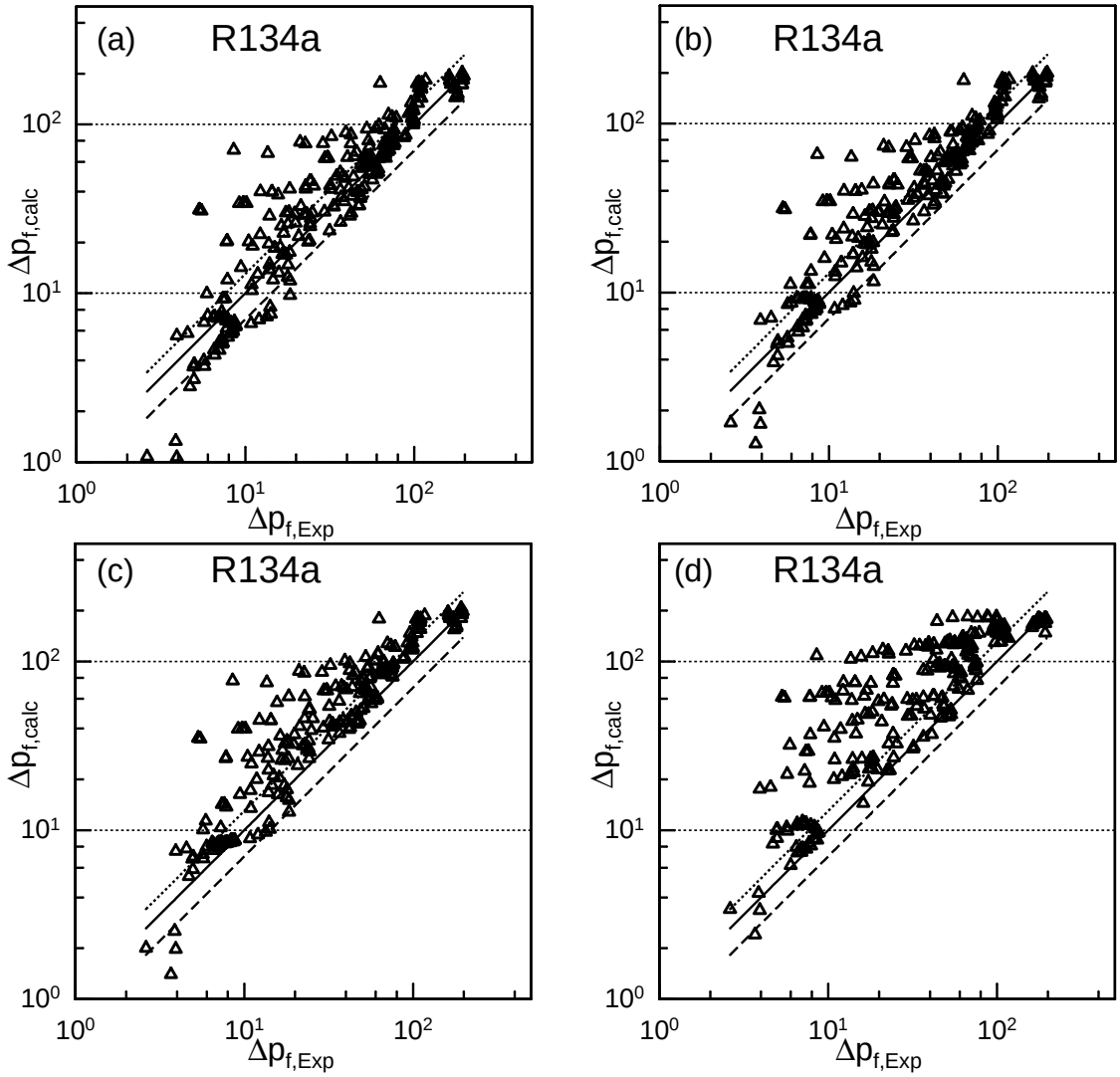

Figure 6.2. Comparison between the experimental frictional pressure drop and correlations for pure R134a: a) homogenous model, b) Friedel [38] correlation, c) Lockhart and Martinelli [85] correlation and d) Chisholm [20] correlation. Legend: (——) correlation, (△) experiment, (· · ·) +30%, (- - -) -30%.

The results indicate that the Friedel [38] correlation gives the best fit to the data with a mean deviation of 25.14 % and standard deviation of 49.38 % and 71.33 % of the experimental data lying within an error band of ±30 %. This is expected because Friedel [38] correlation is recommended for application in the range of $\eta_L/\eta_G < 1000$, where η_L and η_G are the liquid and vapor viscosity respectively. In the present work, the liquid to

Table 6.1. Comparison of four different correlations for the prediction of frictional pressure drop with the experimental data of pure R134a.

Correlation	Mean error %	Standard deviation %	Percentage of data points within an error band of 30%
Lockhart and Martinelli [85]	28.68	59.37	68.87
Friedel [38]	25.14	49.38	71.33
Chisholm [20]	62.92	119.00	17.32
Homogenous	28.62	41.99	57.96

vapor viscosity ratio is less than 50. The models used for the calculation of the liquid and vapor viscosity of R134a are presented in Appendix B. The Chisholm [20] correlation gives the poorest fit to the data. It has a mean deviation of 62.92 % and standard deviation of 119 %. Additionally it systematically overpredicts the result of the present work, only 17.32 % of the data fall within an error band of ±30 %. This could be explained because it is known that the Chisholm [20] correlation is recommended for application in the range of $\eta_L/\eta_G > 1000$ and $\dot{m} < 100$ kg/m^2. The first limitation is beyond the working conditions of the present work. The other two correlations, the homogenous model and Lockhart and Martinelli [85] model, though they are less accurate than the Friedel [38] correlation, give levels of accuracy within the widely accepted threshold of ±30 %. Similar results were previously reported by Wettermann [148] for flow boiling of R134a, however, at relatively high saturation pressures (5-27 bar).

6.2 R134a/R290 mixtures

As for pure R134a the measured frictional pressure drop for R134a/R290 mixture is compared with the homogenous model and the Friedel [38], Lockhart and Martinelli [85] and the Chisholm [20] correlations. Here the R134a/R290 mixture is treated as though it were a pure component with pseudo-properties of the R134a/R290 mixture. Fig. 6.3a-Fig. 6.3d show the results of the comparison between the measured and the predicted frictional pressure drop for a wide range of parameters of R134a/R290 mixtures.

Table 6.2 summarizes the relative errors associated with each correlation. As for the case of pure R134a, the Friedel [38] correlation gives the best fit to the R134a/R290 data. It has mean error of ± 27.23 % and standard deviation of 21.20 % with 64.96 % of the total number of data points lying within an error band of ± 30 %. However, its accuracy for mixtures is less than that for pure R134a. The homogenous model and the Lockhart and Martinelli [85] correlation show a wide error band of 40-55 %. The Chisholm [20] correlation as for the case of pure R134a gives the poorest fit to the R134a/R290 data.

Generally the relatively wide error associated with these correlations for mixtures may be attributed, in addition to their known limitations mentioned in section 6.1, to the high level of inaccuracy associated with calculation of the mixture physical properties. Similar results for mixture were previously reported by Wettermann [148] for R12/R134a

Table 6.2. Comparison of four different correlations for the prediction of frictional pressure drop with the experimental data for R134a/R290 mixtures.

Correlation	Mean error %	Standard deviation %	Percentage of data points within an error band of 30%
Lockhart and Martinelli [85]	34.65	35.70	54.92
Friedel [38]	27.23	21.20	64.96
Chisholm [20]	111.47	91.89	17.01
Homogenous	30.42	18.29	76

mixtures and Niederkrueger [98] for R12/R846 mixtures.

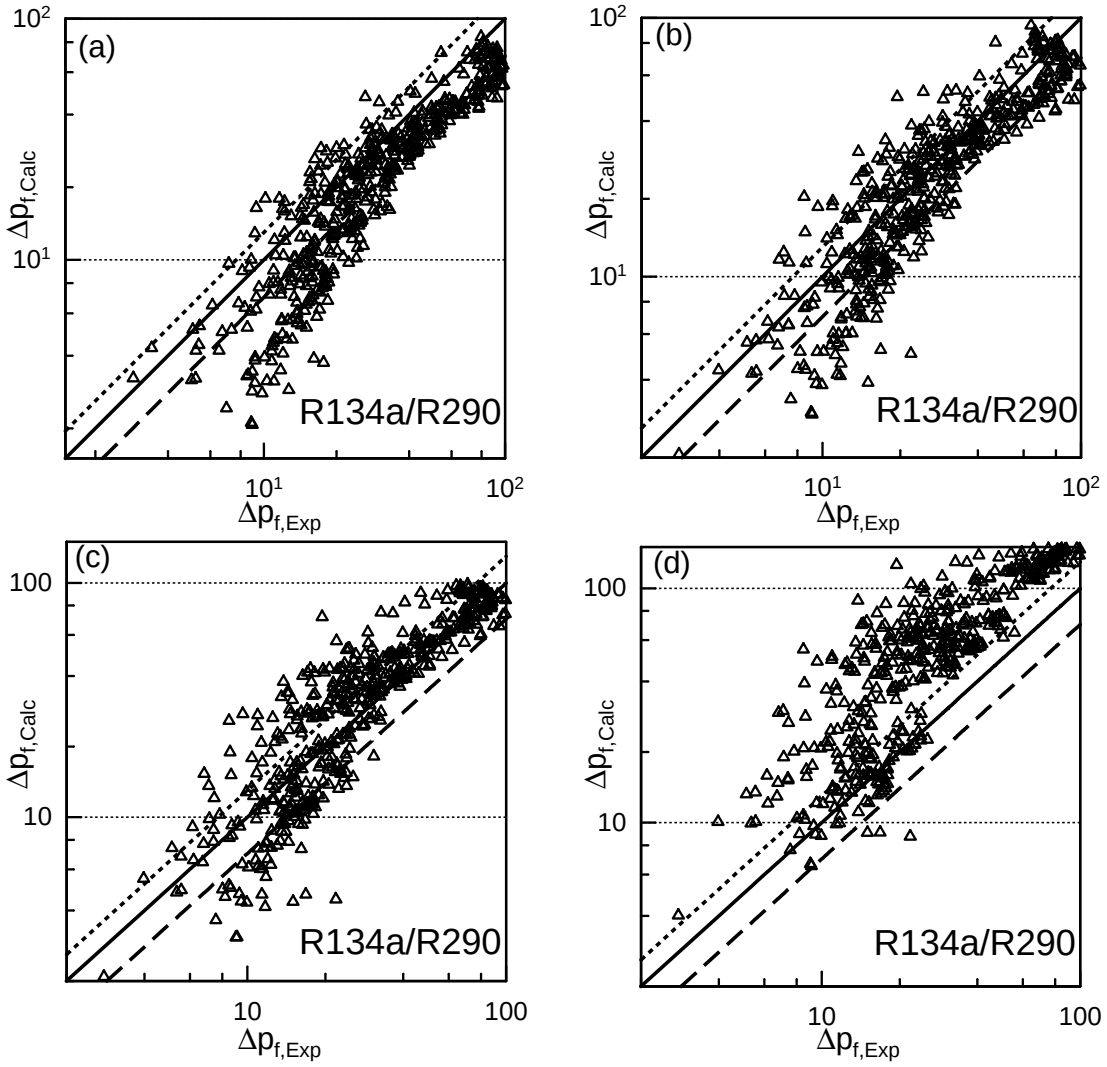

Figure 6.3. Comparison between the experimental frictional pressure drop and correlations for R134a/R290 mixtures: a) homogenous model, b) Friedel [38] correlation, c) Lockhart and Martinelli [85] correlation and d) Chisholm [20] correlation. Legend: (——) correlation, (△) experiment, (· · ·) +30%, (- - -) -30%.

7 Flow pattern

As indicated earlier in the literature review the phase distribution of vapor and liquid of a two-phase flow depends on the conditions of p, $\dot{m}$, $\dot{q}$ and flow geometry. Thus in the design of boiling equipment (*e.g.* heat exchanger) it is desirable to know what the flow pattern is so that a prediction model for the heat transfer coefficient or pressure drop appropriate to that flow pattern can be chosen. For example Steiner's [128] correlation for the prediction of local heat transfer coefficient requires a prior knowledge of flow pattern.

In the present study, parallel to the heat transfer coefficient and pressure drop, the flow patterns were directly visualized and recorded with written hand notes, and in some case a photograph is made. The observed flow patterns are classified in accordance with VDI-Wärmeatlas [143]. Fig. 7.1a from VDI-Wärmeatlas [143] depicts the flow pattern normally observed in flow boiling in a horizontal tube. The various flow patterns are defined as:

a *Bubbly flow*: In bubbly flow the vapor phase is distributed as discrete bubbles in a continuous liquid phase. At moderate velocities of both gas and liquid phases the entire pipe cross-section contain dispersed bubble in the liquid phase. These bubbles tend to congregate near the top of the tube.

b *Plug flow*: In plug flow characteristic bullet-shaped bubbles are observed, but they tend to move in the direction of flow in a position closer to the top of the tube.

c *Stratified flow*: The stratified flow pattern occurs only at very low liquid and vapor velocity. The two phases flow separately with a relatively smooth interface; the liquid flowing at the bottom of the tube and the gas along the top part of the tube; due to gravity.

d *Wavy flow*: As gas velocities is increased the gas-liquid interface becomes disturbed by waves travelling in the direction of flow.

e *Slug flow*: A further increase in vapor velocity causes the waves at the interface to be picked up to form a frothy slug which is propagated along the tube at a high velocity. The upper surface of the tube behind the wave is wetted by a residual film which drains into the bulk of the liquid.

f *Annular flow*: In annular flow pattern the liquid flows on the wall of the tube as a film and the gas flow in the center. The film is generally much thicker at the bottom of the tube than at the top due to the effect of gravity. Usually some of the liquid is entrained as droplets in the gas core.

g *Spray or Mist flow*: In the spray or mist flow region the rest of the liquid phase is entrained in the gas core and dispersed as droplets.

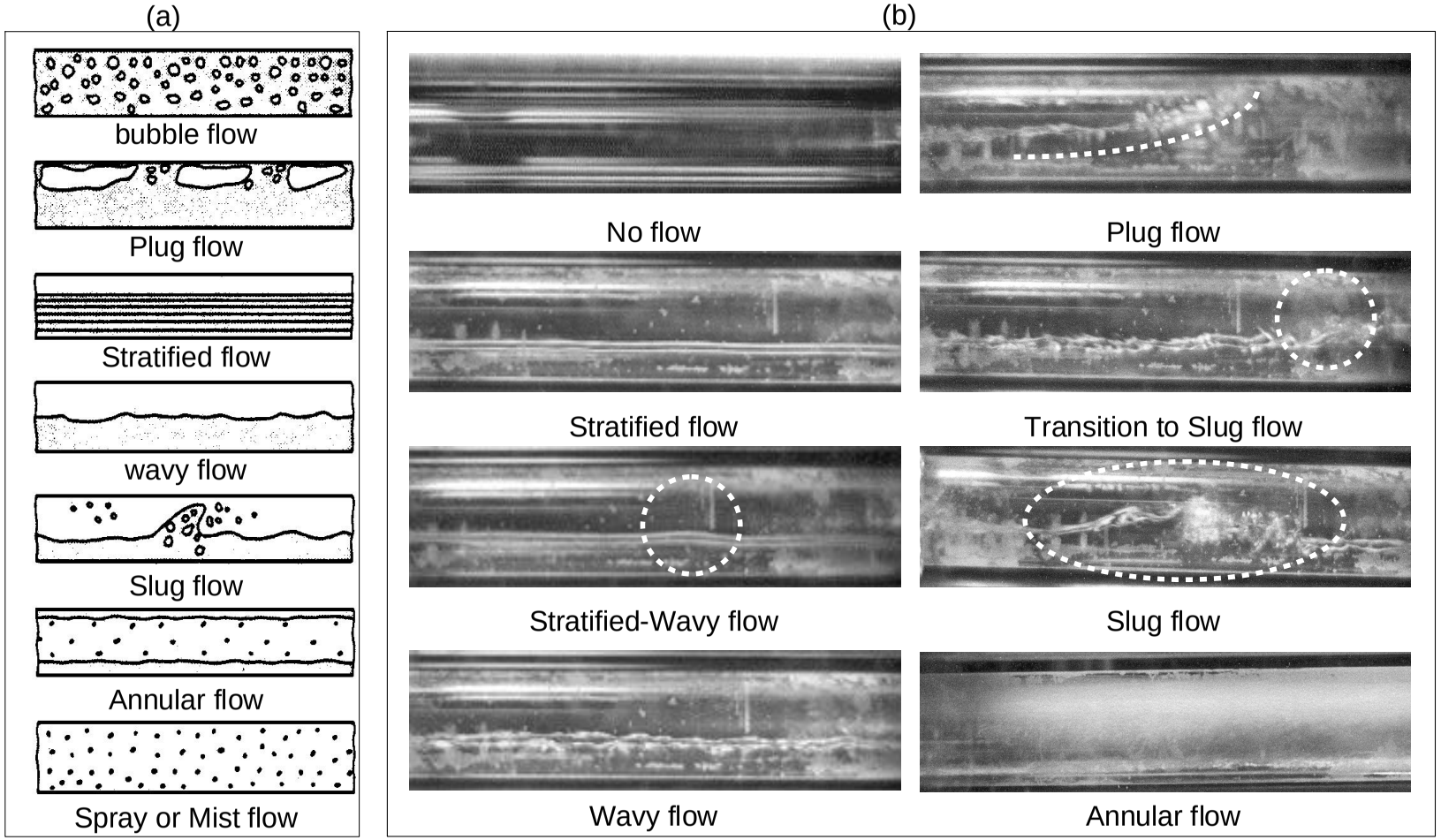

Figure 7.1. a) Flow patterns in horizontal tubes according to VDI-Wärmeatlas [143], b) Specimen of the observed flow pattern in the present work.

Specimens of the actual photographs of the observed flow pattern in the present work are shown in Fig. 7.1b. The photograph pictures clearly feature the flow pattern generally recognized by VDI-Wärmeatlas [143] (cf. Fig. 7.1a). Additionally, some secondary flow patterns for example stratified to wavy flow or transition to slug or annular flow are also observed in the present work.

The quantitative assessment of the flow pattern is generally carried out with a help of flow pattern maps. There exist a number of flow pattern maps, however, among the existing flow pattern maps the Steiner [128] flow pattern map is the most widely accepted one. To facilitate the application of the Steiner [128] flow pattern map, two steps are required to be implemented. The first step is to characterize the transition curves between the various flow patterns. The second step is to convert the observed flow pattern into a suitable dimensionless group that can be superimposed in the flow pattern map. For the first step, the various parameters describing the transition curves between the flow patterns are calculated in small step intervals of the Martinelli parameter X, which is the abscissa of the flow pattern map. These parameters, together with the scheme of their calculation, are described in detail in appendix D. Here these parameters are identified with the index "Gr". In the second step the observed flow flow pattern is converted into it is corresponding dimensionless group as follows:

- for stratified flow pattern the coordinates are F and X, where X is the Lockhart-martinelli parameter defined as

$$X = \left(\frac{1-\dot{x}}{\dot{x}}\right)^{0.875} \left(\frac{\rho_G}{\rho_L}\right)^{0.5} \left(\frac{\eta_L}{\eta_G}\right)^{0.125} , \tag{7.1}$$

  and F is given by

$$F = (Re_L Fr_G)^{0.5} = \sqrt{\frac{\dot{m}^3 \dot{x}^2 (1-\dot{x})}{\rho_G(\rho_L - \rho_G) g \eta_L \cos\Theta}} . \tag{7.2}$$

- for wavy, slug, annular or mist flow pattern the coordinates are Y and X, where Y is taken as the Froude number Fr given by

$$Y = (Fr_{Gm})^{0.5} = \sqrt{\frac{\dot{m}^2 \dot{x}^2}{g d \rho_L \rho_G}} . \tag{7.3}$$

- for bubbly flow pattern the coordinates are R and X where R is given by

$$R = (FrEu)_L^{0.5} = \sqrt{\frac{\xi_L \dot{m}^2 (1-\dot{x})^2}{2 d \rho_G (\rho_L - \rho_G) g \cos\Theta}} , \tag{7.4}$$

where the pressure drop friction factor is given as

$$\xi_L = \frac{0.3164}{Re_L^{0.25}} , \tag{7.5}$$

and the Reynolds number is

$$Re_L = \frac{\dot{m}(1-\dot{x})d}{\eta_L} . \tag{7.6}$$

7.1 Pure R134a

Fig. 7.2a and Fig. 7.2b show the results of the observed flow patterns for flow boiling of pure R134a at saturation temperature of -30 and -10 ^{o}C superimposed on the flow pattern map of Steiner [128].

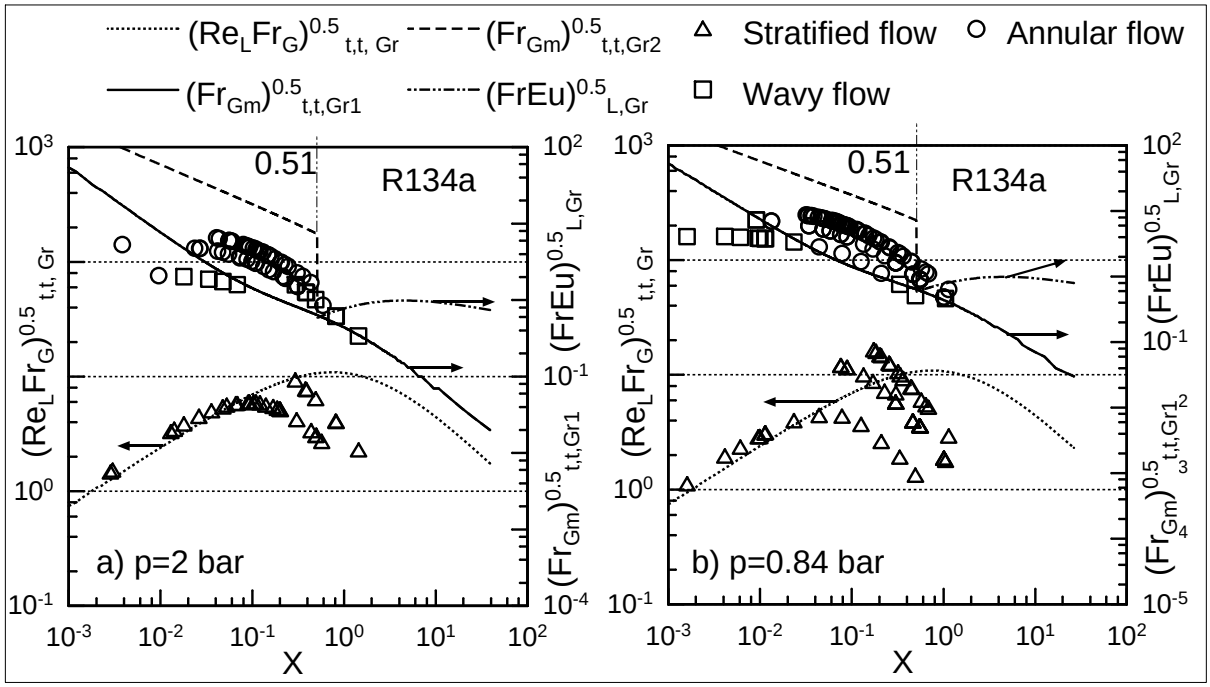

Figure 7.2. Comparison between the Steiner [128] flow pattern map and the observed flow pattern for flow boiling of pure R134a at various working conditions.

Here the symbols (triangle, square,...) represent the observed flow patterns and the lines (solid, dotted, broken,...) represent the calculated transition curves between the various flow patterns. As can be seen only the primary flow patterns (*i.e.* stratified, wavy and annular) are featured in the flow pattern map. Secondary flow patterns are observed in the present work, they are identified with their closest major flow pattern. For example, in some cases the observed flow pattern is stratified-wavy flow pattern (cf. Fig. 7.1b) in this case the flow pattern is classified, subjectively, as stratified flow if the waves contribution is less than the stratified contribution and *vice versa*. In other cases the flow pattern may be a transition to annular, slug to annular or annular with partial dryout. These types of the secondary flow patterns are classified, in most cases, as annular flow.

The results show a consistent match between the Steiner [128] flow pattern map and the observed flow patterns albeit with some scatter; 90 % of the R134a data were correctly predicted. The good agreement between the flow pattern map and the observed ones is expected because, in addition to it is widely known high level of accuracy, the Steiner [128] flow pattern map is known to give good results for low pressure data, $p_r < 0.1$ (Wettermann [148] and Niederkrüger [98]). In the present work $p_r \leq 0.08$ the maximum pressure applied in the present work is 3.4 bar and the critical pressure for R134a is 40.563 bar as given by Tillner-Roth [137]. The relatively wide scatter is associated with stratified

flow (*i.e.* some of the points are above the *stratified-way* transition curve) is a result of the secondary flow pattern (*i.e.* stratified-wavy flow pattern) which is considered in most cases as a stratified flow pattern.

7.2 R134a/R290 mixtures

In contrary to pure substances, the flow pattern map of Steiner [128] has been tested previously with a limited data bank for mixtures. Theses include the flow boiling data of Niederkrüger [98] for R12/R846 and Wettermann [148] for R12/R134a and R12/R134a/R846 mixtures. It is to be remembered that the existing work are at relatively higher saturation pressure of more than 5 bar and mass fluxes of more than 400 kg/m^{2}s. Additionally the existing data are for old refrigerant mixtures. This is in turn necessitates the validation of Steiner [128] flow pattern map to the newly developed mixtures considered here.

With this in mind the Steiner [128] flow pattern map is applied to the R134a/R290 mixture data. Here the mixture is treated as though it were a pure component with pseudo properties of the mixture. Fig. 7.3a,b and Fig. 7.4a,b show the flow pattern data for R134a/R290 mixture at 2 bar for a wide range of bulk compositions, $\widetilde{z}$.

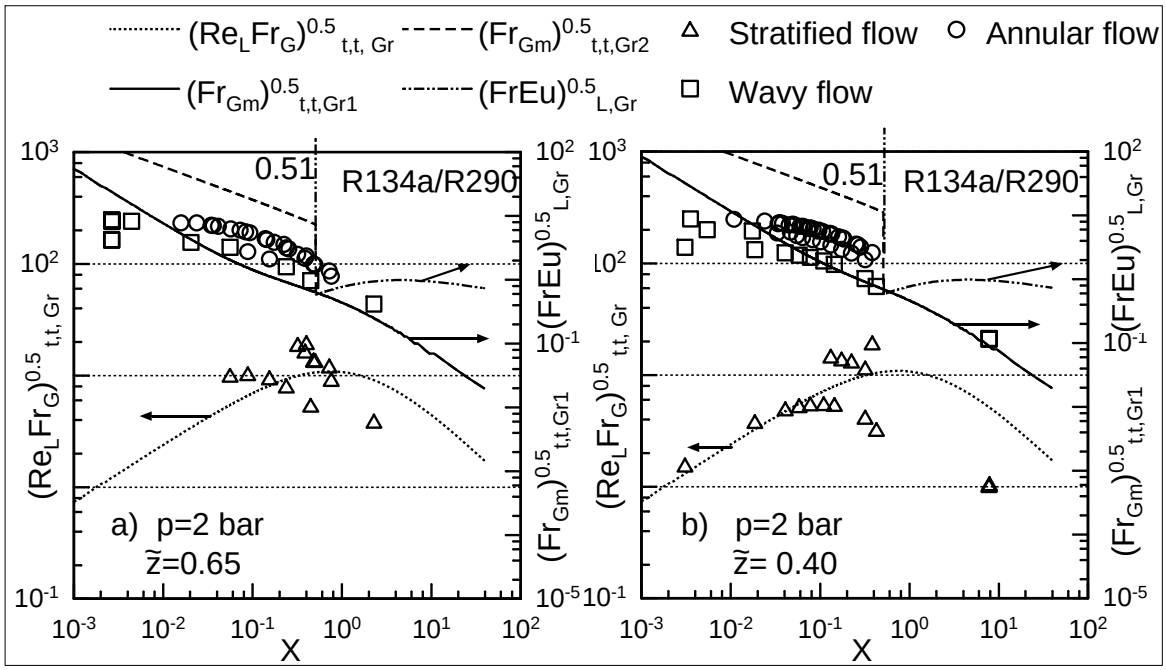

Figure 7.3. Comparison between the Steiner [128] flow pattern map and the observed flow pattern for flow boiling of R134a/R290 mixtures at various working conditions.

The lines (solid, dotted,...) represent the boundaries of the flow pattern map while the symbols (triangle, circle and square) stand for the observed (experimental) flow pattern. As for the case of pure R134a only the primary flow pattern of stratified, wavy and annular are presented. Similar to the flow boiling of pure R134a, the results for R134a/R290 mixture show a consistent prediction of the observed flow patterns, albeit with some

scatter; ∼85 % of R134a/R290 mixture data points match the flow pattern map. As for the case of pure R134a, Steiner's flow pattern map is known to give good accuracy for low pressure mixture data.

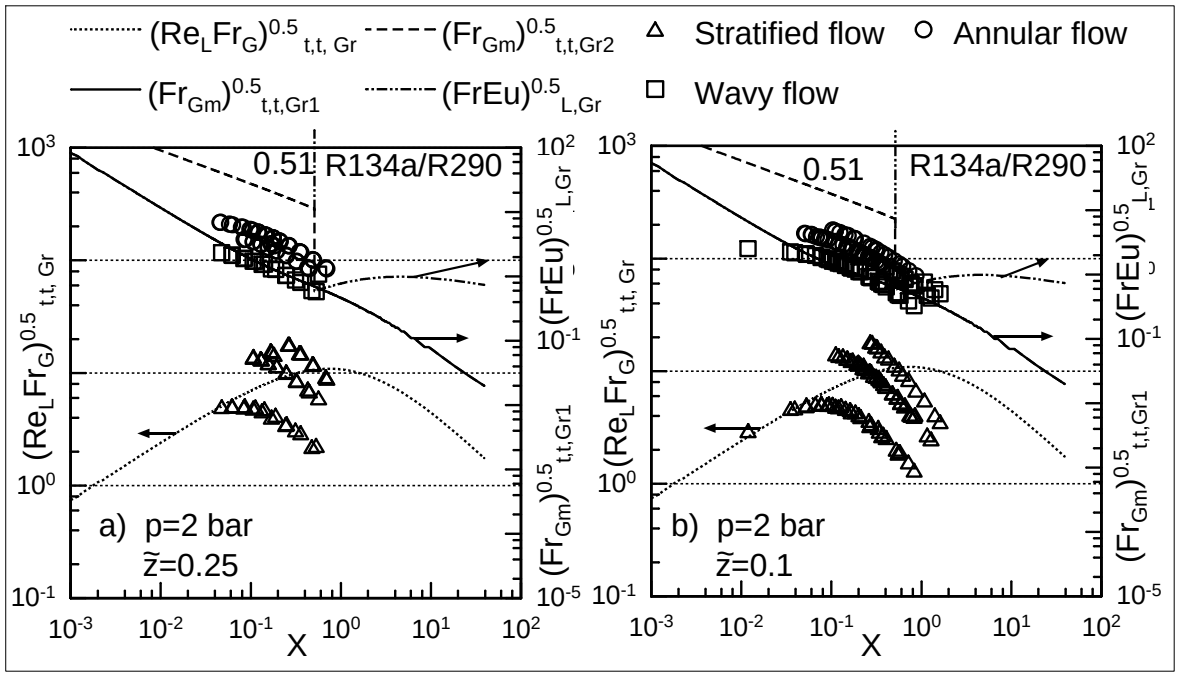

Figure 7.4. Comparison between the Steiner [128] flow pattern map and the observed flow pattern for flow boiling of R134a/R290 mixtures at various working conditions.

8 Recommendation

- Although the existing experiment setup is capable to yield flow boiling data with a high level of accuracy the flowing modifications may be useful if they could be taken into account in future measurements:

  i removal of the adiabatic region between the last set of the preheater and the inlet of the test section. Thus the disturbance of the hydrodynamic and thermal development caused by the adiabatic effect may be eliminated,

  ii visualization of the condensate film on the external tube. This may be realised via a sight glass-window attached to the shell of the test section. This may help to judge the state of the condensation film; the wettability of outside of the test tube,

  iii measurement of the condensate mass flow rate. This may help in the closure of the conservation of mass, momentum and energy equations without necessarily employing a semi-empirical model for the shear stress.

- R134a has been accepted as an alternative to the R12. However, R134a has its limitation if it is intended as a "drop-in" for the existing R12 machines. Most significant is the lack of mineral oil solubility. Nevertheless, in the recent past ester-based lubricants have been developed for the drop-in application. Thus investigations of the local heat transfer coefficient of R134a-Ester oil mixture may be of interest.

- The R22 alternative search has been more difficult with no known single component fluid having a reasonably close saturation pressure curve. As a result mixing of two or more components to obtain all the desired working fluid properties has become important. R134a/R290 mixture is a possible drop-ins known at the present time. The R134a/R290 mixture has the additional advantage of making the mixture soluble for mineral oil. Thus investigations on the influence of mineral oil on the local heat transfer coefficient of R134a/R290 mixtures may be of interest as well.

- In the present study it was observed that there is some enhancement in local heat transfer coefficient in the region prior to the onset of dryout. Further investigation in this phenomena may be useful.

9 Conclusion

In the present study heat transfer characteristics of pure R134a and binary mixtures of R134a/R290 have been studied. The mixture bulk compositions covered the zeotropic region and azeotropic point; $0 < \tilde{z} \leq 65$ mole % R290. The study was carried out using an experimental setup which was built to obtain flow boiling data low saturation temperatures ($T < 0\ ^{\circ}C$). Furthermore, the investigation was carried out under the assumption of a thermal boundary condition of constant wall temperature rather than the conventional one of constant heat flux. The thermal boundary condition of constant wall temperature was tried via film condensation of ammonia at the outside of the horizontal tube. The local heat transfer coefficient and pressure drop were measured for a wide range of parameters of pressure p, mass flux $\dot{m}$ and wall temperature T_w for both pure R134a and R134a/R290 mixtures. Parallel to the local heat transfer coefficient and pressure drop the flow pattern was also observed and recorded with hand notes and, in some cases, documented with a camera.

- **Film condensation**: As indicated above the thermal boundary condition of constant wall temperature was tried via film condensation on the external horizontal tube. The measured wall temperature at the film condensation side was found to possess a profound circumferential cosine profile at high heat fluxes. At relatively low heat fluxes the wall temperature is nearly constant. The complex wall temperature cosine profile is attributed to the non uniform distribution of the condensate film thickness around the tube; the film thickness increases towards the lower part of the tube because of the gravity. Against the background of none uniform wall temperature, the conservation of mass, momentum and energy equation was solved for the condensate film thickness with and without consideration of the vapor shear stress. It was found that the film thickness, also the heat flux, are strong functions of the cosine wall temperature profile. However, the mean heat flux over the perimeter of the tube remained unaffected by the cosine wall temperature distribution. In fact the method of solution of the condensate problem developed in the present study was successfully blended with the original Nusselts theory of film condensation.

- **Heat transfer coefficient for pure R134a**: In the present study the local heat transfer coefficient for pure R134a has been systematically investigated for a wide range of mass flux, saturation temperature and quality. The influence of these parameters on the local heat transfer coefficient has been studied. It was found that the present study confirmed the early investigation reported in Chapter 2 of this work. Furthermore, the result of the local heat transfer coefficient was used to test the validity of ten (**10**) correlations. Namely these are the Steiner [128], Kattan et al. [73], Shah [118], Kandlikar [66], Gungor and Winterton [48], Schrock and Grossman [117], Klimenko [79], Jung et al. [60], Bennett and Chen [7] and Dembi et al. [27] correlations. It was found that most of the correlations fit the R134a data with a mean deviation of less than **30** %, with the Steiner [128] correlation giving the best fit to the R134a data. The Steiner [128] correlation gave a mean deviation

of **15.48** % and **89.2** % of the R134a data were within an error band of ± **30** %.

- **Heat transfer coefficient for R134a/R290 mixtures**: The local heat transfer coefficient for R134a/R290 mixture was measured for the same range of parameters as in the case of pure R134a. The influence of the mixture concentration on the local heat transfer coefficient has been studied. It was found that:

  i the local heat transfer coefficient for the R134a/R290 mixture is smaller than that obtained by the linear interpolation of the heat transfer coefficients of the mixture components,

  ii a maximum decrease in the local heat transfer coefficients occurred at the point where $|\widetilde{y} - \widetilde{x}|$ is maximum. For example for the case at 2 bar and a mass flux of 100 kg/m^{2}s the mixture local heat transfer coefficient decreases by a factor of order **2** in comparison with that of pure R134a under the same working conditions,

  iii the local heat transfer coefficient increases towards the point of the azeotrope. For the case of 2 bar the azeotropic local heat transfer is higher than that for pure R134a by factor **1.2**.

  The result of the measurements were also used to test the validity of five (**5**) correlations. These include the Steiner [128], Jung et al. [60], Kandlikar [67], Bennett and Chen [7] and Palen [104] correlation. It was found that, in comparisons with the results of pure R134a, the correlation possess a relatively higher deviation from the measured local heat transfer. This was attributed in part to the relatively high level of uncertainty associated with prediction of the mixture physical properties. Furthermore, as for the case of pure components the Steiner [128] correlation gave the best fit to the data among the tested correlations. The relatively high level of uncertainty associated with other correlations may be attributed to the neglection of the diffusion effect in the modeling of the convective boiling heat transfer coefficient for the case of a liquid-liquid immiscible mixture.

- **Pressure drop**: Besides the heat transfer coefficient, knowledge of pressure drop is of paramount interest in the design of flow boiling equipment. Against this background, parallel to the measurement of local heat transfer coefficient, the pressure drop was also measured. Firstly, the measured pressure drop facilitated the calculation of the saturation temperature at the exist of the test evaporator. Knowledge of the saturation temperature is a prerequisite for the calculation of the local heat transfer coefficient. Secondly, results of the pressure drop were used to test the validity of existing correlations for the prediction of the pressure drop. The two available models for the homogenous and separated flow models were tested. It was found that the Friedel [38] correlation, which is based on separated flow model, gave the best fit to the R134a and R134a/R290 data with a mean deviation of less than 30 %. The other models gave a wide deviation of more than 30 %.

- **Flow pattern**: Knowledge of the flow pattern is a requirement for the prediction of the heat heat transfer coefficient. For example the application of Steiner [128] correlation for the prediction of the local heat transfer coefficients requires a prior knowledge of flow patterns. Against this background, parallel to the measurement of the local heat transfer coefficients and pressure, the corresponding the flow pattern was observed at the sight glasses and recorded with hand notes and in some case documented with a camera. The results of the observation of the flow pattern were superimposed into the flow pattern of Steiner [128]. The result was found to match the flow pattern map with good agreement. It correctly predicted 90 % of the total number of data points (**2**×**330**) for pure R134a and ∼85 % of the total number of data points (**2**×**800**) for R134a/R290 mixtures.

Bibliography

[1] Adunka, A.: Meßunsicherheiten "Theorie und Praxis" 2.Auflage, VULKAN-Verlag, Essen, Germany, 2000

[2] Baehr, H.D.; Stephan, K.: Wärme-und Stoffübertragung. (2ed), Springer, Berlin, 1996

[3] Baker, O.: Design of pipe lines for simultaneous flow of oil and gas. Oil and Gas J., July 26. Bao, Z.Y., 1954

[4] Bandel, J.: Druckverlust und Wärmeübergang bei der Verdampfung siedender Kältemilttel im durchströmten waagerechten Rohr. Dissertation, Universität Karlsruhe, Germany, 1973

[5] Baumann, P.: Zur Thermohydraulik von Gas/Dampf-flüßigkeitsgemischen in horizontalen Rohren. Dissertation, Universitat Karlsruhe, Germany, 1993

[6] Beattice, D.R.H.; Lawther, K.R.: An examination of wall temperature drop phenomenon during approach to flow boiling crisis. Proc. 8th Int. Heat Transfer Conference, San Francisxo, USA, 1986

[7] Bennet, D.L.; Chen, J.C.: Forced convective boiling in vertical tubes for saturated pure components and binary mixtures. AICHE Journal, Vol. 26, 1980, 454-461

[8] Bertoletti, S.; Lombari, C.; Silvestri, M.: Heat transfer to steam-water mixtures, C.I.S.E., Report R-78, 1964

[9] Boissieux, X.; Heikel, M.R.; Johns, R.A.: Two-phase heat transfer coefficients of three HFC refrigerants inside a horizontal smooth tube, part I: Evaporation. Int. J. of Refrig., Vol. 23, 2000, 269-283

[10] Bonilla, C.F.; Perry, C.W.: Heat transimission to boiling mixtures. Am. Inst. Chem. Eng. J., Vol. 37, 1941, 685-705

[11] Bonn, W.: Wärmeübergang und Druckverlust bei der Verdampfung von Stickstoff und Argon in durchströmten horizontalen Rohr sowie Betrachtungen über die tangentialle Wärmeleitung und die maximal möglische Flüssigkeitsüberhitzung. Dissertation, Universität Karlsruhe (TH), Germany, 1980

[12] Bonn, W.; Iwicki, J.; Krebs, R.; Steiner, D.; Schluender, E. U.: Über die Auswirkung der Ungleichverteilung des Wärmeübergangs am Rohrumfang bei der Verdampfung im durchströmten waagerechten Rohr. Wärme-und Stoffübertragung, 1980, 265-274

[13] Butterworth, D.: "Condensors: basic heat transfer and fluids flow", in Kakac, S.; Bergles, A.E.; Mayinger, F. (eds): Heat exchangers. Hemisphere publishing Corp., New York, USA, 1981, 289-314

[14] Calus, W.F.; di Montegnacco, A.; Denning, R.K.: Heat transfer in a natural circulation single tube reboiler, part II: Binary liquid mixtures. Chem. Eng. J., Vol. 6, 1973, 251-264

[15] Calus, W.F.; Leonidopoulos, D.J.:Pool boiling-binary liquid mixtures. Int. J. of Heat and Mass Transfer, Vol. 17, 1974, 249-256

[16] Carey, V.P.: Liquid-vapor-phase-change phenomina: An introduction to the thermophysics of vaporization and condensation processes in heat transfer equipment. Tayler and Francis, Bristol, UK, 1992

[17] Chen, J.C.: Correlation for boiling heat transfer to saturated fluids in convective flow. I and EC Process Design and Development, Vol. 5, 1966, 322-29

[18] Chen, M.M.: An analytical study of laminar film condensation : Part 1-Flat plates and part 2-Multiple horizontal tubes. J. of Heat Transfer, Vol. 83, 1961, 48-54, 55-60

[19] Chen, L.-T.; Huang, F.; Rong-Fung, M.: Boiling heat transfer to R22/DMF mixtures. Int. Comm. Heat and Mass Transfer, Vol. 12, 1985, 541-549

[20] Chisholm, D.: Pressure gradients due to friction during the flow of evaporating two phase mixtures in smooth tubes and channels. Int. J. of Heat and Mass Transfer, Vol. 16, 1973, 374-358

[21] Churchil, S.W.; Chu, H.H.S.: Correlation equations for laminar and turbulent free convection from a vertical plate. Int. J. of Heat and Mass Transfer, Vol. 18, 1975, 1323-1329

[22] Chwala, J.M.: Wärmeübergang und Druckabfall in waagerechten Rohren bei der Strömung von verdampfenden Kältemitteln. VDI-Forschungsheft Nr. 523, VDI-Verlag GmbH, Düsseldorf, Germany, 1967

[23] Collier, J.G.; Thome, J.R. (ed): Convective boiling and condensation. 3rd ed., Oxford University Press, Oxford, UK, 1994

[24] Collier, J.G.: Gas-liquid flow, in: heat exchanger design handbook. Vol. 2. Hemisphere, Washington, DC, USA, 1983

[25] Cooper, M.G.: Saturation nucleate pool boiling, A simple correlation. 1st UK National Conference on Heat Transfer, Vol. 2, 1984, 785-793

[26] Costigan, G.; Frankum, D.P.; Wadekar, V.V.: Flow boiling measurements on pentane, iso-octane and pentane/iso-octane mixtures. Proc. 10th Int. Heat Tranafer Coeference,Brighton, UK, Vol. 7, 1994,431-436

[27] Dembi, et al.: in Aumann, L.: Verfahren zur Berechnung lokaler Wärmeübergangkoeffizienten von Zweiphasenströmungen in Rohren. Studienarbeit, Institut für Thermodynamik, Universität Hannover, Germany, 1998.

[28] *Der Deutsche Kalibrierdienst* (DKD): Ermittlung von Meßunsicherheiten (DKD-3). Physikalisch-Technische-Bundesanstlt, Braunschweig, 1991

[29] Didion, D.A.; Bivens, D.B.: Role of refrigerant mixtures as alternative to CFCs. Int. J. of Refrig., Vol. 13, 1990, 163-175

[30] Dittus, F.W.; Boelter, L.M.K.: University of California (Berkeley) Publications on Engineering, Vol. 2, University of California, Berkeley, CA, 1930, 443

[31] Domanski, P.A.; Didion, D. A.: Thermodynamic evaluation of R-22 alternative refrigerants and refrigerant mixtures. ASHRAE Trans., Vol. 99, Part 2, 1993, 636-648

[32] Eckels, S.J.; Doerr, T.M.; Pate, M.B.: In-tube heat transfer and pressure drop of R-134a and Ester lubricant mixtures in a smooth tube and a micro-fin tube: Part I-Evaporation. ASHRAE Trans., Vol. 100, 1994, 265-282

[33] Eckels, S.J.; Doerr, T.M.; Pate, M.B.: Heat transfer coefficient and pressure drop for R-134a and an Ester lubricant mixture in a smooth tube and micro fin tube. ASHRAE Trans., Vol. 104, 1998, 366-375

[34] Eckels, S.J.; Doerr, T.M.; Pate, M.B.: A comparison of the heat transfer and pressure drop for R-134a and lubricant mixture in different diameter smooth tubes and nicro fin tubes. ASHRAE Trans., Vol. 104, Part A, 1998, 376-386

[35] Eckels, S.J.; Pate, M.B.: An experimental comparison of evaporation and condensation heat transfer coefficients for HFC-134a and CFC-12. Int. J. Refrig., Vol. 14, March, 1991, 70-78

[36] Fenghour et al.: Transport properties of ammonia. Int. J. Chem. Phys. Ref. Data, Vol. 24, No. 5, 1995, 1649-67

[37] Fletcher, D.F.; Haynes, B.S.: An experimental study of gas-liquid flow in a narrow conduit. Int. J. of Heat and Hass Transfer, Vol. 43, 2000, 2313-24

[38] Friedel, L.: Momentum exchange and pressure drop in two-phase flow. Proceeding NATO Advanced Study Institute, Istanbul, Turkey, 16-17 August, Vol. I, 1976, 239-312

[39] Fuchs, P.H.: Influence of the tube material and external heat load on heat transfer coefficient with separated flow in evaporator. Proc. of the 16th Int. Congr. of Refrig., Venedig, Vol. 2, 1987, 503-506

[40] Fujita, Y.; Bai, Q.: Bubble dynamics and heat transfer in mixture boiling. Proceeding of the 12th Int. Heat Transfer Conference, Gernoble, France, Vol. 1, 2002, 93-104

[41] Fujii, T.; Uehara, H.; Kurata, C.: Laminar filmwise condensation of flowing vapor on a horizontal cylinder. Int. J. of Heat and Mass Transfer, Vol. 15, 1972, 235-246

[42] Gnielinski, V.: New equation for heat and mass transfer in turbulent pipe and channel flow. Int. J. Chemical Engineering, Vol. 16, 1976, 359-368

[43] Gorenflo, D.; Bieling, V.: Heat transfer at pool boiling of mixtures with R22 and R115. XVII Int. Symp. on Heat and Mass Transfer in Cryoeng and Refrig., 1986, 243-257

[44] Goebel, O.: Modeling of two phase stratified and annular flow in heated horitontal tubes. In: Mayinger, F.; Lehner, M.: Convective flow and pool boiling. Taylor and Francis, Philadelphia, USA, 1999

[45] Granryd, E.: Hydrocarbons as refrigerants- an overview. Internationl J. of Refrig., Vol. 24, 2001, 15-24

[46] Gropp, U.:Wärme- und Stoffübertragung bei Oberflächen Verdampfung und beim Blasensieden eines Binäres Gemisches am Riesenfilm. Dissertation, Universität Karlsruhe (TU), Germany, 1989

[47] Gross, U.; Song, Y.W.; Hahne, E.: Thermal conductivity of the new refrigerants R134a, R152a and R123 measured by transient hot-wire method. Int. J. of Thermodynamics, Vol. 13, No. 6, 1992, 957-983

[48] Gungor, K.E.; Winterton, R.H.S.: General correlation for flow boiling in tubes and annuli. Int. J. of Heat and Mass Transfer, Vol. 26, 1986, 351-358

[49] Hambraeus, K.: Heat transfer coefficient during two-phase flow boiling of HFC-134a. Int. J. Refrig, Vol. 14, No. Nov.,1991, 357-362

[50] Hashizume, K.: Flow pattern and void fraction of refrigerant two-phase flow in a horizontal pipe. Bulletin of the JSME, Vol. 26, No. 219, 1983, 1597-1602

[51] Herbst, K.E.; Fechner, A.; Köhler, W.; Goebel, O.; Oberle, B.: Heat transfer behavior of an absorber tube with direct steam generation by water injection. In: Chen, J.C. (ed). Convective flow boiling. Taylor & Francis, 1996

[52] Hewitt, G.F.; Kearcy, H.A.; Lacey, P.M.C.: Burn-out and nucleation in climbing film flow. Int. J. of Heat and Mass Transfer, Vol. 8, 1965, 793-814

[53] Hihara, E.; Tanida, K.; Saito, T.: Forced convection boiling experiments of binary mixtures. Proc. of the ASME-JSME Thermal Engineering joint Conf., Honolulu, Publ. by ASME, Vol 5, 1989, 119-126

[54] Holcomb, C.D.; Magee, J,W.; Scott, J.L.; Outcalt, S.L.; Haynes, W.M.: Selected thermodynamic properties for mixtures of R-32 (Difluoromethane), R125 (pentafluoroethane), R134a (1,1,1,2-tetrafluoroethane), R143a (1,1,1-trifluoroethane),

R41(fluoroethane), propane (R290), and R744 (carbon dioxide). NIST Technical Note No. 1397, U.S. Dept. Commerce, Washington, 1997

[55] ICI: Physikalische Eigenschaften von Klea 134a SI-Einheiten. Mitteilung der Fa. Deutsche ICI GmbH, Frankfurt, Germany, 1993

[56] Jain, V.K.; Dhar, P.L.: Studies on flow boiling of mixture of refrigerants R12 and R13 inside a horizontal tube. Proc. XVI, Int. Congr. Refrig., Paris, 1983

[57] Jallouk, P.A.: Two phase flow pressure drop and heat transfer characteristics of refrigerants in vertical tube. PhD-thesis, University of Tennessee, 1974

[58] Jensen, M. K.; Bensler, H.P.: Saturated forced convection boiling heat transfer with twisted tape inserts. ASME J. Heat Transfer, Vol. 108, 1986, 93-99

[59] Jung, D.S.: Horizontal flow boiling heat transfer using refrigerant mixture. PhD-thesis, University of Maryland, 1988

[60] Jung, D.S.; McLinden, M.; Radermacher, R.; Didion, D.: Horizontal flow boiling heat transfer experiments with a mixture of R22/R114. Int. J. of Heat and Mass Transfer, Vol. 32, 1989, 131-145

[61] Jung, D.S.; Radermacher, R.: Prediction of evaporation heat transfer coefficient and pressure drop of refrigerant mixtures. Int. J. Refrig., Vol. 16, No. 5, 1993, 330-338

[62] Jung, D.; Song, Y.; Park, B.: Performance des melanges de frigorigenes utilises pour remplacer le HCFC22. Int. J. of Refrig., Vol. 23, 2000, 466-474

[63] Kabelac, S.; de Buhr, H-J.: Flow boiling of ammonia in a plain and low finned horizontal tube. Int. J. of Refrig., Vol. 24, 2001, 41-50

[64] Kabelac, S.; de Buhr, H.-J.: Flow boiling of ammonia and ammonia -oil mixtures in a plain and a low finned horizontal tube. Proc. 34th National Heat Transfer Conference, 2000,1-8

[65] Kabelac, S.; Rabah, R.: Flow boiling of R134a-propane mixtures: -experiments and CML modeling-. Proc. of the 12th. Int. Heat Tranasfer Conference, Grenoble, Vol. 4, 2002, 525-530

[66] Kandlikar S.G.: A general correlation for two-phase flow boiling heat transfer inside horizontal and vertical tubes. Int. J. Heat and Mass Transfer, Vol. 112, 1990, 219-228

[67] Kandlikar, S.G.: Boiling heat transfer with binary mixtures: Part II- Flow boiling in plain tubes. Transaction of ASME, Vol. 120, 1998, 388-394

[68] Kandlikar, S.G.: Boiling Heat transfer with binary mixtures: Part I- A theoretical model for pool boiling. Transaction of ASME, vol. 120, 1998, 380-387

[69] Kandlikar, S.G.; Shoji, M. ; Dhir, V. (ed): Hand Book of Phase Change: Boiling and Condensation. Taylor & Francis, Philadelphia, 1999

[70] Kapitza, P.L.: Wave flow of thin viscous fluids. Zh. Eksp. Teoret. Fitz., Vol. 18, 1948, 1-1

[71] Kattan, N.; Thome, J.R.; Favrat, D.: Flow boiling in horizontal tubes. Part 1-Developmment of adiabatic two phase flow pattern map. Trans. of ASME, Vol. 120, 1998, 140-147

[72] Kattan, N.; Thome, J.R.; Favrat D.: Flow boiling in horizontal tubes. Part 2-New heat transfer data for five refrigerants. ASHRAE Trans., Vol. 120, 1998, 148-155.

[73] Kattan, N.; Thome, J.R.; Favrat D.: Flow boiling in horizontal tubes. Part 3-Development of a new heat transfer model based on flow pattern map. ASHRAE Trans., Vol. 120, 1998, 156-165

[74] Kenning, D. B.R.; Cooper, M. G.: Saturated flow boiling of water in vertical tubes. Int. J. of Heat and Mass Transfer, Vol. 31, 1988, 455-458.

[75] Khanpara, J.C.: Augmentation of in tube evaporation and condensation with microfin tubes. PhD-thesis, Iowa State University, Ames, IA, 1986

[76] Kim, M.S.; Mulroy, W.J; Didon, D.A.: Performance evaluation of two azeotropic refrigerant mixtures of HFC-134a with R-290 (propane) and R-600 (isobutane). Trans. of the ASME, Vol. 116, June, 1994, 148-154

[77] Kleemiß, M.: Thermodynamische Eigenschaften zweir ternärer Kältemittelgemische. Dissertation, Universität Hannover, Germany,1997

[78] Kleiber, M.: Vapor-liquid equilibria of binary refrigerant mixtures containing propylene or R134a. Fluid Phase Equil. Vol. 92, 1994, 149-194

[79] Klimenko, in: Aumann, L.: Verfahren zur Berechnung lokaler Wärmeübergangkoeffizient von Zweiphasenströmungen in Rohren. Studienarbeit, Institut für Thermodynamik, Universität Hannover, Germany, 1998.

[80] Koh, C.Y.; Sparrow, E.M.; Harnett, J.P.: The two phase boundary layer in laminar film condensation. Int. J. Heat Mass Transfer, Vol. 2, 1961, 69-82.

[81] Köhler, W.; Kefer, V.; Kastner, W.: Bestimmung des Wärmeübergangs im unbenetzen Teil von Verdampferrohren unter Berücksichtigung zweidimensionaler Wärmeleitung in Wandmaterial. Wärme-Stoffübertragung, Vol. 21, 1987, 133-138

[82] Kon'kov, A.S.: Experimental study of the conditions under which heat exchanger deteriorates when a steam-water mixture flows in heated tubes. Teploenergetika, Vol. 13, No. 12, 1965, 77

[83] Lee, W.C.; Rabbar, S.; Rose, J.W.: Film condensation of refrigerant R113 and ethanediol on a horizontal tube- effect of vapour velocity. ASME J. Heat Transfer, Vol. 106, 1984, 524-530

[84] Liu, Z.; Winterton, R.H.S,: A general correlation for saturated and subcooled flow boiling in tubes and annuli based on a nucleate pool boiling equation. Int. J. of Heat and Mass Transfer, Vol. 34, No. 8, 1990, 2759-2766

[85] Lockhart, R.W.; Martinelli, R.C.: Proposed correaltion for data for two-phase, two-component flow in pipes. Chem. Eng. Prog. Vol. 45, 1949, 39-48

[86] Lucas, K.; Luckas, M.: Berechnungsmethoden für Stoffeigenschaften. VDI-Wärmeatlas. 8. Auflage, Springer, Berlin, 1997

[87] Mathur, G.D.: Heat transfer coefficient for propane (R-290), isobutane (R-600a), and 50/50 mixture of propane and isobutane. ASHRAE Transaction, Vol. 104, No. 2, 1998, 1159-1172

[88] McAdams, W.H.; Woods, W. K.; Heroman, L.C.: Vaporization inside horizontal tube-II, Benzene oil mixtures. Trans. ASME, Vol. 64, 1972, 193-193

[89] McLinden, M.O.: Measurement and formulation of the thermodynamic properties of refrigerants R134a, R123. ASHRAE trans., Vol. 95, No. 2, 1989, 79-103

[90] Melin, P.; Vamling, L.: Flow boiling heat transfer and pressure drop for HFC-134a in a horizontal tube. Proc. of meetings of commissions B1, B2, E1, E2, Padoua, 1994, 575-582

[91] Memory, S.B.; Rose, J.W.: Free convection laminar film condensation on a horizontal tube with variable wall temperature. Int. J. of Heat and Mass Transfer. Vol. 34, No. 11, 1991, 2775-2778.

[92] Moldover, M.R.; Trusler, J.P.M.; Edwards, T.J.; Mehl, J.B.; Davis, R.S.: Measurement of the universal gas consatnat R using a spherical acoustic resonator. J. Research NBS, Vol. 93, No. 2, 1988, 85

[93] Morrison, G; McLinden, M.O.: Azeotropy in refrigerant mixture. Rev. Int. Froid., Vol. 16, No. 2, 1993, 129-137

[94] Müller-Steinhagen, H.: Wärmeübergang und Fouling beim Strömungssieden von Argon und Stickstoff im horizontalen Rohr. Fortschritt-Berichte VDI- Reihe 6 Nr. 143, VDI-Verlag GmbH, Düsseldorf, Germany, 1991

[95] Müller-Steinhagen, H.; Schlünder, E.U.: Über den Einfluß des Wärmeleitvermögens der Rohrwand auf den umfangsmittelen Wärmeübergangs-koeffizienten beim Sieden in horizontalen Verdampferrohren. Chem. Eng. Process, Vol. 18, 1984, 303-316

[96] Murata, K.; Hashizume, K.: Forced convection boiling of non-azeotropic refrigerant mixtures inside tubes. ASME J. of Heat Transfer, Vol. 115, 1993, 680-689

[97] Murata, K.; Hashizume, K.: An experimental invistigation on forced convection boiling of nonazeotropic refrigerant mixtures. Heat transfer Jpn. Res., Vol. 19, No. 2, 1990, 95-109

[98] Niederkrüger, M.: Strömungssieden von reinen Stoffen und binären zeotropen Gemischen im waagerechten Rohr bei mittleren und hohen Drücken. Fortschritt-Berichte VDI- Reihe 3, Nr. 245, VDI-Verlag GmbH, Düsseldorf, Germany, 1991

[99] Niederkrüger, M.; Steiner, D.; Schluender, E.-U.: Horizotal flow boiling experiments of saturated pure components and mixtures of R846-R12 at high pressure. Int. J. Refrig., Vol. 15, No. 1, 1992, 48-58

[100] Niederkrüger, M.; Steiner, D.: Flow boiling heat transfer to saturated pure components and non-azeotropic mixtures in a horizontal tube. Chemical Engineering and Processing, Vol. 33, 1994, 261-274

[101] NIST: REFRPOP. National institute for science and technology. Washington, DC, 1995

[102] Nusselt, W.: Die Oberflächenkondensation des Wasserdampfes. VDI-Z. 60, 1916, 541-546, 569-575

[103] Okubo, T.; Hasuo, T.; Nagashima, H.A.: Measurement of viscosity of HFC 134a in the temperature range 213-423 K and at pressure up to 30 MPa. Int. J. of Thermodynamics, Vol. 13, No. 6, 1992, 931-942

[104] Palen, J.W.: Falling film evaporation of wide-boiling-range mixtures inside a vertical tube. PhD-thesis, Lehigh Univ., 1988

[105] Perry, R.H.; Green, D.W.: Perry's chemical engineers' hand book. 16th (ed), McGraw Hill, New York, 1984

[106] Petukhov, B.S.; Popov, V.N.: Theoretical calculation of the heat exchanger and frictional resistance in turbulent flow in tubes of an incompressible fluid with variable physical properties. teplofiz. Vysok. temperatur (High temperature heat physics) Vol. 1, No. 1, 1963

[107] Rauhani, S.Z.: Subcooled void fraction. AB Atomenergie (Sweden) Report AE-RTV 841, 1969

[108] Reid, R.C.; Prausnitz, J. M.; Poling, B. E.: The properties of gases and liquids. McGraw-Hill, New York, 1987

[109] Rohlin, P.: Heat transfer coefficient of zeotropic mixtures and their pure components in horizontal flow boiling -an experimental study. Proceedings of 1997 ASME International Mechanical Engineering Congress and Exposition, Dallas, USA, 1997

[110] Rohsenow, W.M.; Hartnett, J.P.; Cho, Y.I.: Hand Book of Heat Transfer. McGraw-Hill, New York, 1998

[111] Rose, J.W.: Effect of pressure gradient in forced convection film condensation on a horizontal tube. Int. J. of Heat and Mass Transfer, Vol. 27, No. 1, 1984, 39-47

[112] Rose, J.W.: Condensation heat transfer fundamental. Trans. IchemE, Vol.76, part A, 1998, 143-152

[113] Rose, J.W.: Fundamental of condensation heat transfer: Laminar film condensation. JSME Int. J. of Heat and Mass Transfer, Series II, Vol. 31, No. 3, 1988, 357-375

[114] Ross, H.D.; Radermacher, R.; Di Marzo, M.; Didion, D.: Horizontal flow boiling of pure and mixed refrigerants. Int. J. Heat Mass Transfer, Vol. 30, 1987, 979-992

[115] Schlünder, E.U.: Über den Wärmeübergang bei der Blasenverdampfung von Gemischen. vt Verfahrenstechnik, Vol. 16, No. 9, 1982, 692-698

[116] Schmidt, H.: Beitrag zum Verständnis des Wärmeübergangs im horizontalen Verdampferrohr. Fortschritt-Berichte VDI- Reihe 19, No. 6, VDI-Verlag GmbH, Düsseldorf, Germany, 1986

[117] Schrock, V.E.; Grossman, L. M.: Forced convection in tubes. Nuclear Science and Engineering, Vol. 12, 1962, 474-481

[118] Shah, M.M.: A new correlation for heat transfer during boiling flow through pipes. ASHREE Trans., Vol. 82, 1976, 66-86

[119] Shah, M.M.: Prediction of heat transfer during boiling of cryogenic fluids flowing in tubes. Cryogenics, Vol. 5, 1984, 231-236.

[120] Shah, M.M.: Chart correlation for saturated boiling heat transfer: Equation and further studies. ASHREE Trans. Vol. 88, No. 1, 1982, 80-89

[121] Shao, D.W.; Granryd, E.: Experimental and theoretical study on flow condensation with non-azeotropic refrigerant mixtures of R32/R134a. Int. J. Refrig. Vol. 21, No. 3, 1998, 230-246

[122] Shekriladze, I.G.: Gomelauri, V.I.: Theoretical study of laminar film condensation of flowing vapor. Int. J. of Heat and Mass Transfer. Vol.9, 1966, 581-1

[123] Shin, J.Y.; Kim, M.S.; Ro, S.T.: Experimental study on forced convective boiling heat transfer of pure and refrigerant mixtures in a horizontal tube. Int. J. of Refrig., Vol. 20, No. 4, 1997, 267-275

[124] Shoji, M.: Boiling simulator- a simple theoretical model of boiling-. Proc. of the 3rd Int. Conf. on Multiphase Flow, Lyon, France, June 1998, 8-12

[125] Singal, L.C.; Sharma, C.P.; Varma, H.K.: Heat transfer correlation for the forced convection boiling of R12/R13 mixture. Int. J. Refrig., Vol. 7, No. 5, 1984, 278-284

[126] Sparrow, E.M.; Gregg, J.L.: A boundray-layer treatment of laminar film condensation. J. Heat Transfer, No. 81C, 1959, 13-18,

[127] Spindler, K.: Flow boiling. Proc. Int. Heat Transfer Conference, Brighton, UK, Vol. 1, 1994, 349-369

[128] Steiner, D.: Strömungssieden Gesättiger Flüssigkeiten. in: VDI, VDI-GVC: VDI-Wärmeatlas. 8. Aufl., Springer-Verlag, Berlin, 1997, Abschnitt, Dbb

[129] Stephan, K.: Two-phase heat exchange for new refrigerants and their mixtures. Int. J. Refrig., Vol. 18, No. 3, 1995, 198-209

[130] Stephan, K.; Korner, M.: Berechnung des Warmeübergangs verdampfender binärer Flüßigkeitsgemische. Chem. Ing. Tech., Vol. 2, 1969, 161-169

[131] Stephan, K.; Preusser, P.: Heat transfer and critical heat flux in pool boiling of binary and ternary mixtures. German Chem. engng, Vol. 2, 1979, 161-169

[132] Storek, H.; Brauer, H.: Reibungsdruckverlust der adiabaten Gas/Flüßigkeitsstömung in horizontalen und vertikalen Rohren. VDI-Forschungsheft, Nr. 599, VDI-Verlag GmbH, Düsseldorf, Germany, 1980

[133] Taitel, Y.; Dukler, A.E.: A model for predicting flow regime transitions in horizontal and near horizontal Gas-Liquid flow. AICHE J., Vol. 22, No. 2, 1985, 43-55

[134] Thome, J. R.: Prediction of binary mixture boiling heat transfer coefficient using only phase equilibrium data. Int. J. of Heat and Mass Transfer, Vol. 26, 1983, 965-974

[135] Thome, J. R.: Enhanced boiling of mixture. Chemical Engineering Service, Vol. 42, No. 8, 1986, 1909-1917

[136] Tillner-Roth, R.: Die thermodynamischen Eigenschaften von R152a, R134a und ihren Gemischen-Messungen und Fundamental Gleichungen. Dissertation, Universität Hannover; Germany, 1993

[137] Tillner-Roth, R.: Fundamental equations of state. Shaker-Verlag, Aachen, Germany, 1998

[138] Tillner-Roth, R.; Baehr, H.D.: An international standard formulation of the thermodynamic properties of 1,1,1,2-tetraflouroethane (HFC-134a) covering temperatures from 170 K to 455 K at pressure up to 70 MPa. J. Phys. Chem. Ref. data., Vol. 23, 1994, 657

[139] Tillner-Roth, R.; Li, J.; Yokozenki, A.; Sato, H.; Watanabe, K.: Thermodynamic properties of pure and blended Hydroflourocarbons (HFCs) Refrigerants. Japan Society of Refrigeration and Air Conditioning Engineers, 1997

[140] Urso, M.E.; Wadekar, V.V; Hewitt, G.F.: Heat transfer at the dryout and near dryout regions in flow boiling. 12. Proc. of the 12. Int. Heat Tranasfer Conference, Grenoble, Vol.3. 2002, 701-706.

[141] van Wijk, W.R.; Vos, A.S.; van Stralen, S.J.D.: Heat transfer to boiling binary liquid mixtures. Chem. Engng. Sci., Vol. 5, 1956, 68-80

[142] Verma, H.K.; Sharma, C.P.; Mishra, M.P.: Heat transfer coefficients during forced convective evaporation of R12 and R22 mixtures in annular flow regime. Proc. XV Int. Congr. Refrig., Vol. II, 1979, 479-484

[143] VDI, VDI-GVC: VDI- Wärmeatlas. 8. Aufl., Springer-Verlag, Berlin, 1997

[144] Voskresenskji, K.D.: Heat transfer in film condensation with temperature dependent properties of the condensate. Izv. Akad. Nauk. USSR, 1948, 1023-1028

[145] Wadekar, V.V.: Convective heat transfer to binary mixtures in annular two-phase flow. Proc. of the 10th Int. Heat Transfer Conference, Brington, Vol. 7, 1994, 557-562

[146] Wadekar, V.V.: Boiling hot issues-some resolved and some not-yet-resolved. Trans. IchemE., Vol. 76, Part A, 1998, 133-142

[147] Weisman, J.; Duncan, D.; Bibson, J.; Crawford, T.: Effect of fluid properties and pipe diameter on two phase flow pattern in horizontal pipelines. Int. J. Multiphase flow, Vol. 5, 1979, 437-462

[148] Wettermann, M.: Wärmeübergang beim Sieden von Gemischen bei Zwangskonvektion im horizontalen Verdampferrhor. Fortschritt-Berichte VDI- Reihe 3, Nr. 625, VDI-Verlag GmbH, Düsseldorf, 1999

[149] Wongwises, S.; Disawas, S.; Kaewon, J; Onuari, C.: Two-phase evaporative heat transfer coefficients of refrigerant HFC-134a under forced flow conditions in a small horizotal tube. Int. Comm. Heat Mass Transfer, Vol. 27, No. 1, 2000, 35-48

[150] Yan, Y.; Lin, T.: Evaporation heat transfer and pressure drop of refrigerant R134a in small pipe. Int. J. of Heat and Mass Transfer. Vol. 41, 1997, 4183-4194

[151] Younglove, B.A.; Ely, J.F.: Thermophysical properties of fluids: Methane, Ethane, Propane, Isobutane and Normal Butane. J. of Physical Chemical Reference data, Vol. 16, No. 4, 1987, 577-798

[152] Zahn, W.R.: Flow conditions when evaporating refrigerant R22 in air conditioning coils. ASHRAE trans., Vol. 72, 1965, 82-89

[153] Zhang, L.; Hihara, E.; Saito, T.; Oh, J.-T.: Boiling heat transfer of a ternary refrigerant mixture inside a horizontal smooth tube. Int. J. of Heat and Mass Treansfer, Vol. 40, No. 9, 1997, 2009-2017

[154] Zürcher, O.; Thome, J.R.; Favrat, D.: In tube flow boiling of R407C and R407C/oil mixtures. Part I: microfin tube. ASHRAE Trans., Vol. 4, No. 4, 1998, 347-372

Appendix

A Uncertainty and statistical analysis

A.1 Uncertainty

Fig. A.1 shows the distribution of the pressure and temperature measuring devices on the refrigeration cycle. The distribution of the devices used in the test loop and the secondary evaporator were shown earlier in Chapter 3. Tables A.1 to A.2 present the level of uncertainty of the various devices used for the measurement of pressure, temperature and voltage used in the present study.

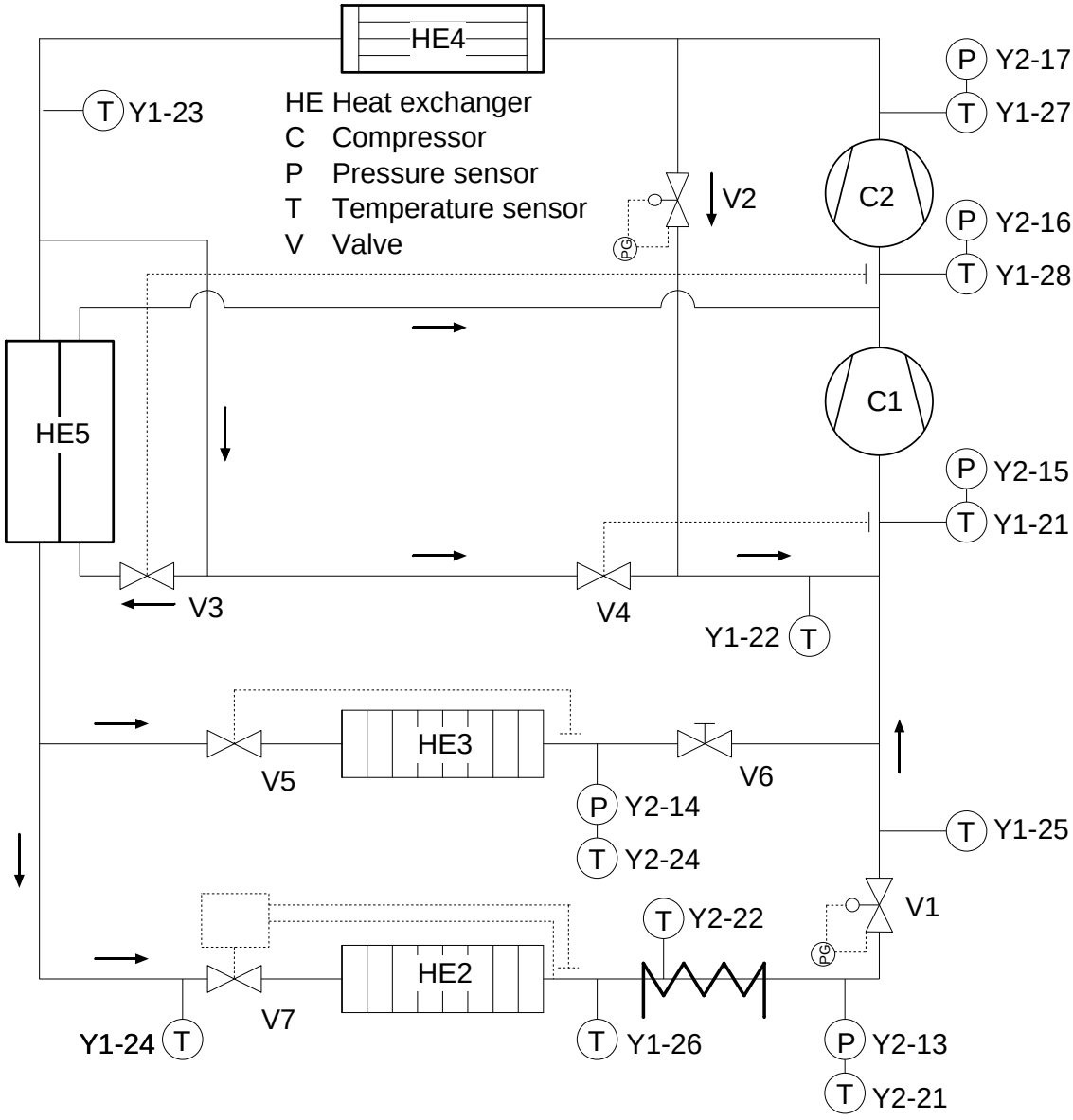

Figure A.1. Distribution of the pressure and temperature measuring devices on the refrigeration cycle.

Table A.1. The level of uncertainty and the coefficients of the calibration equation $T = a + bU$ for the temperature sensors. Abbreviations: **Y1**: hybridrecorder *Yokagawa* HR 3760 1, **Y2**: hybridrecorder *Yokagawa* HR 3760 2 and **K**: *Keithley* 2010 multimer.

Quantity	Multimeter	Number of channel	Temperature sensor	Level of uncertainty	a	b
				mK	°C	°C/V
T	Y2	21	TC-Type K	53.53	-0.272444	1.005231
T	Y2	22	TC-Type K	44.11	-0.104789	1.004089
T	Y2	23	TC-Type K	43.29	-0.344342	1.005296
T	Y2	24	TC-Type K	50.48	0.024347	0.997851
T	Y2	25	TC-Type K	44.35	-0.501147	1.009014
T	Y2	26	TC-Type K	39.72	-0.028944	1.001114
T	Y2	27	TC-Type K	53.41	-0.309052	0.999312
T	Y2	28	TC-Type K	43.45	-0.020262	0.995608
T	Y2	29	TC-Type K	48.77	-0.188612	0.997017
T	Y1	11	PT-100	18.08	0.825519	1.000388
T	Y1	12	PT-100	29.23	0.691602	0.999407
T	Y1	13	PT-100	21.72	0.862451	1.000639
T	Y1	14	PT-100	19.14	0.363798	1.000301
T	Y1	16	PT-100	16.82	0.204539	1.000621
T	Y1	17	PT-100	23.50	0.470446	1.000247
T	Y1	18	PT-100	16.89	0.198149	1.003322
T	Y1	19	PT-100	17.67	0.283839	1.001661
T	K	01	TC-Typ K	10.87	0.307436	0.993844
T	K	02	TC-Typ K	10.54	0.250961	0.996377
T	K	03	TC-Typ K	09.85	0.271730	0.994732
T	K	04	TC-Typ K	10.02	0.305397	0.992951
T	K	05	TC-Typ K	12.44	-0.082072	1.012171
T	K	06	TC-Typ K	10.73	0.256963	0.995941
T	K	07	TC-Typ K	10.24	0.272571	0.994525
T	K	08	TC-Typ K	11.32	0.201222	0.998386
T	K	09	TC-Typ K	11.37	0.205715	0.997792
T	K	10	TC-Typ K	12.19	0.218864	0.998130

For all thermocouples (Type K) which are not listed in the above tables the value of the constant a and b of the calibration equation is 0 and 1 respectively. That is to say the temperature is directly measured using the hybridrecorder *Yokagawa* HR 3760 multimeter. Under such condition the level of uncertainty is ±(0.05% of the reading +0.7 °C). To be remembered is that these temperature sensors are only used as a control.

A.2 Statistical parameters

In the present study a number of characteristic parameters are used in the statistical analysis. These parameters include

Table A.2. The level of uncertainty and the coefficients of the calibration equation $p = a + bU$ for the pressure sensors. Abbreviations: **Y1**: hybridrecorder *Yokagawa* HR 3760 1 and **Y2**: hybridrecorder *Yokagawa* HR 3760 2.

Quantity	Multimeter	Number of	Uncertainty mbar	Type of device	a bar	b bar/V
p	Y2	13	05.7700	DMS	01.2506	01.0049
p	Y2	14	10.1700	DMS	00.8434	00.7734
p	Y2	15	10.9900	DMS	00.9077	01.0069
p	Y2	16	02.9300	DMS	00.9547	01.9153
p	Y2	17	02.5100	DMS	01.3291	02.5500
Δp	Y2	19	00.2429	DMS	-0.1202	99.1305
Δp	Y2	20	00.2352	DMS	-0.2088	99.1815
p	Y1	01	01.9300	Piezometer	-0.0088	00.8994
p	Y1	02	02.0300	Piezometer	-0.0195	00.9018
p	Y1	03	01.4800	DMS	-0.0231	04.1373
p	Y1	04	02.2400	Piezometer	00.0064	00.9001
p	Y1	05	01.3300	DMS	00.0057	02.7545
Δp	Y1	06	0.05408	DMS	-0.1577	20.0205
p	Y1	07	02.5400	DMS	-0.0445	04.1336

Notice: For Δp the constants a and b are in mbar and mbar/V respectively.

- the error

$$e_i = \frac{\phi_i - \Phi_i}{\Phi_i} 100\% \ , \tag{A.1}$$

- the mean error

$$e_m = \frac{1}{N} \sum_{i=1}^{N} e_i \ , \tag{A.2}$$

- the mean absolute error

$$|\overline{e}| = \frac{1}{N} \sum_{i=1}^{N} |e_i| \ , \tag{A.3}$$

- the root mean square error

$$e_{rms} = \sqrt{\frac{1}{N} \sum_{i=1}^{N} e_i^2} \ , \tag{A.4}$$

- the standard deviation

$$\sigma = \sqrt{\frac{1}{N-1} \sum_{i=1}^{N} (e_m - e_i)^2} \ , \tag{A.5}$$

where ϕ_i is the measured parameter and Φ_i is the corresponding calculated parameter.

B Thermophysical properties

In the field of flow boiling, physical properties of high level of accuracy are required for the estimation of the various flow boiling parameters. This is because the flow boiling parameters like the vapor quality and saturation temperature are not directly measured, they are rather calculated from the thermodynamic properties. For example the saturation temperature of the R134a is calculated with knowledge of the saturation pressure from a reliable correlation. The quality is calculated by applying an energy balance between the inlet of the preheater and the inlet of the test section. Here the liquid enthalpy and enthalpy of evaporation are the parameters.

The transport properties like viscosity, thermal conductivity, surface tension, diffusion coefficient are generally calculated from the existing correlations. The thermodynamic properties are best evaluated from the fundamental equation of state for the pure fluid. For the pure R134a, propane and ammonia and the mixture of R134a and propane the fundamental equation of states developed by Tillner-Roth [136] have been adopted in the present work. These equations are already available in a form of a software package under the name "*Progs*" at the Institute for thermodynamic, University of Hannover, Hannover, Germany.

The validation of the of existing correlation for transport properties and thermodynamic properties plays an important role in the present work. Due to the fact there exists a limited number of experimental data on the open literature, the data supplied by the manufacturer of the refrigerant is accepted for the validation of the existing models for the prediction of the physical properties. Additionally, for the saturation temperature of the pure R134a a number of measurement in the adiabatic region are made. For the R134a/propane mixture the p, T, ρ, $\widetilde{x}$, $\widetilde{y}$ experimental data of Kleiber [78] is used to determine the interaction coefficients which are necessary for the correct application of the fundamental equation of state of Tillner-Roth [137]. For the transport properties the author is unaware of any experimental data of R134a/R290 mixture thus the level of uncertainty of each correlation indicated by its author is accepted.

B.1 1,1,1,2- Tetrafluoroethane (R134a)

B.1.1 General specifications and critical properties of R134a

The synonym of 1,1,1,2- Tetrafluorethane (CF_3CH_2F) is HFC-134a and its short name is R134a. Table B.1 presents some general specifications and critical properties of R134a. The general specification are obtained from Mc Linden et al. [89] and the critical properties is taken from Tillner-Roth [137].

B.1.2 Equation of state (EOS) for R134a

The equation of state for a pure refrigerant is given in term of the dimensionless Helmholtz free energy by Tillner-Roth [137] as

$$\Phi(\tau,\delta) = \Phi^o(\tau,\delta) + \Phi^r(\tau,\delta) \ , \tag{B.1}$$

Table B.1. Critical properties of R134a.

T_c	p_c	ϱ_c	$\widetilde{M}$	Acentric factor	Dipole moment
K	bar	kg/m^3	g/mol	-	Debye
374.18	40.563	508	102.032	0.32684	2.058 (polar)

where $\Phi^o(\tau,\delta)$ and $\Phi^r(\tau,\delta)$ is the ideal and the real part of the EOS respectively. Independent variables are the inverse reduced temperature $\tau = T_c/T$ and the reduced density or inverse reduced molar volume $\delta = \varrho/\varrho_c = \overline{V}_c/\overline{V}$. The ideal part of the dimensionless Helmholtz free energy is given by Tillner-Roth and Baehr [138] as

$$\Phi^o(\tau,\delta) = a_1^0 + a_2^o + a_3^o.ln\delta + a_4^o.\tau^{-1/2} + a_5^o\tau^{-3/4} \ . \tag{B.2}$$

The value of the coefficient a_i^o is given in table B.2.

Table B.2. Coefficients of the ideal part of the dimensionless Helmholtz free energy for R134a.

i	1	2	3	4	5	Range of validity
a_i^o	-1.019535	-9.723916	9.047135	-3.92717	-1.629789	$169.85 < T < 455$ K

The real part of the dimensionless Helmholtz free energy is given by Tillner-Roth and Baehr [138] as

$$\Phi^r(\tau,\delta) = \sum_{i=1}^{8} a_i.\tau^{t_i} + exp(-\delta)\sum_{i=9}^{11} a_i.\tau^{t_i}.\delta^{d_i} exp(-\delta^2)\sum_{i=12}^{17} a_i.\tau^{t_i}.\delta^{d_i} + \exp(-\delta^3)\sum_{i=18}^{20} a_i.\tau^{t_i}.\delta^{d_i} + a_{21} exp(-\delta^4)\tau^{t_{21}}.\delta^{d_{21}} \ . \tag{B.3}$$

The value of the constants a_i, τ_i and d_i are given in table B.3.

The saturation properties are determined from the Helmholtz free energy formulation by solving simultaneously the following three equations

$$p_s = p(\varrho_L, T) = RT\varrho_L\left[1 + \delta_L\left(\frac{\partial\Phi^r}{\partial\delta}\right)_L\right] \ , \tag{B.4}$$

$$p_s = p(\varrho_G, T) = RT\varrho_G\left[1 + \delta_G\left(\frac{\partial\Phi^r}{\partial\delta}\right)_G\right] \ , \tag{B.5}$$

$$\frac{p_s}{RT}\left(\frac{1}{\varrho_G} - \frac{1}{\varrho_L}\right) = \ln\frac{\varrho_L}{\varrho_G} + \Phi^r(\tau,\delta_L) - \Phi^r(\tau,\delta_G) \ . \tag{B.6}$$

where the subscript G and L stands for vapor and liquid respectively. The solution of these equations for a given temperature yields the density of the liquid ϱ_L and the density of the vapor ϱ_G and the vapor pressure p_s. Subsequently all other thermodynamic properties of the saturated liquid and vapor can be calculated using the relationships shown in table B.4.

Table B.3. Coefficients of the real part of the dimensionless Helmholtz free energy for R134a (equation B.3).

i	a_i^o	τ_i	d_i^o	i	a_i^o	τ_i	d_i^o
1	0.05586817	-0.5	2	12	$1.017263.10^{-4}$	1	4
2	0.4982230	0	1	13	-0.5184567	5	1
3	0.02458698	0	3	14	$-0.08692288.10^{-2}$	5	4
4	$8.570145.10^{-4}$	0	6	15	0.2057144	6	1
5	$4.788584.10^{-4}$	1.5	6	16	$-5.000457.10^{-3}$	10	2
6	-1.800808	1.5	1	17	$4.603262.10^{-4}$	10	4
7	0.2671641	2	1	18	$-3.497836.10^{-3}$	10	1
8	$-0.04781652.10^{-2}$	2	2	19	$6.995038.10^{-3}$	18	5
9	$0.01423987.10^{-2}$	1	5	20	$-1.452184.10^{-2}$	22	3
10	0.3324062	3	2	21	$-1.285458.10^{-4}$	50	10
11	$-7.485907.10^{-3}$	5	2				
	$169.85 < T < 455$ K				$0 < p < 700$ bar		

Table B.4. Mathematical relationship between the reduced Helmholtz free energy and thermodynamic properties (Tillner-Roth, [137]).

Property		Relationship
Pressure	$\frac{p}{RT\varrho}$	$= 1+\delta\Phi_\delta^r$
Specific isobaric heat capacity	$\frac{c_v}{R}$	$= c_v(\tau,\delta) = -R.\tau^2.(\Phi_{\tau\tau}^o + \Phi_{\tau\tau}^r)$
Specific isochoric heat capacity	$\frac{c_p}{R}$	$= c_v(\tau,\delta) + R\frac{(1+\delta\tau\Phi_{\delta\tau}^r)^2}{1+2\delta\Phi_\delta^r+\delta^2\Phi_{\delta\delta}^r}$
Specific enthalpy	$\frac{h}{RT}$	$\{1 + \tau.[\Phi_\tau^o(\tau,\delta) + \Phi_\tau^r(\tau,\delta)] + \delta.\Phi_\delta^r(\tau,\delta)\}$

Acronyms:

$$\Phi_\delta = \left(\frac{\partial\Phi}{\partial\delta}\right)_\tau,\ \Phi_\tau = \left(\frac{\partial\Phi}{\partial\tau}\right)_\delta,\ \Phi_{\delta\delta} = \left(\frac{\partial^2\Phi}{\partial\delta^2}\right)_\tau$$

$$\Phi_{\delta\tau} = \left(\frac{\partial^2\Phi}{\partial\tau\partial\delta}\right),\ \Phi_{\tau\tau} = \left(\frac{\partial^2\Phi}{\partial\delta^2}\right)_\delta$$

The uncertainty of the equation of state is estimated to be about ±0.03 % or 0.1 kPa at a temperature below 250 K for the vapor pressure, about ±0.1 % in the density for a P, ϱ, T-measurement in the liquid phase and ±0.05 % in the pressure for those in the vapor phase and about ±0.1 % in specific heat capacities in the liquid phase. A software utilizes these models is available under the name *Progs* at the Institute for thermodynamic, University of Hannover, Hannover, Germany.

B.1.3 Liquid dynamic viscosity of R134a

The liquid dynamic viscosity of R134a is calculated using the correlation recommended by Okubo et al.[103] as

$$\eta_L = \left[A + B.p_r + C.ln(1 + p_r)\right].10^{-4} \ , \tag{B.7}$$

where

$$A = \sum_{i=0}^{3} a_i.exp\left(\frac{i-1}{T_r}\right) \ , \tag{B.8}$$

$$B = \sum_{i=0}^{3} b_i.exp\left(\frac{i-1}{T_r}\right) \ , \tag{B.9}$$

$$C = \sum_{i=0}^{3} c_i.T_r^i \ . \tag{B.10}$$

The coefficient a_i, b_i and c_i, the range of validity and level of uncertainty for the liquid thermal conductivity is given in table B.5.

Table B.5. Coefficients of the correlation of the liquid viscosity for R134a.

i	g_i	b_i	c_i	i	g_i	b_i	c_i
0	-28.3390	-203324	3.48185	2	-4.13120	-0.269815	13.2131
1	18.1691	1.29841	-12.4685	3	0.51452	0.0280058	-3.74703

$213 < T < 423$ K and p $\leq$ 300 bar

error= $\pm$1.3 %

B.1.4 Vapor dynamic viscosity of R134a

Lucas and Luckas [86] in VDI-Wärmeatlas [143] have recommended the following procedure for the calculation of the vapor viscosity.

$$\eta = (\eta\xi)^r F_p F_Q \frac{1}{\xi} \ , \tag{B.11}$$

for $T_r \leq 1$ and $p_r \leq p_s/p_c$

$$(\eta\xi)^r = 0.600 + 0.760 p_r^{\alpha} + (6.990 p_r^{\beta} - 0.6)(1 - T_r) \ , \tag{B.12}$$

with

$$\alpha = 3.262 + 14.98 p_r^{5.508} \ and \ \beta = 1.390 + 5.746 p_r \ , \tag{B.13}$$

for $1 \leq T_r \leq 40$ and $0 \leq p_r \leq 100$

$$(\eta\xi)^r = (\eta^o\xi)\left[1 + \frac{A p_r^E}{B p_r^F + (1 + C p_r^D)^{-1}}\right] \ , \tag{B.14}$$

where η^o is the low pressure viscosity given as

$$\eta^o\xi = [0.807T_r^{0.618} - 0.357\exp(-0.449T_r) + 0.340\exp(-4.058T_r) + 0.018]F_p^oF_Q^o \ , \quad \text{(B.15)}$$

and ξ is given as

$$\xi = \frac{[T_c]^{1/6}.[R]^{1/6}[N_a]^{1/3}}{[M]^{1/2}[p_c]^{2/3}} \ , \quad \text{(B.16)}$$

where N_a is the Avagadro number in kmol. The coefficients of equation B.14 are given as

$$A = \frac{a_1}{T_r}\exp(a_2T_r^\gamma) \ , \quad \text{(B.17)}$$

$$B = A(b_1T_r - b_2) \ , \quad \text{(B.18)}$$

$$C = \frac{c_1}{T_r}\exp(c_2T_r^\delta) \ , \quad \text{(B.19)}$$

$$D = \frac{d_1}{T_r}\exp(d_2T_r^\epsilon) \ , \quad \text{(B.20)}$$

$$E = 1.3088 \ , \quad \text{(B.21)}$$

$$F = f_1\exp(f_2T_r^\varsigma) \ . \quad \text{(B.22)}$$

The coefficients $a,\ b,\ c,\ d,\ e$, and f are given in Table B.6

Table B.6. Coefficients of the correlation used for the prediction of the vapor dynamic viscosity of R134a.

a_1	$1.245.10^{-3}$	a_2	5.1726	c_1	0.4489	c_2	3.0578	γ	-0.3286
b_1	1.6553	b_2	1.2723	d_1	1.7368	d_2	2.2310	δ	-37.7332
f_1	0.9425	f_2	-0.1853	ς	0.4489	ϵ	-7.6351		

$$F_p = 1 + (F_p^o - 1)\left[\frac{(\eta\xi)^r}{\eta^o\xi}\right]^{-3} \ , \quad \text{(B.23)}$$

and

$$F_Q = 1 + (F_Q^o - 1)\left[\frac{(\eta\xi)^r}{\eta^o\xi}\right]^{-1} - 0.007\left[\ln\left(\frac{(\eta\xi)^r}{\eta^o\xi}\right)\right]^4 \ , \quad \text{(B.24)}$$

where F_p^o and F_Q^o is low-pressure polarity and quantum factors respectively. These factors are

$$F_p^o = 1 \ , \ 0 \ \leq \mu_r \ < \ 0.022 \ , \quad \text{(B.25)}$$

$$F_p^o = 1 + 30.55(0.292 - Z_c)^{1.7} \ , \ 0.022 \ \leq \mu_r \ < \ 0.075 \ , \quad \text{(B.26)}$$

$$F_p^o = 1 + 30.55(0.292 - Z_c)^{1.7}(|0.96 + 0.1(T_r - 0.7)|) \ , \ 0.075 \ \leq \mu_r \ , \quad \text{(B.27)}$$

where Z_c is the critical compressibility factor and $F_Q^o = 1.0$ for all substances other than He, H_2 and D_2 . The reduced dipole moment μ_r is given as

$$\mu_r = \frac{\mu^2 p_c}{(kT_c)^2} \ , \tag{B.28}$$

where the dipole moment μ for the R134a is given in table B.1

B.1.5 Thermal conductivity of R134a

Goss et al.[47] have recommended a temperature dependent relationship for the prediction of both the liquid and vapor thermal conductivities as

$$\lambda = 10^{-3} \times (a - bT) \ , \tag{B.29}$$

where λ is in W/mK and the values of the coefficient a, b are given in tablel B.7.

Table B.7. Coefficients of equation B.29.

λ	a	b	max. absolute error %
λ_L	210.7	-0.42061	1.2
λ_G	-13.6162	0.09273	1.2

B.1.6 Surface tension of R134a

Lucas and Luckas [86] in VDI-Wärmeatlas [143] have recommended the following correlation for for the calculation of the surface tension

$$\sigma = p_{\mathrm{c}}^{2/3} T_{\mathrm{c}}^{1/3} \left(\frac{1 - T_{\mathrm{r}}}{a} \right)^m b \ , \tag{B.30}$$

where the reduced pressure and temperature are defined as

$$p_{\mathrm{r}} = \frac{p}{p_{\mathrm{c}}}, \ T_{\mathrm{r}} = \frac{T}{T_{\mathrm{c}}}, \ , \tag{B.31}$$

respectively.

For a polar fluid like R134a the following quantities are valid

$$a = 1 \ , \tag{B.32}$$

$$b = 0.1574 + 0.359\omega - 1.769X - 13.69X^2 - 0.510\omega^2 + 1.298\omega X \ , \tag{B.33}$$

$$m = 1.210 + 0.5385\omega - 14.61X - 32.07X^2 - 1.656\omega^2 + 22,03\omega X \ , \tag{B.34}$$

$$X = \lg p_{\mathrm{sr}}(T_{\mathrm{r}} = 0.6) + 1.70\omega + 1.552 \ . \tag{B.35}$$

where ω is the acentric factor and it is given by Pitzer in VDI-Wärmeatlas [143] as

$$\omega = \log(p_{r,(T_r=0.7)}) - 1 \ . \tag{B.36}$$

The surface tension given by equation B.30 is in 10^{-5} N/cm. Its level of uncertainty as given by Reid et al. [108] is 1.2 % in the range of the reduced temperature of $0.56 \leq T_r \leq 0.63$.

B.2 Propane (R290)

B.2.1 General specifications and critical properties of R290

The short name of of propane ($CH_3CH_2CH_3$) is R290. Table B.8 presents some general specifications and critical properties of R290. The general specifications are taken from McLinden et al. [89] and the critical properties are taken from Younglove and Ely [151].

Table B.8. Critical properties of Propane.

T_c	p_c	ϱ_c	$\widetilde{M}$	Acentric factor	Dipole moment
K	bar	m^3/kmol	kg/kmol	-	debye
369.83	42.48	0.2	44.0965	0.1524	0.083 (none polar)

B.2.2 EOS for R290

The ideal and the real part of the dimensionless Helmholtz free energy given by equation B.1 for propane are given by Younglove and Ely [151] as

$$\Phi^o(\tau,\delta) = \ln\delta + a_0^o + a_1^o\tau + a_2^o.ln\tau + a_3^o.(\tau.\ln\tau - \tau) + a_4^o.\ln(1-\exp(-n_4\tau)) + \sum_{i=5}^{9} a_i^o\tau^{n_i} \ , \quad \text{(B.37)}$$

$$\Phi^r(\tau,\delta) = \sum_{i=1}^{3} a_i.\tau^{t_i}.\exp(-\delta^2-1) + \sum_{i=4}^{22} a_i.\tau^{t_i}.\delta^{d_i} + \sum_{i=23}^{37} a_i.\tau^{t_i}.\delta^{d_i}.\exp(-\delta^{e_i}) \ , \quad \text{(B.38)}$$

respectively. The coefficients of the ideal and real part are given in table B.9 and table B.10 respectively.

Table B.9. Coefficients of the ideal part of the dimensionless Helmholtz free energy (equation B.37).

i	a_i^o	i	a_i^o	n_i	Range of validity
0	-8.87133773	4	3.1907016349	4.05569826	$0 < p < 100$ bar
1	9.02469987	5	-.010295701694	3.0	$85.47 < T < 600$ K
2	-6.4041204338	6	0.417257665468	2	$T_o = 273.15$ k
3	-4.048033181019	7	-7.251917626978	-1	s' =1 kJ/kgK^{-1}
3	-4.048033181019	8	0.495607464358	-2	h'=200 kJ/kg^{-1}
		9	-0.020352313275	-3	

The vapor pressure as well as all other thermodynamic properties are calculated following the same procedure used for the evaluation of the thermodynamic properties of R134a.

B.2.3 Dynamic viscosity of R290

The functional form of the liquid and vapor viscosities of propane as given by Younglove and Ely [151] is

$$\eta = \eta_o(T) + \eta_1(T)\rho + \eta_2(\rho,T) \ . \quad \text{(B.39)}$$

Table B.10. Coefficients of the residual part of the dimensionless Helmholtz free energy (equation B.38).

i	a_i	e_i	t_i	n_i	i	a_i	e_i	t_i	n_i
1	0.796570884954	-	3	-	20	$-0.985894180101\times10^{-3}$	-	2	7
2	$0.750795643944\times10^{-3}$	-	4	-	21	$0.115782138023\times10^{-2}$	-	3	7
3	$-0.150861780077\times10^{-3}$	-	5	-	22	$-0.145027445108\times10^{-3}$	-	3	8
4	-0.168644638630	-	0	1	23	$0.158251371231\times10^{1}$	2	3	2
5	$0.369195593593\times10^{1}$	-	0.5	1	24	$-0.637559643886\times10^{0}$	2	4	2
6	$-0.610773043583\times10^{1}$	-	1	1	25	$-0.150861780077\times10^{-3}$	2	5	2
7	$0.247266459364\times10^{1}$	-	2	1	26	$0.520091922107\times10^{0}$	2	3	4
8	$-0.111198258733\times10^{1}$	-	3	1	27	$-0.318779821943\times10^{0}$	2	4	4
9	$-0.685172470782\times10^{-1}$	-	0	2	28	$0.146053023303\times10^{0}$	2	5	4
10	$0.6219577378166\times10^{0}$	-	2	2	29	$0.194724433218\times10^{0}$	2	3	6
11	$-0.118493095237\times10^{1}$	-	2	2	30	$-0.8926609872\times10^{-1}$	2	4	6
12	$0.659145091712\times10^{0}$	-	3	2	31	$0.486843411011\times10^{-1}$	2	5	6
13	$0.332230919248\times10^{-1}$	-	0	3	32	$0.235296026524\times10^{-1}$	2	3	8
14	$-0.840004906444\times10^{-1}$	-	1	3	33	$-0.224066524543\times10^{-1}$	2	4	8
15	$0.247448121180\times10^{0}$	-	2	3	34	$-0.150957482137\times10^{-2}$	2	5	8
16	$0.328898075042\times10^{-1}$	-	1	4	35	$0.386243823311\times10^{-2}$	2	3	10
17	$-0.373926338310\times10^{-1}$	-	2	5	36	$0.247771187669\times10^{-2}$	2	4	10
18	$-0.144516316264\times10^{-1}$	-	3	5	37	$-0.301914964275\times10^{-3}$	2	5	10
19	$0.116730910017\times10^{-1}$	-	2	6					

The first term of the expansion is the dilute gas term which is

$$\eta_o(T) = (5/16)(k(1000\pi N_a)^{1/2}(M_r T)^{1/2}/(\Omega\sigma^2) \ , \tag{B.40}$$

where $N_a = 6.02 \times 10^{26}$ is the Avgadro's number, σ =0.47 nm is the Lorenz-Jones coefficient and $k = 1.38054 \times 10^{-23}$ J/mol K is the Boltzmann's constant.

The collision integral Ω is defined as

$$\Omega(T) = \left[\sum_{n=1}^{9} C(n).\left(\frac{\epsilon}{kT}\right)^{(4-n)/3}\right]^{-1} \ , \tag{B.41}$$

where ϵ/k=358.9 K and the value of the constant C is given in Table B.11.

Table B.11. Coefficients for the Collision integral Ω.

C(1)	-3.0328138281	C(2)	16.918880086	C(3)	-37.189364917
C(4)	41.288861858	C(5)	-24.61592114	C(6)	8.948843096
C(7)	-1.8739245042	C(8)	0.209661014	C(9)	-0.009657044

The second term of equation B.39 represents the contribution of the moderately dense fluid

$$\eta_1(T) = F_v(1) + F_v(2).(F_v(3) - \ln(T/F_v(4))^2 \ , \tag{B.42}$$

where $F_v(1) = 0.0$, $F_v(2) = 0.0$, $F_v(3) = 1.12$ and $F_v(4) = 359$. The third term in equation B.39 is the contribution of the dense gas

$$\eta_2(\rho, T) = \exp[F(\rho, T)] \ , \tag{B.43}$$

where

$$F(\rho, T) = G(T) + [E_v(3) + E_v(4)T^{-3/2}]\rho^{0.1} + \left[\sum_{n=5}^{7} E_v(n)T^{(-n+5)}\right] H(\rho) \ , \tag{B.44}$$

$$G(T) = E_v(1) + E_v(2)/T \ , \tag{B.45}$$

$$H(\rho) = \rho^{0.5}(\rho - \rho_c)/\rho_c \ . \tag{B.46}$$

The coefficients of the third term of the viscosity are given in table B.12

Table B.12. Coefficients of third viscosity term.

$E_v(1)$	$-14.113294896.10^{-2}$	$E_v(2)$	968.22940153	Ev(3)	$13.686545032.10^{2}$
$E_v(4)$	$-12511.628378.10^{-4}$	$E_v(5)$	$0.0168910864.10^{-1}$	$E_v(6)$	43.527109444
$E_v(7)$	7659.4543472				

The uncertainty in the prediction of the vapor viscosity of propane is 2% in the temperature range of $T < T_c$.

B.2.4 Thermal conductivity of R290

The thermal conductivity of the liquid and vapor of propane are calculated using Ross et al. [114] model

$$\lambda_{L/G} = A + B.T + C.T^2 + D.T^3 + E.T^4 \tag{B.47}$$

where λ_L is in mW/mK and the coefficients A, B, C and D are given in table B.13.

B.2.5 Surface tension of R290

The surface tension for propane may be calculated using the method of Mc Linden et al.[89] as

$$\sigma = A(1 - T_r)^B \ , \tag{B.48}$$

where A= $5.092.10^{-2}$ and B= 1.2197. The Mc Linden et al.[89] correlation has a level of uncertainty of 3% in the temperature range 85.47$\leq T \leq$369.93 K.

Table B.13. Coefficients of equation B.47.

	A	B	C	D	Range of validity	Accuracy
λ_L	0.26755	$-6.6457.10^{-4}$	$2.774.10^{-7}$	-	85.47$< T <$350 °C	3%
λ_G	-1.12	$1.0972.10^{-1}$	$-9.8346.10^{3}$	$-7.5358.10^{6}$	85.47$< T <$1000 °C	5%

B.3 Ammonia (R717)

B.3.1 General specifications and critical properties of R717

The short name of of Ammonia (NH_3) is R717. Table B.14 presents some general specifications and critical properties of R717. The general specifications are taken from Tillner-Roth [136].

Table B.14. Critical properties of ammonia.

T_c	p_c	ϱ_c	$\widetilde{M}$	Acentric factor	Dipole moment
K	bar	m^3/kmol	kg/kmol	-	debye
405.40	113.34	0.225	17.03026	0.25	1.5

B.3.2 EOS for R717

The ideal and the real part of the dimensionless Helmholtz free energy (equation B.1) for ammonia is given by Tillner-Roth [136] as

$$\Phi^o(\tau,\delta) = \ln\delta + a_0^o + a_1^o\tau + a_2^o.ln\tau + \sum_{i=3}^{5} a_i^o\tau^{n_i} \ , \tag{B.49}$$

$$\Phi^r(\tau,\delta) = \sum_{i=1}^{5} a_i.\tau^{t_i}.\delta^{d_i} + \sum_{i=6}^{21} a_i.\tau^{t_i}.\delta^{d_i}.\exp(-\delta^{e_i}) \ , \tag{B.50}$$

respectively. The coefficient of the ideal and real part is given in table B.15 and table B.16 respectively.

Table B.15. Coefficient the ideal part of the dimensionless Helmholtz free energy (equation B.49).

i	a_i^o	i	a_i^o	n_i	Range of validity
0	-15.815019	3	11.47434	1/3	$0 < p < 100$ bar, $85.47 < T < 600$ K
1	4.255726	4	-1.296211	-3/2	$T_o = 273.15$ K, $s' = 1$ kJ/(kg.K)$^{-1}$
2	-1.0	5	0.5706757	-7/4	$h' = 200$ kJ/kg^{-1}

Table B.16. Coefficient the real part of the dimensionless Helmholtz free energy (equation B.50).

i	a_i	e_i	t_i	d_i	i	a_i	e_i	t_i	d_i
1	-0.1858814×10^{1}	-	3/2	1	12	0.2397852×10^{-1}	2	3	1
2	0.4554431×10^{-1}	-	-1/2	2	13	-0.4085375×10^{-1}	2	6	1
3	0.7238548	-	1/2	1	14	0.2379275	2	8	2
4	0.1229470×10^{-1}	-	1	4	15	-0.3548972×10^{-1}	2	8	3
5	0.2141882×10^{-10}	-	3	15	16	-0.1823729	2	10	2
6	-0.1430020×10^{-1}	1	0	3	17	-0.150861780077	2	10	4
7	0.3441324	1	3	3	18	-0.6663444×10^{-2}	3	5	3
8	-0.2873571	1	4	1	19	-0.8847486×10^{-2}	3	15/2	1
9	0.2352589×10^{-4}	1	4	8	20	0.2272635×10^{0}	3	15	2
10	-0.3497111×10^{-1}	1	5	2	21	-0.5588655×10^{-3}	3	30	4
11	-0.1831117×10^{-2}	2	5	8					

B.3.3 Thermal conductivity of R717

The thermal conductivity of the liquid and vapor of R290 are calculated using Ross et al. [114] model

$$\lambda_{L/G} = A + BT \ , \tag{B.51}$$

where λ_L is in mW/mK and the coefficients $A,\ B,\ C$ and D are given in table B.17.

Table B.17. Coefficients and the range of validity of the thermal conductivity of ammonia.

Property	A	B	Range of validity	Accuracy
λ_L	0.561	$-2.055.10^{-3}$	85.47< T <350 K	3%
λ_G	0.01573	$0.1222.10^{-3}$	T <0 °C	5%
λ_G	0.02184	$0.1765.10^{-3}$	$T \geq$0 °C	5%

B.3.4 Dynamic viscosity of R717

The functional form of the liquid and vapor viscosity of ammonia as given by Fenghour et al. [36] is

$$\eta = \eta_o(T) + \eta_1(T)\rho + \eta_2(\rho, T) \ , \tag{B.52}$$

The first term of the expansion is the dilute gas term which is given as

$$\eta_o(T) = 100 \left[\frac{0.021357}{0.2957^2}\right] \frac{(\widetilde{M}T)^{1/2}}{\exp(\Omega)} \ , \tag{B.53}$$

where $\widetilde{M}$ is the molecular weight in g/mol, T is the temperature in K. The collision integral Ω is defined as

$$\Omega(T) = \left\{ C(1) + C(2)\log\left(\frac{kT}{\epsilon}\right) + \sum_{n=3}^{4} C(n).\left[\log\left(\frac{kT}{\epsilon}\right)\right]^n \right\} \ , \tag{B.54}$$

where ϵ/k=386 K and the value of the coefficient C is given in table B.18.

Table B.18. Coefficients for the Collision integral Ω (equation B.54).

$C(1)$	4.9931822	$C(2)$	-0.61122364	$C(3)$	0.18535124	$C(4)$	-0.1116094

The second term of equation B.52 represents the contribution of the moderately dense fluid

$$\eta_1(T) = F_v(T)\eta_o(T)\rho \ , \tag{B.55}$$

where

$$F_v(T) = C\left\{A(1) + \sum_{i=2}^{13} A(i)\left[\log\left(\frac{kT}{\epsilon}\right)\right]^{\frac{-(i-1)}{2}}\right\} \ , \tag{B.56}$$

where C=0.6022137/0.2957^3 and the value of the coefficient A is given in table B.19

Table B.19. Coefficients of equation B.56.

i	A	i	A
1	-0.17999496$\times 10^1$	2	0.466692621$\times 10^2$
3	-0.53460794$\times 10^3$	4	0.33604074$\times 10^4$
5	-0.13019164$\times 10^5$	6	0.33414230$\times 10^5$
7	-0.58711743$\times 10^5$	8	0.71426686$\times 10^5$
9	-0.59834012$\times 10^5$	10	0.33652741$\times 10^5$
11	-0.12027350$\times 10^5$	12	0.24348205$\times 10^4$
13	-0.120807957$\times 10^3$		

The third term in the viscosity equation B.52 is the contribution of the dense gas

$$\eta_2(\rho, T) = \sum_{i=1}^{3} F(i,T)\rho^{i+1} \ , \tag{B.57}$$

where

$$F(i,T) = \begin{cases} 1 & 0.219664285\left(\frac{\epsilon}{kT}\right)^2 - 0.83651107\times 10^{-1}\left(\frac{\epsilon}{kT}\right)^4 \\ 2 & 0.17366936\times 10^{-2} - 0.83651107\times 10^{-2}\left(\frac{\epsilon}{kT}\right) \\ 3 & 0.167668649\times 10^{-3}\left(\frac{\epsilon}{kT}\right)^2 - 0.149710093\times 10^{-3}\left(\frac{\epsilon}{kT}\right)^3 + \\ & 0.77012274\times 10^{-4}\left(\frac{\epsilon}{kT}\right)^4 \end{cases}$$

The Fenghour et al. [36] correlation for the vapor viscosity of ammonia has an uncertainty of 2% in the temperature range of $T < T_c$.

B.4 R134a/R290 mixtures

B.4.1 EOS for R134a/R290 mixtures

As for a pure component the dimensionless Helmholtz free energy of a mixture is given by Tillner Roth [137] as

$$\Phi = \frac{\overline{A}}{R_m T} = \Phi^o + \Phi^r \ , \tag{B.58}$$

where $\overline{A}$ is the molar free energy and $R_m = 8.314471$ mol $^{-1}$ K^{-1} is the universal gas constant as reported by Moldover et al. [92]. Similar to the pure fluid equation of state Φ is split into an ideal part Φ^o and residual part Φ^r. The ideal part of a mixture is analytically obtained from the ideal part Φ^o_{0i} of the pure fluid equation of state. At a constant temperature T and a constant molar volume $\overline{V}$ the mixture ideal part is

$$\Phi^o(\tau, \delta, \overrightarrow{x}) = \sum_{i=1}^{l} \widetilde{x}_i \Phi^o_{0i}(\tau, \delta) + \sum_{i=1}^{l} \widetilde{x}_i \ln \widetilde{x}_i \ , \tag{B.59}$$

where l is the number of components, $\overrightarrow{x}$ is the vector of all mole fractions and $\widetilde{x}_i$ is the mole fraction of component i. The second term in the right hand side of equation B.59 represents the mixing effect of the ideal gas mixture. The reduced variables are defined as

$$\delta = \frac{\overline{V}_{c,0i}}{\overline{V}}, \tau = \frac{T_{c,0i}}{T} \ . \tag{B.60}$$

The residual part of the Helmholtz free energy of a mixture is

$$\Phi^r(\tau, V, \widetilde{x}) = \sum_{i=1}^{l} \widetilde{x}_i \Phi^r_{0i}(\tau, \delta) + \sum_{i=1}^{l} \sum_{j=i+1}^{l} \widetilde{x}_i \widetilde{x}_j \Delta\Phi^r_{ij}(\tau, \delta) \ , \tag{B.61}$$

The reduced variables δ and τ are defined as

$$\delta(\overrightarrow{x}) = \frac{\overline{V}_c(\overrightarrow{\widetilde{x}})}{\overline{V}} \quad \tau(\overrightarrow{\widetilde{x}}) = \frac{T_c(\overrightarrow{\widetilde{x}})}{T} \ . \tag{B.62}$$

where $\overline{V}_c(\overrightarrow{\widetilde{x}})$ and $T_c(\overrightarrow{\widetilde{x}})$ is the pseudo-critical molar volume and temperature of the mixture respectively. These are defined as

$$\overline{V}_c(\overrightarrow{x}) = \sum_{i=1}^{l} \sum_{j=1}^{l} \widetilde{x}_i \widetilde{x}_j \overline{V}_{c,ij} \ , \tag{B.63}$$

$$T_c(\overrightarrow{\widetilde{x}}) = \sum_{i=1}^{l} \sum_{j=1}^{l} \widetilde{x}_i \widetilde{x}_j \overline{V}_{c,ij} \ , \tag{B.64}$$

where

$$V_{c,ij} = k_{V,ij} \frac{1}{2}(V_{c,0i} + V_{c,j}), \qquad T_{c,ij} = k_{T,ij} \frac{1}{2}(T_{c,i} + T_{c,j}) \ . \tag{B.65}$$

k_V and k_T are interaction parameters which are determined by fitting the entire fundamental equation of state to the experimental data of the binary mixture. Besides these

parameters the contribution to the Helmholtz free energy from the non-ideal mixing part $\Delta\Phi^r_{ij}(\tau,\delta)$ must be determined. Tillner-Roth [136] has set $\Delta\Phi^r_{ij}(\tau,\delta)=0$.

The available experimental VLE-data of Holcomb et al. [54] and Kleiber [78] between 255 K and 350 K and the liquid densities by Holcomb et al. [54] between 275 K and 345 K are used to determine the interaction coefficients k_V and k_T for this work. These were determined iteratively until the objective function

$$O.F = \sum_{1}^{i=2}\left(\frac{p_{cal}-p_{meas}}{p_{meas}}\right)^2 + \sum_{1}^{i=2}\left(\frac{\widetilde{y}_{cal,i}-\widetilde{y}_{meas,i}}{\widetilde{y}_{meas,i}}\right)^2 , \tag{B.66}$$

is minimized, where $\widetilde{y}_{meas}$ and p_{meas} is the experimental value of the vapor mole fraction and pressure at constant temperature respectively. The result of the optimization yields k_T= 1.04225 and k_v= 0.8955.

Fig. B.1 shows comparison of experimental VLE-data of Kleiber [78] with the present formulation. The average deviation is 1.48 % for the bubble pressure and it is 0.017 for the vapor mole fraction $\widetilde{y}$ (propane). The R134a-propane mixture has an azeotrope at approximately 65 mol % propane. Relationship between the thermodynamic properties

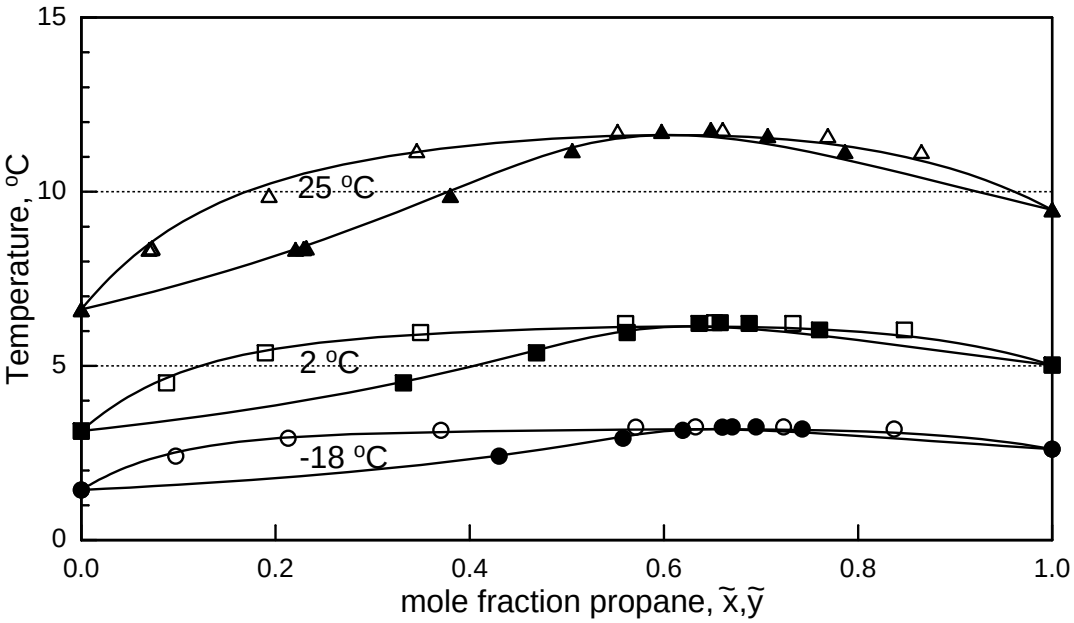

Figure B.1. Phase diagram for the system of propane-R134a mixtures. The symbols represent the experimental VLE-data of Kleiber [78].

and the Helmholtz function for mixtures are similar to those for pure fluid. The mathematical relationships for calculating the thermodynamic properties of a binary mixture are summarized in table B.20.

Table B.20. Mathematical relationship between the reduced Helmholtz free energy and thermodynamic properties of a mixture (Tillner-Roth [137]).

Property		Relationship
Pressure	$\frac{p}{RT\varrho}$	$= 1+\delta\Phi^r_\delta$
Specific isobaric heat capacity	$\frac{c_v}{R}$	$= c_v(\tau,\delta) = -R.\tau^2.(\Phi^o_{\tau\tau} + \Phi^r_{\tau\tau})$
Specific isochoric heat capacity	$\frac{c_p}{R}$	$= = c_v(\tau,\delta) + R\frac{(1+\delta\tau\Phi^r_{\delta\tau})^2}{1+2\delta\Phi^r_\delta+\delta^2\Phi^r_{\delta\delta}}$
Specific enthalpy	$\frac{h}{RT}$	$=\{1 + \tau.[\Phi^o_\tau(\tau,\delta) + \Phi^r_\tau(\tau,\delta)] + \delta.\Phi^r_\delta(\tau,\delta)\}$
Fugacity coefficient	$ln\varphi$	$=-lnZ + \Phi^r_{0i} + \delta\Phi^r_\delta + \delta\Phi^r_\delta\frac{n}{V_c}\frac{\partial V_c}{\partial n_i} + \tau\Phi^r_\tau\frac{n}{T_c}\frac{\partial Tc}{\partial n_i}$
		$n\frac{\partial V_c}{\partial n_i} = 2\left(\sum \widetilde{x}_i V_{c,ij} - V_{c(\widetilde{x})}\right)$
		$n\frac{\partial T_c}{\partial n_i} = 2\left(\sum \widetilde{x}_i T_{c,ij} - T_{c(\widetilde{x})}\right)$

B.4.2 Liquid dynamic viscosity of R134a/R290 mixtures

For a liquid mixture which contains one or more polar constituents Reid et al. [108] recommended the following model for the calculation of the mixture liquid viscosity

$$\ln \eta_m = \sum_{i=1}^{n} x_i . \ln \eta_{L,i} + 2.\widetilde{x}_1.\widetilde{x}_2.G_{12} \ , \tag{B.67}$$

where $\widetilde{x}_i$ is the mole fraction of the component i, $\eta_{L,i}$ is the viscosity of the component i in kg/ms and G_{12} is an adjustable parameter normally obtained from experimental data. For a polar-nonpolar mixture G_{12}= -0.22. The Reid et al. [108] model give the thermal conductivity with a mean error of less then 5%.

B.4.3 Vapor dynamic viscosity of R134a/R290 mixtures

The viscosity of a gas mixture can be approximated by using the principle of the kinetic theory (Reid et al. [108]) as

$$\eta_m = \eta^o_m + \Delta\eta \ , \tag{B.68}$$

where η^o_m is the mixture gas viscosity at a low pressure and $\Delta\eta$ is a correction factor for the high pressure viscosity

$$\eta^o_m = \sum_{i=1}^{n} \frac{\widetilde{y}_i.\eta_{G,i}}{\sum_{j=1}^{n} \widetilde{y}_i\phi_{ij}} \ , \tag{B.69}$$

where $\widetilde{y}_i$ is the mole fraction of the component i and η_i is the viscosity of the pure component i. ϕ_{ij} is a parameter which may be estimated as

$$\phi_{ij} = \frac{\left[1 + (\eta_{G,i}/\eta_{G,j})^{0.5}(\widetilde{M}_j/\widetilde{M}_i)^{0.25}\right]^2}{[8(1 + \widetilde{M}_i/\widetilde{M}_j)]^{0.5}} \ , \tag{B.70}$$

$$\phi_{ji} = \frac{\eta_{G,j}}{\eta_{G,i}} \frac{\widetilde{M}_j}{\widetilde{M}_i} . \phi_{ij} \ . \tag{B.71}$$

The high pressure correction term is estimated as

$$\Delta\eta = \frac{0.497.10^{-6}. \left[\exp(1.439\rho_{r,m}) - \exp(-1.111\rho_{r,m}^{1.858})\right]}{T_{c,m}^{1/6} \widetilde{M}_m^{-0.5} p_{c,m}^{-2/3}} \ . \tag{B.72}$$

The pseudo critical properties of the mixture are calculated as

$$T_{c,m} = \sum_{j=1} \widetilde{y}_j T_{c,j}, \quad \upsilon_{c,m} = \sum_j \widetilde{y}_j . \upsilon_{c,j}, \quad \widetilde{Z}_{c,j} = \frac{p_{c,j}\upsilon_{c,j}}{RT_{c,j}}, \quad \widetilde{Z}_m = \sum_j . y_j . \widetilde{Z}_{c,j}, \tag{B.73}$$

$$\widetilde{M}_m = \sum_{j=1} \widetilde{y}_j \widetilde{M}_j, \quad \rho_{c,m} = \frac{\widetilde{M}_m/1000}{\upsilon_{c,m}}, \quad \rho_{r,m} = \frac{\rho_m}{\upsilon_{c,m}}, \quad p_{c,m} = \frac{R.T_{c,m}\widetilde{Z}_{c,m}}{\upsilon_{c,m}} \ , \tag{B.74}$$

where T is in K, p is in Mpa, $\upsilon_{c,m}$ is in m^3/kmol, $\rho_{r,m}$ is in kg/m^3, M is in g/mol and η_m is in kg/ms. The error associated with this model is seldom exceeded 3 to 4% (Perry and Green [105]).

B.4.4 Liquid thermal conductivity of R134a/R290 mixtures

Reid et al. [108] have recommended a Filippov-like model for the prediction of the thermal conductivity of a liquid mixture as

$$\lambda_m = \sum_{i=1}^{2} \widetilde{X}_i \lambda_{L,i} - 0.72 X_1 . \widetilde{X}_2 . |\lambda_{L,2} - \lambda_{L,1}| \ , \tag{B.75}$$

where $\widetilde{X}_1$ and $\widetilde{X}_2$ is the weight fraction of the component 1 and 2 respectively and λ_1 and λ_2 is the thermal conductivity of the component 1 and 2 in W/mK respectively.

B.4.5 Vapor thermal conductivity of R134a/R290 mixtures

The thermal conductivity of a low-pressure gas mixture can be determined from the relationship given by Reid et al. [108]

$$\lambda_{G,m} = \sum_{i=1}^{n} \frac{\widetilde{y}_i . \lambda_{G,i}}{\sum_{j=1}^{n} \widetilde{y}_i . A_{ij}} \ , \tag{B.76}$$

where $\lambda_{G,m}$ is the low-pressure gas mixture thermal conductivity, $\lambda_{G,i}$ is the low-pressure thermal conductivity of the pure component i. For a binary mixture of two non-polar gases or a non-polar and a polar gas, A_{ij} may be calculated by the model given by Perry and Green [105] as

$$A_{ij} = \frac{\left[1 + (\lambda_{tr,i}/\lambda_{tr,j})^{0.5} (\widehat{M}_j/\widetilde{M}_i)^{0.25}\right]^2}{[8(1 + \widetilde{M}_i/\widetilde{M}_j)]^{0.5}} \ , \tag{B.77}$$

with

$$\frac{\lambda_{tr,i}}{\lambda_{tr,j}} = \frac{\Gamma_j}{\Gamma_i} \frac{\exp(0.0464.T_{r,i}) - \exp(-0.2412.T_{r,i})}{\exp(0.0464.T_{r,j}) - \exp(-0.2412.T_{r,j})} \ , \tag{B.78}$$

where $\widetilde{M}$ is the molecular weight and Γ is defined as

$$\Gamma_i = 210 \left[\frac{T_{c,i}.\widetilde{M}_i^3}{P_{ci}^4} \right]^{(1/6)} , \tag{B.79}$$

where T is in K, p is in bar, $\widetilde{M}$ is in g/mol and λ is in W/mK. This model yields an error of less than 5% in the prediction of the thermal conductivity of the gas mixture.

B.4.6 Surface tension of R134a/R290 mixtures

Lucas and Luckas [86] in VDI-Wärmeatlas [143] recommended the following method for calculation of the mixture surface tension

$$\sigma_m = p_{c,m}^{2/3} T_{c,m}^{1/3} \left(\frac{1 - t_{r,m}}{a_m} \right)^{n_m} b_m , \tag{B.80}$$

where

$$b_i = 0.1196. \left[1 + \frac{T_{s,ri} \ln(p_{c,m}/1.01325)}{1 - T_{s,ri}} \right], \quad b_m = \sum \widetilde{x}_i b_i , \tag{B.81}$$

$$a_m = 1, \quad n_m = 11/9, \quad T_{c,m} = \sum_{j=1} \widetilde{x}_i T_{c,j}, \quad \upsilon_{c,m} = \sum_j x_j \upsilon_{c,j}, \quad \widetilde{Z}_{c,j} = \frac{p_{c,j} \upsilon_{c,j}}{R T_{c,j}} , \tag{B.82}$$

$$\widetilde{Z}_m = \sum_j \widetilde{x}_j \widetilde{Z}_{c,j}, \quad p_{c,m} = \frac{R T_{c,m} \widetilde{Z}_{c,m}}{\upsilon_{c,m}}, \quad T_{s,ri} = \frac{T_{b,i}}{T_{c,i}} , \tag{B.83}$$

where $T_{b,i}$=T (p=1.01325 bar) is the normal boiling point temperature of the pure component i. T is in K, p is in bar and σ is in N/m. The Lucas and Luckas correlation yields an error of <5%.

C Heat transfer coefficient

C.1 Two phase flow: Pure fluid

C.1.1 Steiner [128] correlation

Steiner [128] has considered the two phase heat transfer coefficient α as a combination of the convective and the nucleate part using an asymptotic model as:

$$\alpha = \left(\alpha_n^3 + \alpha_c^3\right)^{1/3} \ , \tag{C.1}$$

where α_n and α_c is the nucleate and convective boiling heat transfer coefficient respectively. The convective boiling heat transfer coefficient for a completely wetted tube (*i.e.* all types of flow patterns save stratified and stratified-wavy flow) is calculated as

$$\frac{\alpha_c}{\alpha_{L0}} = \left\{ \left[(1-\dot{x}) + 1.2\dot{x}^{0.4}(1-\dot{x})^{0.01} \left(\frac{\rho_L}{\rho_G}\right)^{0.37} \right] + \left[\frac{\alpha_{G0}}{\alpha_{L0}} \dot{x}^{0.01} \left(1 + 8(1-\dot{x})^{0.7} \left(\frac{\rho_L}{\rho_G}\right)^{0.67} \right) \right]^{-2} \right\}^{-0.5} . \tag{C.2}$$

The heat transfer coefficients α_{L0} and α_{G0} are those of single phase flow, assuming that the total mass velocity is pure liquid or pure vapor respectively. They are calculated in the case of a fully developed turbulent flow from the Gnielinski [42] model

$$Nu = \frac{(\xi/8)(Re - 1000)Pr}{1 + 12.7(\xi/8)^{0.5}(Pr^{2/3} - 1)} \ , \tag{C.3}$$

taken in to account the respective dimensionless group Nu_{L0}, Nu_{G0}, Re_{L0}, Re_{G0}, Pr_l and Pr_g. These dimensionless groups are defined as

$$Nu_{L0/G0} = \frac{\alpha_{L0/G0} d}{\lambda_{L/G}}, \tag{C.4}$$

$$Re_{L0/G0} = \frac{\dot{m} d}{\eta_{L/G}}, \tag{C.5}$$

$$Pr_{L/G} = \frac{\eta_{L/G} c_{p,L/G}}{\lambda_{L/G}}. \tag{C.6}$$

The friction factor is

$$\xi = (1.82 log Re - 1.62)^{-2}. \tag{C.7}$$

For a partial wetting of the tube (stratified or stratified-wavy flow) the average heat transfer coefficient at the tube circumference under the thermal boundary condition of a constant wall temperature is given as

$$\alpha_c = \alpha_{wet}(1 - \Phi) + \alpha_G \Phi \ , \tag{C.8}$$

where α_{wet} is the convective boiling heat transfer coefficient at the wetted part of the tube and it is calculated by using equation C.2. In the non-wetted part of the tube,

the convective heat transfer coefficient α_g is calculated from the Gnielinski [42] model (equation C.3). In this case Re and Nu are defined with the hydraulic diameter of the vapor-occupied part of the tube cross-section

$$d_h = d\left(\frac{\varphi - \sin\varphi}{d + 2\sin(\varphi/2)}\right) \ , \tag{C.9}$$

where φ is the stratified angle. The Reynolds number is given as

$$Re_G = \frac{\dot{m}\dot{x}d_{hyd}}{\epsilon\eta_G} \ , \tag{C.10}$$

and

$$\alpha_G = \frac{Nu_G\lambda_G}{d_{hyd}} \ . \tag{C.11}$$

The void fraction is calculated using the Rauhani [107] model given as

$$\varepsilon = \frac{\dot{x}}{\rho_G}\left\{(1 + 0.12(1-\dot{x}))\left(\frac{\dot{x}}{\rho_G} + \frac{1-\dot{x}}{\rho_L}\right) + \frac{1.18(1-\dot{x})[g\sigma(\rho_L - \rho_G)]^{1/4}}{\dot{m}\rho_{\cdot L}^{1/2}}\right\}^{-1} \tag{C.12}$$

The wetting boundary can be estimated (see Fig. C.1) from the void fraction as

$$\varepsilon = \frac{f_G}{f_G + f_L} \ . \tag{C.13}$$

With some mathematical manipulation of equation C.13 the non-wetted perimeter can calculated iteratively from the following relationship

$$\varphi = 2.\pi.\varepsilon + sin\varphi \ , \tag{C.14}$$

with the assumption that no bubbles in the liquid phase and no entrainment (hold-up) in the vapor phase, the scaling parameter Φ of equation C.8 can thus be calculated as

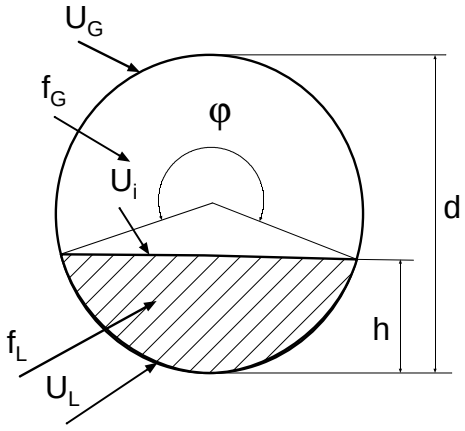

Figure C.1. Cross-section and perimeter parts of the vapor flow in a horizontal tube.

$$\Phi = \frac{\varphi_G}{2\pi} \ , \tag{C.15}$$

where $\varphi_G = 0.5\varphi$.

The local nucleate boiling heat transfer coefficient α_{nb} of a horizontal tube is estimated as

$$\frac{\alpha_{nb}}{\alpha_o} = \psi C_f \left(\frac{\dot{q}}{\dot{q}_o}\right)^{n(pr)} F(p_r)F(R_a)F(d)F(\dot{m},\dot{x}) \ . \tag{C.16}$$

The value with a subscript "o" is a reference value.

The pressure function is given as

$$F(p_r) = 2.692p_r^{0.43} + \left(\frac{1.6p_r^{6.5}}{1-p_r^{4.4}}\right) \ , \tag{C.17}$$

and the mass flux function is given as

$$F(\dot{m},\dot{x}) = \frac{\dot{m}}{\dot{m}_o}^{0.25} \left[1 - p_r^{0.1}\left(\frac{\dot{q}}{q_{cr,nb}}\right)^{0.3}\dot{x}\right] \ , \tag{C.18}$$

where

$$\dot{q}_{cr,cb} = 2.79\dot{q}_{cr,0,1}p_r^{0.4}(1-p_r) \ . \tag{C.19}$$

The critical value of $\dot{q}_{cr,0,1}$ at a reduced pressure p_r of 0.1 is given as

$$\dot{q}_{cr,0.1} = 0.13\Delta h_{V,0}\rho_{G,0}^{0.5}[\sigma_o g(\rho_{L,0}-\rho_{G,0})]^{0.25} \ . \tag{C.20}$$

The function for the effect of surface roughness and tube diameter is $F(R_a) = (R_a/R_{ao})^{0.133}$ and $F(d) = (d_o/d)^{0.5}$ respectively. The pressure dependence of the heat flux exponent $n(p_r)$ can be predicted as

$$n(p_r) = 0.9 - 0.3p_r^{0.3} \ . \tag{C.21}$$

The experimental value of the specific constant C_f for a number of substances is be found in VDI-Wärmeatlas[143], for example for water it is 0.72. In absence of an experimental value it can be estimated as

$$C_f = 0.789\left(\frac{\widetilde{M}}{\widetilde{M}_{H_2}}\right)^{0.11} \ , \tag{C.22}$$

where $\widetilde{M}$ is the molecular weight and $\widetilde{M}_{H_2}$= 2.016. The correction factor ψ for a stratified and a stratified-wavy flow pattern under the thermal boundary condition of a constant wall temperature is 0.86 for all other type of flow patterns it is taken as unity (VDI-Wärmeatlas[143]).

Table C.1 shows the reference factors for the nucleate boiling heat transfer coefficient for R134a and R290.

C.1.2 Kattan et al. [73] correlation

For a stratified-wavy flow pattern or annular flow pattern with a partial dryout the two phase heat transfer coefficient is

$$\alpha = \frac{\varphi_{dry}\alpha_G + (2\pi - \varphi_{dry})\alpha_{wet}}{2\pi} \ . \tag{C.23}$$

Table C.1. Values of the reference parameters used in evaluation of the local nucleate boiling heat transfer coefficient.

Refrigerant	α_o	$\dot{q}_o$	R_{ao}	d_o
	W/m^{2}K	W/m^2	m	m
R134a	3,500	20,000	10^{-6}	0.01
R290	4,000	20,000	10^{-6}	0.01

The vapor heat transfer coefficient α_G is determined by using the Dittus-Boelter [30] correlation as

$$\alpha_G = 0.023 Re_G^{0.8} P_{rG}^{0.4} \frac{\lambda_G}{d} \ , \tag{C.24}$$

with Reynold number given as

$$Re_G = \frac{\dot{m}\dot{x}d}{\varepsilon\eta_G} \ , \tag{C.25}$$

where ε is the void fraction given by the Rauhani [107] model (equation C.12). The heat transfer coefficient on the wetted portion of the tube is

$$\alpha_{wet} = \sqrt[3]{\alpha_n^3 + \alpha_c^3} \ . \tag{C.26}$$

The nucleate boiling heat transfer coefficient α_n is given by the Cooper [25] model as

$$\alpha_n = 55 p_r^{0.12} (-0.4343 \ln p_r)^{-0.55} \widetilde{M}^{-05} \dot{q} \ . \tag{C.27}$$

The convective heat transfer coefficient is given by a modified form of the Dittus-Boelter [30] model as

$$\alpha_c = 0.0133 Re_L^{0.69} P_{rL}^{0.4} \frac{\lambda_L}{d} \ . \tag{C.28}$$

The liquid Reynolds number is given as

$$Re_L = \frac{4\dot{m}(1-\dot{x})\delta}{(1-\varepsilon)\eta_G} \ . \tag{C.29}$$

where δ is the liquid film thickness it is given as

$$\delta = \frac{\pi d(1-\varepsilon)}{2(2\pi - \varphi_{dry})} \ , \tag{C.30}$$

where φ_{dry} is

$$\varphi_{dry} = \varphi_{strat} \frac{(\dot{m}_{wavy} - \dot{m})}{(\dot{m}_{wavy} - \dot{m}_{strat})} \ , \tag{C.31}$$

where φ_{strat} is calculated iteratively from equation C.14. The mass flux under a stratified and wavy flow pattern is

$$\dot{m}_{strat} = \frac{(226.3)^2 f_L f_G^2 \rho_G (\rho_L - \rho_G) \eta_L g \cos\Theta}{0.3164(1-\dot{x})^{1.75} \pi^2 \eta_L^{0.25}} \ , \tag{C.32}$$

and

$$\dot{m}_{wavy} = \left\{ \frac{16 f_G^3 g d \rho_L \rho_G}{\dot{x}^2 \pi^2 (1-(2h_L-1)^2)^{0.5}} \left[\frac{\pi^2}{25 h_L^2} (1-x)^{F_1(\dot{q})} \times \left(\frac{We}{Fr} \right)_L^{F_2(\dot{q})} + \frac{1}{\cos\Theta} \right] \right\}^{0.5} + 50 \ , \tag{C.33}$$

respectively. The parameters f_L, f_G, h_L are defined in Fig.C.1. Θ is the angle of inclination to the horizontal and

$$F_1(\dot{q}) = 646.0 \left(\frac{\dot{q}}{\dot{q}_{crit}} \right)^2 + 64.8 \left(\frac{\dot{q}}{\dot{q}_{crit}} \right); \quad F_2(\dot{q}) = 18.8 \left(\frac{\dot{q}}{\dot{q}_{crit}} \right) + 1.023 \ . \tag{C.34}$$

The stratified-wavy flow model is also valid for the stratified flow patten with φ_{strat} replacing φ_{dry} and for the annular flow condition with φ_{dry} is set to zero and the film thickness δ is set to $(1-\varepsilon)d/4$.

C.1.3 Kandlikar [66] correlation

The flow boiling heat transfer coefficient for a pure fluid is given by Kandlikar [66] as

$$\alpha = max(\alpha_n, \alpha_c) \ , \tag{C.35}$$

wher the subscript n and c in equation C.35 refers to the nucleate and convective boiling respectively. The convective and the nucleate boiling part is given as

$$\alpha_n = 0.6683 Co^{-0.2} (1-\dot{x})^{0.8} \alpha_{L0} f(F_{rL0}) + 1058.0 Bo^{0.7} (1-\dot{x})^{0.8} F_{Fl} \alpha_{L0} \ , \tag{C.36}$$

and

$$\alpha_c = 1.136 Co^{-0.9} (1-\dot{x})^{0.8} \alpha_{L0} f(F_{rL0}) + 667.2 Bo^{0.7} (1-\dot{x})^{0.8} F_{Fl} \alpha_{L0} \ , \tag{C.37}$$

respectively, where Fr_{L0} is the liquid Froude number, Bo is the boiling number and Co is the convection number. These dimensionless groups are defined as

$$Fr_{L0} = \frac{\dot{m}}{\rho_L g d}, \quad Bo = \frac{\dot{q}}{\dot{m} \Delta h_v}, \quad Co = \left(\frac{\rho_G}{\rho_L} \right)^{0.5} \left(\frac{1-\dot{x}}{\dot{x}} \right)^{0.8} \ . \tag{C.38}$$

The function $f(F_{rL0})$ is defined as

$$f(F_{rL0}) = (25 F_{rL0})^{0.324} \quad F_{rL0} < 0.04 \ ,$$

$$f(F_{rL0}) = 1 \qquad\qquad F_{rL0} \geq 0.04 \ ,$$

where F_{Fl} is a fluid-surface parameter related to the nucleation characteristic. For all type of fluids flowing in a stainless tube it is taken as 1. The single phase heat transfer coefficient α_{L0} is obtained from the Petukhov and Popov [106] correlation or Gnielinski [42] correlation. The Petukhov and Popov [106] correlation is valid in the range of $0.5 \leq P_{rL} \leq 2000$ and $10^4 \leq Re_{L0} \leq 5 \times 10^6$ and it is given as

$$Nu_{L0} = \frac{\alpha_{L0} d}{\lambda} = \frac{Re_{L0} Pr_L (\xi/2)}{1.07 + 12.7 (P_{rL}^{2/3} - 1)(\xi/2)^{0.5}} \ . \tag{C.39}$$

The Gnielinski [42] correlation (equation C.3) is valid in the range of $0.5 \leq P_{rL} \leq 2000$ and $2300 \leq Re_{L0} \leq 5 \times 10^4$. The friction factor ξ in equation C.39 is given by equation C.7.

C.1.4 Chen [17] correlation

Chen [17] postulated that the heat transfer coefficient is made of two parts: a) a micro-convective (or nucleate boiling) portion α_n and b) a macro-convective (or forced convective) portion α_c as

$$\alpha = \alpha_c F + \alpha_n S \ , \tag{C.40}$$

where α_c is calculated using the Dittus and Boelter [30] correlation as

$$\alpha_c = 0.023 \frac{\lambda_L}{d} Re_L^{0.8} Pr_L^{0.4} \ , \tag{C.41}$$

where

$$Re_L = \frac{(1-\dot{x})\dot{m}d}{\eta_L}, \quad Pr_L = \frac{c_{pL}\eta_L}{\lambda_L} \ , \tag{C.42}$$

The suppression factor for the convection part is

$$F = \begin{cases} 1 & if \quad 1/X_{tt} > 0.1 \\ \\ 2.35\left[\frac{1}{X_{tt}} + 0.213\right]^{0.736} & if \quad 1/X_{tt} \leq 0.1 \end{cases} \ ,$$

and the Martinelli parameter X_{tt} is given as

$$X = \left(\frac{1-\dot{x}}{\dot{x}}\right)^{0.875} \left(\frac{\rho_G}{\rho_L}\right)^{0.5} \left(\frac{\eta_L}{\eta_G}\right)^{0.125} \ . \tag{C.43}$$

The nucleate boiling heat transfer coefficient is

$$\alpha_n = 0.00122 \frac{\lambda_L^{0.79} c_{p,L}^{0.45} \rho_L^{0.49}}{\sigma^{0.5} \eta_L^{0.29} \rho_G^{0.24} \Delta h_V^{0.24}} \Delta T_{sat}^{0.24} \Delta p_{sat}^{0.75} \ , \tag{C.44}$$

where

$$\Delta T_{sat} = T_w - T_s; \quad \Delta p_{sat} = p(T_w) - p(T_s); \quad Re_{tp} = Re_L F^{1.25} \ . \tag{C.45}$$

The suppression factor for the nucleate part is

$$S = \frac{1}{1 + 2.53 \times 10^{-6} Re_{tp}} \ . \tag{C.46}$$

C.1.5 Gungor and Winterton [48] correlation

The Gungor and Winterton [48] correlation is a modified form of the Chen [17] correlation given by equation C.40 with the nucleate boiling calculated from the Cooper [25] correlation given by equation C.27. The suppression factor for the convection part is defined as

$$F = \begin{cases} (1 + 24,000 Bo^{1.16} + 1.37(1/x_{tt})^{0.86}) Fr_L^{(0.1-2Fr_L)} & if \quad Fr < 0.05 \\ \\ 1 + 24,000 Bo^{1.16} + 1.37(1/x_{tt})^{0.86} & if \quad Fr \geq 0.05 \end{cases} \ ,$$

and the suppression factor for the nucleate part is

$$S = \begin{cases} (1 + 0.00000115F^2 Re_L)^{-1} Fr_L^{1/2} & if \quad Fr < 0.05 \\ \\ (1 + 0.00000115F^2 Re_L)^{-1} & if \quad Fr \geq 0.05 \end{cases} ,$$

The convective boiling part is calculated from the Dittus-Boelter [30] correlation (equation C.41).

C.1.6 Shah [118] correlation

The Shah [118] correlation is given as

$$\alpha = max(\alpha_c, \alpha_n) \ , \tag{C.47}$$

where the subscript n and c in equation C.47 refers to the nucleate and convective boiling respectively. The convective heat transfer coefficient is defined as

$$\alpha_c = 1.8\alpha_L N^{-0.8} \ , \tag{C.48}$$

where

$$N = \begin{cases} Co & Fr_L > 0.04 \\ \\ 0.38 Fr_L^{-0.4} Co & Fr_L < 0.04 \end{cases} ,$$

where α_L is calculated using the Dittus-Boelter [30] correlation (equation C.41). The nucleate boiling heat transfer coefficient is calculated as follows

- For $N > 1$

$$\alpha_n = \begin{cases} 230\alpha_L Bo^{0.5} & Bo > 0.0003 \\ \\ 1 + 46\alpha_L Bo^{0.5} & Bo < 0.0003 \end{cases} .$$

- For $1 > N > 0.1$

$$\alpha_n = F\alpha_L Bo^{0.5} \exp(2.74 N^{-0.1}) \ . \tag{C.49}$$

- For $N < 0.1$

$$\alpha_n = F\alpha_L Bo^{0.5} \exp(2.47 N^{-0.15}) \ , \tag{C.50}$$

where

$$F = \begin{cases} 14.7 & Bo > 0.0011 \\ \\ 15.43 & Bo < 0.0011 \end{cases} .$$

C.1.7 Schrock and Grossman [117] correlation

A very simple correlation is given by Schrock and Grossman [117] as

$$\alpha = 1.91\alpha_L \left[10^4 \times Bo + 1.5 \left(\frac{1}{X_{tt}} \right)^{2/3} \right]^{0.6} \ , \tag{C.51}$$

where α_L is calculated using Dittus-Boelter [30] correlation equation C.41.

C.1.8 Dembi et al. [27] correlation

The Dembi et al. [27] correlation is based on the asymptotic model given by equation C.1 with the nucleate and convection part given as

$$\alpha_n = 23388.5\frac{\lambda_L}{d}\left(\frac{\dot{q}}{\rho_G \Delta h_V \varpi}\right)^{0.64}\left(\frac{gd}{\Delta h_V}\right)^{0.27}\left(\frac{\dot{m}^2 d}{\rho_L \Delta h_V \varpi}\right)^{0.14} , \tag{C.52}$$

and

$$\alpha_c = 0.115\frac{\lambda_L}{d}\left[\dot{x}^4(1-\dot{x})^2\right]^{0.11}\left(\frac{\dot{m}^2 \Delta h_V}{\rho_L g \sigma}\right)^{0.14} P_{rL}^{0.27} , \tag{C.53}$$

respectively. The parameter ϖ is defined as

$$\varpi = 0.36 \times 10^{-3} p_r^{-1.4} . \tag{C.54}$$

C.1.9 Klimenko [79] correlation

The Klimenko [79] correlation is based on the asymptotic model given by equation C.1 with the convection part given by the Dittus-Boelter [30] correlation equation C.41 and the nucleate boiling is

$$\alpha_n = \begin{cases} \alpha_{n1} & N_{CB} < 1.6 \times 10^4 \\ \alpha_{n2} & N_{CB} > 1.6 \times 10^4 \end{cases} ,$$

where

$$\alpha_{n1} = 7.4 \times 10^{-3}\left(\frac{\lambda_w}{\lambda_L}\right)^{0.15} Pe^{0.6} K_p^{0.5} Pr_L^{-1/3} , \tag{C.55}$$

$$\alpha_{n2} = 0.087\frac{\lambda_L}{b}\left(\frac{\lambda_w}{\lambda_L}\right)^{0.09} Re_m^{0.6}\left(\frac{\rho_G}{\rho_L}\right)^{0.2} Pr_L^{1/6} , \tag{C.56}$$

$$Pe = \left(\frac{qb}{\Delta h_V \rho_G a_L}\right), \quad Kp = \frac{p}{\sqrt{\sigma g(\rho_L - \rho_G)}}, \quad b = \sqrt{\frac{2\sigma}{g(\rho_L - \rho_G)}} , \tag{C.57}$$

$$Re_m = \frac{w_m b}{\nu_L}, \quad w_m = \frac{\dot{m}}{\rho_L}\left[1 + x\left(\frac{\rho_L}{\rho_G} - 1\right)\right], \quad Re_* = \frac{qb}{\Delta h_V \rho_G \nu_L}, \quad N_{CB} = \frac{Re_m}{Re_*}\left(\frac{\rho_L}{\rho_G}\right) . \tag{C.58}$$

C.1.10 Jung et al. [60] correlation

The Jung et al. [60] correlation is a modified form of the Chen [17] correlation. The convection heat transfer coefficient is calculated using the Dittus-Boelter [30] correlation (equation C.41) and the nucleate part is calculated from the Stephan and Abdelsalm in VDI-Wärmeatlas [143] correlation as

$$\alpha_n = 207\frac{\lambda_L}{b.d}\left[\frac{\dot{q}(b.d)}{\lambda_L T_s}\right]^{0.745}\left(\frac{\rho_G}{\rho_L}\right)^{0.581} P_{rL}^{0.533} , \tag{C.59}$$

where

$$(b.d) = 0.511 \left(\frac{2\sigma}{g(\rho_L - \rho_G)} \right)^{0.5} , \tag{C.60}$$

$$F = 2.37 \left(0.29 + \frac{1}{X_{tt}} \right) , \tag{C.61}$$

$$S = \begin{cases} 4048 X_{tt}^{1.22} Bo^{1.13} & Xtt < 1 \\ 2.0 - 0.1 X_{tt}^{-0.28} Bo^{-0.33} & 1 \leq X_{tt} \leq 5 \end{cases} .$$

C.2 Two phase flow: Mixture

C.2.1 Steiner [128] correlation

Steiner [128] has extended his pure component asymptotic model to mixture. The nucleate part of the heat transfer coefficient is suppressed using the Schlünder [115] suppression factor for the nucleate boiling. The Schlünder [115] suppression factor is based on the heat and mass transfer laws it is defined as

$$F_n = \left\{ 1 + \frac{\alpha_{id,n}}{\dot{q}} (T_{b,k} - T_{b,j})(\widetilde{y}_j - \widetilde{x}_j) \left[1 - \exp \frac{B_o q}{\rho_L \Delta h_V \beta_L} \right] \right\} , \tag{C.62}$$

where T_b is the saturated (boiling) temperature of the pure component, the index j and k stands for the more volatile and less volatile component respectively. $\beta_L / B_0 = 5 \times 10^5$ is the mass transfer coefficient. The ideal nucleate boiling heat transfer coefficient for a mixture $\alpha_{id,n}$ is calculated from the heat transfer coefficient of pure components as

$$\alpha_{id,n} = \left[\sum \frac{\widetilde{x}_i}{\alpha_{i,n}} \right]^{-1} , \tag{C.63}$$

and $B_o / \beta_L = 5.10^3$ and ρ_L and Δh_V is the ideal density and enthalpy of evaporation of the mixture respectively. $\widetilde{x}$ and $\widetilde{y}$ is the liquid and vapor mole fraction of the more volatile component respectively.

The same approach applies also to the convective part for the liquid-liquid immiscible mixture. That is to say for a liquid-liquid miscible mixture the convective suppression factor made analogous to that for the nucleate boiling heat transfer coefficient as

$$F_c = \left\{ 1 + \frac{\alpha_{id,c}}{\dot{q}} (T_{b,k} - T_{b,j})(\widetilde{y}_j - \widetilde{x}_j) \left[1 - \exp \frac{B_o q}{\rho_L \Delta h_V \beta_L} \right] \right\} . \tag{C.64}$$

C.2.2 Kandlikar [67] correlation

Kandlikar [67] has extended his pure component correlation (Kandlikar [66]) to mixtures as

- Region I: Near-azeotropic region

$$\alpha = max(\alpha_n, \alpha_c) , \tag{C.65}$$

where α_n and α_c is obtained from equation C.67 and equation C.37 respectively using the mixture properties.

- Region II: Moderate diffusion-induced suppression region

$$\alpha = \alpha_c \ , \tag{C.66}$$

where α_c is given by equation C.67 with the properties of the mixture.

- Region III: Severe diffusion-induced suppression region: $0.03 < V_1 < 0.2$ and $Bo \leq 1E^{-4}$; $V_1 \geq 0.2$

$$\alpha = 1.136 Co^{-0.9}(1-\dot{x})^{0.8}\alpha^{L0} f(F_{rL0}) + 667.2 Bo^{0.7}(1-\dot{x})^{0.8} F_{Fl}\alpha_{L0} F_D \ , \tag{C.67}$$

where

$$V_1 = \left[\left(\frac{c_{pL}}{\Delta h_V}\right)\left(\frac{a}{D_{12}}\right)^{0.5} |\widetilde{y} - \widetilde{x}| \left(\frac{dT}{d\widetilde{x}}\right)\right] \ , \tag{C.68}$$

$$F_D = \frac{0.678}{1+V_1} \ . \tag{C.69}$$

C.2.3 Bennett and Chen [7] correlation

Bennett and Chen [7] has extended the Chen [17] correlation (equation C.40) for mixture. Here both the convective and the nucleate parts are suppressed. The convection part which is calculated for the original Chen [17] correlation with mixture properties is suppressed using the following suppression factor

$$F_c = \frac{T_w - T_{ph}}{T_w - T_s} \ , \tag{C.70}$$

where T_w, T_{ph}, and T_s is the wall, equilibrium temperature and saturation temperature respectively. The nucleate part is also calculated using the original Chen [17] model for the pure substance with mixture properties. It suppressed using the the suppression factor given by equation C.69.

C.2.4 Palen [104] correlation

Palen [104] has extended the original Chen [17] correlation for pure component (equation C.40) to mixture similar to the Bennett and Chen [7] correlation. However, only the nucleate part is suppressed using the following suppression factor

$$F_d = \exp(-0.027 \Delta T_{bp}) \ , \tag{C.71}$$

where ΔT_{bp} is difference between the dew and bubble point temperature of the mixture.

C.2.5 Jung et al. [60] correlation

Jung et al. [60] have extended their pure substance correlation to the mixture. The nucleate boiling heat transfer coefficient is replaced by the ideal one given by equation C.63. The convective part is suppressed using the following suppression factor

$$F_c = 1.0 - 0 - 35|\widetilde{y}_1 - \widetilde{x}_1|^{1.56} \ . \tag{C.72}$$

For the nucleate part the following suppression factor is employed

$$F_n = \frac{1}{\{[1 + (b_2 + b_3)(1 + b_4)](1 + b_5)\}^2} \ , \tag{C.73}$$

where

$$b_2 = (1 - \widetilde{x}_1) \ln\left(\frac{1.01 - \widetilde{x}_1}{1.01 - \widetilde{y}_1}\right) + \widetilde{x}_1 \ln\left(\frac{\widetilde{x}_1}{\widetilde{y}_1}\right) + |\widetilde{y}_1 - \widetilde{x}_1|^{1.5} \ , \tag{C.74}$$

$$b_3 = \begin{cases} 0 & x_1 \geq 0.01 \\ \left(\frac{\widetilde{x}_1}{\widetilde{y}_1}\right)^{0.1} - 1 & \widetilde{x}_1 < 0.01 \end{cases} \ ,$$

$$b_4 = 152 \left(\frac{p}{p_{c,1}}\right)^{0.66} \ , \tag{C.75}$$

$$b_5 = 0.92|\widetilde{y}_1 - \widetilde{x}_1|^{0.001} \left(\frac{p}{p_{c,1}}\right)^{0.66} \ , \tag{C.76}$$

and

$$\frac{\widetilde{x}_1}{\widetilde{y}_1} = 1 \quad \text{for} \quad \widetilde{x}_1 = \widetilde{y}_1 = 0 \ ,$$

$\widetilde{x}_1$ and $\widetilde{y}_1$ is the liquid and vapor mole fraction of the more volatile component respectively. p and $p_{c,1}$ is system pressure and critical pressure of the more volatile component respectively.

C.3 Single phase

C.3.1 Free convection

The air heat transfer coefficient due to the free convection at the outside surface of the insulation is calculated using the Churchill and Chu [21] correlation given by

$$\alpha = \frac{\lambda}{d_o} \left\{ 0.60 + \frac{0.387 Ra^{1/6}}{[1 + (0.559/Pr)^{9/16}]^{8/27}} \right\}^2 \qquad \left(10^{-5} < Ra < 10^{12}\right) \ , \tag{C.77}$$

where P_r is the Prandtl number, $Ra = GrP_r$ is the Rayleigh number and Gr is the Graschhof number. These dimensionless groups are defined as

$$Pr = \frac{c_p \eta}{\lambda}, \qquad Gr = \frac{g\beta(T_{so} - T_\infty)d^3}{\nu^2} \ , \tag{C.78}$$

where β is the thermal expansion coefficient, for a perfect gas (*e.g* air) where ρ=RT/p it is

$$\beta = -\frac{1}{\rho}\frac{\partial \rho}{\partial T} = \frac{1}{T} \ . \tag{C.79}$$

C.3.2 Radiation

To estimate the heat transfer coefficient due to the radiation, the outer surface of the insulation is assumed to be a diffuse gray and the surrounding is large. With these assumptions the net rate of radiation heat transfer between the insulation surface and the surrounding may then be expressed as (VDI-Wärmeatlas [143])

$$Q_{rad} = \varepsilon A \sigma (T_{s,o}^4 - T_{sur}^4) = \alpha_r A (T_{s,o} - T_{sur}) \tag{C.80}$$

where ε is the insulation emissivity which is taken as 0.9. The Stefan-Boltzmann constant is $\sigma = 5.67^{-8}\mathrm{KW/m^2K^4}$. α_r is the heat transfer coefficient due to radiation. T_{sur} is the surrounding temperature which is assumed to be equal to the ambient temperature T_∞ and $T_{s,o}$ is the insulation outside surface temperature. Mathematical manipulation of equation C.80 yields

$$\alpha_r = \varepsilon \sigma (T_{s,o}^2 + T_\infty^2)(T_{s,o} + T_\infty) \ . \tag{C.81}$$

The determination of the radiation heat transfer coefficient requires knowledge of the outside surface temperature of the insulation. This may be determined by applying an energy balance between the insulation and the surrounding as

$$\dot{Q}_{cond} = \dot{Q}_{conv} + \dot{Q}_{rad} \ , \tag{C.82}$$

$$\frac{2\pi\lambda_s(T_{s,i} - T_{s,o})}{\ln\left(\frac{r_{s,o}}{r_{s,i}}\right)} = \alpha_o \pi d_o (T_{s,o} - T_\infty) + \pi d_o \varepsilon \sigma (T_{s,o}^4 - T_{sur}^4) \ , \tag{C.83}$$

with the measured inside surface temperature of the insulation ($T_{s,i} = T_{w,o}$) and the ambient temperature, the outside surface temperature of the insulation can be calculated iteratively from equation C.83. The physical properties of the air are evaluated at the mean temperature $T = (T_{s,o} + T_\infty)/2$ from Chapter: Db of VDI-Wärmeatlas [143].

D Steiner [128] flow pattern map

The abscissa of the flow pattern map of Steiner [128] is the Martinelli parameter given by equation C.43 The ordinate of the map is defined by four curves which characterize the transition between the various flow pattern. The parameters of the transition curves are defined as

- Stratified to wavy flow pattern

$$(Re_L Fr_G)_{tt,Gr} = \frac{226.3^2 \widetilde{f}_L \widetilde{f}_G^2}{\pi^3} \ , \tag{D.1}$$

- Wavy to annular flow and wavy to slug flow pattern

$$(Fr_{Gm})_{tt,Gr1} = \frac{16\widetilde{f}_G^3}{\pi^2\sqrt{1-(2h_L-1)^2}} \left(\frac{\pi^2}{25hL} \frac{Fr_L}{We_L} + \frac{1}{\cos\Theta} \right) \ , \tag{D.2}$$

  where Θ is the angle of inclination, for a horizontal tube it is set to zero.

- Bubble to slug flow pattern

$$(FrEu)_L \geq (FrEu)_{Gr} = 128 \frac{\widetilde{f}_G \widetilde{f}_L^2}{\pi^2 \widetilde{U}_i} \ . \tag{D.3}$$

- Mist to annular flow pattern $X < 0.51$

$$Fr_{Gm} \geq (Fr_{Gm})_{Gr2} = \frac{7680\widetilde{f}_G^2}{\pi^2 \xi_{ph}} \left(\frac{Fr}{We} \right)_L \ , \tag{D.4}$$

  where

$$\xi_{ph} = \left[1.138 + 2\log\left(\frac{\pi}{1.5\widetilde{f}_L} \right) \right]^{-2} \ . \tag{D.5}$$

The following dimensionless variables needed to be defined (see Fig. C.1)

$$\begin{cases} \widetilde{h}_L & = \mathrm{h/d} \ , \\ \widetilde{U}_{L,G,i} & = U_{L,G,i}/\mathrm{d} \ , \\ \widetilde{f}_{L,G} & = f_{L,G}/\mathrm{d}^2 \ . \end{cases} \tag{D.6}$$

The dimensionless peripheral and cross-sectional area variables that are required for the analysis can be derived from the geometry of the flow configuration for a given height h (cf. Fig. C.1) of a liquid or for a given reference liquid level $\widetilde{h}_L$ as

- for $\widetilde{h}_L \leq 0.5$

$$\widetilde{U}_L = \left(8\sqrt{\widetilde{h}_L} - 2\sqrt{\widetilde{h}_L(1-\widetilde{h}_L)} \right) /3 \ , \tag{D.7}$$

$$\widetilde{U}_G = \pi - \widetilde{U}_L \ , \tag{D.8}$$

$$\widetilde{f}_L = \left(8\sqrt{\widetilde{h}_L} + 12\sqrt{\widetilde{h}_L(1-\widetilde{h}_L)}\right)\widetilde{h}_L/15 \ , \tag{D.9}$$

$$\widetilde{f}_G = \pi/4 - \widetilde{f}_L \ . \tag{D.10}$$

- for $\widetilde{h}_L > 0.5$

$$\widetilde{U}_G = \left(8\sqrt{1-\widetilde{h}_L} - 2\sqrt{\widetilde{h}_L(1-\widetilde{h}_L)}\right)/3 \ , \tag{D.11}$$

$$\widetilde{U}_L = \pi - \widetilde{U}_G \ , \tag{D.12}$$

$$\widetilde{f}_G = \left(12\sqrt{\widetilde{h}_L(1-\widetilde{h}_L)} + 12\sqrt{(1-\widetilde{h}_L)}\right)(1-\widetilde{h}_L)/15 \ , \tag{D.13}$$

$$\widetilde{f}_L = \pi/4 - \widetilde{f}_G \ . \tag{D.14}$$

- for $0 \leq \widetilde{h}_L \leq 1$

$$\widetilde{U}_i = 2\sqrt{\widetilde{h}_L(1-\widetilde{h}_L)} \ . \tag{D.15}$$

An iterative method of solution on the basis of the following equation is necessary to calculate the reference liquid level, $\widetilde{h}_L$

$$X^2 = \left[\left(\frac{\widetilde{U}_G + \widetilde{U}_i}{\pi}\right)^{0.25}\left(\frac{\pi^2}{64\widetilde{f}_G^2}\right)\left(\frac{\widetilde{U}_G + \widetilde{U}_i}{\widetilde{f}_G} + \frac{\widetilde{U}_i}{\widetilde{f}_L}\right) - \frac{1}{(FrEu)_G}\right]\left(\frac{\pi}{\widetilde{U}_L}\right)^{0.25}\left(\frac{64\widetilde{f}_L^3}{\pi^2\widetilde{U}_L}\right) \ , \tag{D.16}$$

where

$$(FrEu)_G = \frac{\xi_G(\dot{m}\dot{x})^2}{2dg\rho_G(\rho_L - \rho_G\sin\Theta)} \ , \tag{D.17}$$

$$\xi_{G/L} = \frac{0.3164}{Re_{G/L}^{0.25}} \ , \tag{D.18}$$

$$Re_G = \frac{\dot{m}\dot{x}d}{\eta_G} \ , \tag{D.19}$$

$$\left(\frac{We}{Fr}\right)_L = \frac{gd^2\rho_L}{\sigma} \ , \tag{D.20}$$

$$(Fr_{Gm})^{0.5} = \frac{\dot{m}^2\dot{x}^2}{gd\rho_L\rho_G} \ , \tag{D.21}$$

$$(Re_L Fr_G)^{0.5} = \left(\frac{\dot{m}^3 \dot{x}^2 (1-\dot{x})}{\rho_G (\rho_{Ll} - \rho_G) g \eta_L \cos\Theta} \right)^{0.5} , \tag{D.22}$$

$$(FrEu)_L^{0.5} = \left(\frac{\xi_L \dot{m}^2 (1-\dot{x})^2}{2d\rho_G (\rho_L - \rho_G) g \cos\Theta} \right)^{0.5} . \tag{D.23}$$

E Pressure drop

There exists a number of correlations for the prediction of the two phase multiplier Ψ of the separated flow model. These models are presented in the following subsections.

E.1 Friedel [38] model

$$\Psi_{L0} = E + \frac{3.24FH}{Fr^{0.045}We^{0.035}} \ , \tag{E.1}$$

where

$$E = (1-\dot{x})^2 + \dot{x}^2 \frac{\rho_L f_{G0}}{\rho_G f_{L0}} \ , \tag{E.2}$$

$$F = \dot{x}^{0.78}(1-\dot{x})^{0.24} \ , \tag{E.3}$$

$$H = \left(\frac{\rho_L}{\rho_G}\right)^{0.91} \left(\frac{\eta_G}{\eta_L}\right)^{0.19} \left(1 - \frac{\eta_G}{\eta_L}\right)^{0.7} \ , \tag{E.4}$$

$$Fr = \frac{\dot{m}^2}{gd\rho_H^2} \ , \tag{E.5}$$

$$We = \frac{\dot{m}^2 d}{\sigma \rho_H} \ , \tag{E.6}$$

d is tube diameter, σ is the surface tension and ϱ_H is the homogenous density given by equation 6.9. f_{G0} and f_{L0} are the friction factors defined by a Blasius-type model as

$$f_{L0/G0} = \frac{0.079}{Re_{L0/G0}^{0.25}} \ , \tag{E.7}$$

where $Re = \dot{m}d/\eta$. The range of the validity of the Friedel [38] model is $\eta_L/\eta_G < 1000$

E.2 Lockhart and Martinelli [85] model

In the Lockhart and Martinelli [85] model the two phase friction multiplier is

$$\psi_L^2 = 1 + \frac{C}{X} + \frac{1}{X^2} \ , \tag{E.8}$$

$$\psi_G^2 = 1 + C.X + X^2 \ , \tag{E.9}$$

where X is the Martinelli parameter and the value of the coefficient C is given in Table E.1.

The range of the applicability of the Lockhart and Martinelli [85] correlation is η_L/η_G >1000 and $\dot{m}$ <100 kg/m^{2}s.

Table E.1. Value of C for the Lockhart and Martinelli [85] correlation.

Liquid	Gas	Subscript	C
Turbulent	Turbulent	tt	20
Viscous	Turbulent	vt	12
Turbulent	Viscous	tv	10
Viscous	Viscous	vv	05

E.3 Chisholm [20] model

In the Chisholm [20] model the two phase friction multiplier is

$$\Psi_{L0} = 1 + (Y^2 - 1)\left[B\dot{x}^{(2/n-1)}(1-\dot{x})^{(2/n-1)} + \dot{x}^{1-n}\right] , \tag{E.10}$$

where

$$Y^2 = \frac{(dp_f/dz)_{G0}}{(dp_f/dz)_{L0}} , \tag{E.11}$$

n is 0.25 for a Blasius model. The parameter B is given by

$$B = \frac{55}{\dot{m}^{1/2}} \quad 0 < Y < 9.5 , \tag{E.12}$$

$$B = \frac{520}{Y\dot{m}^{1/2}} \quad 9.5 < Y < 28 , \tag{E.13}$$

$$B = \frac{15000}{Y^2\dot{m}^{1/2}} \quad 28 < Y . \tag{E.14}$$

The range of the validity of the Chisholm [20] correlation is $\eta_L/\eta_G > 1000$ and $\dot{m} > 100$ kg/m^{2}s.

F Experimental Data

Table F.1. Experimental data for the local heat transfer coefficient and pressure drop for the pure R134a and R134a-R290 mixtures. Symbols: $\widetilde{x}$: liquid mole fraction of propane, $\widetilde{z}$: bulk mole fraction of propane. Abbreviations: S1: measurement at section 1, S2: measurement at section 2 and S3:measurement at section 3.

$\dot{m}$	p_s	T	Δp	p_c	$\overline{\dot{q}}$		T_w		$\widetilde{x}$		$\dot{x}$			α	
$\frac{kg}{m^2 s}$	bar	°C	mbar	bar	$\frac{kW}{m^2}$		°C		-		-			kW/m^{2}K	
						S1	S2	S3		S1	S2	S3	S1	S2	S3
						$\widetilde{\mathbf{z}} = \mathbf{0}$ (**Pure R134a**)									
99.6	3.36	3.9	10.1	5.9	6.1	8.6	8.6	8.8	0.00	0.43	0.45	0.47	1.15	1.26	1.32
100.0	3.39	4.1	11.4	5.9	6.0	8.3	8.3	8.4	0.00	0.55	0.57	0.59	1.30	1.45	1.52
99.1	3.39	4.1	12.5	5.9	6.1	8.6	8.6	8.7	0.00	0.69	0.71	0.74	1.22	1.35	1.42
99.4	3.39	4.1	13.2	5.9	6.0	8.9	8.9	9.1	0.00	0.82	0.84	0.86	1.14	1.25	1.30
99.2	3.38	4.0	12.6	6.1	6.1	9.2	9.3	9.4	0.00	0.92	0.94	0.96	1.05	1.14	1.19
99.1	3.37	3.9	11.9	6.8	6.0	12.0	12.3	12.8	0.00	0.95	0.97	0.99	0.65	0.69	0.70
100.0	3.36	3.8	11.6	6.7	6.0	11.9	12.1	12.5	0.00	0.93	0.96	0.98	0.65	0.70	0.72
99.9	3.34	3.7	10.1	5.9	6.0	8.4	8.4	8.5	0.00	0.40	0.43	0.45	1.15	1.26	1.33
100.5	3.37	3.9	11.6	5.4	2.7	6.5	6.5	6.4	0.00	0.60	0.61	0.62	0.92	1.01	1.11
99.9	3.39	4.1	12.6	5.4	2.6	6.7	6.7	6.7	0.00	0.77	0.78	0.79	0.89	0.98	1.06
100.2	3.36	3.9	10.3	6.4	10.5	10.9	10.8	10.9	0.00	0.33	0.36	0.40	1.36	1.52	1.63
99.2	3.40	4.2	11.7	6.4	10.4	10.9	10.8	10.9	0.00	0.51	0.55	0.58	1.41	1.59	1.68
99.1	3.39	4.1	13.2	6.4	10.6	11.0	11.0	11.1	0.00	0.73	0.77	0.80	1.41	1.55	1.63
99.9	3.38	4.1	13.7	6.6	10.6	11.4	11.5	11.7	0.00	0.82	0.86	0.89	1.31	1.43	1.49
99.3	3.38	4.0	13.0	6.8	10.7	12.4	12.5	12.8	0.00	0.90	0.93	0.97	1.15	1.26	1.30
100.0	3.37	3.9	12.6	7.6	10.7	15.2	15.7	16.4	0.00	0.93	0.97	1.01	0.84	0.89	0.90
99.3	3.36	3.9	9.1	6.2	10.8	9.8	9.7	9.9	0.00	0.07	0.11	0.15	1.70	1.88	1.99
100.6	3.35	3.8	8.3	6.3	10.8	9.9	9.9	10.0	0.00	0.10	0.14	0.17	1.64	1.84	1.94
99.9	3.38	4.0	12.1	6.4	10.6	10.3	10.4	10.6	0.00	0.54	0.58	0.61	1.55	1.69	1.77
99.4	1.30	-20.4	14.2	3.2	23.2	-9.7	-9.7	-9.1	0.00	0.09	0.16	0.24	2.06	2.26	2.28
99.9	1.32	-20.1	21.8	4.1	50.4	-5.5	-5.9	-5.1	0.00	0.13	0.29	0.45	3.62	4.09	4.14
99.9	1.34	-19.8	31.2	4.5	62.1	-5.2	-5.3	-4.2	0.00	0.28	0.48	0.68	4.70	5.21	5.10
99.1	1.31	-20.3	31.6	5.9	62.1	-2.2	1.7	7.9	0.00	0.53	0.73	0.93	3.59	3.09	2.50
99.4	1.34	-19.8	28.8	5.4	72.0	-2.6	-2.7	0.8	0.00	0.21	0.44	0.67	4.61	5.12	4.33
99.3	1.30	-20.5	10.3	2.8	10.5	-11.9	-11.8	-11.6	0.00	0.07	0.10	0.14	1.09	1.18	1.24
99.1	1.29	-20.6	16.0	2.6	11.1	-13.7	-13.4	-13.1	0.00	0.32	0.36	0.39	1.48	1.55	1.58
99.4	1.30	-20.4	22.1	2.4	11.0	-15.4	-15.2	-14.9	0.00	0.59	0.62	0.66	2.09	2.17	2.17
99.5	1.29	-20.7	21.4	3.0	10.9	-11.8	-10.1	-9.3	0.00	0.88	0.91	0.94	1.08	0.98	0.98
99.7	0.82	-30.7	16.5	2.0	15.9	-20.3	-20.6	-20.4	0.00	0.17	0.22	0.27	1.39	1.57	1.65
102.8	0.85	-29.8	26.9	1.8	16.2	-22.6	-22.9	-22.4	0.00	0.44	0.49	0.54	2.12	2.38	2.35
100.6	0.85	-29.9	31.4	1.7	16.5	-24.0	-24.0	-23.2	0.00	0.72	0.77	0.82	2.67	2.88	2.60
100.0	0.83	-30.4	24.5	3.2	16.4	-9.7	-7.2	-7.2	0.00	0.95	1.00	1.05	0.69	0.67	0.73
100.3	0.83	-30.3	30.1	2.5	15.9	-18.7	-15.0	-13.9	0.00	0.83	0.88	0.92	1.22	0.99	0.99
101.6	0.83	-30.3	28.5	2.2	16.3	-21.1	-18.1	-17.0	0.00	0.86	0.91	0.96	1.62	1.30	1.27

Continued on next page.

Continued from previous page.

$\dot{m}$	p_s	T	Δp	p_c	$\overline{\dot{q}}$		T_w		$\widetilde{x}$		$\dot{x}$		α		
$\frac{kg}{m^2 s}$	bar	°C	mbar	bar	$\frac{kW}{m^2}$		°C		-		-		kW/m^{2}K		
						S1	S2	S3		S1	S2	S3	S1	S2	S3
102.3	0.83	-30.3	27.2	3.3	16.5	-10.6	-6.5	-6.5	0.00	0.90	0.95	1.00	0.73	0.66	0.71
200.4	0.86	-29.7	13.9	1.9	16.3	-19.8	-19.8	-20.1	0.00	0.01	0.03	0.06	1.51	1.65	1.84
199.6	0.84	-30.1	22.0	1.9	16.3	-21.3	-21.5	-21.2	0.00	0.08	0.11	0.13	1.69	1.88	1.94
199.6	0.89	-28.9	73.9	1.8	16.5	-23.1	-24.1	-23.9	0.00	0.46	0.48	0.51	2.65	3.29	3.10
199.2	0.89	-28.9	74.2	1.7	16.5	-24.6	-25.0	-24.9	0.00	0.58	0.60	0.63	3.65	4.05	3.83
199.5	0.92	-28.3	76.8	1.7	16.5	-24.5	-24.8	-24.7	0.00	0.71	0.73	0.76	4.26	4.48	4.14
199.2	0.92	-28.3	65.9	1.9	16.5	-23.8	-21.2	-20.5	0.00	0.88	0.91	0.93	3.52	2.21	2.07
200.5	1.34	-19.8	13.6	2.5	10.5	-14.3	-14.2	-13.8	0.00	0.07	0.09	0.10	1.77	1.87	1.88
199.8	1.45	-18.0	23.4	3.8	39.8	-6.6	-6.6	-6.0	0.00	0.08	0.15	0.21	3.64	3.99	4.05
200.6	1.32	-20.1	33.3	3.5	39.9	-8.9	-9.0	-8.5	0.00	0.14	0.20	0.27	3.72	4.12	4.15
200.1	1.29	-20.7	44.0	2.5	17.0	-14.7	-15.2	-14.7	0.00	0.28	0.31	0.34	2.74	3.22	3.06
201.9	1.31	-20.3	54.5	2.5	16.6	-15.5	-15.8	-15.4	0.00	0.50	0.53	0.55	3.42	3.92	3.66
199.8	1.37	-19.3	56.3	2.5	16.9	-15.1	-15.4	-15.0	0.00	0.68	0.71	0.74	4.09	4.67	4.21
200.4	1.35	-19.6	56.1	2.5	16.4	-15.4	-15.7	-15.2	0.00	0.85	0.88	0.90	4.03	4.48	3.98
201.0	1.36	-19.5	46.7	2.7	16.5	-14.7	-12.8	-11.9	0.00	0.95	0.98	1.00	3.47	2.48	2.29
200.2	1.18	-22.7	26.6	2.6	16.5	-14.8	-15.3	-14.6	0.00	0.18	0.20	0.23	1.97	2.32	2.23
200.0	1.34	-19.8	49.0	2.8	23.8	-12.7	-12.9	-12.6	0.00	0.37	0.41	0.44	3.36	3.75	3.71
199.7	1.35	-19.6	58.5	2.8	23.3	-13.1	-13.5	-13.1	0.00	0.50	0.53	0.57	3.66	4.14	3.99
199.5	1.36	-19.4	63.6	2.7	23.1	-13.5	-13.8	-13.3	0.00	0.64	0.68	0.72	4.01	4.46	4.18
200.5	1.38	-19.1	61.4	2.7	22.2	-13.4	-13.6	-13.0	0.00	0.58	0.61	0.65	3.98	4.31	3.99
199.9	1.36	-19.5	42.8	5.7	22.5	7.4	7.8	7.8	0.00	0.93	0.97	1.00	0.73	0.79	0.85
200.8	1.28	-20.9	17.8	2.9	22.2	-11.8	-11.7	-11.3	0.00	0.03	0.06	0.10	2.38	2.56	2.62
201.0	1.30	-20.5	24.3	2.9	22.6	-12.7	-12.5	-12.0	0.00	0.13	0.16	0.20	2.88	3.06	3.04
200.8	1.97	-10.5	16.4	4.2	22.4	-2.8	-2.7	-2.4	0.00	0.08	0.12	0.15	2.91	3.15	3.23
200.6	1.97	-10.5	23.2	4.1	22.5	-3.6	-3.5	-3.1	0.00	0.21	0.25	0.28	3.35	3.61	3.60
200.4	1.99	-10.2	11.4	4.0	15.2	-3.3	-3.2	-3.1	0.00	0.01	0.04	0.06	2.08	2.27	2.42
200.3	2.01	-10.0	12.9	4.0	15.6	-2.9	-2.8	-2.7	0.00	0.06	0.08	0.11	2.10	2.28	2.42
200.4	2.02	-9.8	21.4	3.8	15.5	-3.8	-3.7	-3.5	0.00	0.22	0.25	0.27	2.52	2.68	2.76
200.1	2.01	-9.9	26.5	3.8	15.7	-4.0	-3.9	-3.7	0.00	0.30	0.32	0.35	2.61	2.79	2.87
200.5	2.03	-9.7	37.3	3.7	15.5	-4.6	-4.6	-4.4	0.00	0.45	0.47	0.50	2.98	3.24	3.27
200.3	2.01	-10.0	42.2	3.7	15.6	-5.1	-5.1	-4.9	0.00	0.53	0.56	0.58	3.17	3.46	3.45
201.5	2.02	-9.9	46.4	3.6	15.7	-5.1	-5.2	-4.9	0.00	0.61	0.64	0.66	3.31	3.62	3.55
200.7	2.01	-9.9	47.8	3.6	15.5	-5.6	-5.6	-5.4	0.00	0.74	0.76	0.79	3.67	3.90	3.81
199.8	2.03	-9.7	46.6	3.6	15.5	-5.6	-5.6	-5.4	0.00	0.81	0.84	0.86	4.00	4.19	4.12
200.4	2.02	-9.8	36.2	4.1	15.7	-3.7	-2.0	-1.2	0.00	0.92	0.95	0.97	2.47	2.06	1.96
200.0	2.01	-10.0	29.7	7.9	15.7	17.1	17.3	17.5	0.00	1.00	1.04	1.07	0.50	0.55	0.59
302.2	0.86	-29.6	32.6	2.0	21.9	-20.9	-21.3	-21.2	0.00	0.05	0.07	0.10	2.42	2.76	2.86
300.6	0.92	-28.2	57.8	2.0	21.9	-21.0	-21.7	-21.7	0.00	0.15	0.17	0.20	2.92	3.44	3.54
301.6	0.94	-27.7	96.5	1.9	21.9	-21.4	-22.3	-22.4	0.00	0.34	0.36	0.39	3.29	3.86	3.84
300.5	0.98	-26.9	115.5	1.9	21.9	-21.9	-22.7	-22.9	0.00	0.48	0.50	0.52	4.19	4.83	4.73
301.1	0.97	-27.0	119.0	1.9	21.9	-22.2	-23.0	-23.2	0.00	0.56	0.58	0.60	4.44	5.07	4.87
300.7	0.97	-27.0	121.6	1.9	21.9	-22.5	-23.1	-23.3	0.00	0.58	0.60	0.62	4.71	5.17	5.01
298.0	0.97	-27.0	112.7	1.9	22.5	-22.2	-23.2	-23.1	0.00	0.56	0.59	0.61	4.48	5.51	5.02
296.8	1.04	-25.5	111.2	1.9	22.6	-21.3	-22.0	-22.1	0.00	0.73	0.75	0.78	5.44	6.39	5.94

Continued on next page.

Continued from previous page.

$\dot{m}$	p_s	T	Δp	p_c	$\bar{\dot{q}}$		T_w		$\widetilde{x}$		$\dot{x}$		α		
$\frac{kg}{m^2 s}$	bar	°C	mbar	bar	$\frac{kW}{m^2}$		°C		-		-		kW/m^{2}K		
						S1	S2	S3		S1	S2	S3	S1	S2	S3
300.4	1.24	-21.5	47.0	2.4	15.8	-15.7	-16.1	-15.8	0.00	0.19	0.21	0.22	2.63	2.99	2.93
300.7	1.34	-19.8	54.3	2.5	15.8	-15.0	-15.2	-15.0	0.00	0.28	0.30	0.31	3.20	3.54	3.47
300.3	1.40	-18.8	71.5	2.5	15.8	-14.7	-15.0	-14.8	0.00	0.32	0.34	0.36	3.81	4.15	3.98
300.2	1.43	-18.3	81.9	2.5	15.8	-14.6	-14.9	-14.7	0.00	0.41	0.43	0.45	4.25	4.58	4.34
300.9	1.40	-18.7	91.5	2.5	15.8	-15.3	-15.6	-15.5	0.00	0.54	0.55	0.57	4.64	5.01	4.69
300.1	1.42	-18.4	90.3	2.5	15.8	-15.2	-15.5	-15.4	0.00	0.60	0.62	0.64	4.99	5.41	4.95
300.3	1.39	-19.0	93.4	2.4	15.8	-15.8	-16.1	-15.9	0.00	0.69	0.70	0.72	5.10	5.29	4.82
302.3	0.87	-29.4	32.2	2.6	40.3	-16.6	-17.0	-17.0	0.00	0.01	0.05	0.09	3.18	3.61	3.84
299.3	0.90	-28.7	59.0	2.5	40.3	-17.1	-17.9	-18.3	0.00	0.10	0.14	0.19	3.52	4.11	4.49
301.2	0.94	-27.8	92.2	2.4	40.3	-17.5	-18.4	-19.0	0.00	0.20	0.24	0.29	4.00	4.61	5.06
299.2	0.96	-27.2	115.8	2.4	40.3	-17.6	-18.6	-19.3	0.00	0.31	0.36	0.40	4.25	4.92	5.35
300.1	1.00	-26.3	120.1	2.4	40.3	-17.4	-18.3	-19.2	0.00	0.37	0.41	0.45	4.75	5.39	6.04
298.9	0.98	-26.7	121.0	2.4	40.3	-17.9	-18.9	-19.8	0.00	0.46	0.50	0.54	4.73	5.54	6.15
299.0	0.99	-26.6	119.8	2.4	39.8	-17.7	-18.7	-19.0	0.00	0.45	0.49	0.53	4.66	5.36	5.56
298.4	1.01	-26.2	121.2	2.4	40.3	-17.7	-18.7	-19.0	0.00	0.51	0.56	0.60	4.98	5.78	5.95
299.5	1.02	-25.9	116.4	2.4	40.0	-17.6	-18.6	-18.3	0.00	0.59	0.63	0.67	5.16	6.02	5.64
299.0	1.01	-26.0	117.9	2.4	40.4	-18.1	-19.1	-18.3	0.00	0.66	0.70	0.74	5.52	6.47	5.57
297.7	0.86	-29.6	29.3	1.9	16.5	-21.9	-22.4	-21.8	0.00	0.07	0.09	0.11	2.00	2.35	2.28
296.7	0.94	-27.6	62.7	1.8	16.5	-22.4	-23.0	-22.9	0.00	0.20	0.22	0.24	3.05	3.58	3.49
297.4	0.95	-27.4	92.9	1.7	16.5	-23.1	-23.8	-23.9	0.00	0.33	0.35	0.37	3.66	4.23	4.05
296.6	0.99	-26.5	102.2	1.8	16.5	-22.9	-23.5	-23.6	0.00	0.47	0.48	0.50	4.25	4.79	4.52
298.3	0.98	-26.8	106.2	1.7	16.5	-23.3	-23.9	-23.9	0.00	0.55	0.57	0.59	4.30	4.88	4.36
297.2	1.01	-26.2	106.3	1.8	16.5	-23.0	-23.5	-23.5	0.00	0.64	0.66	0.68	4.86	5.25	4.78
297.5	1.01	-26.2	113.8	1.8	16.5	-22.4	-23.3	-23.1	0.00	0.72	0.74	0.76	4.01	4.80	4.09
199.6	0.86	-29.6	13.9	2.0	16.0	-19.1	-19.2	-19.5	0.00	0.01	0.03	0.06	1.39	1.55	1.71
199.6	0.93	-27.8	17.2	2.0	16.0	-19.1	-19.0	-18.8	0.00	0.07	0.09	0.12	1.69	1.83	1.91
199.0	0.85	-29.8	30.5	1.8	16.6	-21.6	-21.9	-21.8	0.00	0.15	0.18	0.20	1.89	2.12	2.20
199.6	0.88	-29.0	51.0	1.8	17.1	-22.6	-23.1	-23.1	0.00	0.28	0.30	0.33	2.49	2.85	2.95
200.4	0.86	-29.7	13.9	1.9	16.3	-19.8	-19.8	-20.1	0.00	0.01	0.03	0.06	1.51	1.65	1.84
199.6	0.84	-30.1	22.0	1.9	16.3	-21.3	-21.5	-21.2	0.00	0.08	0.11	0.13	1.69	1.88	1.94
199.6	0.89	-28.9	73.9	1.8	16.5	-23.1	-24.1	-23.9	0.00	0.46	0.48	0.51	2.65	3.29	3.10
199.2	0.89	-28.9	74.2	1.7	16.5	-24.6	-25.0	-24.9	0.00	0.58	0.60	0.63	3.65	4.05	3.83
199.5	0.92	-28.3	76.8	1.7	16.5	-24.5	-24.8	-24.7	0.00	0.71	0.73	0.76	4.26	4.48	4.14
199.2	0.92	-28.3	65.9	1.9	16.5	-23.8	-21.2	-20.5	0.00	0.88	0.91	0.93	3.52	2.21	2.07
196.7	2.07	-9.2	24.8	3.8	16.7	-4.1	-4.0	-3.9	0.00	0.41	0.44	0.47	3.33	3.52	3.72
202.5	2.07	-9.2	36.0	3.7	16.7	-4.6	-4.5	-4.5	0.00	0.56	0.59	0.62	3.81	4.03	4.22
198.3	2.01	-10.0	39.4	3.6	16.2	-5.4	-5.4	-5.4	0.00	0.68	0.70	0.73	3.65	3.96	4.07
198.1	2.07	-9.2	36.6	3.7	16.2	-5.2	-5.2	-5.1	0.00	0.93	0.96	0.98	4.33	4.65	4.71
303.3	2.02	-9.8	23.9	3.8	16.6	-4.9	-4.9	-4.8	0.00	0.21	0.23	0.24	3.52	3.81	3.98
296.3	2.09	-9.0	44.2	3.8	16.5	-4.9	-4.9	-4.9	0.00	0.35	0.37	0.38	4.25	4.53	4.73
298.6	2.00	-10.0	61.9	3.5	16.5	-6.3	-6.4	-6.4	0.00	0.49	0.51	0.52	4.77	5.08	5.09
296.8	1.96	-10.6	67.5	3.4	16.5	-7.3	-7.4	-7.4	0.00	0.67	0.69	0.71	5.65	5.86	5.86
303.8	1.94	-10.9	63.1	3.5	17.0	-6.4	-6.4	-6.4	0.00	0.46	0.48	0.50	3.82	4.02	4.15
299.0	2.03	-9.7	29.1	4.0	23.3	-3.8	-3.9	-3.6	0.00	0.23	0.25	0.28	4.24	4.71	4.72

Continued on next page.

Continued from previous page.

$\dot{m}$	p_s	T	Δp	p_c	$\bar{\dot{q}}$		T_w		$\widetilde{x}$		$\dot{x}$		α		
$\frac{kg}{m^2 s}$	bar	°C	mbar	bar	$\frac{kW}{m^2}$		°C		-		-		kW/m^{2}K		
						S1	S2	S3		S1	S2	S3	S1	S2	S3
298.8	1.96	-10.5	51.3	3.8	23.8	-4.9	-5.1	-4.9	0.00	0.36	0.39	0.41	4.53	5.02	5.06
298.6	2.03	-9.7	66.7	3.8	23.2	-4.2	-4.3	-4.2	0.00	0.48	0.51	0.54	4.46	4.85	4.90
300.5	2.00	-10.1	70.4	3.7	23.2	-4.7	-4.8	-4.8	0.00	0.56	0.58	0.61	4.67	5.02	5.09
301.4	2.09	-8.9	66.9	3.9	23.1	-4.0	-4.2	-4.1	0.00	0.55	0.58	0.60	5.18	5.64	5.67
302.6	1.97	-10.4	59.8	4.3	42.4	-2.5	-2.7	-2.4	0.00	0.37	0.42	0.46	6.41	7.00	7.00
304.1	2.06	-9.3	69.7	4.5	42.4	-1.1	-1.3	-1.0	0.00	0.46	0.51	0.56	6.05	6.61	6.61
298.0	2.02	-9.9	76.5	4.4	42.4	-1.8	-2.0	-1.7	0.00	0.64	0.68	0.73	6.10	6.70	6.67
297.1	2.04	-9.6	58.5	4.6	41.3	-1.0	-1.1	-0.9	0.00	0.69	0.74	0.78	5.44	5.92	6.06
99.6	3.36	3.9	10.1	5.9	6.1	8.6	8.6	8.8	0.00	0.43	0.45	0.47	1.15	1.26	1.32
100.0	3.39	4.1	11.4	5.9	6.0	8.3	8.3	8.4	0.00	0.55	0.57	0.59	1.30	1.45	1.52
99.1	3.39	4.1	12.5	5.9	6.1	8.6	8.6	8.7	0.00	0.69	0.71	0.74	1.22	1.35	1.42
99.4	3.39	4.1	13.2	5.9	6.0	8.9	8.9	9.1	0.00	0.82	0.84	0.86	1.14	1.25	1.30
99.2	3.38	4.0	12.6	6.1	6.1	9.2	9.3	9.4	0.00	0.92	0.94	0.96	1.05	1.14	1.19
99.1	3.37	3.9	11.9	6.8	6.0	12.0	12.3	12.8	0.00	0.95	0.97	0.99	0.65	0.69	0.70
100.0	3.36	3.8	11.6	6.7	6.0	11.9	12.1	12.5	0.00	0.93	0.96	0.98	0.65	0.70	0.72
99.9	3.34	3.7	10.1	5.9	6.0	8.4	8.4	8.5	0.00	0.40	0.43	0.45	1.15	1.26	1.33
100.5	3.37	3.9	11.6	5.4	2.7	6.5	6.5	6.4	0.00	0.60	0.61	0.62	0.92	1.01	1.11
99.9	3.39	4.1	12.6	5.4	2.6	6.7	6.7	6.7	0.00	0.77	0.78	0.79	0.89	0.98	1.06
100.2	3.36	3.9	10.3	6.4	10.5	10.9	10.8	10.9	0.00	0.33	0.36	0.40	1.36	1.52	1.63
99.2	3.40	4.2	11.7	6.4	10.4	10.9	10.8	10.9	0.00	0.51	0.55	0.58	1.41	1.59	1.68
99.1	3.39	4.1	13.2	6.4	10.6	11.0	11.0	11.1	0.00	0.73	0.77	0.80	1.41	1.55	1.63
99.9	3.38	4.1	13.7	6.6	10.6	11.4	11.5	11.7	0.00	0.82	0.86	0.89	1.31	1.43	1.49
99.3	3.38	4.0	13.0	6.8	10.7	12.4	12.5	12.8	0.00	0.90	0.93	0.97	1.15	1.26	1.30
100.0	3.37	3.9	12.6	7.6	10.7	15.2	15.7	16.4	0.00	0.93	0.97	1.01	0.84	0.89	0.90
99.3	3.36	3.9	9.1	6.2	10.8	9.8	9.7	9.9	0.00	0.07	0.11	0.15	1.70	1.88	1.99
100.6	3.35	3.8	8.3	6.3	10.8	9.9	9.9	10.0	0.00	0.10	0.14	0.17	1.64	1.84	1.94
99.9	3.38	4.0	12.1	6.4	10.6	10.3	10.4	10.6	0.00	0.54	0.58	0.61	1.55	1.69	1.77
99.4	1.30	-20.4	14.2	3.2	23.2	-9.7	-9.7	-9.1	0.00	0.09	0.16	0.24	2.06	2.26	2.28
99.9	1.32	-20.1	21.8	4.1	50.4	-5.5	-5.9	-5.1	0.00	0.13	0.29	0.45	3.62	4.09	4.14
99.9	1.34	-19.8	31.2	4.5	62.1	-5.2	-5.3	-4.2	0.00	0.28	0.48	0.68	4.70	5.21	5.10
99.1	1.31	-20.3	31.6	5.9	62.1	-2.2	1.7	7.9	0.00	0.53	0.73	0.93	3.59	3.09	2.50
99.4	1.34	-19.8	28.8	5.4	72.0	-2.6	-2.7	0.8	0.00	0.21	0.44	0.67	4.61	5.12	4.33
99.3	1.30	-20.5	10.3	2.8	10.5	-11.9	-11.8	-11.6	0.00	0.07	0.10	0.14	1.09	1.18	1.24
99.1	1.29	-20.6	16.0	2.6	11.1	-13.7	-13.4	-13.1	0.00	0.32	0.36	0.39	1.48	1.55	1.58
99.4	1.30	-20.4	22.1	2.4	11.0	-15.4	-15.2	-14.9	0.00	0.59	0.62	0.66	2.09	2.17	2.17
99.5	1.29	-20.7	21.4	3.0	10.9	-11.8	-10.1	-9.3	0.00	0.88	0.91	0.94	1.08	0.98	0.98
99.7	0.82	-30.7	16.5	2.0	15.9	-20.3	-20.6	-20.4	0.00	0.17	0.22	0.27	1.39	1.57	1.65
102.8	0.85	-29.8	26.9	1.8	16.2	-22.6	-22.9	-22.4	0.00	0.44	0.49	0.54	2.12	2.38	2.35
100.6	0.85	-29.9	31.4	1.7	16.5	-24.0	-24.0	-23.2	0.00	0.72	0.77	0.82	2.67	2.88	2.60
100.0	0.83	-30.4	24.5	3.2	16.4	-9.7	-7.2	-7.2	0.00	0.95	1.00	1.05	0.69	0.67	0.73
100.3	0.83	-30.3	30.1	2.5	15.9	-18.7	-15.0	-13.9	0.00	0.83	0.88	0.92	1.22	0.99	0.99
101.6	0.83	-30.3	28.5	2.2	16.3	-21.1	-18.1	-17.0	0.00	0.86	0.91	0.96	1.62	1.30	1.27
102.3	0.83	-30.3	27.2	3.3	16.5	-10.6	-6.5	-6.5	0.00	0.90	0.95	1.00	0.73	0.66	0.71
200.4	0.86	-29.7	13.9	1.9	16.3	-19.8	-19.8	-20.1	0.00	0.01	0.03	0.06	1.51	1.65	1.84

Continued on next page.

Continued from previous page.

$\dot{m}$	p_s	T	Δp	p_c	$\bar{\dot{q}}$	T_w			$\widetilde{x}$	$\dot{x}$			α		
$\frac{kg}{m^2 s}$	bar	°C	mbar	bar	$\frac{kW}{m^2}$	°C			-	-			kW/m^{2}K		
						S1	S2	S3		S1	S2	S3	S1	S2	S3
199.6	0.84	-30.1	22.0	1.9	16.3	-21.3	-21.5	-21.2	0.00	0.08	0.11	0.13	1.69	1.88	1.94
199.6	0.89	-28.9	73.9	1.8	16.5	-23.1	-24.1	-23.9	0.00	0.46	0.48	0.51	2.65	3.29	3.10
199.2	0.89	-28.9	74.2	1.7	16.5	-24.6	-25.0	-24.9	0.00	0.58	0.60	0.63	3.65	4.05	3.83
199.5	0.92	-28.3	76.8	1.7	16.5	-24.5	-24.8	-24.7	0.00	0.71	0.73	0.76	4.26	4.48	4.14
199.2	0.92	-28.3	65.9	1.9	16.5	-23.8	-21.2	-20.5	0.00	0.88	0.91	0.93	3.52	2.21	2.07
200.5	1.34	-19.8	13.6	2.5	10.5	-14.3	-14.2	-13.8	0.00	0.07	0.09	0.10	1.77	1.87	1.88
199.8	1.45	-18.0	23.4	3.8	39.8	-6.6	-6.6	-6.0	0.00	0.08	0.15	0.21	3.64	3.99	4.05
200.6	1.32	-20.1	33.3	3.5	39.9	-8.9	-9.0	-8.5	0.00	0.14	0.20	0.27	3.72	4.12	4.15
200.1	1.29	-20.7	44.0	2.5	17.0	-14.7	-15.2	-14.7	0.00	0.28	0.31	0.34	2.74	3.22	3.06
201.9	1.31	-20.3	54.5	2.5	16.6	-15.5	-15.8	-15.4	0.00	0.50	0.53	0.55	3.42	3.92	3.66
199.8	1.37	-19.3	56.3	2.5	16.9	-15.1	-15.4	-15.0	0.00	0.68	0.71	0.74	4.09	4.67	4.21
200.4	1.35	-19.6	56.1	2.5	16.4	-15.4	-15.7	-15.2	0.00	0.85	0.88	0.90	4.03	4.48	3.98
201.0	1.36	-19.5	46.7	2.7	16.5	-14.7	-12.8	-11.9	0.00	0.95	0.98	1.00	3.47	2.48	2.29
200.2	1.18	-22.7	26.6	2.6	16.5	-14.8	-15.3	-14.6	0.00	0.18	0.20	0.23	1.97	2.32	2.23
200.0	1.34	-19.8	49.0	2.8	23.8	-12.7	-12.9	-12.6	0.00	0.37	0.41	0.44	3.36	3.75	3.71
199.7	1.35	-19.6	58.5	2.8	23.3	-13.1	-13.5	-13.1	0.00	0.50	0.53	0.57	3.66	4.14	3.99
199.5	1.36	-19.4	63.6	2.7	23.1	-13.5	-13.8	-13.3	0.00	0.64	0.68	0.72	4.01	4.46	4.18
200.5	1.38	-19.1	61.4	2.7	22.2	-13.4	-13.6	-13.0	0.00	0.58	0.61	0.65	3.98	4.31	3.99
199.9	1.36	-19.5	42.8	5.7	22.5	7.4	7.8	7.8	0.00	0.93	0.97	1.00	0.73	0.79	0.85
200.8	1.28	-20.9	17.8	2.9	22.2	-11.8	-11.7	-11.3	0.00	0.03	0.06	0.10	2.38	2.56	2.62
201.0	1.30	-20.5	24.3	2.9	22.6	-12.7	-12.5	-12.0	0.00	0.13	0.16	0.20	2.88	3.06	3.04
200.8	1.97	-10.5	16.4	4.2	22.4	-2.8	-2.7	-2.4	0.00	0.08	0.12	0.15	2.91	3.15	3.23
200.6	1.97	-10.5	23.2	4.1	22.5	-3.6	-3.5	-3.1	0.00	0.21	0.25	0.28	3.35	3.61	3.60
200.4	1.99	-10.2	11.4	4.0	15.2	-3.3	-3.2	-3.1	0.00	0.01	0.04	0.06	2.08	2.27	2.42
200.3	2.01	-10.0	12.9	4.0	15.6	-2.9	-2.8	-2.7	0.00	0.06	0.08	0.11	2.10	2.28	2.42
200.4	2.02	-9.8	21.4	3.8	15.5	-3.8	-3.7	-3.5	0.00	0.22	0.25	0.27	2.52	2.68	2.76
200.1	2.01	-9.9	26.5	3.8	15.7	-4.0	-3.9	-3.7	0.00	0.30	0.32	0.35	2.61	2.79	2.87
200.5	2.03	-9.7	37.3	3.7	15.5	-4.6	-4.6	-4.4	0.00	0.45	0.47	0.50	2.98	3.24	3.27
200.3	2.01	-10.0	42.2	3.7	15.6	-5.1	-5.1	-4.9	0.00	0.53	0.56	0.58	3.17	3.46	3.45
201.5	2.02	-9.9	46.4	3.6	15.7	-5.1	-5.2	-4.9	0.00	0.61	0.64	0.66	3.31	3.62	3.55
200.7	2.01	-9.9	47.8	3.6	15.5	-5.6	-5.6	-5.4	0.00	0.74	0.76	0.79	3.67	3.90	3.81
199.8	2.03	-9.7	46.6	3.6	15.5	-5.6	-5.6	-5.4	0.00	0.81	0.84	0.86	4.00	4.19	4.12
200.4	2.02	-9.8	36.2	4.1	15.7	-3.7	-2.0	-1.2	0.00	0.92	0.95	0.97	2.47	2.06	1.96
200.0	2.01	-10.0	29.7	7.9	15.7	17.1	17.3	17.5	0.00	1.00	1.04	1.07	0.50	0.55	0.59
302.2	0.86	-29.6	32.6	2.0	21.9	-20.9	-21.3	-21.2	0.00	0.05	0.07	0.10	2.42	2.76	2.86
300.6	0.92	-28.2	57.8	2.0	21.9	-21.0	-21.7	-21.7	0.00	0.15	0.17	0.20	2.92	3.44	3.54
301.6	0.94	-27.7	96.5	1.9	21.9	-21.4	-22.3	-22.4	0.00	0.34	0.36	0.39	3.29	3.86	3.84
300.5	0.98	-26.9	115.5	1.9	21.9	-21.9	-22.7	-22.9	0.00	0.48	0.50	0.52	4.19	4.83	4.73
301.1	0.97	-27.0	119.0	1.9	21.9	-22.2	-23.0	-23.2	0.00	0.56	0.58	0.60	4.44	5.07	4.87
300.7	0.97	-27.0	121.6	1.9	21.9	-22.5	-23.1	-23.3	0.00	0.58	0.60	0.62	4.71	5.17	5.01
298.0	0.97	-27.0	112.7	1.9	22.5	-22.2	-23.2	-23.1	0.00	0.56	0.59	0.61	4.48	5.51	5.02
296.8	1.04	-25.5	111.2	1.9	22.6	-21.3	-22.0	-22.1	0.00	0.73	0.75	0.78	5.44	6.39	5.94
300.4	1.24	-21.5	47.0	2.4	15.8	-15.7	-16.1	-15.8	0.00	0.19	0.21	0.22	2.63	2.99	2.93
300.7	1.34	-19.8	54.3	2.5	15.8	-15.0	-15.2	-15.0	0.00	0.28	0.30	0.31	3.20	3.54	3.47

Continued on next page.

Continued from previous page.

$\dot{m}$	p_s	T	Δp	p_c	$\bar{\dot{q}}$		T_w		$\widetilde{x}$		$\dot{x}$		α		
$\frac{kg}{m^2 s}$	bar	°C	mbar	bar	$\frac{kW}{m^2}$		°C		-		-		kW/m^{2}K		
						S1	S2	S3		S1	S2	S3	S1	S2	S3
300.3	1.40	-18.8	71.5	2.5	15.8	-14.7	-15.0	-14.8	0.00	0.32	0.34	0.36	3.81	4.15	3.98
300.2	1.43	-18.3	81.9	2.5	15.8	-14.6	-14.9	-14.7	0.00	0.41	0.43	0.45	4.25	4.58	4.34
300.9	1.40	-18.7	91.5	2.5	15.8	-15.3	-15.6	-15.5	0.00	0.54	0.55	0.57	4.64	5.01	4.69
300.1	1.42	-18.4	90.3	2.5	15.8	-15.2	-15.5	-15.4	0.00	0.60	0.62	0.64	4.99	5.41	4.95
300.3	1.39	-19.0	93.4	2.4	15.8	-15.8	-16.1	-15.9	0.00	0.69	0.70	0.72	5.10	5.29	4.82
302.3	0.87	-29.4	32.2	2.6	40.3	-16.6	-17.0	-17.0	0.00	0.01	0.05	0.09	3.18	3.61	3.84
299.3	0.90	-28.7	59.0	2.5	40.3	-17.1	-17.9	-18.3	0.00	0.10	0.14	0.19	3.52	4.11	4.49
301.2	0.94	-27.8	92.2	2.4	40.3	-17.5	-18.4	-19.0	0.00	0.20	0.24	0.29	4.00	4.61	5.06
299.2	0.96	-27.2	115.8	2.4	40.3	-17.6	-18.6	-19.3	0.00	0.31	0.36	0.40	4.25	4.92	5.35
300.1	1.00	-26.3	120.1	2.4	40.3	-17.4	-18.3	-19.2	0.00	0.37	0.41	0.45	4.75	5.39	6.04
298.9	0.98	-26.7	121.0	2.4	40.3	-17.9	-18.9	-19.8	0.00	0.46	0.50	0.54	4.73	5.54	6.15
299.0	0.99	-26.6	119.8	2.4	39.8	-17.7	-18.7	-19.0	0.00	0.45	0.49	0.53	4.66	5.36	5.56
298.4	1.01	-26.2	121.2	2.4	40.3	-17.7	-18.7	-19.0	0.00	0.51	0.56	0.60	4.98	5.78	5.95
299.5	1.02	-25.9	116.4	2.4	40.0	-17.6	-18.6	-18.3	0.00	0.59	0.63	0.67	5.16	6.02	5.64
299.0	1.01	-26.0	117.9	2.4	40.4	-18.1	-19.1	-18.3	0.00	0.66	0.70	0.74	5.52	6.47	5.57
297.7	0.86	-29.6	29.3	1.9	16.5	-21.9	-22.4	-21.8	0.00	0.07	0.09	0.11	2.00	2.35	2.28
296.7	0.94	-27.6	62.7	1.8	16.5	-22.4	-23.0	-22.9	0.00	0.20	0.22	0.24	3.05	3.58	3.49
297.4	0.95	-27.4	92.9	1.7	16.5	-23.1	-23.8	-23.9	0.00	0.33	0.35	0.37	3.66	4.23	4.05
296.6	0.99	-26.5	102.2	1.8	16.5	-22.9	-23.5	-23.6	0.00	0.47	0.48	0.50	4.25	4.79	4.52
298.3	0.98	-26.8	106.2	1.7	16.5	-23.3	-23.9	-23.9	0.00	0.55	0.57	0.59	4.30	4.88	4.36
297.2	1.01	-26.2	106.3	1.8	16.5	-23.0	-23.5	-23.5	0.00	0.64	0.66	0.68	4.86	5.25	4.78
297.5	1.01	-26.2	113.8	1.8	16.5	-22.4	-23.3	-23.1	0.00	0.72	0.74	0.76	4.01	4.80	4.09
199.6	0.86	-29.6	13.9	2.0	16.0	-19.1	-19.2	-19.5	0.00	0.01	0.03	0.06	1.39	1.55	1.71
199.6	0.93	-27.8	17.2	2.0	16.0	-19.1	-19.0	-18.8	0.00	0.07	0.09	0.12	1.69	1.83	1.91
199.0	0.85	-29.8	30.5	1.8	16.6	-21.6	-21.9	-21.8	0.00	0.15	0.18	0.20	1.89	2.12	2.20
199.6	0.88	-29.0	51.0	1.8	17.1	-22.6	-23.1	-23.1	0.00	0.28	0.30	0.33	2.49	2.85	2.95
200.4	0.86	-29.7	13.9	1.9	16.3	-19.8	-19.8	-20.1	0.00	0.01	0.03	0.06	1.51	1.65	1.84
199.6	0.84	-30.1	22.0	1.9	16.3	-21.3	-21.5	-21.2	0.00	0.08	0.11	0.13	1.69	1.88	1.94
199.6	0.89	-28.9	73.9	1.8	16.5	-23.1	-24.1	-23.9	0.00	0.46	0.48	0.51	2.65	3.29	3.10
199.2	0.89	-28.9	74.2	1.7	16.5	-24.6	-25.0	-24.9	0.00	0.58	0.60	0.63	3.65	4.05	3.83
199.5	0.92	-28.3	76.8	1.7	16.5	-24.5	-24.8	-24.7	0.00	0.71	0.73	0.76	4.26	4.48	4.14
199.2	0.92	-28.3	65.9	1.9	16.5	-23.8	-21.2	-20.5	0.00	0.88	0.91	0.93	3.52	2.21	2.07
196.7	2.07	-9.2	24.8	3.8	16.7	-4.1	-4.0	-3.9	0.00	0.41	0.44	0.47	3.33	3.52	3.72
202.5	2.07	-9.2	36.0	3.7	16.7	-4.6	-4.5	-4.5	0.00	0.56	0.59	0.62	3.81	4.03	4.22
198.3	2.01	-10.0	39.4	3.6	16.2	-5.4	-5.4	-5.4	0.00	0.68	0.70	0.73	3.65	3.96	4.07
198.1	2.07	-9.2	36.6	3.7	16.2	-5.2	-5.2	-5.1	0.00	0.93	0.96	0.98	4.33	4.65	4.71
303.3	2.02	-9.8	23.9	3.8	16.6	-4.9	-4.9	-4.8	0.00	0.21	0.23	0.24	3.52	3.81	3.98
296.3	2.09	-9.0	44.2	3.8	16.5	-4.9	-4.9	-4.9	0.00	0.35	0.37	0.38	4.25	4.53	4.73
298.6	2.00	-10.0	61.9	3.5	16.5	-6.3	-6.4	-6.4	0.00	0.49	0.51	0.52	4.77	5.08	5.09
296.8	1.96	-10.6	67.5	3.4	16.5	-7.3	-7.4	-7.4	0.00	0.67	0.69	0.71	5.65	5.86	5.86
303.8	1.94	-10.9	63.1	3.5	17.0	-6.4	-6.4	-6.4	0.00	0.46	0.48	0.50	3.82	4.02	4.15
299.0	2.03	-9.7	29.1	4.0	23.3	-3.8	-3.9	-3.6	0.00	0.23	0.25	0.28	4.24	4.71	4.72
298.8	1.96	-10.5	51.3	3.8	23.8	-4.9	-5.1	-4.9	0.00	0.36	0.39	0.41	4.53	5.02	5.06
298.6	2.03	-9.7	66.7	3.8	23.2	-4.2	-4.3	-4.2	0.00	0.48	0.51	0.54	4.46	4.85	4.90

Continued on next page.

Continued from previous page.

$\dot{m}$	p_s	T	Δp	p_c	$\bar{\dot{q}}$		T_w		$\widetilde{x}$		$\dot{x}$		α		
$\frac{kg}{m^2 s}$	bar	°C	mbar	bar	$\frac{kW}{m^2}$		°C		-		-		kW/m^{2}K		
						S1	S2	S3		S1	S2	S3	S1	S2	S3
300.5	2.00	-10.1	70.4	3.7	23.2	-4.7	-4.8	-4.8	0.00	0.56	0.58	0.61	4.67	5.02	5.09
301.4	2.09	-8.9	66.9	3.9	23.1	-4.0	-4.2	-4.1	0.00	0.55	0.58	0.60	5.18	5.64	5.67
302.6	1.97	-10.4	59.8	4.3	42.4	-2.5	-2.7	-2.4	0.00	0.37	0.42	0.46	6.41	7.00	7.00
304.1	2.06	-9.3	69.7	4.5	42.4	-1.1	-1.3	-1.0	0.00	0.46	0.51	0.56	6.05	6.61	6.61
298.0	2.02	-9.9	76.5	4.4	42.4	-1.8	-2.0	-1.7	0.00	0.64	0.68	0.73	6.10	6.70	6.67
297.1	2.04	-9.6	58.5	4.6	41.3	-1.0	-1.1	-0.9	0.00	0.69	0.74	0.78	5.44	5.92	6.06
							$\widetilde{\mathbf{z}} = \mathbf{0.10}$								
99.3	1.89	-20.8	7.0	3.2	10.5	-10.0	-9.1	-9.0	0.05	0.15	0.17	0.18	1.04	0.85	0.94
97.5	1.93	-17.7	9.0	3.3	10.5	-8.5	-8.1	-7.9	0.03	0.28	0.29	0.30	1.23	1.05	1.15
98.6	2.01	-15.1	11.1	3.4	10.4	-7.4	-7.1	-6.9	0.02	0.42	0.43	0.44	1.48	1.28	1.39
99.1	2.10	-12.8	13.9	3.4	10.8	-7.0	-6.7	-6.7	0.02	0.59	0.60	0.61	2.08	1.80	1.97
98.2	2.14	-11.7	14.5	3.5	10.4	-6.1	-5.6	-5.5	0.01	0.74	0.75	0.76	2.11	1.72	1.86
98.0	2.18	-10.9	14.0	3.8	10.8	-4.5	-3.9	-3.8	0.01	0.80	0.82	0.82	1.85	1.52	1.67
99.0	1.80	-22.0	6.9	2.6	2.0	-13.5	-13.3	-13.1	0.04	0.16	0.16	0.16	0.24	0.21	0.23
98.0	1.92	-21.1	11.8	4.4	44.9	-2.8	-2.2	-1.2	0.05	0.13	0.20	0.25	2.90	2.52	2.63
99.4	1.44	-27.1	9.0	2.6	10.1	-14.5	-14.2	-14.0	0.04	0.17	0.18	0.19	0.85	0.74	0.82
100.5	1.43	-25.9	9.7	2.5	10.1	-15.4	-15.1	-14.6	0.03	0.22	0.24	0.25	1.02	0.89	0.94
99.9	1.41	-24.1	12.2	2.4	10.1	-16.2	-16.1	-15.9	0.02	0.35	0.37	0.38	1.40	1.24	1.33
100.2	1.39	-23.1	17.0	2.2	10.1	-17.5	-17.4	-17.1	0.02	0.51	0.52	0.53	2.03	1.80	1.88
99.0	1.39	-22.2	19.9	2.2	10.1	-17.4	-17.2	-16.9	0.01	0.67	0.68	0.69	2.43	2.08	2.16
100.4	1.43	-21.1	18.8	2.3	10.1	-16.5	-15.8	-15.7	0.01	0.80	0.81	0.82	2.52	1.95	2.08
99.4	1.41	-21.1	16.6	2.8	10.2	-12.7	-11.4	-11.2	0.01	0.90	0.92	0.92	1.31	1.01	1.10
99.2	1.41	-21.2	15.6	3.3	10.2	-8.1	-6.8	-6.6	0.01	0.91	0.92	0.93	0.82	0.67	0.73
100.1	1.47	-26.7	9.3	2.8	16.8	-13.0	-12.5	-12.0	0.04	0.16	0.19	0.20	1.33	1.16	1.23
100.4	1.45	-24.3	12.8	2.8	16.7	-13.2	-12.6	-12.2	0.03	0.29	0.31	0.33	1.64	1.40	1.50
98.6	1.45	-22.6	16.1	2.7	16.9	-13.2	-13.0	-12.7	0.02	0.45	0.47	0.48	2.03	1.78	1.91
98.7	1.49	-21.1	19.7	2.8	16.7	-12.7	-12.6	-12.1	0.01	0.57	0.59	0.60	2.24	2.00	2.09
99.7	1.49	-20.5	19.1	2.9	16.7	-12.4	-11.2	-10.8	0.01	0.72	0.74	0.75	2.37	1.82	1.92
100.4	1.47	-20.5	17.4	3.5	17.1	-7.7	-5.5	-5.2	0.01	0.78	0.80	0.81	1.46	1.11	1.20
99.3	2.08	-14.7	11.0	3.8	10.0	-4.9	-4.4	-4.3	0.03	0.36	0.38	0.39	1.09	0.93	1.02
99.9	2.13	-12.9	12.6	3.6	9.9	-5.3	-5.0	-4.8	0.02	0.50	0.51	0.52	1.40	1.22	1.33
99.7	2.21	-11.2	14.1	3.6	9.7	-5.2	-4.9	-4.8	0.02	0.65	0.66	0.66	1.81	1.55	1.68
100.7	2.32	-9.4	14.3	3.9	10.2	-3.2	-2.6	-2.6	0.01	0.78	0.79	0.80	1.83	1.48	1.64
99.8	2.31	-9.2	10.6	5.7	10.2	6.7	7.8	7.8	0.01	0.91	0.92	0.93	0.67	0.56	0.63
100.3	1.97	-18.1	8.7	3.3	10.4	-7.9	-7.4	-7.2	0.04	0.23	0.24	0.25	1.09	0.93	1.02
98.7	1.90	-23.0	7.2	2.9	10.2	-11.2	-10.4	-10.3	0.06	0.08	0.10	0.11	0.91	0.77	0.85
200.9	1.98	-20.5	12.1	3.0	15.4	-11.3	-10.7	-10.4	0.05	0.13	0.14	0.15	1.87	1.57	1.68
199.1	2.03	-18.0	16.1	3.1	15.9	-10.4	-10.0	-9.7	0.04	0.20	0.21	0.21	2.39	2.02	2.16
198.5	2.11	-15.9	20.4	3.2	15.9	-8.8	-8.5	-8.2	0.03	0.25	0.26	0.27	2.57	2.21	2.36
201.0	2.16	-14.1	28.7	3.4	16.2	-6.8	-6.6	-6.3	0.03	0.34	0.35	0.35	2.56	2.26	2.38
198.8	2.21	-12.6	34.1	3.4	16.2	-6.5	-6.3	-6.0	0.02	0.42	0.43	0.44	3.12	2.75	2.88
200.2	2.06	-14.0	41.2	3.4	15.2	-7.9	-8.1	-7.6	0.02	0.48	0.49	0.50	2.91	2.74	2.80
199.4	2.11	-12.4	44.0	3.4	15.2	-7.7	-7.7	-7.5	0.02	0.66	0.67	0.67	4.02	3.65	3.79
198.0	1.45	-29.4	13.0	2.3	15.9	-17.5	-17.5	-16.8	0.06	0.10	0.11	0.12	1.46	1.32	1.37

Continued on next page.

Continued from previous page.

$\dot{m}$	p_s	T	Δp	p_c	$\bar{\dot{q}}$		T_w		$\widetilde{x}$		$\dot{x}$		α		
$\frac{kg}{m^2 s}$	bar	°C	mbar	bar	$\frac{kW}{m^2}$		°C		-		-		kW/m^{2}K		
						S1	S2	S3		S1	S2	S3	S1	S2	S3
198.7	1.41	-27.4	19.3	2.2	15.7	-18.6	-18.4	-17.5	0.04	0.17	0.18	0.19	1.99	1.75	1.76
199.9	1.43	-25.5	26.4	2.2	15.7	-18.0	-17.9	-17.2	0.03	0.24	0.25	0.26	2.38	2.11	2.12
199.7	1.45	-24.1	36.9	2.2	16.0	-17.4	-17.4	-16.9	0.03	0.30	0.31	0.32	2.79	2.48	2.56
198.2	1.47	-22.9	44.9	2.3	15.9	-16.6	-16.7	-16.3	0.02	0.39	0.40	0.40	3.02	2.77	2.82
197.7	1.46	-22.3	50.9	2.3	16.0	-16.6	-16.6	-16.2	0.02	0.46	0.46	0.47	3.38	3.08	3.13
199.0	1.48	-20.9	55.3	2.4	16.0	-16.0	-16.1	-15.6	0.01	0.63	0.64	0.64	4.03	3.73	3.71
197.5	1.49	-20.1	37.9	4.1	16.0	-3.1	-0.7	-0.8	0.01	0.82	0.82	0.83	1.00	0.79	0.88
199.0	1.97	-21.7	11.9	3.3	23.5	-9.2	-9.2	-8.3	0.06	0.10	0.11	0.13	2.11	1.90	1.96
198.9	2.04	-18.7	16.4	3.3	23.0	-8.6	-8.2	-7.7	0.05	0.16	0.18	0.19	2.64	2.28	2.39
200.0	2.10	-16.4	21.1	3.5	23.2	-7.2	-6.9	-6.4	0.04	0.23	0.25	0.26	2.97	2.59	2.70
198.2	2.04	-15.7	29.8	3.5	23.9	-7.0	-6.8	-6.3	0.03	0.32	0.33	0.34	3.32	2.90	3.03
201.9	2.00	-15.3	40.2	3.4	24.0	-7.0	-7.0	-6.5	0.02	0.40	0.42	0.43	3.51	3.15	3.27
198.1	2.04	-14.4	39.2	3.5	22.5	-6.7	-6.8	-6.4	0.02	0.45	0.47	0.47	3.58	3.29	3.39
200.4	2.03	-13.6	45.4	3.5	22.5	-6.8	-6.9	-6.5	0.02	0.59	0.61	0.62	4.09	3.79	3.89
198.9	2.09	-12.4	44.7	3.6	22.6	-5.9	-6.0	-5.6	0.02	0.68	0.69	0.70	4.39	4.07	4.15
299.9	1.47	-30.3	20.0	2.6	22.5	-17.0	-17.3	-16.1	0.07	0.07	0.08	0.09	1.87	1.74	1.75
299.6	1.49	-27.5	26.4	2.4	22.5	-18.2	-18.3	-17.5	0.05	0.13	0.14	0.15	2.86	2.59	2.62
298.6	1.48	-25.4	47.5	2.3	23.4	-18.3	-18.6	-18.0	0.03	0.21	0.22	0.23	4.10	3.88	3.88
300.2	1.51	-23.2	71.7	2.4	23.4	-17.6	-17.9	-17.4	0.03	0.30	0.31	0.31	5.51	5.44	5.30
298.9	1.55	-21.7	79.7	2.5	23.3	-16.3	-16.7	-16.2	0.02	0.37	0.38	0.39	5.88	5.88	5.77
299.3	1.54	-21.2	85.2	2.5	23.4	-15.9	-16.4	-15.9	0.02	0.45	0.46	0.46	6.16	6.28	6.06
299.9	1.45	-31.2	26.9	3.0	42.6	-12.3	-13.3	-11.8	0.07	0.06	0.08	0.10	2.62	2.52	2.54
300.1	1.47	-27.7	41.8	2.9	42.6	-12.8	-13.2	-12.2	0.05	0.13	0.15	0.17	3.48	3.23	3.30
298.7	1.52	-24.4	63.7	3.0	43.0	-12.0	-12.2	-11.6	0.03	0.23	0.25	0.26	4.40	4.03	4.23
299.0	1.57	-22.0	88.0	3.1	43.0	-11.0	-11.3	-11.0	0.02	0.33	0.34	0.35	5.10	4.74	5.09
299.8	1.58	-20.5	94.3	3.2	43.0	-10.6	-10.9	-10.8	0.02	0.46	0.48	0.49	5.91	5.60	6.06
298.7	1.56	-20.2	91.4	3.1	43.0	-10.7	-11.1	-11.0	0.02	0.54	0.56	0.57	6.25	6.05	6.51
299.1	1.41	-30.3	15.8	2.1	11.5	-19.3	-19.8	-19.0	0.06	0.09	0.10	0.10	1.12	1.06	1.08
300.2	1.43	-27.9	28.4	2.1	11.4	-19.6	-19.7	-19.1	0.04	0.14	0.15	0.15	1.49	1.35	1.40
299.0	1.47	-25.5	48.5	2.1	11.3	-19.2	-19.3	-18.8	0.03	0.21	0.22	0.22	2.01	1.83	1.88
301.6	1.50	-23.6	63.3	2.1	11.3	-18.4	-18.5	-18.1	0.03	0.28	0.29	0.29	2.52	2.31	2.35
298.2	1.55	-21.8	79.2	2.2	11.3	-17.4	-17.4	-17.1	0.02	0.37	0.37	0.38	3.02	2.79	2.85
299.3	1.53	-21.1	85.5	2.3	11.3	-17.1	-17.2	-16.9	0.02	0.47	0.48	0.48	3.35	3.18	3.22
299.6	2.12	-16.0	40.2	3.2	10.6	-10.1	-10.1	-9.8	0.04	0.25	0.25	0.25	2.02	1.83	1.91
299.3	2.23	-13.3	52.2	3.3	10.6	-8.8	-8.9	-8.6	0.03	0.33	0.34	0.34	2.79	2.55	2.64
298.8	2.16	-12.8	70.6	3.2	10.6	-9.1	-9.2	-8.9	0.02	0.47	0.48	0.48	3.38	3.15	3.27
299.2	2.19	-12.0	70.7	3.3	10.4	-8.5	-8.7	-8.5	0.02	0.55	0.55	0.56	3.70	3.49	3.60
300.3	2.00	-19.4	20.3	2.9	10.4	-12.0	-11.9	-11.6	0.05	0.15	0.16	0.16	1.53	1.37	1.45
299.6	2.00	-21.6	12.7	2.8	10.4	-12.1	-12.1	-11.7	0.06	0.08	0.09	0.09	1.19	1.06	1.14
100.1	2.40	-9.4	14.5	4.8	10.5	0.3	1.2	1.5	0.02	0.58	0.60	0.60	1.16	0.95	1.03
99.7	2.24	-12.2	13.2	4.1	10.4	-3.0	-2.3	-2.2	0.02	0.43	0.45	0.46	1.22	1.02	1.11
100.0	2.15	-14.8	10.5	3.9	10.4	-4.5	-3.9	-3.7	0.03	0.30	0.31	0.32	1.09	0.92	1.00
98.7	2.07	-17.5	9.4	3.7	10.4	-5.7	-4.9	-4.8	0.04	0.19	0.21	0.22	0.93	0.79	0.86
98.2	1.99	-21.6	7.3	3.5	10.5	-8.0	-6.8	-6.7	0.06	0.09	0.11	0.12	0.81	0.67	0.74

Continued on next page.

Continued from previous page.

$\dot{m}$	p_s	T	Δp	p_c	$\bar{\dot{q}}$	T_w			$\widetilde{x}$	$\dot{x}$			α		
$\frac{kg}{m^2 s}$	bar	°C	mbar	bar	$\frac{kW}{m^2}$	°C			-	-			kW/m^{2}K		
						S1	S2	S3		S1	S2	S3	S1	S2	S3
101.5	2.42	-8.7	14.3	4.4	10.4	-0.6	0.0	0.1	0.02	0.69	0.70	0.70	1.38	1.17	1.27
99.8	2.55	-6.8	11.6	6.1	10.4	7.6	9.2	9.7	0.01	0.85	0.86	0.87	0.76	0.61	0.66
202.3	2.20	-18.8	11.5	3.6	16.0	-6.4	-5.6	-5.5	0.06	0.09	0.10	0.11	1.40	1.18	1.29
199.2	2.17	-17.6	12.4	3.4	16.0	-8.2	-7.3	-7.3	0.05	0.15	0.16	0.17	1.90	1.56	1.72
200.5	2.28	-14.6	16.2	3.5	16.0	-6.9	-6.4	-6.2	0.04	0.22	0.23	0.24	2.40	2.01	2.18
200.1	2.36	-12.4	20.9	3.6	16.2	-5.8	-5.5	-5.3	0.03	0.29	0.30	0.31	2.88	2.46	2.64
199.1	2.54	-9.5	26.8	3.9	16.2	-3.4	-3.2	-3.0	0.03	0.38	0.39	0.40	3.17	2.75	2.93
202.3	2.63	-7.4	35.1	4.1	16.2	-2.2	-2.1	-1.9	0.02	0.52	0.53	0.54	3.82	3.41	3.59
198.6	2.44	-8.8	40.5	3.9	16.7	-3.6	-3.6	-3.3	0.02	0.63	0.64	0.65	4.00	3.65	3.78
199.0	2.40	-9.6	39.4	3.8	16.7	-4.2	-4.1	-3.8	0.02	0.57	0.58	0.58	3.79	3.40	3.54
199.4	1.50	-28.4	11.1	2.5	16.1	-15.7	-16.1	-15.4	0.05	0.10	0.11	0.12	1.38	1.29	1.35
198.7	1.51	-26.3	15.7	2.3	16.3	-16.8	-16.7	-16.2	0.04	0.15	0.16	0.17	1.90	1.71	1.79
198.2	1.52	-24.4	24.2	2.4	16.6	-16.3	-16.2	-15.8	0.03	0.22	0.23	0.24	2.37	2.09	2.20
197.4	1.54	-22.8	33.7	2.4	16.6	-16.0	-15.9	-15.6	0.03	0.30	0.31	0.32	2.86	2.56	2.68
201.1	1.56	-21.3	42.8	2.4	16.7	-15.5	-15.5	-15.2	0.02	0.40	0.40	0.41	3.46	3.14	3.26
199.4	1.97	-23.0	11.5	3.4	16.6	-9.5	-8.7	-8.6	0.07	0.06	0.07	0.08	1.33	1.13	1.24
199.9	2.02	-20.3	11.2	3.2	16.3	-11.5	-10.8	-10.6	0.05	0.12	0.13	0.14	2.10	1.73	1.88
199.8	2.00	-18.5	16.6	3.1	16.7	-11.7	-11.3	-11.1	0.04	0.19	0.20	0.21	2.94	2.45	2.63
201.4	1.94	-18.0	23.5	3.2	16.4	-10.1	-10.0	-9.4	0.03	0.26	0.27	0.27	2.38	2.14	2.17
198.9	1.99	-16.3	29.0	3.2	16.4	-10.0	-10.0	-9.7	0.03	0.33	0.34	0.35	3.11	2.78	2.93
201.4	1.97	-15.3	39.2	3.1	16.9	-10.1	-10.2	-9.9	0.02	0.44	0.45	0.46	4.03	3.72	3.85
197.8	1.96	-14.4	47.0	3.1	16.9	-9.9	-10.0	-9.7	0.02	0.61	0.62	0.62	4.86	4.47	4.60
201.3	1.96	-14.0	48.2	3.1	16.9	-9.4	-9.4	-9.2	0.01	0.70	0.71	0.72	4.79	4.33	4.45
202.0	1.95	-14.1	46.5	3.1	16.5	-9.5	-9.5	-9.2	0.01	0.70	0.71	0.72	4.59	4.18	4.31
200.3	1.47	-30.1	11.8	2.5	16.4	-15.4	-16.1	-15.3	0.06	0.07	0.09	0.10	1.20	1.14	1.19
199.8	1.47	-28.1	13.5	2.3	16.2	-18.0	-17.8	-17.4	0.05	0.12	0.14	0.14	1.78	1.58	1.67
199.6	1.51	-25.3	20.2	2.3	16.6	-17.3	-17.1	-16.7	0.04	0.19	0.20	0.21	2.39	2.08	2.19
197.8	1.48	-24.2	30.1	2.3	16.6	-17.3	-17.2	-16.8	0.03	0.27	0.28	0.29	2.80	2.50	2.61
200.5	1.50	-22.9	38.9	2.3	16.1	-17.0	-17.0	-16.7	0.02	0.34	0.35	0.36	3.30	2.97	3.09
199.2	1.51	-21.7	47.3	2.3	16.4	-16.5	-16.5	-16.2	0.02	0.44	0.45	0.46	3.84	3.52	3.63
201.6	1.52	-20.5	53.8	2.4	17.0	-15.6	-15.8	-15.3	0.01	0.60	0.60	0.61	4.35	4.13	4.12
198.6	1.52	-20.0	53.1	2.4	16.4	-15.6	-15.6	-15.3	0.01	0.71	0.72	0.72	4.84	4.45	4.46
199.7	1.51	-19.8	42.1	2.7	16.4	-14.3	-12.8	-12.2	0.01	0.81	0.82	0.82	3.62	2.48	2.47
298.8	1.51	-29.1	29.0	3.1	41.6	-12.3	-12.6	-11.5	0.06	0.08	0.10	0.12	2.92	2.68	2.77
299.6	1.59	-25.4	38.8	3.2	41.6	-11.5	-11.5	-10.9	0.05	0.14	0.16	0.18	3.66	3.29	3.48
299.2	1.56	-24.0	59.4	3.1	41.2	-11.6	-11.6	-11.3	0.03	0.21	0.23	0.24	4.16	3.76	4.04
299.1	1.57	-22.5	76.9	3.1	40.8	-11.3	-11.4	-11.2	0.03	0.28	0.30	0.31	4.67	4.25	4.59
300.3	1.56	-21.6	91.0	3.1	41.0	-11.2	-11.4	-11.3	0.02	0.38	0.39	0.40	5.17	4.78	5.26
298.3	1.56	-20.5	94.2	3.1	41.2	-10.9	-11.1	-11.1	0.02	0.49	0.51	0.52	5.75	5.39	5.91
298.0	1.61	-19.4	86.6	3.2	41.0	-10.2	-10.6	-10.3	0.02	0.57	0.58	0.59	6.19	5.90	6.19
301.1	1.60	-19.3	78.2	4.0	41.0	-6.9	-6.1	-2.6	0.01	0.58	0.60	0.61	4.12	3.44	2.88
299.7	1.50	-29.3	22.5	2.5	23.5	-16.3	-17.1	-16.1	0.06	0.08	0.09	0.10	2.03	1.95	1.99
299.2	1.51	-26.4	31.0	2.4	23.5	-16.8	-17.0	-16.5	0.04	0.15	0.16	0.17	2.86	2.66	2.75
298.9	1.54	-24.2	49.2	2.4	23.3	-16.3	-16.6	-16.1	0.03	0.22	0.23	0.24	3.61	3.38	3.49

Continued on next page.

Continued from previous page.

$\dot{m}$	p_s	T	Δp	p_c	$\bar{\dot{q}}$		T_w		$\widetilde{x}$		$\dot{x}$		α		
$\frac{kg}{m^2 s}$	bar	°C	mbar	bar	$\frac{kW}{m^2}$		°C		-		-		kW/m^{2}K		
						S1	S2	S3		S1	S2	S3	S1	S2	S3
300.5	1.55	-22.6	69.4	2.4	23.2	-16.1	-16.4	-16.0	0.03	0.31	0.32	0.32	4.61	4.41	4.50
299.6	1.55	-21.4	81.8	2.5	23.0	-15.8	-16.1	-15.7	0.02	0.40	0.41	0.42	5.43	5.35	5.40
299.4	1.56	-20.5	87.0	2.5	23.0	-15.4	-15.8	-15.4	0.02	0.49	0.50	0.51	6.14	6.15	6.12
299.4	1.61	-19.1	84.8	2.6	23.1	-14.0	-14.2	-13.9	0.01	0.61	0.62	0.62	6.11	5.89	6.01
299.8	1.97	-23.6	8.4	2.7	16.7	-13.0	-12.4	-12.2	0.08	0.04	0.05	0.06	1.73	1.47	1.60
299.9	2.13	-19.2	11.3	3.0	16.7	-10.7	-10.2	-10.0	0.06	0.11	0.12	0.12	2.24	1.90	2.06
299.6	2.08	-17.7	27.4	3.0	16.9	-10.6	-10.4	-10.1	0.04	0.18	0.19	0.20	2.80	2.44	2.59
300.7	2.05	-16.7	43.1	2.9	16.6	-10.7	-10.7	-10.4	0.03	0.25	0.26	0.26	3.31	3.00	3.15
300.1	2.10	-14.9	55.4	3.0	16.4	-9.9	-10.0	-9.7	0.03	0.33	0.34	0.34	4.07	3.74	3.92
298.8	2.00	-15.0	70.1	3.0	16.7	-10.5	-10.6	-10.4	0.02	0.44	0.45	0.45	4.69	4.42	4.56
298.7	2.03	-13.8	72.1	3.1	16.6	-9.6	-9.8	-9.6	0.02	0.56	0.57	0.57	5.36	5.12	5.23
300.1	1.51	-29.0	16.0	2.2	16.3	-19.1	-19.5	-18.9	0.06	0.08	0.09	0.10	1.82	1.72	1.79
299.8	1.48	-28.1	20.1	2.1	16.3	-19.8	-19.9	-19.4	0.05	0.12	0.13	0.13	2.23	2.02	2.11
299.3	1.51	-25.6	36.7	2.1	16.7	-19.1	-19.1	-18.7	0.04	0.18	0.19	0.19	3.10	2.78	2.88
299.1	1.53	-23.7	56.5	2.2	16.9	-18.6	-18.6	-18.3	0.03	0.26	0.27	0.27	4.12	3.78	3.85
298.1	1.56	-22.0	72.7	2.3	16.8	-17.7	-17.8	-17.5	0.02	0.34	0.35	0.35	5.02	4.67	4.74
300.1	1.56	-21.0	84.8	2.3	16.7	-17.2	-17.4	-17.1	0.02	0.43	0.44	0.45	5.99	5.78	5.85
299.3	1.56	-20.3	81.4	2.3	16.8	-16.6	-16.8	-16.5	0.02	0.54	0.55	0.55	6.25	6.11	6.20
300.0	1.61	-19.2	82.7	2.5	16.8	-15.0	-15.1	-14.9	0.01	0.59	0.60	0.60	5.26	4.93	5.08
300.2	1.62	-18.8	83.5	2.5	16.8	-15.0	-15.1	-15.0	0.01	0.66	0.66	0.67	6.14	5.71	6.00
98.8	1.99	-20.0	7.6	3.7	16.9	-5.7	-5.4	-5.2	0.05	0.14	0.16	0.18	1.27	1.12	1.22
99.6	2.04	-16.4	9.4	3.8	15.3	-4.9	-4.5	-4.3	0.03	0.28	0.30	0.31	1.46	1.26	1.37
99.1	2.06	-14.0	12.4	3.8	17.1	-4.1	-3.9	-3.6	0.02	0.46	0.48	0.50	1.92	1.70	1.83
98.8	1.98	-14.3	14.5	3.5	16.4	-6.3	-6.0	-5.7	0.02	0.60	0.62	0.63	2.38	2.03	2.18
98.9	1.96	-14.0	14.8	3.6	17.1	-6.1	-5.5	-5.4	0.01	0.68	0.70	0.71	2.49	2.07	2.23
99.6	1.94	-13.9	12.5	4.8	16.9	0.8	2.4	3.1	0.01	0.77	0.79	0.81	1.23	1.00	1.06
99.0	1.48	-27.1	8.1	2.7	16.6	-12.9	-12.4	-12.1	0.04	0.15	0.17	0.19	1.26	1.09	1.19
99.7	1.48	-24.1	10.7	2.8	16.6	-12.5	-12.1	-11.9	0.03	0.28	0.30	0.31	1.58	1.37	1.49
99.5	1.49	-22.0	15.0	2.7	16.9	-13.0	-12.9	-12.8	0.02	0.45	0.47	0.48	2.12	1.90	2.05
98.5	1.49	-20.7	17.2	2.7	16.9	-13.0	-12.6	-12.3	0.01	0.67	0.69	0.70	2.54	2.18	2.32
100.1	1.48	-20.4	17.1	2.8	16.9	-12.4	-11.3	-11.2	0.01	0.76	0.78	0.79	2.42	1.90	2.08
99.4	1.40	-29.6	5.7	2.4	10.7	-15.7	-14.5	-14.5	0.05	0.11	0.13	0.14	0.81	0.67	0.74
100.3	1.39	-26.9	7.9	2.4	10.7	-16.0	-15.0	-15.1	0.03	0.21	0.22	0.23	1.04	0.86	0.96
99.6	1.42	-23.6	11.9	2.3	10.7	-15.8	-15.6	-15.5	0.02	0.39	0.41	0.41	1.49	1.30	1.43
101.0	1.40	-22.6	16.4	2.2	10.8	-16.9	-16.8	-16.6	0.01	0.56	0.58	0.58	2.15	1.88	2.02
97.8	1.40	-21.8	17.2	2.3	10.8	-16.8	-16.4	-16.3	0.01	0.76	0.77	0.78	2.51	2.07	2.25
98.0	1.37	-21.8	14.3	2.9	10.9	-11.1	-9.8	-9.7	0.01	0.90	0.91	0.91	1.08	0.87	0.96
299.7	2.07	-21.4	16.0	3.3	23.2	-9.4	-9.7	-9.1	0.07	0.07	0.08	0.09	2.20	2.05	2.14
299.9	2.06	-19.1	19.2	3.2	20.6	-9.9	-9.8	-9.3	0.05	0.14	0.15	0.15	2.58	2.31	2.40
298.9	2.04	-17.4	35.8	3.2	23.3	-9.8	-9.8	-9.5	0.04	0.22	0.23	0.24	3.72	3.36	3.55
299.7	2.01	-16.7	49.5	3.2	23.2	-9.8	-9.9	-9.6	0.03	0.28	0.29	0.30	4.22	3.90	4.07
300.0	2.08	-14.8	59.7	3.3	23.0	-8.5	-8.7	-8.4	0.03	0.36	0.37	0.38	4.72	4.41	4.57
300.6	1.99	-14.9	73.4	3.2	23.1	-9.0	-9.3	-8.9	0.02	0.48	0.49	0.50	5.23	4.95	5.07
299.8	2.00	-22.3	19.9	3.8	40.6	-6.6	-6.3	-5.7	0.07	0.07	0.09	0.10	3.05	2.70	2.86

Continued on next page.

Continued from previous page.

$\dot{m}$	p_s	T	Δp	p_c	$\bar{\dot{q}}$		T_w		$\widetilde{x}$		$\dot{x}$		α		
$\frac{kg}{m^2 s}$	bar	°C	mbar	bar	$\frac{kW}{m^2}$		°C		-		-		kW/m^{2}K		
						S1	S2	S3		S1	S2	S3	S1	S2	S3
298.6	2.06	-18.1	36.3	3.9	41.4	-5.9	-5.5	-4.8	0.04	0.18	0.20	0.21	4.26	3.70	3.86
299.1	2.03	-16.6	56.1	3.9	41.4	-5.8	-5.5	-5.0	0.03	0.27	0.29	0.30	4.98	4.35	4.57
299.5	1.99	-15.9	76.1	3.9	41.3	-5.7	-5.7	-5.3	0.02	0.37	0.38	0.40	5.40	4.85	5.10
99.3	1.86	-23.2	7.3	3.1	10.5	-10.7	-9.5	-9.4	0.06	0.09	0.11	0.12	0.88	0.72	0.80
98.5	1.92	-19.1	8.2	3.2	10.5	-9.3	-8.7	-8.4	0.04	0.21	0.22	0.23	1.15	0.97	1.04
100.2	1.97	-16.3	10.2	3.4	10.5	-7.9	-7.5	-7.4	0.03	0.34	0.36	0.37	1.36	1.17	1.27
97.9	2.05	-13.8	12.4	3.4	10.6	-7.1	-6.8	-6.7	0.02	0.52	0.53	0.54	1.76	1.53	1.66
98.8	2.11	-12.4	14.7	3.5	10.3	-6.5	-6.2	-6.0	0.02	0.65	0.66	0.67	1.94	1.68	1.80
99.1	2.20	-10.7	13.7	3.8	10.4	-4.1	-3.5	-3.5	0.01	0.82	0.84	0.84	1.76	1.45	1.60
97.6	2.16	-10.8	11.0	5.7	10.9	6.8	7.8	7.8	0.01	0.94	0.95	0.96	0.64	0.55	0.61
99.6	1.85	-21.8	9.1	3.5	25.0	-7.3	-6.7	-6.1	0.05	0.14	0.18	0.20	1.92	1.66	1.77
98.4	1.78	-22.4	6.6	2.3	0.1	-16.1	-15.8	-15.7	0.05	0.15	0.15	0.15	0.02	0.02	0.02
98.9	1.43	-25.8	9.7	2.5	10.1	-15.2	-14.9	-14.6	0.03	0.23	0.24	0.25	1.02	0.88	0.96
99.7	1.43	-24.8	11.1	2.5	10.1	-15.5	-15.3	-15.0	0.03	0.29	0.30	0.31	1.17	1.03	1.11
100.1	1.40	-23.5	15.5	2.3	10.1	-17.0	-17.0	-16.7	0.02	0.43	0.45	0.45	1.72	1.54	1.63
99.9	1.39	-22.6	19.4	2.2	10.1	-17.6	-17.4	-17.1	0.01	0.58	0.59	0.60	2.26	1.99	2.06
99.6	1.43	-21.2	19.1	2.3	10.0	-17.0	-16.6	-16.4	0.01	0.76	0.77	0.78	2.76	2.23	2.35
99.4	1.42	-21.2	18.0	2.4	10.0	-15.8	-14.8	-14.7	0.01	0.81	0.82	0.83	2.10	1.55	1.69
99.4	1.41	-21.1	16.6	2.8	10.2	-12.7	-11.4	-11.2	0.01	0.90	0.92	0.92	1.31	1.01	1.10
99.6	1.47	-28.7	9.4	2.9	16.8	-12.8	-12.5	-11.8	0.05	0.10	0.13	0.15	1.12	1.00	1.06
100.8	1.46	-25.4	11.7	2.8	16.7	-13.2	-12.5	-11.9	0.03	0.23	0.25	0.26	1.50	1.28	1.34
99.7	1.45	-23.2	14.9	2.7	16.8	-12.9	-12.6	-12.3	0.02	0.38	0.40	0.41	1.81	1.58	1.70
99.5	1.46	-22.0	18.4	2.6	16.8	-13.5	-13.5	-13.1	0.02	0.51	0.53	0.54	2.25	2.00	2.12
100.1	1.49	-20.7	21.0	2.8	16.7	-12.9	-12.5	-12.1	0.01	0.65	0.67	0.68	2.47	2.09	2.19
99.3	1.48	-20.4	18.3	3.0	16.9	-11.8	-10.4	-10.2	0.01	0.78	0.80	0.81	2.25	1.71	1.84
100.4	1.47	-20.4	16.2	4.5	17.1	-0.1	1.5	1.5	0.01	0.84	0.86	0.87	0.89	0.74	0.82
99.7	2.10	-13.9	11.8	3.7	9.9	-5.0	-4.7	-4.6	0.02	0.43	0.44	0.45	1.21	1.05	1.14
98.4	2.16	-12.2	12.7	3.6	9.8	-5.3	-5.1	-5.0	0.02	0.57	0.58	0.59	1.57	1.37	1.49
99.3	2.29	-10.0	14.5	3.8	10.2	-4.1	-3.6	-3.5	0.01	0.74	0.75	0.76	1.94	1.60	1.74
100.7	2.31	-9.3	12.4	4.6	10.3	0.6	1.4	1.8	0.01	0.85	0.86	0.87	1.11	0.93	0.99
99.1	2.00	-16.9	10.0	3.5	10.4	-6.6	-6.0	-5.9	0.03	0.28	0.29	0.30	1.07	0.91	1.00
100.0	1.93	-20.6	7.5	3.1	10.6	-9.6	-9.0	-8.6	0.05	0.14	0.16	0.17	1.01	0.87	0.93
198.9	1.93	-22.1	10.2	3.1	15.6	-11.3	-10.7	-10.4	0.06	0.10	0.11	0.12	1.59	1.35	1.45
200.4	2.00	-19.2	13.5	3.0	15.5	-11.0	-10.5	-10.2	0.05	0.16	0.17	0.18	2.14	1.79	1.91
199.6	2.07	-17.0	18.0	3.1	15.9	-9.7	-9.4	-9.1	0.04	0.22	0.23	0.24	2.50	2.16	2.29
198.4	2.16	-14.9	23.5	3.3	15.9	-7.8	-7.6	-7.3	0.03	0.29	0.30	0.30	2.62	2.26	2.42
199.3	2.17	-13.5	32.0	3.4	16.0	-6.9	-6.7	-6.3	0.03	0.37	0.38	0.39	2.83	2.48	2.56
199.0	2.25	-12.2	33.4	3.5	16.2	-6.1	-6.0	-5.7	0.02	0.43	0.44	0.44	3.20	2.81	2.95
200.9	2.07	-13.4	43.8	3.3	15.2	-8.1	-8.3	-7.9	0.02	0.55	0.56	0.56	3.50	3.28	3.36
198.8	1.44	-31.0	9.9	2.4	15.8	-16.6	-16.8	-16.0	0.07	0.06	0.08	0.09	1.18	1.08	1.13
203.1	1.41	-28.4	15.6	2.2	15.9	-18.4	-18.2	-17.7	0.04	0.14	0.15	0.16	1.75	1.54	1.62
198.9	1.42	-26.3	22.6	2.2	15.6	-18.3	-18.1	-17.6	0.03	0.21	0.22	0.23	2.19	1.92	2.01
200.0	1.44	-24.8	33.9	2.2	15.8	-17.7	-17.7	-17.2	0.03	0.27	0.28	0.29	2.57	2.31	2.37
198.2	1.49	-23.0	41.0	2.3	15.8	-16.2	-16.3	-15.8	0.02	0.35	0.36	0.36	2.68	2.47	2.52

Continued on next page.

Continued from previous page.

$\dot{m}$	p_s	T	Δp	p_c	$\bar{\dot{q}}$	T_w			$\widetilde{x}$	$\dot{x}$			α		
$\frac{kg}{m^2 s}$	bar	°C	mbar	bar	$\frac{kW}{m^2}$	°C			-	-			kW/m^{2}K		
						S1	S2	S3		S1	S2	S3	S1	S2	S3
201.2	1.46	-22.5	49.7	2.3	16.1	-16.6	-16.7	-16.0	0.02	0.44	0.44	0.45	3.32	3.06	2.92
200.3	1.47	-21.8	54.7	2.3	16.0	-16.4	-16.5	-16.1	0.02	0.51	0.52	0.53	3.66	3.38	3.40
199.4	1.49	-20.5	53.4	2.4	16.0	-15.8	-15.8	-15.4	0.01	0.74	0.75	0.75	4.41	3.95	3.95
200.3	2.00	-22.8	13.6	3.5	23.7	-7.9	-8.3	-7.3	0.07	0.05	0.08	0.09	1.76	1.64	1.68
198.7	1.99	-20.3	13.3	3.3	23.3	-9.2	-8.8	-8.1	0.05	0.13	0.15	0.16	2.40	2.10	2.18
198.8	2.06	-17.4	17.4	3.4	23.0	-7.9	-7.6	-7.0	0.04	0.21	0.22	0.23	2.87	2.48	2.57
201.2	2.04	-16.1	27.3	3.5	24.1	-7.2	-6.9	-6.5	0.03	0.29	0.30	0.31	3.22	2.81	2.93
199.6	2.09	-14.7	33.3	3.6	23.9	-6.4	-6.2	-5.7	0.03	0.36	0.37	0.38	3.51	3.07	3.20
199.6	1.98	-15.5	39.5	3.4	23.9	-7.3	-7.3	-6.6	0.02	0.41	0.43	0.44	3.53	3.15	3.17
198.3	2.01	-14.3	45.1	3.5	22.4	-7.0	-7.2	-6.7	0.02	0.51	0.52	0.53	3.76	3.48	3.59
198.6	2.04	-13.3	47.1	3.5	22.5	-6.6	-6.7	-6.2	0.02	0.62	0.63	0.64	4.19	3.87	3.93
200.0	2.10	-12.5	46.0	3.6	22.7	-5.8	-6.0	-5.5	0.02	0.65	0.66	0.67	4.25	3.96	4.03
300.2	1.46	-29.0	22.4	2.5	22.4	-17.7	-17.9	-16.9	0.05	0.10	0.11	0.12	2.25	2.07	2.09
300.0	1.47	-26.6	40.8	2.3	23.4	-18.5	-18.7	-18.1	0.04	0.17	0.18	0.19	3.50	3.26	3.28
301.7	1.50	-24.2	62.1	2.4	23.3	-17.9	-18.3	-17.8	0.03	0.25	0.26	0.27	4.82	4.68	4.65
299.8	1.52	-22.7	75.9	2.4	23.3	-17.1	-17.5	-17.0	0.02	0.32	0.33	0.34	5.58	5.52	5.43
298.8	1.54	-21.4	84.8	2.5	23.3	-16.1	-16.5	-16.0	0.02	0.42	0.43	0.44	5.92	6.00	5.89
298.5	1.54	-21.0	86.0	2.5	23.5	-15.6	-16.0	-15.5	0.02	0.47	0.47	0.48	5.89	5.95	5.83
299.8	1.45	-29.4	32.4	2.9	42.5	-12.9	-13.4	-12.1	0.06	0.10	0.12	0.14	3.06	2.87	2.90
299.8	1.49	-25.9	55.0	3.0	43.0	-12.5	-12.8	-12.1	0.04	0.18	0.20	0.21	3.98	3.70	3.85
300.2	1.57	-22.5	77.4	3.1	42.9	-11.2	-11.5	-11.2	0.03	0.29	0.31	0.32	4.96	4.59	4.92
299.8	1.57	-21.3	92.6	3.1	42.4	-10.9	-11.3	-11.1	0.02	0.39	0.40	0.41	5.41	5.13	5.54
298.5	1.56	-20.4	92.7	3.2	42.9	-10.7	-11.1	-10.9	0.02	0.51	0.52	0.54	6.08	5.81	6.30
299.1	1.47	-30.8	19.6	2.5	11.4	-16.0	-16.8	-15.8	0.07	0.06	0.06	0.07	0.81	0.77	0.80
298.8	1.42	-29.1	21.5	2.1	11.5	-19.5	-19.7	-19.0	0.05	0.11	0.12	0.12	1.29	1.19	1.22
298.5	1.45	-26.6	41.8	2.1	11.3	-19.5	-19.6	-19.1	0.04	0.18	0.19	0.19	1.79	1.64	1.67
299.9	1.49	-24.5	57.5	2.1	11.3	-18.8	-18.9	-18.4	0.03	0.25	0.25	0.26	2.30	2.10	2.12
299.5	1.54	-22.5	70.2	2.2	11.3	-17.8	-17.9	-17.5	0.02	0.32	0.33	0.33	2.84	2.60	2.65
298.9	1.54	-21.3	82.3	2.3	11.3	-17.2	-17.3	-17.0	0.02	0.43	0.44	0.44	3.24	3.02	3.13
299.7	1.53	-20.8	83.8	2.3	11.5	-16.8	-17.0	-16.7	0.02	0.52	0.53	0.53	3.49	3.33	3.38
299.2	2.17	-14.9	44.9	3.2	10.6	-9.6	-9.7	-9.4	0.03	0.28	0.28	0.29	2.30	2.11	2.19
298.8	2.17	-13.3	62.0	3.2	10.4	-9.2	-9.3	-9.1	0.02	0.41	0.41	0.41	3.09	2.83	2.98
298.4	2.18	-12.1	71.3	3.3	10.5	-8.7	-8.8	-8.7	0.02	0.55	0.55	0.56	3.83	3.57	3.71
298.6	1.99	-18.5	29.6	2.9	10.4	-11.9	-11.9	-11.6	0.04	0.20	0.20	0.21	1.75	1.59	1.67
300.6	2.02	-20.1	15.6	2.9	10.4	-12.1	-12.0	-11.7	0.05	0.12	0.13	0.13	1.42	1.27	1.35
299.9	1.97	-23.4	8.2	2.8	10.5	-12.1	-12.2	-11.8	0.08	0.05	0.05	0.06	0.98	0.89	0.96
99.2	2.32	-10.7	13.5	4.4	10.4	-1.5	-0.6	-0.4	0.02	0.51	0.52	0.53	1.21	0.99	1.08
100.6	2.22	-13.1	11.4	4.1	10.4	-3.5	-2.7	-2.6	0.03	0.37	0.39	0.39	1.17	0.97	1.06
100.8	2.15	-15.7	9.6	3.8	10.4	-5.1	-4.3	-4.1	0.04	0.24	0.25	0.26	1.04	0.88	0.95
100.0	2.03	-19.6	8.0	3.6	10.4	-6.8	-6.0	-5.8	0.05	0.13	0.15	0.16	0.85	0.72	0.79
99.8	2.37	-9.4	13.5	4.3	10.4	-1.1	-0.8	-0.6	0.02	0.64	0.66	0.66	1.35	1.17	1.27
99.0	2.48	-7.6	12.6	4.8	10.4	1.5	2.3	2.5	0.01	0.80	0.81	0.82	1.22	1.01	1.09
99.1	2.53	-7.0	11.3	6.3	10.5	8.3	10.0	10.6	0.01	0.85	0.87	0.87	0.72	0.58	0.62
199.4	2.15	-18.6	13.2	3.5	16.0	-7.6	-6.7	-6.6	0.06	0.12	0.13	0.14	1.60	1.33	1.46

Continued on next page.

Continued from previous page.

$\dot{m}$	p_s	T	Δp	p_c	$\bar{\dot{q}}$		T_w		$\widetilde{x}$		$\dot{x}$		α		
$\frac{kg}{m^2 s}$	bar	°C	mbar	bar	$\frac{kW}{m^2}$		°C		-		-		kW/m^{2}K		
						S1	S2	S3		S1	S2	S3	S1	S2	S3
199.8	2.22	-16.2	12.8	3.4	14.3	-7.9	-7.2	-7.0	0.04	0.18	0.19	0.19	1.91	1.57	1.72
200.9	2.37	-13.1	16.2	3.5	16.0	-6.3	-5.9	-5.7	0.04	0.24	0.25	0.26	2.73	2.32	2.50
201.2	2.42	-11.2	24.7	3.7	16.2	-5.0	-4.8	-4.6	0.03	0.34	0.35	0.36	3.09	2.68	2.85
199.1	2.60	-8.4	28.5	4.0	16.2	-3.0	-2.8	-2.7	0.02	0.44	0.45	0.46	3.66	3.17	3.42
198.9	2.49	-8.0	39.8	4.0	16.7	-3.0	-3.0	-2.8	0.02	0.67	0.68	0.68	4.19	3.78	3.93
198.8	2.41	-9.2	40.5	3.8	16.7	-3.9	-3.9	-3.6	0.02	0.60	0.61	0.62	3.88	3.48	3.60
200.3	1.52	-28.9	12.7	2.8	16.3	-13.2	-13.8	-13.0	0.06	0.08	0.09	0.10	1.11	1.04	1.09
198.8	1.51	-27.3	14.3	2.4	16.1	-16.6	-16.6	-16.1	0.05	0.12	0.14	0.15	1.65	1.49	1.58
200.4	1.52	-25.2	19.3	2.3	16.2	-16.7	-16.6	-16.2	0.04	0.19	0.20	0.21	2.18	1.93	2.03
200.5	1.53	-23.5	27.9	2.4	16.6	-16.2	-16.0	-15.7	0.03	0.26	0.27	0.28	2.61	2.31	2.43
199.4	1.55	-21.9	37.3	2.4	16.7	-15.7	-15.7	-15.4	0.02	0.36	0.37	0.37	3.24	2.93	3.04
200.9	1.56	-21.1	46.0	2.4	16.6	-8.4	-8.5	-8.3	0.02	0.42	0.43	0.44	1.42	1.29	1.41
199.9	2.08	-20.3	9.5	3.3	16.5	-10.0	-9.3	-9.1	0.06	0.09	0.10	0.11	1.76	1.48	1.61
199.5	2.04	-19.2	11.7	3.1	16.2	-11.8	-11.0	-10.9	0.05	0.15	0.16	0.17	2.53	2.04	2.22
200.5	2.10	-16.5	19.1	3.5	16.6	-7.9	-7.6	-7.4	0.04	0.23	0.24	0.25	2.17	1.90	2.05
199.3	1.96	-17.2	25.4	3.2	16.4	-10.1	-10.0	-9.7	0.03	0.29	0.30	0.31	2.70	2.41	2.54
198.4	2.04	-15.1	31.1	3.2	16.4	-9.6	-9.6	-9.3	0.02	0.38	0.39	0.39	3.59	3.23	3.40
201.8	1.96	-14.9	44.5	3.1	16.8	-10.0	-10.1	-9.8	0.02	0.53	0.54	0.55	4.39	4.06	4.20
198.9	1.96	-14.3	46.9	3.1	16.7	-9.9	-10.0	-9.7	0.02	0.65	0.66	0.66	5.05	4.62	4.74
199.6	1.96	-13.9	46.1	3.2	17.1	-9.4	-9.4	-9.1	0.01	0.74	0.75	0.75	4.87	4.43	4.51
200.4	1.94	-14.0	45.2	3.1	16.4	-9.5	-9.5	-9.1	0.01	0.74	0.75	0.76	4.68	4.23	4.13
199.7	1.47	-28.9	14.6	2.4	16.4	-16.6	-17.0	-16.3	0.05	0.10	0.11	0.12	1.45	1.35	1.41
199.3	1.48	-26.8	15.0	2.2	16.2	-18.0	-17.8	-17.4	0.04	0.15	0.16	0.17	2.06	1.80	1.91
199.0	1.47	-25.0	23.4	2.3	16.6	-17.5	-17.4	-17.0	0.03	0.23	0.24	0.25	2.56	2.27	2.38
201.1	1.49	-23.6	32.8	2.3	16.3	-17.3	-17.3	-16.6	0.03	0.30	0.31	0.32	3.05	2.75	2.72
199.8	1.50	-22.3	42.9	2.3	16.0	-16.5	-16.6	-16.3	0.02	0.39	0.40	0.40	3.34	3.03	3.18
200.3	1.52	-20.9	52.9	2.4	17.0	-15.5	-15.7	-15.2	0.02	0.52	0.53	0.54	3.83	3.65	3.65
200.1	1.52	-20.3	53.0	2.4	16.6	-15.6	-15.7	-15.4	0.01	0.62	0.63	0.64	4.49	4.19	4.18
200.5	1.52	-19.8	51.7	2.4	16.4	-15.6	-15.7	-15.4	0.01	0.75	0.76	0.77	5.22	4.76	4.80
300.1	1.50	-29.8	22.4	3.3	41.7	-11.0	-11.5	-10.3	0.07	0.06	0.09	0.11	2.55	2.38	2.45
299.9	1.53	-27.2	36.6	3.1	41.4	-12.3	-12.4	-11.4	0.05	0.12	0.14	0.16	3.33	3.03	3.12
299.6	1.60	-24.3	49.6	3.2	41.4	-11.3	-11.3	-10.8	0.04	0.18	0.20	0.21	3.98	3.58	3.80
299.6	1.54	-23.5	69.1	3.1	41.0	-11.8	-11.9	-11.6	0.03	0.25	0.27	0.28	4.43	4.04	4.35
298.4	1.56	-22.1	84.7	3.1	41.1	-11.2	-11.3	-11.1	0.02	0.33	0.34	0.36	4.91	4.48	4.89
299.8	1.56	-21.2	96.6	3.1	41.0	-11.1	-11.3	-11.3	0.02	0.42	0.43	0.44	5.39	5.01	5.55
300.0	1.56	-20.3	90.2	3.1	41.0	-10.8	-11.2	-11.1	0.02	0.53	0.55	0.56	5.89	5.63	6.10
300.8	1.60	-19.3	72.1	4.6	41.0	-4.3	0.0	1.7	0.01	0.61	0.63	0.64	3.29	2.20	2.21
300.1	1.50	-30.2	18.9	2.7	22.9	-14.7	-15.9	-14.6	0.07	0.06	0.07	0.08	1.62	1.60	1.62
298.3	1.50	-28.1	24.8	2.4	23.5	-16.9	-17.3	-16.5	0.05	0.11	0.12	0.13	2.41	2.26	2.33
299.9	1.53	-25.2	40.2	2.4	23.6	-16.7	-16.9	-16.5	0.04	0.18	0.19	0.20	3.34	3.10	3.21
300.2	1.55	-23.2	58.5	2.4	23.1	-16.2	-16.5	-16.0	0.03	0.26	0.27	0.28	4.11	3.89	3.97
299.1	1.56	-21.9	74.7	2.5	23.1	-15.9	-16.2	-15.8	0.02	0.35	0.36	0.36	5.06	4.93	4.97
							$\widetilde{z} = 0.25$								
197.4	1.97	-28.6	9.8	2.1	16.0	-18.8	-18.6	-18.4	0.17	0.15	0.17	0.18	1.79	1.59	1.73

Continued on next page.

Continued from previous page.

$\dot{m}$	p_s	T	Δp	p_c	$\bar{\dot{q}}$		T_w		$\widetilde{x}$		$\dot{x}$		α		
$\frac{kg}{m^2 s}$	bar	°C	mbar	bar	$\frac{kW}{m^2}$		°C		-		-		kW/m^{2}K		
						S1	S2	S3		S1	S2	S3	S1	S2	S3
198.8	1.98	-26.5	17.5	2.1	16.1	-18.6	-18.1	-18.0	0.12	0.26	0.28	0.29	2.34	1.95	2.14
196.6	2.01	-23.5	30.2	2.3	16.1	-16.7	-16.2	-16.0	0.08	0.39	0.40	0.41	2.76	2.30	2.50
197.4	2.01	-21.3	40.3	2.4	16.3	-15.3	-14.9	-14.7	0.06	0.51	0.52	0.53	3.24	2.70	2.91
95.7	1.97	-28.7	4.5	2.5	16.4	-14.7	-14.1	-14.0	0.17	0.14	0.18	0.21	1.25	1.08	1.19
96.8	1.99	-26.2	5.8	2.8	16.4	-13.0	-12.0	-12.0	0.12	0.27	0.30	0.33	1.34	1.12	1.24
103.0	2.00	-23.1	9.7	2.9	16.2	-11.7	-10.9	-10.9	0.08	0.41	0.44	0.46	1.55	1.30	1.44
100.3	1.98	-20.8	12.3	2.9	16.1	-11.5	-11.1	-11.0	0.05	0.57	0.59	0.61	1.94	1.66	1.83
97.2	1.33	-38.7	10.0	1.8	16.2	-24.3	-22.8	-22.7	0.16	0.15	0.20	0.23	1.21	0.98	1.08
95.1	1.33	-36.2	8.0	1.7	16.0	-24.3	-22.7	-22.8	0.10	0.26	0.30	0.33	1.46	1.15	1.28
98.2	1.35	-32.2	13.0	1.9	16.2	-22.2	-21.4	-21.3	0.06	0.41	0.44	0.46	1.78	1.49	1.63
104.2	1.34	-30.2	18.6	1.9	16.1	-21.8	-21.4	-21.2	0.05	0.53	0.55	0.57	2.17	1.87	2.00
102.2	1.35	-27.8	20.3	2.0	16.6	-20.2	-19.5	-19.4	0.03	0.71	0.73	0.75	2.51	2.06	2.23
101.8	1.33	-27.4	17.6	3.5	16.7	-8.1	-6.1	-5.5	0.03	0.81	0.83	0.84	0.91	0.74	0.80
195.8	1.38	-37.9	13.0	1.4	16.0	-27.9	-28.1	-27.6	0.16	0.15	0.18	0.19	1.77	1.64	1.72
195.7	1.35	-36.0	28.1	1.5	16.7	-27.0	-26.9	-26.4	0.11	0.25	0.27	0.29	2.07	1.84	1.93
198.6	1.38	-32.8	43.9	1.6	16.9	-26.2	-25.6	-25.4	0.07	0.36	0.38	0.39	3.00	2.48	2.64
197.9	1.38	-30.3	53.1	1.7	16.6	-24.4	-24.1	-23.9	0.05	0.49	0.50	0.51	3.41	2.90	3.09
300.7	1.97	-29.3	15.4	2.2	22.7	-18.0	-18.6	-18.0	0.20	0.10	0.12	0.13	2.28	2.18	2.27
297.6	2.02	-27.4	24.2	2.2	23.6	-18.2	-18.2	-17.7	0.15	0.19	0.21	0.22	3.07	2.77	2.89
297.6	2.03	-25.0	51.7	2.3	23.6	-17.2	-17.3	-16.8	0.11	0.30	0.32	0.33	3.73	3.38	3.52
294.9	2.00	-23.2	66.3	2.4	23.6	-16.1	-16.1	-15.7	0.08	0.41	0.42	0.43	4.19	3.79	3.95
295.1	1.98	-21.5	76.6	2.5	22.8	-15.1	-15.2	-14.9	0.06	0.52	0.53	0.54	4.56	4.24	4.42
296.4	2.00	-19.2	74.1	2.7	23.3	-13.1	-13.4	-13.1	0.05	0.68	0.69	0.70	4.98	4.79	5.00
295.2	1.99	-18.9	58.3	4.2	40.8	-5.2	-2.4	-1.1	0.04	0.74	0.76	0.77	3.66	2.64	2.67
295.6	1.99	-20.4	80.8	3.2	40.4	-10.1	-10.1	-9.9	0.05	0.59	0.61	0.63	5.17	4.63	5.06
297.2	1.99	-22.2	81.6	3.1	40.4	-11.3	-11.3	-11.0	0.07	0.46	0.49	0.50	4.76	4.28	4.61
298.5	2.04	-23.7	67.4	3.0	40.8	-12.2	-12.0	-11.9	0.09	0.35	0.38	0.40	4.51	3.98	4.36
298.6	2.00	-26.5	47.2	2.9	41.3	-13.2	-13.1	-12.9	0.13	0.25	0.28	0.30	3.80	3.40	3.70
296.8	2.03	-28.0	22.2	3.0	41.0	-12.3	-12.5	-12.3	0.18	0.14	0.17	0.19	3.11	2.84	3.10
100.7	2.00	-27.7	5.7	2.5	16.4	-15.9	-14.8	-14.5	0.15	0.19	0.23	0.25	1.50	1.23	1.34
100.9	2.01	-24.5	7.8	2.8	16.7	-13.0	-11.9	-11.8	0.10	0.33	0.36	0.39	1.60	1.30	1.43
98.8	2.01	-21.4	11.5	2.9	16.7	-11.6	-10.9	-10.9	0.06	0.50	0.53	0.55	1.90	1.58	1.75
99.4	1.99	-19.6	12.9	3.0	16.3	-10.8	-10.4	-10.3	0.05	0.66	0.68	0.70	2.09	1.79	1.97
296.7	1.99	-29.1	9.9	2.1	16.4	-19.0	-18.9	-18.8	0.20	0.10	0.11	0.12	1.80	1.61	1.76
297.1	2.00	-27.6	22.1	2.0	16.4	-20.6	-20.3	-20.1	0.15	0.19	0.20	0.21	2.75	2.36	2.53
300.7	2.01	-25.1	48.5	2.0	16.6	-20.1	-19.9	-19.1	0.10	0.31	0.32	0.32	4.13	3.54	3.32
298.5	1.98	-23.6	65.6	2.2	16.0	-17.9	-17.8	-17.5	0.08	0.39	0.40	0.41	3.37	3.00	3.14
299.1	2.01	-21.3	75.6	2.3	15.9	-16.5	-16.5	-16.3	0.06	0.51	0.52	0.52	4.18	3.70	3.92
229.4	2.00	-24.5	37.1	2.6	15.8	-14.8	-14.4	-14.2	0.09	0.34	0.36	0.36	1.81	1.57	1.70
202.8	2.40	-24.0	7.3	2.8	16.7	-12.3	-12.6	-12.1	0.21	0.08	0.10	0.11	1.56	1.45	1.53
201.1	2.36	-23.0	10.5	2.7	16.9	-13.6	-13.3	-13.1	0.15	0.20	0.22	0.23	2.03	1.75	1.90
200.0	2.39	-20.4	21.3	2.7	16.7	-12.9	-12.6	-12.4	0.11	0.32	0.34	0.35	2.61	2.22	2.42
200.6	2.40	-18.3	29.7	2.8	16.5	-11.8	-11.6	-11.4	0.08	0.43	0.44	0.45	2.98	2.57	2.77
202.1	2.38	-16.5	35.1	3.0	16.4	-10.7	-10.5	-10.3	0.06	0.56	0.57	0.58	3.38	2.94	3.16

Continued on next page.

Continued from previous page.

$\dot{m}$	p_s	T	Δp	p_c	$\bar{\dot{q}}$	T_w			$\widetilde{x}$	$\dot{x}$			α		
$\frac{kg}{m^2 s}$	bar	°C	mbar	bar	$\frac{kW}{m^2}$	°C			-	-			kW/m^{2}K		
						S1	S2	S3		S1	S2	S3	S1	S2	S3
198.4	2.36	-15.2	42.0	3.1	16.6	-9.8	-9.7	-9.5	0.05	0.68	0.69	0.70	3.75	3.30	3.54
200.5	1.94	-29.0	8.5	2.1	17.1	-19.3	-19.8	-19.2	0.17	0.16	0.18	0.19	1.97	1.90	1.96
201.0	1.96	-26.7	17.6	2.2	16.9	-18.8	-18.5	-18.2	0.12	0.26	0.28	0.29	2.46	2.14	2.28
198.1	1.98	-23.9	32.5	2.3	16.9	-17.3	-17.1	-16.8	0.08	0.38	0.40	0.41	3.08	2.64	2.81
200.7	1.98	-21.8	40.3	2.4	16.9	-15.8	-15.7	-15.4	0.06	0.50	0.51	0.52	3.46	3.00	3.17
196.5	2.00	-28.7	11.2	2.3	16.3	-16.8	-17.0	-16.7	0.19	0.11	0.13	0.14	1.49	1.36	1.48
196.0	1.99	-27.5	12.4	2.1	16.2	-18.9	-18.4	-18.4	0.14	0.21	0.23	0.24	2.15	1.82	2.00
200.1	1.99	-24.9	25.4	2.2	16.0	-17.8	-17.3	-17.2	0.10	0.32	0.34	0.35	2.61	2.16	2.37
200.5	1.99	-22.7	36.3	2.3	16.3	-16.3	-15.8	-15.7	0.07	0.44	0.46	0.47	3.00	2.50	2.70
195.7	2.01	-20.4	42.5	2.5	16.2	-14.7	-14.4	-14.3	0.05	0.58	0.59	0.60	3.43	2.91	3.14
98.8	2.00	-27.2	4.8	2.6	16.5	-13.9	-13.1	-13.1	0.14	0.21	0.25	0.28	1.34	1.13	1.26
96.1	1.98	-24.3	7.4	2.9	16.4	-11.4	-10.5	-10.5	0.09	0.36	0.39	0.41	1.38	1.16	1.28
101.3	1.99	-22.0	10.7	2.9	16.0	-11.8	-11.2	-11.2	0.07	0.48	0.51	0.53	1.73	1.47	1.63
100.0	1.99	-19.5	13.0	2.9	16.2	-11.0	-10.5	-10.5	0.05	0.66	0.69	0.70	2.13	1.82	2.00
99.9	1.32	-37.9	7.3	1.6	16.2	-25.6	-24.3	-24.3	0.13	0.19	0.24	0.27	1.42	1.15	1.28
100.7	1.34	-34.5	10.7	1.8	15.9	-23.5	-22.4	-22.4	0.08	0.32	0.35	0.38	1.58	1.28	1.42
96.8	1.34	-30.8	16.4	1.9	16.3	-21.4	-20.8	-20.7	0.05	0.49	0.52	0.54	1.93	1.64	1.78
102.6	1.34	-28.9	20.3	1.9	16.2	-21.0	-20.5	-20.3	0.04	0.63	0.65	0.67	2.37	1.99	2.14
101.8	1.33	-27.4	17.6	3.5	16.7	-8.1	-6.1	-5.5	0.03	0.81	0.83	0.84	0.91	0.74	0.80
195.8	1.38	-37.9	13.0	1.4	16.0	-27.9	-28.1	-27.6	0.16	0.15	0.18	0.19	1.77	1.64	1.72
195.7	1.35	-36.0	28.1	1.5	16.7	-27.0	-26.9	-26.4	0.11	0.25	0.27	0.29	2.07	1.84	1.93
198.6	1.38	-32.8	43.9	1.6	16.9	-26.2	-25.6	-25.4	0.07	0.36	0.38	0.39	3.00	2.48	2.64
197.9	1.38	-30.3	53.1	1.7	16.6	-24.4	-24.1	-23.9	0.05	0.49	0.50	0.51	3.41	2.90	3.09
300.7	1.97	-29.3	15.4	2.2	22.7	-18.0	-18.6	-18.0	0.20	0.10	0.12	0.13	2.28	2.18	2.27
297.6	2.02	-27.4	24.2	2.2	23.6	-18.2	-18.2	-17.7	0.15	0.19	0.21	0.22	3.07	2.77	2.89
297.6	2.03	-25.0	51.7	2.3	23.6	-17.2	-17.3	-16.8	0.11	0.30	0.32	0.33	3.73	3.38	3.52
294.9	2.00	-23.2	66.3	2.4	23.6	-16.1	-16.1	-15.7	0.08	0.41	0.42	0.43	4.19	3.79	3.95
295.1	1.98	-21.5	76.6	2.5	22.8	-15.1	-15.2	-14.9	0.06	0.52	0.53	0.54	4.56	4.24	4.42
296.4	2.00	-19.2	74.1	2.7	23.3	-13.1	-13.4	-13.1	0.05	0.68	0.69	0.70	4.98	4.79	5.00
295.2	1.99	-18.9	58.3	4.2	40.8	-5.2	-2.4	-1.1	0.04	0.74	0.76	0.77	3.66	2.64	2.67
295.6	1.99	-20.4	80.8	3.2	40.4	-10.1	-10.1	-9.9	0.05	0.59	0.61	0.63	5.17	4.63	5.06
297.2	1.99	-22.2	81.6	3.1	40.4	-11.3	-11.3	-11.0	0.07	0.46	0.49	0.50	4.76	4.28	4.61
298.5	2.04	-23.7	67.4	3.0	40.8	-12.2	-12.0	-11.9	0.09	0.35	0.38	0.40	4.51	3.98	4.36
298.6	2.00	-26.5	47.2	2.9	41.3	-13.2	-13.1	-12.9	0.13	0.25	0.28	0.30	3.80	3.40	3.70
296.8	2.03	-28.0	22.2	3.0	41.0	-12.3	-12.5	-12.3	0.18	0.14	0.17	0.19	3.11	2.84	3.10
100.7	2.00	-27.7	5.7	2.5	16.4	-15.9	-14.8	-14.5	0.15	0.19	0.23	0.25	1.50	1.23	1.34
100.9	2.01	-24.5	7.8	2.8	16.7	-13.0	-11.9	-11.8	0.10	0.33	0.36	0.39	1.60	1.30	1.43
98.8	2.01	-21.4	11.5	2.9	16.7	-11.6	-10.9	-10.9	0.06	0.50	0.53	0.55	1.90	1.58	1.75
99.4	1.99	-19.6	12.9	3.0	16.3	-10.8	-10.4	-10.3	0.05	0.66	0.68	0.70	2.09	1.79	1.97
296.7	1.99	-29.1	9.9	2.1	16.4	-19.0	-18.9	-18.8	0.20	0.10	0.11	0.12	1.80	1.61	1.76
297.1	2.00	-27.6	22.1	2.0	16.4	-20.6	-20.3	-20.1	0.15	0.19	0.20	0.21	2.75	2.36	2.53
300.7	2.01	-25.1	48.5	2.0	16.6	-20.1	-19.9	-19.1	0.10	0.31	0.32	0.32	4.13	3.54	3.32
298.5	1.98	-23.6	65.6	2.2	16.0	-17.9	-17.8	-17.5	0.08	0.39	0.40	0.41	3.37	3.00	3.14
299.1	2.01	-21.3	75.6	2.3	15.9	-16.5	-16.5	-16.3	0.06	0.51	0.52	0.52	4.18	3.70	3.92

Continued on next page.

Continued from previous page.

$\dot{m}$	p_s	T	Δp	p_c	$\bar{\dot{q}}$		T_w		$\widetilde{x}$	$\dot{x}$			α		
$\frac{kg}{m^2 s}$	bar	°C	mbar	bar	$\frac{kW}{m^2}$		°C		-	-			kW/m^{2}K		
						S1	S2	S3		S1	S2	S3	S1	S2	S3
229.4	2.00	-24.5	37.1	2.6	15.8	-14.8	-14.4	-14.2	0.09	0.34	0.36	0.36	1.81	1.57	1.70
202.8	2.40	-24.0	7.3	2.8	16.7	-12.3	-12.6	-12.1	0.21	0.08	0.10	0.11	1.56	1.45	1.53
201.1	2.36	-23.0	10.5	2.7	16.9	-13.6	-13.3	-13.1	0.15	0.20	0.22	0.23	2.03	1.75	1.90
200.0	2.39	-20.4	21.3	2.7	16.7	-12.9	-12.6	-12.4	0.11	0.32	0.34	0.35	2.61	2.22	2.42
200.6	2.40	-18.3	29.7	2.8	16.5	-11.8	-11.6	-11.4	0.08	0.43	0.44	0.45	2.98	2.57	2.77
202.1	2.38	-16.5	35.1	3.0	16.4	-10.7	-10.5	-10.3	0.06	0.56	0.57	0.58	3.38	2.94	3.16
198.4	2.36	-15.2	42.0	3.1	16.6	-9.8	-9.7	-9.5	0.05	0.68	0.69	0.70	3.75	3.30	3.54
200.5	1.94	-29.0	8.5	2.1	17.1	-19.3	-19.8	-19.2	0.17	0.16	0.18	0.19	1.97	1.90	1.96
201.0	1.96	-26.7	17.6	2.2	16.9	-18.8	-18.5	-18.2	0.12	0.26	0.28	0.29	2.46	2.14	2.28
198.1	1.98	-23.9	32.5	2.3	16.9	-17.3	-17.1	-16.8	0.08	0.38	0.40	0.41	3.08	2.64	2.81
							$\widetilde{\mathbf{z}} = \mathbf{0.40}$								
202.8	2.04	-29.2	10.9	2.0	16.3	-20.4	-20.7	-20.4	0.33	0.23	0.25	0.26	2.11	1.98	2.09
197.0	2.06	-28.4	20.5	2.0	16.2	-20.7	-20.7	-20.3	0.26	0.37	0.38	0.39	2.41	2.17	2.28
199.0	2.04	-27.5	30.7	1.9	16.2	-21.0	-20.8	-20.5	0.18	0.50	0.52	0.54	2.93	2.57	2.68
198.5	2.05	-25.8	37.3	2.0	16.2	-19.9	-19.6	-19.3	0.13	0.63	0.65	0.66	3.27	2.78	2.93
201.7	2.06	-23.5	45.2	2.2	16.2	-18.0	-17.6	-17.4	0.09	0.79	0.80	0.81	3.57	2.98	3.16
204.4	2.05	-20.9	40.7	2.4	15.9	-15.3	-15.3	-15.1	0.10	0.77	0.79	0.80	3.45	3.10	3.26
203.2	2.31	-25.8	13.6	2.2	16.2	-17.7	-17.7	-17.4	0.31	0.27	0.29	0.30	2.28	2.04	2.19
205.6	2.30	-25.3	19.8	2.2	16.2	-18.0	-17.8	-17.6	0.25	0.40	0.41	0.42	2.57	2.25	2.41
206.0	2.47	-22.5	30.8	2.4	16.2	-16.1	-15.8	-15.0	0.19	0.53	0.54	0.55	3.03	2.59	2.50
205.7	2.47	-20.5	40.0	2.5	16.2	-14.8	-14.5	-14.3	0.13	0.68	0.70	0.71	3.42	2.88	3.08
200.8	2.48	-18.4	39.3	2.7	16.3	-12.8	-12.5	-12.3	0.09	0.85	0.87	0.88	3.54	3.04	3.23
298.3	2.04	-30.0	9.8	2.1	16.3	-19.9	-20.5	-20.0	0.47	0.01	0.01	0.02	1.78	1.72	1.81
297.6	2.04	-28.7	35.0	1.8	16.3	-22.6	-23.0	-22.5	0.27	0.35	0.37	0.37	3.18	3.12	3.12
300.1	2.05	-27.9	51.4	1.8	16.0	-23.2	-23.4	-22.9	0.21	0.44	0.46	0.46	4.22	4.00	3.98
300.8	2.07	-26.2	66.7	1.9	16.0	-22.1	-22.0	-21.7	0.15	0.58	0.59	0.60	5.17	4.44	4.55
301.6	2.07	-24.5	76.4	2.0	16.1	-20.3	-20.1	-19.8	0.11	0.70	0.71	0.72	4.98	4.17	4.29
296.8	2.07	-22.7	72.7	2.2	16.0	-18.2	-18.0	-17.8	0.08	0.85	0.86	0.86	4.56	3.93	4.14
301.1	2.06	-29.8	16.5	2.3	23.7	-17.5	-18.7	-17.9	0.47	0.01	0.02	0.02	2.19	2.22	2.26
303.4	2.06	-28.7	40.8	2.0	23.7	-20.5	-21.2	-20.6	0.31	0.27	0.29	0.30	3.48	3.53	3.52
300.9	2.09	-27.6	56.8	2.0	23.7	-20.8	-21.3	-20.7	0.22	0.43	0.45	0.46	4.43	4.43	4.39
298.7	2.10	-26.1	72.1	2.1	23.7	-19.8	-19.9	-19.4	0.16	0.56	0.58	0.59	4.85	4.43	4.47
297.1	2.10	-24.5	76.1	2.2	23.7	-18.3	-18.1	-17.8	0.11	0.69	0.70	0.72	5.03	4.38	4.51
97.9	2.04	-29.3	7.8	2.4	16.2	-16.0	-16.6	-15.9	0.35	0.18	0.21	0.22	1.32	1.25	1.31
103.5	2.05	-28.2	9.1	2.2	16.2	-18.3	-18.1	-17.6	0.23	0.41	0.45	0.47	1.81	1.61	1.69
102.8	2.03	-26.8	11.0	2.4	16.2	-16.9	-16.3	-16.1	0.15	0.58	0.61	0.64	1.83	1.55	1.67
102.0	2.02	-24.6	13.1	2.5	16.2	-15.7	-15.2	-15.0	0.10	0.74	0.77	0.80	2.06	1.75	1.90
300.5	2.07	-29.5	20.3	2.8	41.6	-14.1	-15.6	-14.2	0.43	0.01	0.03	0.04	3.24	3.30	3.26
297.9	2.09	-28.0	61.3	2.5	41.8	-16.5	-17.1	-16.4	0.27	0.36	0.38	0.40	4.66	4.48	4.61
289.3	2.12	-26.3	74.9	2.7	41.8	-15.0	-15.1	-13.8	0.17	0.53	0.56	0.58	4.78	4.32	4.20
292.5	2.11	-24.7	78.6	2.8	41.7	-13.6	-13.6	-13.0	0.12	0.66	0.69	0.71	4.86	4.38	4.55
287.3	2.12	-22.9	72.7	3.0	40.9	-10.3	-10.3	-10.0	0.10	0.79	0.81	0.83	4.03	3.66	3.93
202.8	2.04	-29.2	10.9	2.0	16.3	-20.4	-20.7	-20.4	0.33	0.23	0.25	0.26	2.11	1.98	2.09
197.0	2.06	-28.4	20.5	2.0	16.2	-20.7	-20.7	-20.3	0.26	0.37	0.38	0.39	2.41	2.17	2.28

Continued on next page.

Continued from previous page.

$\dot{m}$	p_s	T	Δp	p_c	$\bar{\dot{q}}$	T_w			$\widetilde{x}$	$\dot{x}$			α		
$\frac{kg}{m^2 s}$	bar	°C	mbar	bar	$\frac{kW}{m^2}$	°C			-	-			kW/m^{2}K		
						S1	S2	S3		S1	S2	S3	S1	S2	S3
199.0	2.04	-27.5	30.7	1.9	16.2	-21.0	-20.8	-20.5	0.18	0.50	0.52	0.54	2.93	2.57	2.68
198.5	2.05	-25.8	37.3	2.0	16.2	-19.9	-19.6	-19.3	0.13	0.63	0.65	0.66	3.27	2.78	2.93
201.7	2.06	-23.5	45.2	2.2	16.2	-18.0	-17.6	-17.4	0.09	0.79	0.80	0.81	3.57	2.98	3.16
204.4	2.05	-20.9	40.7	2.4	15.9	-15.3	-15.3	-15.1	0.10	0.77	0.79	0.80	3.45	3.10	3.26
203.2	2.31	-25.8	13.6	2.2	16.2	-17.7	-17.7	-17.4	0.31	0.27	0.29	0.30	2.28	2.04	2.19
205.6	2.30	-25.3	19.8	2.2	16.2	-18.0	-17.8	-17.6	0.25	0.40	0.41	0.42	2.57	2.25	2.41
206.0	2.47	-22.5	30.8	2.4	16.2	-16.1	-15.8	-15.0	0.19	0.53	0.54	0.55	3.03	2.59	2.50
205.7	2.47	-20.5	40.0	2.5	16.2	-14.8	-14.5	-14.3	0.13	0.68	0.70	0.71	3.42	2.88	3.08
200.8	2.48	-18.4	39.3	2.7	16.3	-12.8	-12.5	-12.3	0.09	0.85	0.87	0.88	3.54	3.04	3.23
298.3	2.04	-30.0	9.8	2.1	16.3	-19.9	-20.5	-20.0	0.47	0.01	0.01	0.02	1.78	1.72	1.81
297.6	2.04	-28.7	35.0	1.8	16.3	-22.6	-23.0	-22.5	0.27	0.35	0.37	0.37	3.18	3.12	3.12
300.1	2.05	-27.9	51.4	1.8	16.0	-23.2	-23.4	-22.9	0.21	0.44	0.46	0.46	4.22	4.00	3.98
300.8	2.07	-26.2	66.7	1.9	16.0	-22.1	-22.0	-21.7	0.15	0.58	0.59	0.60	5.17	4.44	4.55
301.6	2.07	-24.5	76.4	2.0	16.1	-20.3	-20.1	-19.8	0.11	0.70	0.71	0.72	4.98	4.17	4.29
296.8	2.07	-22.7	72.7	2.2	16.0	-18.2	-18.0	-17.8	0.08	0.85	0.86	0.86	4.56	3.93	4.14
301.1	2.06	-29.8	16.5	2.3	23.7	-17.5	-18.7	-17.9	0.47	0.01	0.02	0.02	2.19	2.22	2.26
303.4	2.06	-28.7	40.8	2.0	23.7	-20.5	-21.2	-20.6	0.31	0.27	0.29	0.30	3.48	3.53	3.52
300.9	2.09	-27.6	56.8	2.0	23.7	-20.8	-21.3	-20.7	0.22	0.43	0.45	0.46	4.43	4.43	4.39
298.7	2.10	-26.1	72.1	2.1	23.7	-19.8	-19.9	-19.4	0.16	0.56	0.58	0.59	4.85	4.43	4.47
297.1	2.10	-24.5	76.1	2.2	23.7	-18.3	-18.1	-17.8	0.11	0.69	0.70	0.72	5.03	4.38	4.51
97.9	2.04	-29.3	7.8	2.4	16.2	-16.0	-16.6	-15.9	0.35	0.18	0.21	0.22	1.32	1.25	1.31
103.5	2.05	-28.2	9.1	2.2	16.2	-18.3	-18.1	-17.6	0.23	0.41	0.45	0.47	1.81	1.61	1.69
102.8	2.03	-26.8	11.0	2.4	16.2	-16.9	-16.3	-16.1	0.15	0.58	0.61	0.64	1.83	1.55	1.67
102.0	2.02	-24.6	13.1	2.5	16.2	-15.7	-15.2	-15.0	0.10	0.74	0.77	0.80	2.06	1.75	1.90
300.5	2.07	-29.5	20.3	2.8	41.6	-14.1	-15.6	-14.2	0.43	0.01	0.03	0.04	3.24	3.30	3.26
						$\widetilde{z} = 0.65$ (Azeotropic point)									
202.2	2.12	-28.9	54.4	1.6	16.6	-24.5	-25.0	-24.6	0.65	0.31	0.32	0.32	4.87	5.15	5.04
198.6	2.10	-29.0	54.4	1.6	16.6	-25.1	-25.5	-25.1	0.65	0.90	0.91	0.91	5.79	5.96	5.70
205.1	2.10	-29.4	51.0	1.6	17.4	-24.7	-25.1	-24.8	0.65	0.62	0.62	0.63	4.77	4.83	4.93
198.0	2.09	-29.4	40.4	1.6	17.4	-24.5	-24.8	-24.5	0.65	0.50	0.51	0.51	4.48	4.41	4.50
200.5	2.06	-30.1	13.6	1.7	17.4	-23.3	-23.3	-22.9	0.65	0.21	0.22	0.23	2.98	2.69	2.79
103.3	2.08	-29.7	5.4	1.8	16.0	-22.7	-22.8	-22.2	0.65	0.23	0.24	0.25	2.63	2.43	2.46
102.2	2.07	-29.5	11.5	1.8	16.0	-23.0	-23.1	-22.7	0.65	0.48	0.49	0.50	2.89	2.66	2.74
100.8	2.08	-29.4	16.3	1.7	16.0	-23.7	-23.8	-23.5	0.65	0.73	0.75	0.75	3.38	3.17	3.26
202.9	2.32	-27.4	6.2	2.1	16.0	-20.2	-20.3	-19.8	0.65	0.05	0.06	0.06	2.54	2.35	2.40
197.9	2.35	-26.4	31.6	1.9	16.0	-21.4	-21.7	-21.3	0.65	0.43	0.44	0.44	4.04	3.91	3.94
198.4	2.47	-24.9	42.4	1.9	16.0	-20.9	-21.0	-20.8	0.65	0.63	0.64	0.64	5.18	4.85	4.95
200.1	2.45	-24.9	49.7	1.9	16.0	-21.4	-21.5	-21.2	0.65	0.85	0.85	0.86	6.11	5.81	5.80
233.8	2.08	-30.6	7.6	1.8	16.3	-22.8	-22.8	-22.3	0.65	0.06	0.07	0.07	2.40	2.16	2.24
229.1	2.12	-29.2	21.3	1.7	16.2	-23.3	-23.5	-23.2	0.65	0.25	0.26	0.26	3.28	3.09	3.21
206.9	2.17	-28.3	52.1	1.6	16.2	-24.3	-24.5	-24.3	0.65	0.68	0.69	0.69	5.45	5.33	5.44
202.1	2.09	-29.6	29.0	2.2	23.9	-19.4	-20.9	-19.9	0.65	0.21	0.22	0.22	2.72	2.98	2.89
198.5	2.13	-29.0	55.0	1.9	24.1	-22.4	-23.5	-23.0	0.65	0.73	0.74	0.75	4.73	5.46	5.37
206.5	2.09	-29.4	62.7	2.1	41.1	-21.0	-21.8	-21.9	0.65	0.87	0.88	0.89	6.94	7.28	8.26

Continued on next page.

Continued from previous page.

$\dot{m}$	p_s	T	Δp	p_c	$\bar{\dot{q}}$		T_w		$\widetilde{x}$		$\dot{x}$		α		
$\frac{kg}{m^2 s}$	bar	°C	mbar	bar	$\frac{kW}{m^2}$		°C		-		-		kW/m^{2}K		
						S1	S2	S3		S1	S2	S3	S1	S2	S3
202.1	2.08	-29.5	56.5	2.1	40.9	-20.6	-21.4	-21.4	0.65	0.64	0.66	0.67	6.33	6.61	7.26
203.5	2.06	-30.0	31.6	2.2	40.9	-19.3	-20.2	-19.9	0.65	0.37	0.38	0.39	5.00	5.09	5.43
200.4	2.04	-31.3	17.2	2.3	40.9	-19.6	-20.0	-19.5	0.65	0.15	0.16	0.17	4.47	4.22	4.41
104.1	2.09	-29.8	2.5	1.6	3.1	-24.2	-24.2	-23.9	0.65	0.04	0.05	0.05	0.58	0.52	0.55
104.0	2.09	-29.9	3.5	1.9	16.9	-22.1	-22.1	-21.8	0.65	0.12	0.14	0.14	2.49	2.27	2.39
103.3	2.09	-29.8	6.3	2.1	31.3	-19.9	-20.2	-19.6	0.65	0.22	0.24	0.26	3.91	3.67	3.79
202.2	2.12	-28.9	54.4	1.6	16.6	-24.5	-25.0	-24.6	0.65	0.72	0.73	0.73	4.87	5.15	5.04
198.6	2.10	-29.0	54.4	1.6	16.6	-25.1	-25.5	-25.1	0.65	0.90	0.91	0.91	5.79	5.96	5.70
205.1	2.10	-29.4	51.0	1.6	17.4	-24.7	-25.1	-24.8	0.65	0.62	0.62	0.63	4.77	4.83	4.93
198.0	2.09	-29.4	40.4	1.6	17.4	-24.5	-24.8	-24.5	0.65	0.50	0.51	0.51	4.48	4.41	4.50
200.5	2.06	-30.1	13.6	1.7	17.4	-23.3	-23.3	-22.9	0.65	0.21	0.22	0.23	2.98	2.69	2.79
103.3	2.08	-29.7	5.4	1.8	16.0	-22.7	-22.8	-22.2	0.65	0.23	0.24	0.25	2.63	2.43	2.46
102.2	2.07	-29.5	11.5	1.8	16.0	-23.0	-23.1	-22.7	0.65	0.48	0.49	0.50	2.89	2.66	2.74
100.8	2.08	-29.4	16.3	1.7	16.0	-23.7	-23.8	-23.5	0.65	0.73	0.75	0.75	3.38	3.17	3.26
202.9	2.32	-27.4	6.2	2.1	16.0	-20.2	-20.3	-19.8	0.65	0.05	0.06	0.06	2.54	2.35	2.40
197.9	2.35	-26.4	31.6	1.9	16.0	-21.4	-21.7	-21.3	0.65	0.43	0.44	0.44	4.04	3.91	3.94
198.4	2.47	-24.9	42.4	1.9	16.0	-20.9	-21.0	-20.8	0.65	0.63	0.64	0.64	5.18	4.85	4.95
200.1	2.45	-24.9	49.7	1.9	16.0	-21.4	-21.5	-21.2	0.65	0.85	0.85	0.86	6.11	5.81	5.80
233.8	2.08	-30.6	7.6	1.8	16.3	-22.8	-22.8	-22.3	0.65	0.06	0.07	0.07	2.40	2.16	2.24
229.1	2.12	-29.2	21.3	1.7	16.2	-23.3	-23.5	-23.2	0.65	0.25	0.26	0.26	3.28	3.09	3.21
206.9	2.17	-28.3	52.1	1.6	16.2	-24.3	-24.5	-24.3	0.65	0.68	0.69	0.69	5.45	5.33	5.44
202.1	2.09	-29.6	29.0	2.2	23.9	-19.4	-20.9	-19.9	0.65	0.21	0.22	0.22	2.72	2.98	2.89

Lebenslauf

Persönliche Daten

Name	Rabah
Vorname	Ali Abdelrahman
Geburtsdatum	1 Januar 1967
Gerburtsort	El Obeid
Staatangehörigkeit	sudanese

Schulbildung

Juli 1971-März 1978	Malit "Primary school", Sudan
Juli 1979-April /1981	Malit "Intermediate secondary school", Sudan
Juli 1981-März 1984	Elfashir " Higher secondary school", Sudan

Studium

Juli 1984-Nov. 1989	Bachlor-Studiengang "Chemical Engineering", Universität Khartum, Sudan Abschluss: Bachelor of Science (BSc)
Dez. 1993-Dez. 1996	Master-Studiengang "Mechanical Engineering", Universität Nairobi, Kenei Abschluss: Master of Science in Engineering (MSc)

Berufliche Tätigkeiten

seit April 2000	Wissenschaftlicher Mitarbeiter am Institut für Thermodynamik der Universität Hannover
Dez. 1996-	Wissenschaftlicher Mitarbeiter am "Department of Chemical Engineering" der Universität Khartum, Sudan
Dez. 1993-Dez. 1996	Wissenschaftlicher Mitarbeiter am "Department of Mechanical Engineering" der Universität Nairobi, Kenei
Jan. 1990-Nov. 1993	Wissenschaftlicher Mitarbeiter am "Department of Chemical Engineering" der Universität Khartum, Sudan

Hannover, im Juni 2003